EPITAXIAL GROWTH OF SPUTTERED THIN FILMS

by

C.K. Layton, Dip. Tech.

A Thesis submitted for the degree of

Doctor of Philosophy

Department of Electrical Engineering,

Imperial College of Science and Technology,

London.

June, 1969.

ABSTRACT

The deposition of thin films has attracted much attention in recent years. The merits of the various deposition techniques are largely consequent upon the requirements for the film. This Thesis describes the technique of D.C. sputtering as it may be applied to the growth of epitaxial thin films of metals and semiconductors. A review of nucleation theory and sputtering in general is given.

The results presented herein are those of a structural study and also, for semiconductor films, a study of galvanomagnetic properties. It is found that both metal and semiconductor films are epitaxial at temperatures considerably lower than the temperature required for evaporated epitaxial films. Increasing orientation is observed to occur for increasing substrate temperature, increasing film thickness and decreasing deposition rate. The effect is observed for growth by both diode and triode sputtering, but in the case of semiconductors, diode sputtering appears to be less effective.

Since one of the features of sputtering is that the ejected atoms have kinetic energy of ~10 eV, it is thought that this may be responsible for the observed epitaxy at lower temperatures. A computer calculation of the arrival energy at the substrate as a function of discharge gas pressure is presented. This shows a rapid decline in the arrival energy above 10^{-2} torr. A semi-quantitative model is presented in terms of the arrival energy being dissipated in the growing islands, the effect being dependent upon island size. The results are also discussed in relation to modern nucleation theories.

The results of the electrical study, made predominantly on germanium films, shows the galvanomagnetic properties to be considerably inferior

to those of the bulk material. It is demonstrated that the results are
due almost entirely to defects in the film structure. The mean free
path of the charge carriers is found to be of the same order as the
grain size.

ACKNOWLEDGEMENTS

CONTENTS

INTRODUCTION

1.1   INTRODUCTION

This Thesis describes the preparation and properties of thin films of metals and semiconductors by the technique of sputtering. The purpose of this introductory chapter is to examine the need for thin films in fundamental and applied terms, and to discuss briefly the various methods by which such films may be prepared. A historical survey of the evolution of sputtering as a technique is included and the types of film which may be prepared by sputtering are discussed. The experimental trends which determined the nature of the present investigation are indicated and in the light of these the aims of the thesis are outlined.

1.2.   THE DEVELOPMENT OF THIN FILM APPLICATIONS

The study of thin films per se first became necessary as a result of their application to the physics of optics, e.g. lens blooming, towards the end of the last century. Wavelengths of around $5000\overset{o}{A}$ require films of similar dimensions to act as quarter-wave retarders, filters etc. There was thus a need for the study of parameters controlling film growth and deposition so that films of the desired properties could be obtained.

From a physical investigation viewpoint, there was in the early part of this century, much interest in the conduction process, particularly in relation to electron mean free path behaviour. If the conductor has one dimension reduced to approximately the mean free path (typically $\sim 500\overset{o}{A}$), such a study becomes practicable. It was in this field that the electrical properties of thin films was first studied by J.J. Thompson (1901).

Practical requirements of modern technology have led to the need for electrical components in the form of small lightweight devices. Thus there has emerged a strong practical incentive for thorough investigations of the properties of thin films as a function of the many variables involved in their preparation. In this new technology, application of thin films falls into two main classes a) passive devices and b) active devices. The former class includes resistors and capacitors. In these the magnitude of both resistance and capacitance are inversely proportional to the thickness of the film. Theoretically it is therefore possible to produce thin film passive devices of any required characteristic simply by controlling the film thickness. In practice this is of course not so, and it is the reasons behind this not being so which form broadly the basis for the investigation of passive thin films. The first films deliberately prepared as resistors were made by Longden in 1900, but it was not until ∼1950 that any commercial products became available. The first reference to the use of thin films in the manufacture of capacitors, at the turn of the century, was not with respect to the dielectric layer, but to the electrodes. Metallised paper or plastic capacitors were thus conceived. The use of a deposited thin film dielectric was not achieved for another 50 years, one of the main drawbacks to the satisfactory development of the devices being the technical problems of achieving good vacuum.

Active devices broadly span semiconducting materials, particularly Si and Ge suitably doped. The carrier transport action may be bipolar (current carriers holes and electrons) or unipolar (one type of carrier only). A transistor made up of p-n junctions falls into the first category and it was to this that thin film efforts were directed initially. Results were not very encouraging because of the need for good single crystal growth so that minority carriers do not rapidly recombine with the majority carriers. Techniques have therefore concentrated on the production of single crystal films. The unipolar action, however, does not rely upon single crystallinity and this has led to

much activity in the development of the field effect transistor. The first device of such a kind prepared entirely by vacuum evaporation was by Weimer in 1961. Nowadays since the advent of integrated circuit techniques, it is possible to form an entire circuit on a single semiconductor substrate by suitable deposition of metal, semiconductor and insulating film. The need to understand and control the properties of these films is thus of paramount importance.

A further type of film which cannot be strictly termed active or passive is the magnetic film. Since these are generally metallic (elemental or compound) they lend themselves very readily to preparation by several of the methods described below. Magnetic devices in thin film form are particularly useful in computers where a large amount of information is required to be stored in as small a space as possible. A physical study of magnetic properties such as coercivity, hysterisis etc. is thus fundamental if an efficient fast computer store is required.

1.3. THIN FILM DEPOSITION METHODS

The deposition of a thin film layer on a suitable substrate relies upon the material being in atomic ionic or molecular form. Thus a technique is only suitable for a given material if that material can be reduced to this form. The techniques exist in two main classes, physical and chemical. Into the former class fall evaporation, sublimation and sputtering. The second class contains electro- and electro-less deposition, thermal decomposition from the vapour phase, etc.

1.3.1. Physical Deposition

In order to obtain a thin film from a bulk material it is necessary to give sufficient energy to the atoms in the material for them to break away from the bulk surface into free space. Once in free space they will condense on a cool surface to form a film, unless they are forced back to the source, e.g. by back diffusion. Hence the need for reduced pressure. The energy required

for the atoms to leave the surface may be imparted thermally by heating the material (evaporation, sublimation) or by momentum transfer on impact with an energetic particle (sputtering). Whether a material can be deposited by evaporation or not, depends on how much energy is required for dissociation and upon the pressure just above the surface of the material, i.e. the process is vapour pressure dependent. Because of this, different materials evaporate at different rates for a given temperature and/or pressure. Thus most alloys and compounds do not form thin films with the same stoichiometry as the source material. However, evaporation does have a very important place in deposition techniques because a) it is a very contamination-free method, b) it relies only upon the provision of sufficient heat, and for most materials, a moderate vacuum of only $\sim 10^{-6}$ torr is required and c) it is often possible to overcome the non-stoichiometry problem in alloy by suitable technique, e.g. flash evaporation, three-temperature method etc.

The second process, that of sputtering, is not vapour pressure dependent, since it relies only upon the transfer of energy from a bombarding particle to a lattice atom. The process will be discussed at greater length in Chapter 3. At this stage it is sufficient to say that virtually any material, elemental or compound, metal or dielectric can be sputtered using an appropriate technique. However, because it relies upon the existence of a dense ion cloud or beam for adequate deposition rates, it has often been described as a dirty method. This description arose from a misconceived idea over the method of production of the ions. Nowadays, it is possible to deposit films by sputtering under conditions matching those of evaporation.

Because evaporation techniques were developed more rapidly than sputtering techniques, most applications involve evaporation rather than sputtering. This is justifiably so since the requirements for evaporation are generally simpler than for sputtering though sputtering does have other advantages which will be discussed in Section 1.4.

1.3.2. Chemical Deposition

It is often possible to produce a layer of material on a suitable substrate by precipitation from a compound of that material. The compound may exist in solid, liquid or gas form and the transfer of material may be ionic or atomic. The chemical techniques commonly used are electro- and electro-less deposition and vapour phase deposition, which includes disproportionation, thermal decomposition and reduction or oxidation. The processes are somewhat limited in that not all materials lend themselves to the process. They are used nevertheless for thin film preparation and are superior to physical techniques in some cases. However, since these methods are not of direct relevance to the present work, they will not be discussed further. A recent and complete review of chemical deposition techniques has been given by Campbell (1968).

1.4. SPUTTERING

1.4.1. Early Work

The term sputtering refers to the removal of atoms from a bulk surface due to the bombardment of the surface by energetic particles, usually ions. It was first observed as a by-product of the investigation of discharges in gases in 1852 by Grove, who noticed a metallic deposit on the walls of the discharge tube. At the time it was considered an interesting nuisance and no attention was paid to its physical significance. It was not until 1877 that Wright again observed the deposition of a metal film during glow discharge experiments. Wright's observation followed the insertion of a gold foil into the discharge in an attempt to eliminate mercury vapour from the discharge he was studying. He then saw that a gold film was depositing on the wall of the discharge tube and that the film was thickest near the negative end of the foil. He realised the significance of this and was able to repeat his experiments making the negative electrode of the material he wished to deposit. Thus he was able to make qualitative and substantially correct statements regarding the relative sputtering efficiency of different materials.

The literature on the subject then increased rapidly as the simplicity of the technique was realized. A very moderate vacuum ($<10^{-2}$ torr) was required plus a suitable high potential source such as an induction coil. It was therefore within most workers' capabilities to set up an apparatus for the deposition of films by this technique. The really early work was concerned with the interesting phenomenon of obtaining thin films and a long list of references dating from 1852 is given by Fruth (1932). The study of the physical properties of the films so produced was not so thoroughly carried out. The electrical and magnetic properties were only earnestly investigated from about 1925. The effects observed were not so much peculiar to sputtered films as to thin films in general. A review up to 1938 is given by Lewis (1938).

All the early sputtering work, prior to 1940, was carried out in a glow discharge environment. As will be discussed in Chapter 3, this results in the mean free path for sputtered atoms and bombarding ions being reduced by collision with free gas atoms in the discharge. For accurate quantitative studies of the sputtering phenomenon, e.g. sputtering yield, this condition is clearly unsatisfactory. It was shown by von Hippel (1926) that at a pressure of 0.1 mm Hg and with a collector placed at the edge of the cathode fall the back diffusion of material amounts to 90%. This effect is clearly shown in Fig. 1.1, which represents the results of Guntherschulze and Meyer (1932). (Results given in this form by Penney and Moubis, 1940.) The sputtering yield for positive ions (energy 500eV) is plotted against the product pd, where p is the gas pressure in mm Hg and d is cathode-collector separation in cm.

Efforts to overcome the effects of back diffusion were initially directed towards reducing the surface area of the target electrode, e.g. by using a cylindrical wire. This was found to be unsatisfactory, however, on account of geometrical differences in the nature of the experiments. The first attempts to reduce the pressure in the system so that the yield did not vary with pd (see Fig.1.1) were made by Guntherschulze and Meyer (1932) using a hot
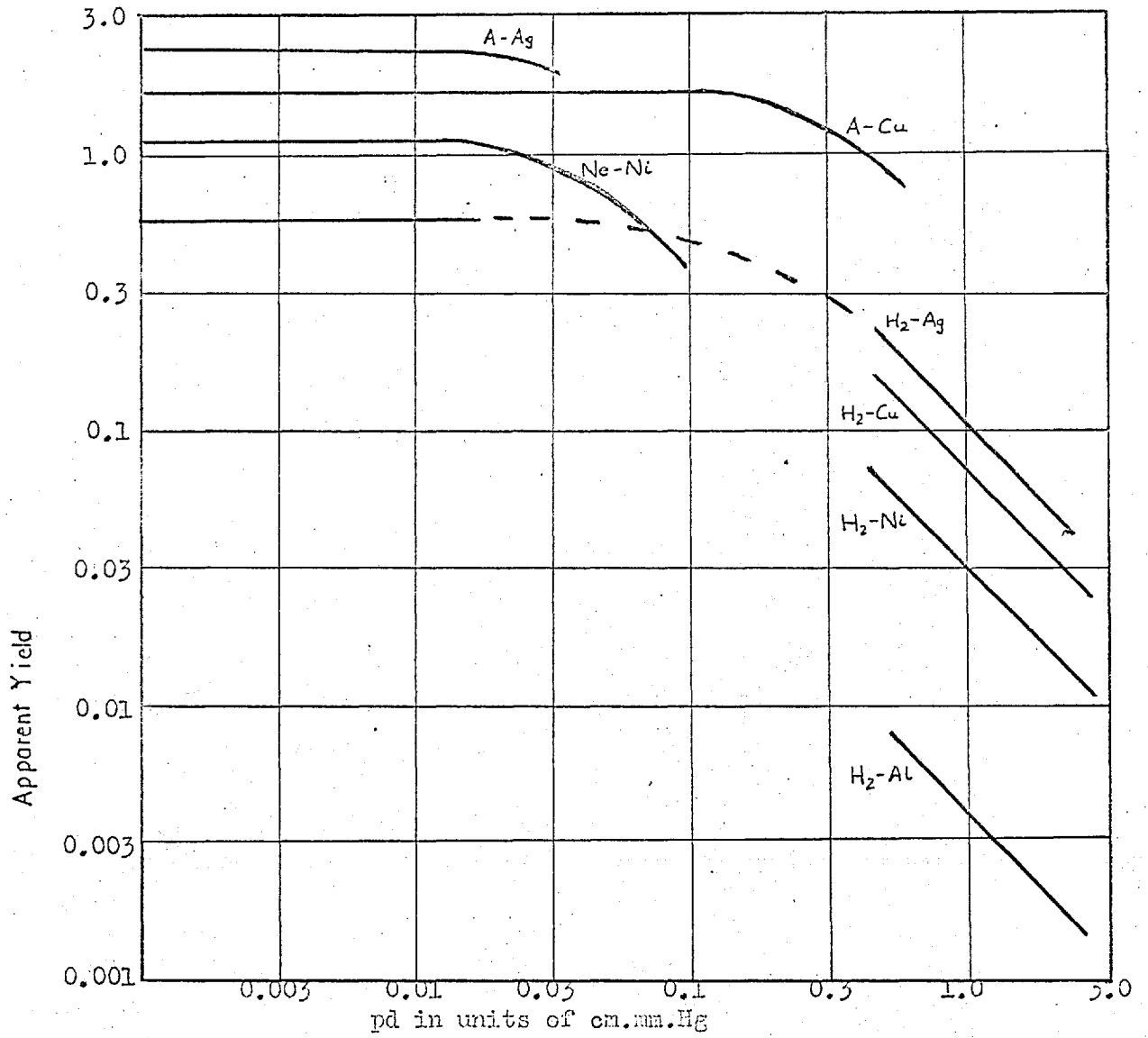
FIGURE 1.1

Apparent Sputtering Yield as a function of the product of the
Pressure and Anode-Cathode Separation, illustrating the
effect of Diffusion.

cathode. They found that the sputtering rate of silver by argon was constant at pressures below .01 mm Hg. Penney and Moubis (1940) attempted to lower the required pressure for the discharge by employing an axial magnetic field with a normal glow discharge. The field was coaxial with a cylindrical electrode arrangement. Its purpose was to increase the path length of the electrons, thereby increasing the probability of ionisation at lower pressures. Their arrangement allowed operation at current densities as high as $20mA/cm^2$ and with such a current and a cathode fall of 500V, a sputtering rate of 3000 Å/min. at 0.014 mm Hg could be achieved for copper bombarded by argon! The major purpose of their experiments however was to determine sputtering yields for various materials as a function of applied voltage, gas pressure and current density. It is a feature of sputtering at low pressures that these three parameters can be separately varied whereas in a glow discharge they are interdependent. Their results compared very favourably with those obtained by Guntherschulze and Meyer.

A feature of early work was an attempt to establish the lowest voltage at which sputtering occurred. An excellent review of these early observations is given by Wehner (1955). Oliphant (1928) measured the sputtering yield and found that no sputtering occurred until the energy of the ions was at least 300-400 volts. The major difficulty encountered is that near the threshold the sputtering yield is very low. Early experiments were simply not sensitive enough to detect the very small changes which occurred. Also, the yield is not linear with energy, which precludes accurate extrapolation. Many techniques have been evolved in an attempt to establish a true starting point, including radio-tracers (Morgulis and Tishenko, 1956) and optical spectroscopy (Stuart and Wehner, 1962). Such techniques have shown that the threshold (~20eV) was much less than originally determined. It is an interesting result that the threshold is virtually independent of the relative masses of target atom and bombarding ion. Stuart et al (1960) have shown that the threshold energies are very similar to the displacement energies in solids.

Following Penney and Moubis (1940), it became very clear that investigations of the sputtering mechanism were unreliable unless the pressure in the system could be reduced such that the mean free paths of the sputtered atoms and the bombarding ions were of the same order as the interelectrode dimensions. Thus emphasis after 1940 was on the design and operation of low pressure sputtering systems purely as a means of studying the mechanisms of sputtering. A study of the resultant films was not made to any extent except insofar as they represented a measure of the sputtered material. Wehner's review of 1955 and also that by Kaminsky (1965) give a very complete survey of the work up to the time of their publication.

The growth of thin films by sputtering, although known, was not given serious consideration largely because it was thought to compare badly with evaporation as far as film purity was concerned. In fact, where an inert bombarding gas is used, the only impurity problem arises from inclusion of gas in the growing film and not by chemical reaction with the film. The amount of reactive gas in the environment depends entirely upon the residual pressure of the vacuum system as is the case for evaporation. The techniques used in sputtering to overcome contamination will be discussed in Chapter 3.

1.4.2 TYPES OF FILM WHICH MAY BE DEPOSITED BY SPUTTERING

Generally, there is no exception to the type of material which may be deposited by sputtering, given the right technique. Because the process is basically one of momentum transfer between bombarding ion and target atom, there is no limitation due to vapour pressure etc. Films of metals, insulators and semiconductors can therefore be produced and their properties reasonably controlled by control of the deposition parameters. Historically, metal films were the first to be studied because of their lack of complexity, and resistivity, superconductivity, optical and magnetic properties were investigated. Since 1960 these investigations have hardened in their intent and sputtering is an

viable a process as evaporation for the formation of superconducting (Fierichs, 1962) and magnetic (Francombe and Noreika, 1961) films, particularly since sputtering enables alloy films to be easily deposited. Insulating films may be prepared by sputtering but not normally by the d.c. method. If the target is an insulator, charge effects are such that ion bombardment stops after a very short time, thereby preventing sputtering. An a.c. method is therefore employed in which the target is made periodically positive and negative. The frequency is usually >100 KHz. This technique, known as R.F. sputtering, was used by Davidse and Maissel (1965) to deposit glass films. The technique is however fairly recent and early work on sputtering insulating films was by reactive sputtering. Deliberate production of insulating films by sputtering was carried out in 1944 by Janeff (published in 1955). Bickley and Campbell (1962) deposited mixed oxides by sputtering for capacitor applications.

The use of sputtering for the deposition of semiconductor films has been one of slow development, based again on the mistaken idea that the technique is a dirty one. Several papers appeared in 1962 which showed that epitaxial films of elemental and compound semiconductors could be prepared by sputtering (Francombe et al, 1962, Reizman and Basseches, 1962) though the electrical properties of such films were not very good (Moulton, 1962).

1.5. FACTORS LEADING TO THIS WORK

One of the many applications of thin films described in the earlier section is in the field of electronics. Certainly in the case of semiconductors it is an advantage to have a single crystal film deposited on a suitable substrate (e.g. for bipolar transistors). The need for single crystal metal layers is not so apparent except for cases in which certain properties are anisotropic. However, the value in studying sputtered metal film lies in the comparative wealth of information regarding the growth of metal films by evaporation. The interest in epitaxy by sputtering was generated by Campbell

and Stirland (1964). They demonstrated that gold and silver deposited on to rocksalt by sputtering grew epitaxially at substrate temperatures low in comparison to evaporated films. This fact, if applicable to the growth of semiconductors, would enable epitaxial overlayers to be grown on substrates which had been previously treated (e.g. diffusion processes) at relatively low temperatures. Other methods of deposition, for example vapour phase deposition, require substrate temperatures around $1,000^{\circ}C$ for epitaxial growth. Such a temperature would cause large diffusion and alter the characteristics of a pre-formed device. Because of the small amount of diffusion which would result at the low epitaxy temperature, any junctions formed between opposite types of semiconductor would be very sharp. This would enhance the high frequency characteristics of the device. A further point in favour of sputtering as a deposition technique for epitaxial semi-conductors is the observation that compound films can be grown with the stoichiometry of the original source material (Francombe et al, 1962).

1.6. OBJECTS OF THIS WORK

The above benefits which would result if epitaxial semiconductor films could be grown at low temperatures formed the basis on which the present work was founded. Since the observations had been largely qualitative, it was considered necessary to investigate the growth of films by sputtering, particularly the phenomenon of epitaxy, as a function of deposition and discharge parameters.

Thus the aims of the experimental work were set up as follows:

a) To investigate the phenomenon of sputtering insofar as it may be applied to the controlled growth of thin films.

b) To investigate the experimental parameters influencing the growth of such films.

c) To examine the epitaxial growth in particular in an attempt to
    establish the reasons for epitaxy occurring at lower temperatures
    for sputtering than for evaporation.

d) To establish any correlation between the growth of semiconductor
    films by sputtering and their galvanomagnetic properties.

CHAPTER II

NUCLEATION AND GROWTH

2.1. INTRODUCTION

Fundamental to any physical study of thin film phenomena is the need

for a detailed picture of the way a film develops. It is therefore necessary

to study the stages of development of a film on a substrate from zero thick-

ness (i.e. bare substrate) up to a finite, continuous, thickness of film.

From such a study it should be possible to predict the nature and behaviour

of a film according to the parameters known to be controlling its growth. It

is therefore the purpose of this chapter to discuss the nucleation and growth

of films in the light of various theoretical models. Particular attention is

to be given to the effect sputtered atoms may have on the nucleation and growth

process.

2.2. HIGH ENERGY ELECTRON DIFFRACTION

By far the most widely used tool for examination of thin films is that

of high energy electron diffraction. The resolution of a good well aligned

electron microscope is $\sim 5\overset{o}{A}$ which enables films to be studied, if not from their

very initial stages, then certainly from their embryonic stage. There has

been much literature on the methods and application of electron diffraction

to thin films and there are several reviews of note (Stirland 1966 and Pashley

1965). The most common techniques are briefly described below :

a) Bright field electron microscopy, in which the field of view of the spec-

    imen is a function of the magnification.. Typical magnification is

    20-40,000X. The image contrast depends upon the extent of diffraction

    by the specimen.

b) Selected area diffraction. In this case an aperture is placed in the back focal plane of the projector lens so as to limit the area of specimen contributing to the final image. The magnification is reduced to zero so that the final image is composed of an electron distribution according to the crystallinity of the specimen. A single crystal specimen will diffract electrons from discrete sets of planes to form a spot pattern on the final screen analogous to the reciprocal lattice of the specimen. If the specimen is composed of randomly oriented crystallites (i.e. it is polycrystalline) a ring pattern will result. Amorphous films (or polycrystalline films with grain size $<5\overset{\circ}{A}$) will yield a diffuse ring pattern. The use of selected area diffraction also reduces the effect of lens aberration on the final image.

c) Dark field electron microscopy in which an objective aperture is placed so as to isolate a single diffraction spot. Then only those parts of the film which have contributed to that spot will appear bright on the magnified image, since the direct beam has been excluded by the aperture. It is thus a reversal in contrast to the technique described in (a). The technique is useful for establishing twinning planes in crystals.

d) General area diffraction in which no aperture is used. All parts of the film on which the electron beam is incident contribute to the diffraction pattern. This method allows examination of a much larger area of film but has the disadvantage that induced damage (e.g. tearing or folding of the film during the mounting procedure) also contributes to the final image.

All the above techniques are for transmission microscopy and diffraction in which the beam passes through the film.

It is limited therefore by the thickness of film which may be examined. The limitations for metal and semiconductor film is ~2000Å. It also requires that the film be removed from its substrate. In most cases this is not possible without the danger of film damage. However, a reflection technique can be employed, known as glancing angle electron diffraction, in which the electron beam is "reflected" from the first few lattice planes of the film which act like a reflection diffraction grating. The technique is more dependent upon surface topography than the transmission technique but is more accurate for lattice parameter determination because there are no lenses between specimen and image recorder (photographic plate) to distort the diffracted beam paths. In the work described in this Thesis, all the above techniques have been used.

2.3. STAGES IN THIN FILM GROWTH

On a semi-quantitative basis it is relevant here to discuss what happens when a clean substrate area is exposed to a flux of atoms from any source.

Consider a substrate made up of a series of building blocks of unit cell size. If the surface is perfect, it is flat on an atomic scale. In practice it is imperfect and so has a topography resembling that of Fig. 2.1. The incident atom flux can be defined in terms of the supersaturation. This is given by P/Pe where P is the equivalent vapour pressure at a given surface temperature that would give the observed impingement flux and Pe is the thermodynamic equilibrium value corresponding to bulk condensate at the same temperature. If P < Pe there is a net vaporisation from the surface, i.e. condensation cannot occur. Assuming the supersaturation is greater than unity, there will be a net gain of adatoms to the surface. If the atom is thermally accommodated, it equilibrates with the substrate lattice and its mobility on the surface will be determined by the surface temperature. There are now three
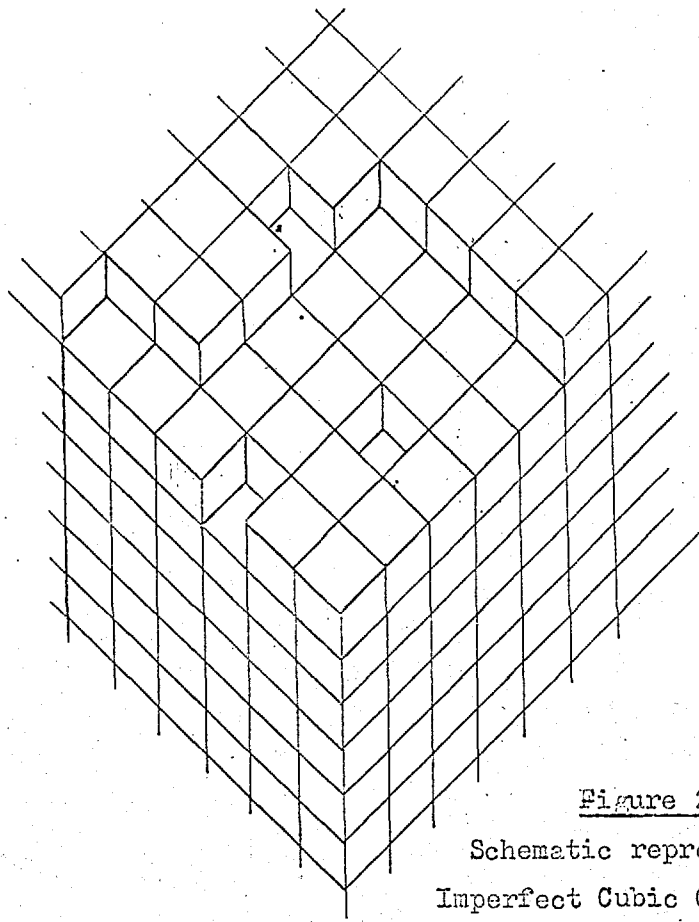
Figure 2.1

Schematic representation of
Imperfect Cubic Crystal Surface
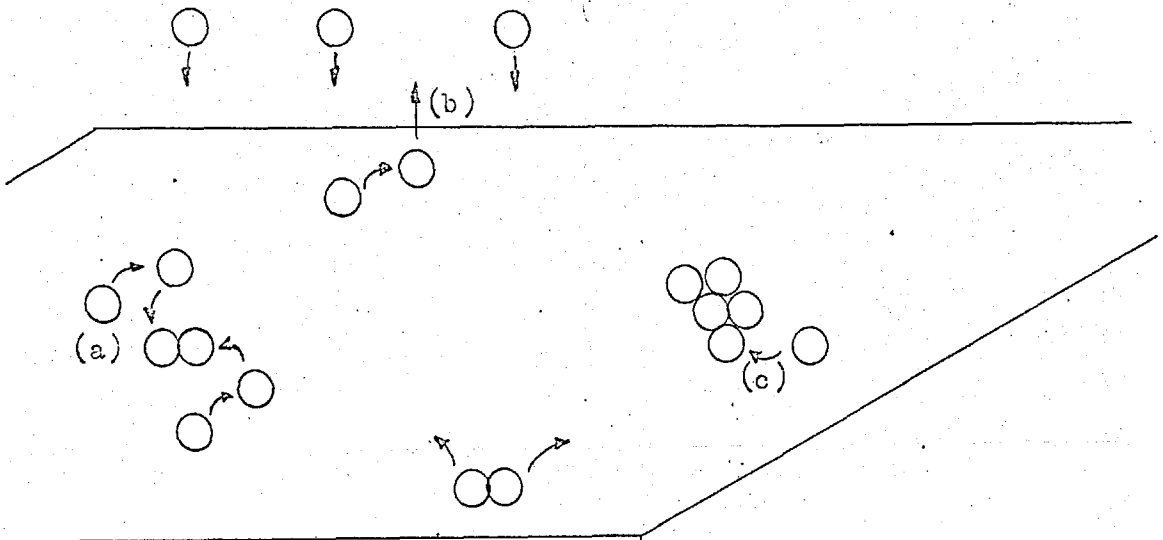
Figure 2.2

Schematic representation of the Behaviour of
Adatoms on a Crystal Surface

possible mechanisms governing the behaviour of the adatom :

a) It may meet another single adatom to form a pair. Such a pair will be

    less mobile than a single atom and will also require a greater energy

    from the substrate in order to re evaporate, i.e. it is more stable.

    It is possible, however, for it to break up and it will require an amount

    of energy equivalent to the pair-bonding energy for this to occur.

b) The atom may receive sufficient energy to de-sorb, or re-evaporate,

    provided it does not meet another atom or group of atoms. The probability

    of re-evaporation is an exponential function of the desorption energy

    and the temperature. This will be discussed more fully later.

c) The atom may meet a group of atoms, to form a stable group, or it may

    meet an already stable group. It is then absorbed and will lead to

    growth of the film. As in (a) there is a finite probability of it break-

    ing away from the group, proportional to the number of bonds it has with

    the group.

These three mechanisms are represented schematically by Fig. 2.2. The
statistics and kinetics governing the process are considered in a later section.

The growth of a thin film depends upon mechanism (c) above. Addition of
atoms to a group of atoms at a rate faster than the rate of atoms leaving the
group, leads to an increase in size of the group. By the time they become large
enough for resolution by an electron microscope ($\sim 10 \overset{\circ}{A}$ diameter) they consist
of ~ 10 atoms and are therefore very stable. These groups or islands have a
substrate surface density determined by the kinetics of the system as discussed
below. For given conditions they will grow in size eventually touching. When
this occurs coalescence takes place which will reduce the number density of
the islands but the average island size will increase. As the growth proceeds
the coalescence occurs between larger and larger islands and the film becomes
continuous but for the fissures between the coalesced areas. Eventually the

fissures close up so material lands in them and on the existing film, to form a continuous layer of deposit. A series of micrographs depicting the process of film development is shown in Fig. 2.3. which is for increasing thickness of deposit at constant rate (0.05Å/s) and substrate temperature (300°C). It will be noticed from the micrographs that, from an early stage, the film consists of many defects (twins and stacking faults - evident from the diffraction contrast). The origin of these faults may be the substrate, but is also because the substrate/deposit lattice match is not perfect, so that strain exists in the overlayer which may be relieved by way of defects. Also, due to the lattice mismatch, when islands coalesce there is most likely to be a fault at the island interface

2.4. ADSORPTION

In a discussion of the formation of one phase from another, the interaction between molecules or atoms in the phases is of extreme importance. Since all such phase transformations are energy activated, the magnitude of the interaction determines the conditions for the transformation. It is necessary to know therefore the various types of force which can exist between atoms or molecules and the relative importance of these forces in controlling the behaviour of the atoms.

The forces between atoms on the surface and atoms in the surface, though commonly known as adsorption forces, are of the same nature exactly as any other interatomic forces. The forces fall into two classes characterised by the magnitude of the binding energy. So-called chemical bonding or chemisorption is characterised by a binding energy of the order of 1-10eV per bond. Physisorption on the other hand is characterised by a binding energy of the order of 0.5eV per bond.

10Å

50Å

150Å
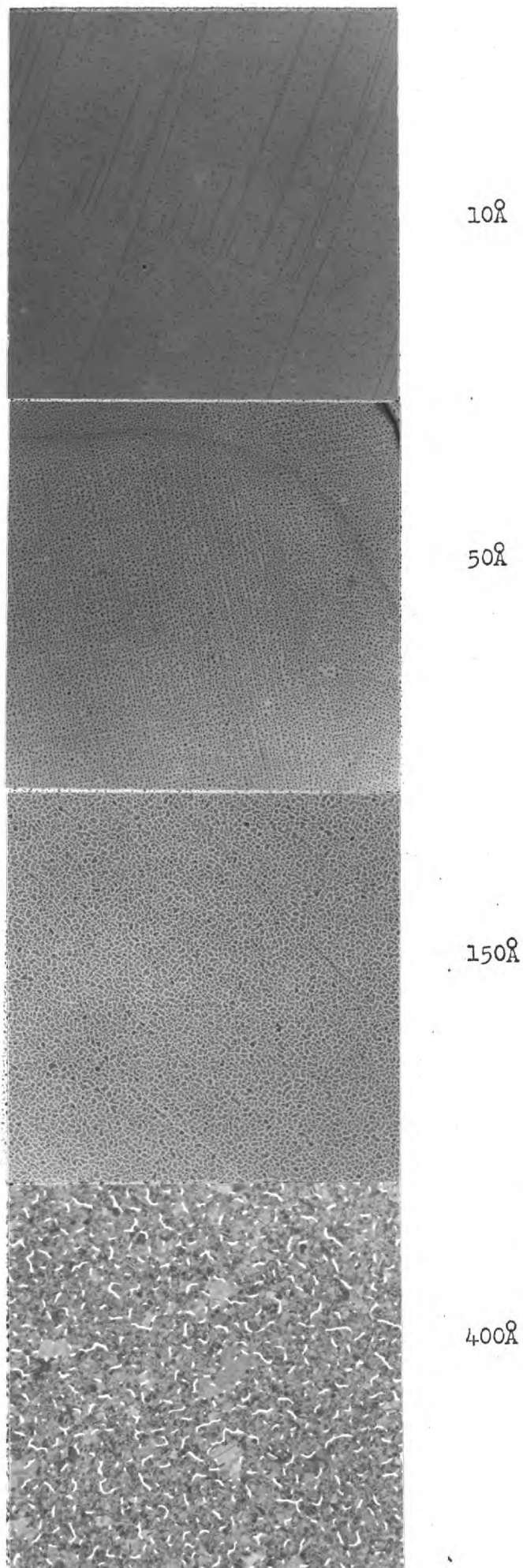
Figure 2.3

Thin film growth sequence
Au/NaCl. Rate of deposition
0.05Å/sec. Substrate temp.
300°C.

400Å

2.4.1. Chemisorption

Ionic, covalent and metallic bonds are all examples of chemisorption. Each involves the giving up or sharing of an electron to or with other atoms or molecules. Generally nearest neighbour interaction is insufficient to account for the large forces which in the case of ionic bonds decrease as the square of the distance. Of the three types of bonding in this class, ionic bonding is by far the strongest, ranging from 5-10eV per bond. Covalent bonds are approximately 1-6eV and typical of substances with such bonding are diamond, silicon and germanium. Often bonds are of partial ionic and partial covalent nature, e.g. SiO, HCl. Metallic bonds (typically 1-3eV per bond) are more difficult to analyse due to the considerable effect which can result from the ion core, in addition to the interaction of conduction electrons.

2.4.2. Physisorption

Physisorption does not rely on electron exchange in any way and is therefore weaker in nature than the chemisorption bond. It may be regarded as interaction between dipoles, which are a result of the charge distribution within a molecule. Some molecules possess a permanent dipole moment and are termed polar molecules, water or acetone are examples. The magnitude of the interaction of dipoles is dependent upon whether one or both of the molecules is polar. There are thus three main types of interaction:

a)   Polar-polar, in which the binding energy is ~5 kcal/mole (1eV ≃ 23kcal/mole). The dipoles will tend to line up end to end and are a function of temperature since increased temperature destroys the alignment.

b)   Polar-non polar, in which for instance a neutral atom of spherical symmetry has its symmetry distorted by an electric field so that a resultant dipole moment is induced, i.e. it becomes polarised. The electric field may be produced by a neighbouring dipole. For a flat surface the effect is small (typically 0.5 kcal/mole) but it may become important at discontinuities in the surface, e.g. steps or dislocations.

c) Non polar - non polar. These non-polar forces are the most important of the attractive forces. The interaction can be likened to the case of two simple harmonic oscillators such that the mutual polarisation of adatom and substrate atom dipoles fluctuate in phase giving rise to an attraction. The magnitude of the interaction for a dielectric substrate is ~ 10kcal/mole.

The types of interaction above are commonly known as Van der Waal interactions. For the case of non-polar forces the most favourable position for an adatom is when it is as close to as many highly polarisable sub-atoms as possible, e.g. at the centre of a cube face. For polar forces, generally important only on ionic substrates, adsorption is favoured directly above one type of sub-atom. Since the adatom is generally not ionised the former interaction is expected to predominate.

If the adatom is ionised, additional interaction can occur. A dielectric substrate may be polarised by an ad-ion. In addition, if the substrate is ionic then normal Coulomb interaction between charges will exist. This will be particularly important at irregularities in the surface and as a result defects will act as strongly preferred sites for ad-ions. For a metal substrate image charges are also important.

It would be expected from the above considerations that neutral and charged atoms would be adsorbed at different sites. This may be important in the sputtering environment. For a real surface there will exist many defects which will modify the interaction. More important perhaps, particularly when applied to considerations of epitaxy, the strain energy introduced by interfacial misfit between substrate and adsorbate may well swamp the normal interaction energy and therefore dominate the adsorption.

The review of nucleation theory which follows deals only with physisorption. As a first approximation the case of chemisorption might be expected to modify the theories only in the magnitude of the surface diffusion energy.

2.5. NUCLEATION THEORIES

2.5.1. Introduction

As has already been intimated the fundamental phenomenon on which nucleation theory rests is that of single atom adsorption onto a substrate and the subsequent behaviour of that atom in relation to the substrate and to other atoms. The theories attempt to analyse statistically the dependence of the behaviour on such terms as impingement rate, substrate temperature, etc. It is useful at this stage to define certain terms, particularly with regard to energy.
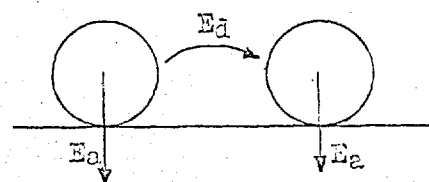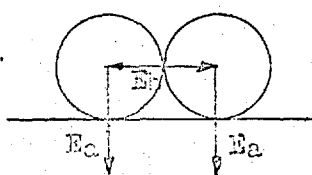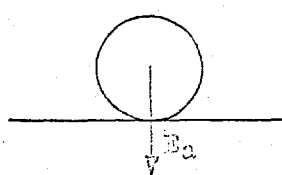
Ea = Adsorption Energy   Eb = Cohesive Energy   Ed = Surface Diffusion Energy

If the substrate is considered as a periodic potential surface then it may be represented by the energy diagram shown below :
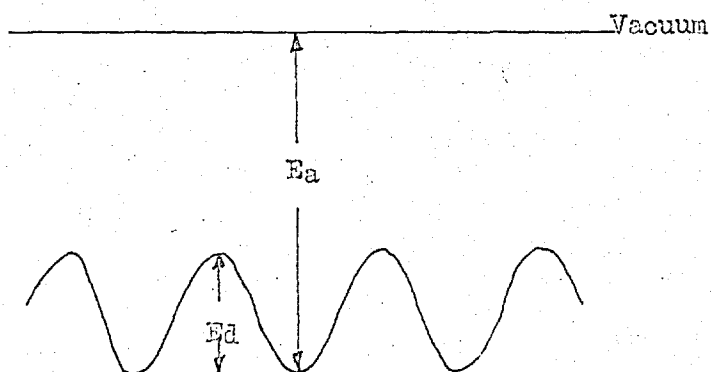
Ea = Adsorption Energy
Ed = Surface Diffusion
                Energy

Single atom adsorption was first analytically considered by Frenkel (1923). He made two fundamental assumptions which formed the basis of later theoretical work on the problem. These were (a) when an atom strikes the substrate it will stay on the surface for a certain time before re-evaporating, dependent upon the surface temperature, and (b) during its time on the surface it will move about and may collide with another atom to form a pair which is more stable, i.e. it has a much longer lifetime on the surface. Frenkel derived expressions for the lifetimes of singles and pairs as :

$$\tau_1 = \tau_0 \exp Ea/kT$$

$$\tau_2 = \tau^{-1} \exp \frac{Ea + Eb}{kT}$$

where $\tau_0 = 1/\nu_0$, and $\tau^{-1} = 1/\nu^1$, ν_0 and ν^1 are characteristic frequencies for the system and are constants ($\sim 10^{12}$). He then considered the equilibrium condition when $\frac{dn}{dt}$ (the rate of increase of nuclei) is zero, and derived a critical impingement rate. Above this critical rate, nucleation will occur while below it there is no net condensation. The critical rate is given by :

$$Rc = \frac{1}{4 \, \sigma_0 \, \tau_0} \exp - \frac{(Ea + Ed)}{kT}$$

and the slope of ln Rc against $1/T$ gives (Ea + Ed) which was typically 5-6 kcal/mole.

A criticism of this early work was that (a) it only considered the equilibrium conditions, (b) no account was taken of arrival temperature, (c) a unique value of Ea was assumed and (d) critical states of pairs and above were not considered. Of these four points, only (d) has been re-examined since the other three present quite complex problems analytically.

2.5.2. Modern Concepts

The basis of modern theories of nucleation stems from the earlier work of Volmer and Weber (1925) and Becker and Doering (1935) who considered the homogeneous nucleation in the vapour phase from a super-saturated vapour, in which clusters grew by the addition of single atoms or molecules. By considering the change in the free energy of a cluster as a function of its size, the Gibbs free energy of formation of a cluster may be found. If one assumes these clusters to possess macroscopic thermodynamic properties then, if σ is the surface free energy per unit area and ΔG_V is the difference in volume free energy between cluster and vapour per unit volume, the free energy of formation is given by :

$$G = \underbrace{4\pi r^2 \sigma}_{\text{Surface}} + \underbrace{\frac{4}{3}\pi r^3 \Delta G_V}_{\text{Volume}} \qquad - \quad 2.1$$

ΔG_V is given by $\quad - \dfrac{(kT)}{(\Omega)} \ln P/Pe \quad - \quad$ 2.1(a)

Ω = molecular volume and P/Pe = supersaturation ratio as defined in an earlier section of this chapter. This expression is obtained by integration of the expression $dG_V = Vdp$ where $V = \dfrac{kT}{\Omega P}$. A plot of equation 2.1. gives a curve of the form

ΔG^*

ΔG

r^* r
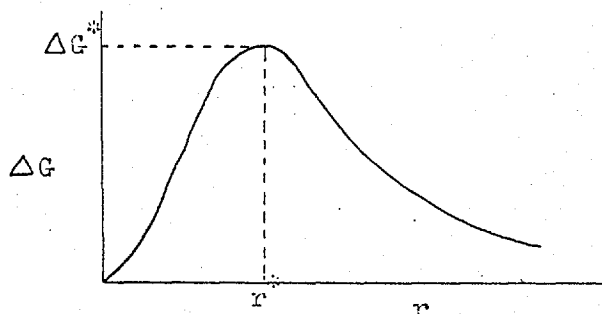
(This curve assumes only a single maximum of ΔG).

Initially, addition of a single atom will increase the free energy. When $r = r^*$, ΔG is a maximum and further addition decreases the free energy. Maximising ΔG gives

$$r^* = \dfrac{-2\sigma}{\Delta G_V} \quad - \quad 2.2(a)$$

and $\quad \Delta G^* = \dfrac{16 \pi \sigma^3}{3 \; \Delta G_V^2} \quad - \quad$ 2.2(b)

The critical radius r^* thus defines the critical cluster size, whose free energy will decrease on the addition of one or more atoms, or by the removal of an atom, i.e. it has equal chance of growth and decay. A cluster one atom greater than the critical size has a greater probability of growth than of decay and is termed the smallest stable cluster..

A natural extension of the theory of homogeneous nucleation is to that of heterogeneous nucleation, of which atoms striking a substrate is an example. The problem has been approached in two ways, the capillarity model and the atomistic model. The former model based on the application of macroscopic thermodynamic properties to microscopic clusters (Hirth and Pound, 1963) has now been largely discounted and will not be discussed.

2.5.2.1. Atomistic Model

By considering the adsorption of single atoms onto a surface and their subsequent diffusion about the surface, Walton et al (1963) considered a maximum density of nuclei determined by the capture area of stable clusters. When these areas overlap, further fresh nucleation stops. Since the diffusion distance is defined as :

$$d = A_o \exp \frac{Ea-Ed}{2kT}$$

a knowledge of the saturation nucleation density should yield values of (Ea-Ed).

A general expression for the nucleation rate is obtained from the expression :

$$J_i^* = \omega_{i*} \, N_{i*} \qquad - \qquad 2.3.$$

where J_{i*} = formation rate of stable nuclei from critical nuclei of i* atoms

N_{i*} is the number of critical nuclei and is given by considering the equilibrium between growth and decay of the critical nucleus. By a step-by-step method, an equation is obtained, viz:

$$N_{i*} = No \, \frac{(N_1)^{i^*}}{(N_0)} \, \exp. \, \frac{E_i^*}{kT} \qquad - \qquad 2.4.$$

where $E_{i*} = \sum_{i=1}^{i^*} \Delta E_{i-1}^i$ = energy required to break bond with cluster.

ω_{i*} is the rate at which single atoms join a critical nucleus and is given by considering the capture area of a critical nucleus. This is given by $^{Ma}/No$ where Ma = V $\mathcal{T}$a = no. of sites covered by a single atom travelling at velocity V sites per second in its lifetime $\mathcal{T}$a seconds, and No = total number of available sites. The total capture rate is thus R, $^{Ma}/No$ where R = arrival rate.

$$\text{Thus} \qquad J_{i*} = R \, Ma \, \frac{N_{i*}}{No}$$

$$= R \, (\frac{R}{No \mathcal{V}o})^{i^*} \, \exp \, (E_{i*} + (i+1) \, Ea - Ed) \, /kT \qquad - \qquad 2.5$$

This defines J in terms of fraction of total sites filled per unit area per second. Walton et al considered the conditions under which i^* increased from unity. At high supersaturation (high rate or low substrate temperature) $i^* = 1$ so that substituting in the above equation :

$$J_1 = R \left(\frac{R}{N_o\nu_o}\right) \exp. \left(\frac{2E_a-E_d}{kT}\right) \qquad - \qquad 2.6(a)$$

and $i^* = 2$

$$J_2 = R \left(\frac{R}{N_o\nu_o}\right)^2 \exp. \left(\frac{E_2 + 3E_a - E_d}{kT}\right) \qquad - \qquad 2.6(b)$$

Since Waltons equations give J in terms of absolute numbers atom captured it is necessary to multiply the above equations by the total number of sites, No.

For each value of i^*, one can plot ln J as a function of $^1/T$ and obtain straight lines of varying slope according to the energy terms. At the points of intersection of the various lines, a temperature is defined at which the critical nucleus changes from one value of i^* to another. The value of the transition temperature is obtained by equating the nucleation rates. Thus :

$$T_{1-2} = \frac{-(E_2+E_a)}{k \ln \left(R/N_o\nu_o\right)} = \text{Temperature at which critical nucleus goes from } i^* = 1 \text{ to } i^* = 2$$

$$T_{2-3} = \frac{-(E_3+E_a - E_2)}{k \ln \left(R/N_o\nu_o\right)} = \text{Temperature at which critical nucleus goes from } i^* = 2 \text{ to } i^* = 3$$

Walton et al (1963) attempts to define the epitaxial temperature on the basis of the size of the smallest stable cluster (which is one atom larger than the critical nucleus). T_{2-3} corresponds to a change in the smallest stable cluster from 3 atoms to 4 atoms, the 4 atoms arranging themselves in a square array. Both a triangular array of 3 atoms and a square array of 4 atoms have

a minimum of two bonds per atom, and the type which predominates at a given temperature will depend on the energies E_3 and E_2. If $E_3 = 2E_2$ then $T_{1-2} = T_{2-3}$ so that triangles will not exist. Only if $E_3 > 2E_2$ will the triangular configuration occur. Walton has shown E_3 to be ~2.1eV for silver on rocksalt which is greater than $2E_2$ since E_2 is equivalent to the dissociation energy of a pair ($\simeq 0.9$ according to Walton). Thus it is to be expected that decreasing the supersaturation would result in the film going from polycrystalline to $\langle 111 \rangle$ predominated to $\langle 001 \rangle$ predominated to $\langle 001 \rangle$ perfect orientation for silver or gold on rocksalt. By putting $T_{1-2} = T_{2-3} = T_{1-3}$ Walton predicts an $\langle 001 \rangle$ epitaxial temperature given by

$$T_e \simeq \frac{E_2 + Ea}{k \ln \left(\frac{No \nu o}{R} \right)}$$

Putting in suitable values gives a temperature of $250^\circ C$ for silver on rocksalt, in fair agreement with observed values. It should be emphasised that the above is Waltons own interpretation and may not be correct. It is included here as it formed the basis of the atomistic theory application to nucleation and epitaxy.

Lewis (1967) has carried the atomistic model a stage further and has calculated the saturation island density under various conditions by defining the catchment areas of a critical nucleus.

In the case of initially incomplete condensation, the supersaturation is such that the formation of pairs is unlikely and most atoms complete their lifetime on the surface and re-evaporate. The formation rate of stable nuclei is given by :

$$\frac{dns}{dt} = \underbrace{R.Ma \times Ni^* \times}_{\substack{\text{critical nucl}^n \\ \text{rate}}} \underbrace{\left(1 - \frac{Ns\ Ma}{No}\right)}_{\substack{\text{fresh nucl}^n \\ \text{area}}} \qquad - \qquad 2.7.$$

The final saturation density is given by :

$$N_S = No\ exp\ - (Ea - Ed)/kT \qquad - \qquad 2.8.$$

The instantaneous condensation coefficient $x = \dfrac{\dot{n}s}{Ns}$ so that condensation is complete when $\dot{n}s = Ns$. $\dot{n}s$ rises exponentially towards Ns with time constant Ns/J_{i*}, J_{i*} being given by equation 2.5 (i.e. function of R).

When condensation is complete from the onset, then the formation of pairs is highly probable and there are an average two atoms in the catchment area $^{Ma}/No$. By defining another area Mc sites, such that there is one single atom for every Mc sites, $Mc^2 = No\ ^{Ma}/_{R\ \tau a}$

and

$$N_S = \frac{(NoR)^{\frac{1}{2}}}{(\nu o)} \exp \frac{Ed}{2kT} \qquad - \qquad 2.9.$$

If Ns is plotted as a function of $^1/T$ from equations 2.8. and 2.9. the curve shown in Fig. 2.4. will result.

There will be a family of curves for different values of Ea, Ed and R. It will be noted that only the complete condensation curve is rate-dependent.

The above condition for complete condensation is for i* = 1 so that a pair is stable. At lower supersaturations i* = 2 or more. For i* = 2, Ns is given by :

$$Ns = \frac{(R^2\ No)^{1/3}}{(\nu o^2)} \exp \frac{E_2 + 2E_d}{3kT} \qquad - \qquad 2.10.$$

This will result in a lower saturation density than would be expected if i* were equal to one. Similarly if i* = 3 an even lower Ns would result.

The fact that Ns is of the order of 10^{11} cm^{-2} even in the case of epitaxial films and gives an intercept of the order $\dfrac{(R\ No)^{\frac{1}{2}}}{(\nu o)}$ suggests that i* = 1. If this is so, it tends to contradict Waltons proposal that i* = 3 for epitaxy. There is thus some disagreement as to what exactly constitutes epitaxial nucleation. A stable cluster of two atoms certainly has directional properties and may well therefore influence the subsequent orientation of the nucleus.

It is equally probable that while several orientations may nucleate, the growth of all but one orientation may be supressed because it involves the
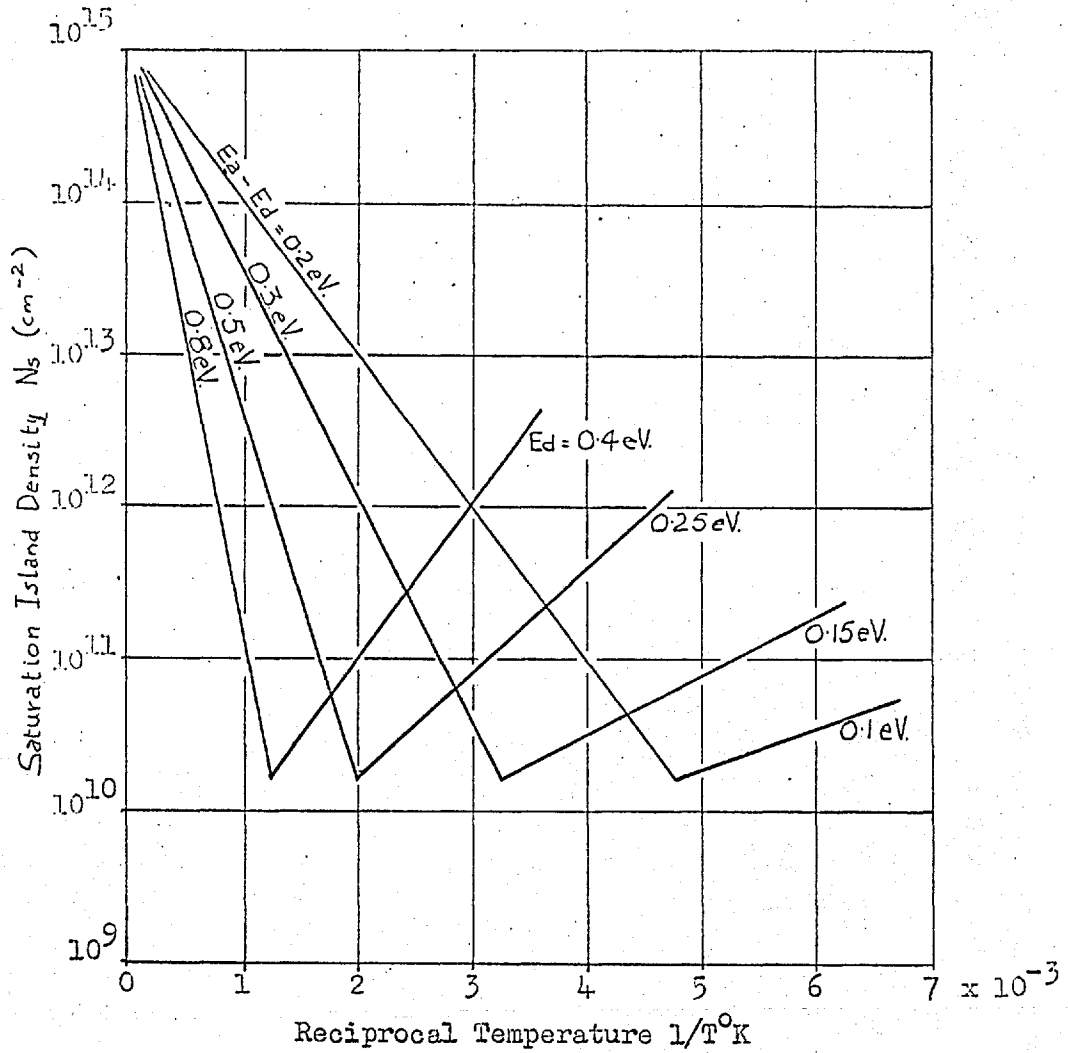
FIGURE 2.4

Theoretical variation of saturation island density Ns with temperature T for an incidence rate of $1\overset{\circ}{A}$ sec^{-1} and for a range of values of adsorption energy E_a and surface diffusion energy E_d. (Lewis and Campbell, 1967)

addition of atoms into energetically unfavourable positions. Thus there
may be local free energy minima associated with certain values of i^*,
which would lead to stability of that particular "phase". This is the
basis of the Alternate Path Theory (Halpern, 1967). The theory allows
for clusters of size i to exist in various states, j. The proportion of
clusters in a given state, j_i, will depend upon the substrate temperature
and the rate of impingement.

Thus the resultant orientation depends upon the number of stable
clusters in a given state.

The conclusion of the various nucleation approaches seems to be that,
although useful in defining the initial stages of formation of nuclei and
for determining the various energy terms, they do not adequately predict
the phenomenon of epitaxy. Epitaxial nucleation as such is impossible
to examine experimentally since at the highest resolution of observation,
clusters . . . (contd. overleaf)

already comprise ~10 atoms, i.e. growth has occurred. Growth concepts are
therefore equally important, e.g. recrystallisation, coalescence, rates of
growth etc.

A further basic assumption of the above theories is that atoms are
thermally accommodated by the substrate or they are lost completely. According
to Cabrera's condition (1959) an atom is thermally accommodated if its arrival
energy is $<25E_a$. E_a is typically $\sim 0.4eV$ so that thermal accommodation occurs
if the arrival energy of the atom is $<10eV$. However, in sputtering, as will
be shown in the next chapter, the arriving atoms may have energies well in
excess of this and so do not satisfy the above condition. It is a criticism
of the atomistic model that no account is taken of the arrival energy. While
this may be satisfactory for films grown by evaporation it will certainly not
be so for sputtered films. It is possible, therefore, for a sputtered atom
to retain a fair amount of its energy and virtually "bounce" about the surface.
By so doing, it may move large distances and contribute large amounts of
energy to any island with which it comes into contact. Thus epitaxy may be
improved by virtue of this energy. The possible effect of large amounts of
energy transfer is discussed in Chapter 6.

Thus, while nucleation theory provides useful guide-lines in interpret-
ation of results obtained under conditions of relatively low super-saturation
and complete thermal accommodation, its overall predictions must be treated
with caution.

2.5.3. Active-Site Theory

This theory bridges the gap between nucleation concepts and growth con-
cepts. The following is based on the theory proposed by Rhodin et al (1968),

It has been shown by Stirland (1967) and others that electron irradiation
enhances epitaxy at lower substrate temperatures. It has also been found that
considerable orientation changes occur during the growth stages (Pashley 1965),

Matthews 1965, Layton and Campbell 1966.) The understanding of surface features in the substrate is therefore of extreme importance.

The role of point defects in the substrate surface has been largely ignored because of the difficulties in preparing well defined defect surfaces. The effect of electron irradiation is found to favour growth of (100) orientation of Au and Ag on cleaved NaCl, though no specific interpretation is given. Palmberg et al (1967) found that epitaxy of Au and Ag depended critically on exposure of the substrate surface to an electron beam prior to deposition. They concluded that the incident electrons formed nucleation sites leading to epitaxial growth which were thermally stable only below $80^{\circ}C$. It was observed that these sites could be stabilised by deposition of a monolayer of metal. Thick epitaxial layers could be subsequently grown at substrates from $70^{\circ}C$ to $300^{\circ}C$.

Quantitative measurements of the ions and atoms emitted from NaCl and KCl surfaces as a result of electron irradiation at $300^{\circ}C$ have been made by Palmberg and Rhodin (1968). It was concluded that K and Cl were removed from KCl stoichiometrically above $100^{\circ}C$. Below $100^{\circ}C$, bulk defects are essentially immobile and vacuum desorption occurs only if the initial interaction is localised near the surface. Occurrence of Cl depletion through ejection of negative Cl ions led to the suggestion that production of Cl vacancies at the surface is the predominant effect below $\sim 50^{\circ}C$. Single ion vacancies appear to anneal out at about $50^{\circ}C$.

Rhodin observed that epitaxial growth of Ag on KCl was not obtained unless the vacuum cleaved surface was irradiated prior to deposition. The conditions are summarised in Fig. 2.5. The 45° line corresponds to equivalent nucleation and growth temperatures. The plot indicates that in Rhodin's experiments, except for a very narrow range, two stage deposition is required.
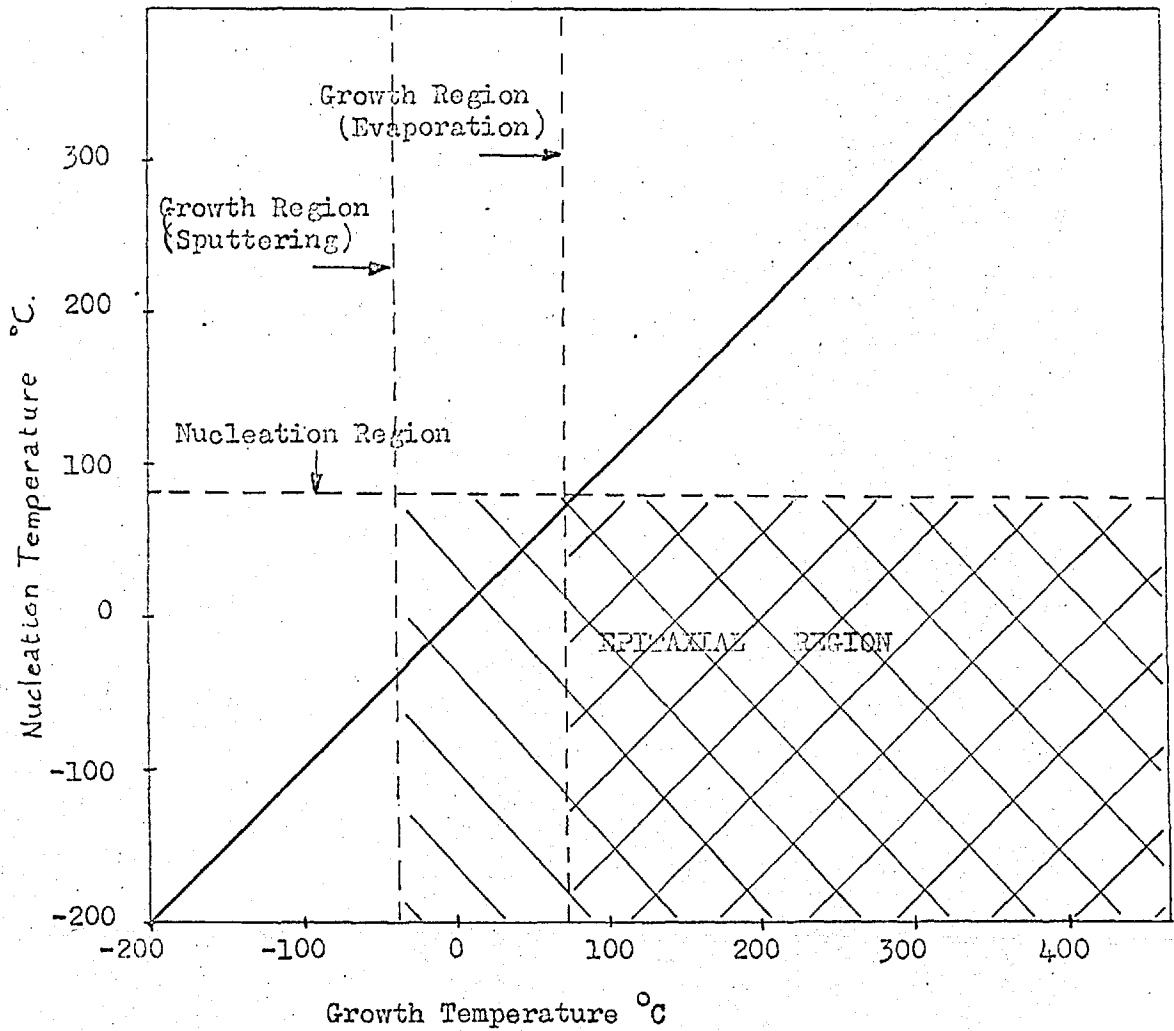
FIGURE 2.5

Range of temperatures corresponding to nucleation and to growth
resulting in epitaxial silver film formation on irradiated
KCl (Rhodin et al 1968) with condition for epitaxy by sputtering
superimposed.

The 45° line corresponds to equivalent nucleation and growth
temperatures.

Rhodins results indicate therefore that surface vacancies are effective in promoting the (100) orientation for nuclei formed at substrate temperatures up to the thermal annealing limit of 80°C. Simultaneous irradiation and deposition suggests that surface vacancies are effective in nucleating epitaxial films at much higher substrate temperatures.

Application of these results to sputtering, must take into account the existence of the discharge and also the existence of high energy sputtered particles, as discussed in the next chapter. It is possible that both phenomena, charged particles and energetic particles, could produce surface vacancies or defects which act as preferred sites for epitaxial growth, particularly in the case of ionic substrates. In the experiments described later, nucleation and growth were carried out at the same substrate temperature. This theory is applicable to the single temperature deposition when epitaxy is observed for low growth temperatures. On figure 2.5 this would result in the dotted line and shaded epitaxial area. It is shown in Chapter 5 that epitaxy clearly does occur at low substrate temperatures. However, as Rhodin points out, the experimental parameters such as surface contamination and impurity atoms may also influence epitaxy through their effect on surface structure.

2.6. POST-NUCLEATION GROWTH CONCEPTS

Matthews and Allinson (1963) have observed an orientation dependence on thickness for gold evaporated onto rocksalt. They discuss this in terms of a rotation of the smaller crystallites and Bassett (1960) has actually observed that isolated silver nuclei will change their orientation on the substrate. Matthews and Allinson show that large crystallites are better aligned than small ones and they contend that when two crystallites coalesce, the smaller of the two will rotate to parallel or twin relationship to the larger. There will be an increase in alignment in the film, though they did not discuss why the initial nuclei should appear to be oriented. Matthews

(1965) has shown that it is possible for certain orientations to grow preferentially by virtue of their lower surface free energies. The actual crystal planes that are preferred and their rates of growth will depend on the energetics of the system and the presence of impurities may play a considerable part. Indeed, Matthews finds that when there are no contaminants present the (100) orientation predominates. He concludes that since the observed island density is an order of magnitude lower for clean substrates, the (111) nucleus has time to grow larger than the (100) nucleus so that on coalescence the (111) type orientation overwhelms the (100).

Another model of re-orientation rather than on relative growth rates, is based on the van der Merwe's misfit concept (1966) for the case of an f.c.c. material growing on a close-packed substrate plane (e.g. (111) plane for f.c.c.) he calculates that the energy per atom as a function of lattice misfit shows a maximum. For nearest neighbour interaction this maximum is at 10%. Above a lattice misfit of 14% the coherent state is unstable.

From this model, van der Merwe proposed that for a lattice misfit of >9% the energy per atom will be reduced by the film growing in a polycrystalline manner. For misfits <9% the deposit lattice would prefer to exist in a strained but oriented state. In an attempt to reduce the total strain the film will contain dislocations. Matthews (1961) work on PbS films or PbSe for which the misfit is <9% shows a dislocation density in agreement with this proposal.

The suggested application to an observed increase in orientation with thickness is in terms of an increase in the lattice spacing of the initial deposit consisting of only a few atoms. If, in the case of growth on a (111) surface, the lattice spacing in the crystallite is >9% the crystallite will tend to be randomly oriented. As the crystallite size increases the lattice parameter becomes the same as the bulk value and the crystallite will prefer

to be strained but oriented. To apply the concept to growth of on (100) faces, the energy per atom versus misfit curve must be determined in order to ascertain whether the change in lattice spacing would be sufficient to change the low energy state from a random to an oriented structure.

The concepts of growth have been thoroughly reviewed by Matthews (1967) who has considered the orientation of nuclei and the changes in orientation with subsequent growth. An important stage in the growth sequence is that of coalescence, mentioned briefly above. When islands coalesce a liquid-like behaviour has been observed (Bassett 1960), particularly if one or both of the coalescing nuclei is very small. This results from the rapid diffusion of atoms over the surfaces of nuclei. The stage at which coalescence occurs depends upon contact angle, deposition rate, substrate temperature, contamination and the substrate surface nature.

A feature of coalescence is the formation of lattice defects, e.g. stacking faults, twins. This may be due to a variety of mechanisms but one of the major factors is the misfit between the lattice of substrate and deposit. As a result the lattice of one nucleus may be separated from the lattice of another by a non-lattice vector so that on coalescence the displacement may be taken up by a stacking fault. These have been directly observed by Jacobs et al (1966) studying the moiré fringe pattern produced by deposition of gold on molybdenite. Dislocations may also result at coalescence due to the fact that lattices of adjacent nuclei are often rotated relative to one another. Twins are commonly found in deposited films, particularly f.c.c. metals on NaCl. The twinning planes are the four (111) planes inclined to the (001) deposit plane. Several mechanisms have been proposed to explain their formation. In a way similar to that for the formation of stacking faults, it has been suggested that twins are formed to accommodate the displacement between coalescing nuclei. Hall and Thompson (1961) suggest

that for hexagonal substrates there is equal probability of the formation
of nuclei having a twin relationship (double positioning) while on a cubic
substrate lattice the origin of twins is due to imperfect condensation on the
(111) facets of the growing nuclei. Another mechanism suggested by Matthews
and Allinson (1963) is that of rotation mentioned above. If coalescing nuclei
are nearly in twin relationship before coalescence then the formation of a
twin is highly probable.

Coalescence need not necessarily lead to a faulted island. Depending
upon the relative sizes of the coalescing nuclei, the subsequent alignment
of the deposit may be more or less perfect. Pashley and Stowell (1963) have
observed that the coalescence of doubly positioned gold on molybdenite may be
followed by the migration of the twin boundary through the smaller of the
two nuclei, the driving force being the decrease in boundary area and hence
energy.

CHAPTER III

SPUTTERING: THEORY & APPLICATIONS

3.1 INTRODUCTION

In the introductory chapter some of the historical back-ground to the evaluation of sputtering as a technique for film deposition was discussed. It is now a widely used process and there is much research into the further, perhaps more efficient, techniques to which it may be applied. In order to comprehend fully the process, however, it is necessary to investigate the mechanisms by which material is released from the bombarded target. It is the purpose of this chapter therefore to review the various theories in the light of experimental observation and to discuss their relevance to thin film deposition. A dis-cussion of the various sputtering methods which may be employed precedes the theoretical section and includes a semi-theoretical analysis of the attenuation-by-collision of sputtered atoms between source and substrate.

3.2 SPUTTERING METHODS

Since sputtering is the ejection of atoms from a material by ion bombardment, the most important single factor to consider is the production of the ions. The method used is to some extent dependent upon the pressure which can be tolerated in the experiment. The simplest method is that of the glow discharge (diode sputtering) in which ions are generated in the space between an anode and a cathode and these bombard the cathode which is made of the material to be sputtered. The second method is to produce the ions independently of the region in which the sputtering is to take place and then to direct them onto the target (low pressure and triode sputtering).

3.2.1 Glow Discharge

The glow discharge is only part of the processes which can occur when a potential is applied between two electrodes in a reduced atmosphere. The type of discharge which occurs depends upon a) the pressure, b) applied voltage, and c) electrode geometry. A schematic of the voltage-current discharge is seen in Fig. 3.1 and from this it is seen that the discharge of interest is that in the milliamp range. The discharge is maintained by electrons produced at the cathode as a result of positive ion bombardment. Fig. 3.2 shows the potential as a function of the position in the discharge, at pressures $\sim 100\mu$. The existence of a glow depends upon the energy of the electrons. Electrons leaving the cathode accumulate and neutralize positive ions, whose excitation energy decay gives rise to the cathode glow.
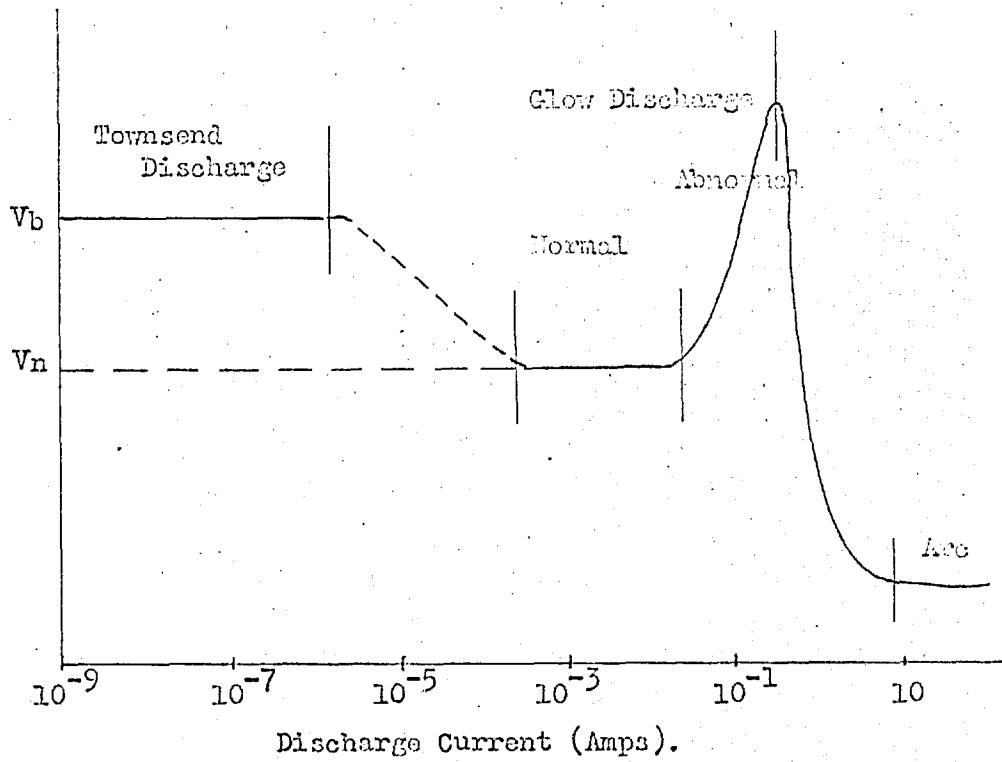
Vb=Breakdown Voltage
Vn=Normal cathode fall

FIGURE 3.1

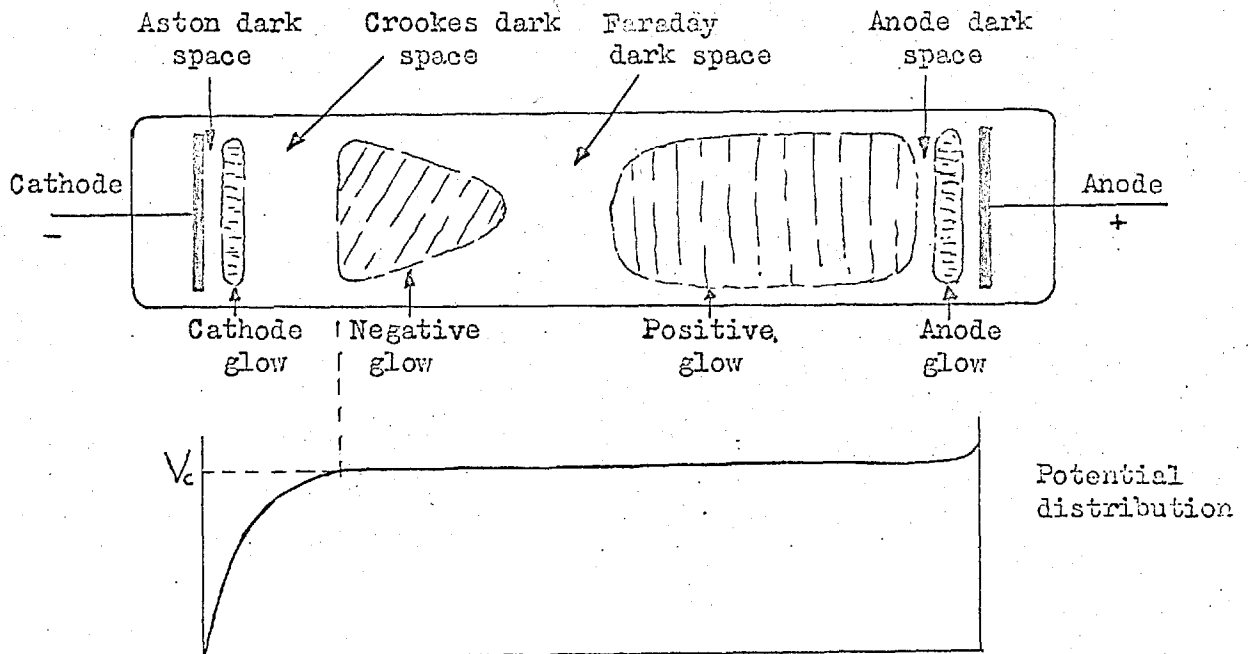Relationship between current and voltage in a reduced pressure
discharge tube.

FIGURE 3.2

Distribution of glow and potential as a function of
position in a glow discharge. Gas pressure ~100μ.

Electrons passing through the Crookes dark space gain
energy in doing so and may excite or ionise neutral atoms.
The subsequent decay of these atoms gives rise to the neg-
ative glow, the sharp boundary to which is due to the back
diffusion of low energy electrons from the essentially field
free negative glow region. The opposite (anode) end of the
negative glow is due to electrons giving up sufficient
energy only to excite the neutral atoms. In the Faraday
dark space, the electrons slowly regain energy which is sub-
sequently given up by ionisation in the positive column.
The positive column acts as an effective anode to the dis-
charge, it being a conducting path between the anode and the
negative glow region. As the pressure is reduced, the pos-
itive column shrinks and the Crookes dark space expands. The
discharge is extinguished when the anode enters the dark
space. In most sputtering experiments carried out at $\sim 10\mu$
the voltage is such that the anode is somewhere in the neg-
ative glow region and the potential between the electrodes
is almost equal to the cathode fall.

From Fig. 3.1 it is noted that there are two regions in the
glow discharge part of the spectrum. In the normal cathode
fall region, the cathode fall is independent of current and
pressure. Only a portion of the cathode is covered by the
discharge and the current density remains constant. In the
abnormal fall region, the whole of the cathode is covered, so
that the current density increases with current. As will be
seen later, the rate of ejection of material from the cathode
is proportional to the current density so that variation of
rate is effected by altering the current density. Hence,
the abnormal glow discharge is the method used almost univers-
ally for thin film deposition.

The width of the cathode, or Crookes, dark space is a function of the gas pressure and the applied potential. It also depends upon the secondary electron emission coefficient for the ion-target combination used.

For argon the product of pressure and dark space thickness is ~ 0.3 torr.cm. If the electrodes are placed such that the pressure x separation product is less than the above figure, the applied voltage has to be increased to restore the glow. Empirically it is found that the following relations hold between pressure, voltage and current changes :

$$\left(\frac{di}{dV}\right)_p = +^{ve} \qquad \left(\frac{di}{dp}\right)_V = +^{ve} \qquad \left(\frac{dV}{dp}\right)_i = -^{ve}$$

i.e. $i = f(p.V)$

Of these only pressure and voltage are independently variable, and the current is directly proportional to any change in these parameters.

The glow discharge system is very useful in that it can be very easily set up. From the quantitative point of view, however, it has several inherent disadvantages. Because of the relatively high gas pressure the mean free path of ions, λ_i, is small compared to the length of the cathode fall region. Hence any collisions occuring within this region will result in a spread in the energy and angle of incidence of the bombarding ions. For instance, it has been shown (von Hippel, 1926) that for a cathode fall of 1,000V at pressures ~ 100μ, the average ion energy is only 250eV. There is also the possibility of the formation of multiply charged ions.

A second disadvantage is due to the short mean free path of the sputtered atoms, λ_s. Since $\lambda_s < d$, the source-substrate separation, collisions inevitably occur and, at higher pressures the problem of transport becomes one of diffusion. Von Hippel (1926b) has calculated that for a planar arrangement with the collector at the edge of the cathode fall, 90% of the sputtered material diffuses back to the cathode when the pressure is 100μ. However this assumes the atoms to have only thermal velocities on leaving the target, which is certainly not the case.

Although these drawbacks are not too prohibitive when dealing with the general production of thin films, they are certainly important when depositing epitaxial or controlled-property films. Also, if any quantitative data on the sputtering process is required, the discharge process should be as well defined as possible. The three most important characterising properties of the sputtering process are (1) Yield, (2) Angular distribution and (3) Energy distribution of the sputtered atoms. None of these can be measured unless a) the angle, energy and mass of the incident ions is fairly well defined and b) there is no interference with the sputtered material between source and collector. At 10^{-3} torr, the mean free path of thermal gas atoms is $\sim$ 5 cm. - comparable to the apparatus dimensions. However, the lowest pressure at which the discharge can be maintained and still have useful ion current densities is $\sim 5\mu$, at which pressure there are still sufficient collisions to make analysis of the process unreliable. The system is also limited to higher ion
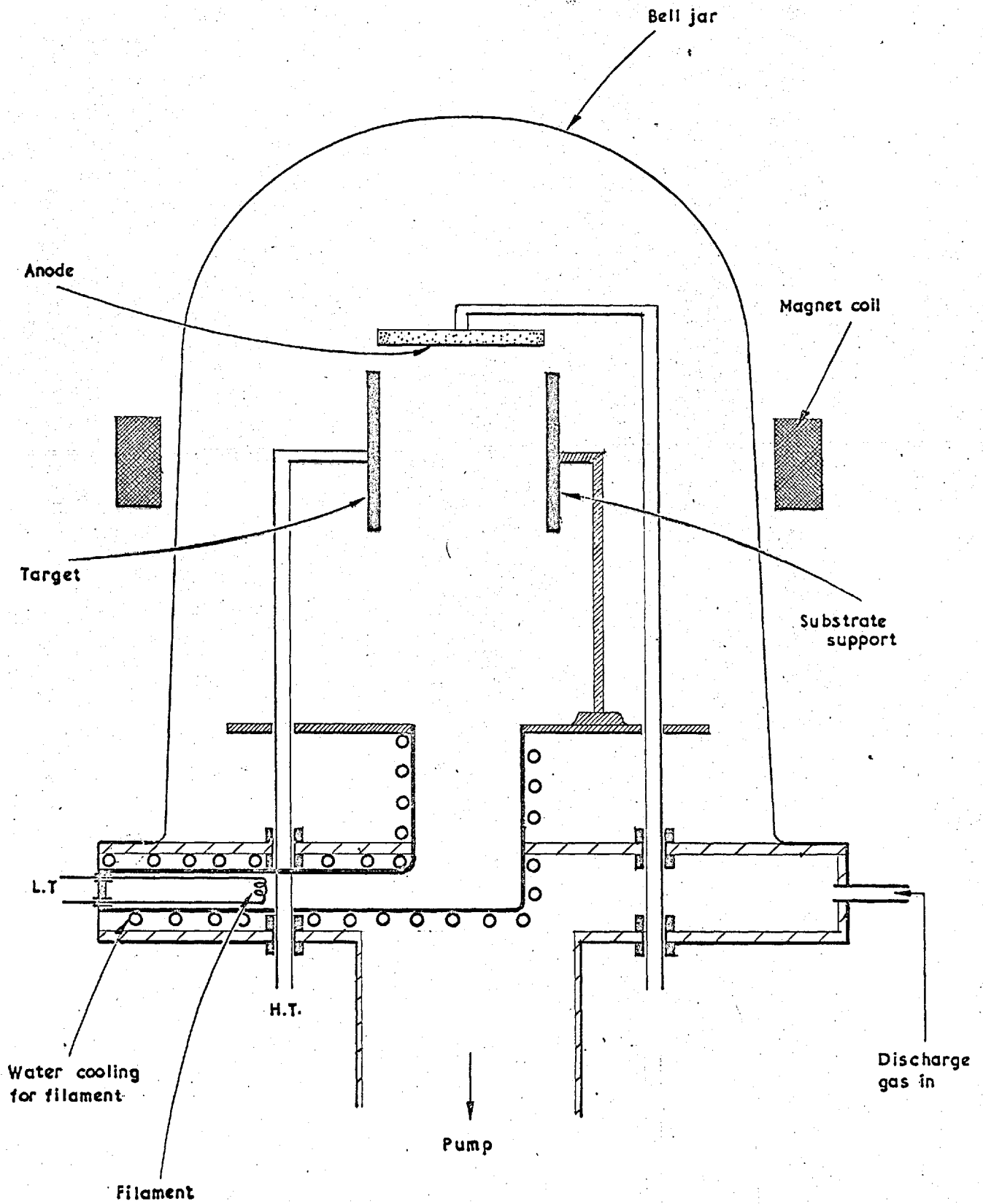
energies, since the voltage required to maintain the dis-
charge is $\sim$300V. In order, therefore, to extend invest-
igation to lower energies and pressures, an assisted dis-
charge is required.

3.2.2 Assisted Low Pressure Discharge

Because of the limitations given above, it is necessary to
provide a source of ionising radiation. This may be R.F.
radiation, but the more common technique is to employ a
thermal source of electrons. Then, although the probab-
ility of ionisation per electron is low, the number of events
is still usefully high. The source acts as a cathode and a
suitably placed collector plate as the anode. A schematic
of a typical assembly is shown in Fig. 3.3. The purpose of
the magnetic field, arranged parallel to the electron beam,
is to constrain the electrons so that recombination at the
walls of the apparatus is reduced. The target is introduced
as a Langmuir-type probe into the system and extracts ions
from the plasma. This mode of sputtering is often termed
triode sputtering. The pressure at which the system can be
operated depends upon the electron current and the magnetic
field. For an electron current of $\sim$3A, an ion current of
$\sim$1mA/cm^2 can be extracted from a discharge at 10^{-3} torr with
a magnetic field of $\sim$20oe. If the field is increased to 40oe
the system can be used at 10^{-4} torr or lower.

Wehner (1962) used a slightly different method of producing
the ions. He used a modified mercury-pool rectifier in
which electrons generated by a low pressure mercury arc drawn
through a grid into the sputtering chamber, held at a lower

FIG 3.3
SCHEMATIC DIAGRAM OF LOW PRESSURE SPUTTERING APPARATUS
BASED ON TRIODE SYSTEM OF SPUTTERING.
ANODE – FILAMENT = 50V TARGET:= UP TO −1600V.

Bell jar

Anode

Magnet coil

Target

Substrate
support

L.T

H.T.

Water cooling
for filament

Filament

Pump

Discharge
gas in

pressure. The system was very useful but had the dis-
advantage that mercury vapour was always present in the
sputtering chamber.

In the case of an R.F. induced plasma, ionisation can be
produced at low pressures without the need for electrodes
within the discharge chamber. A simple set-up is shown in
Fig. 3.4 in which the ions are produced in the upper portion
and diffuse into the lower portion where the target and sub-
strate are situated. Gawehn (1962) has obtained deposition
rates of $\sim 1\text{Å}/\text{sec}$. with a target voltage of -500V and power
input to R.F. field of 200W. The operating frequency was
~ 10 Mc/s and pressure 2.10^{-3} torr.

Bearing in mind the requirements listed in the previous sect-
ion, the advantages of low pressure sputtering are several.
Provided the size of the target is large compared to the width
of the Langmuir sheath surrounding it the ions impinge on the
target along the normal. The width of the Langmuir sheath is
given by the "three halves" power law; (Langmuir and Tonks
1929).

$$d^2 = \frac{4Eo}{9j} \left(\frac{2q}{m}\right)^{\frac{1}{2}} V^{3/2}$$

where Eo = permittivity of free space.

j = current density

V = probe potential (relative to plasma)

$\frac{q}{m}$ = charge-mass ratio of ion.

For argon gas, singly ionised.

$$d^2 = 8.75 \times 10^{-9} \frac{V^{3/2}}{j} \text{ cm.}$$

The variation of d with j at various voltages is shown in
Fig. 3.5. At 1,500V and 0.1mA/cm^2 which are typical values
employed in the present experiments the sheath thickness is
2.4 cm which is much less than the mean free path at 10^{-3} torr

FIGURE 3.4

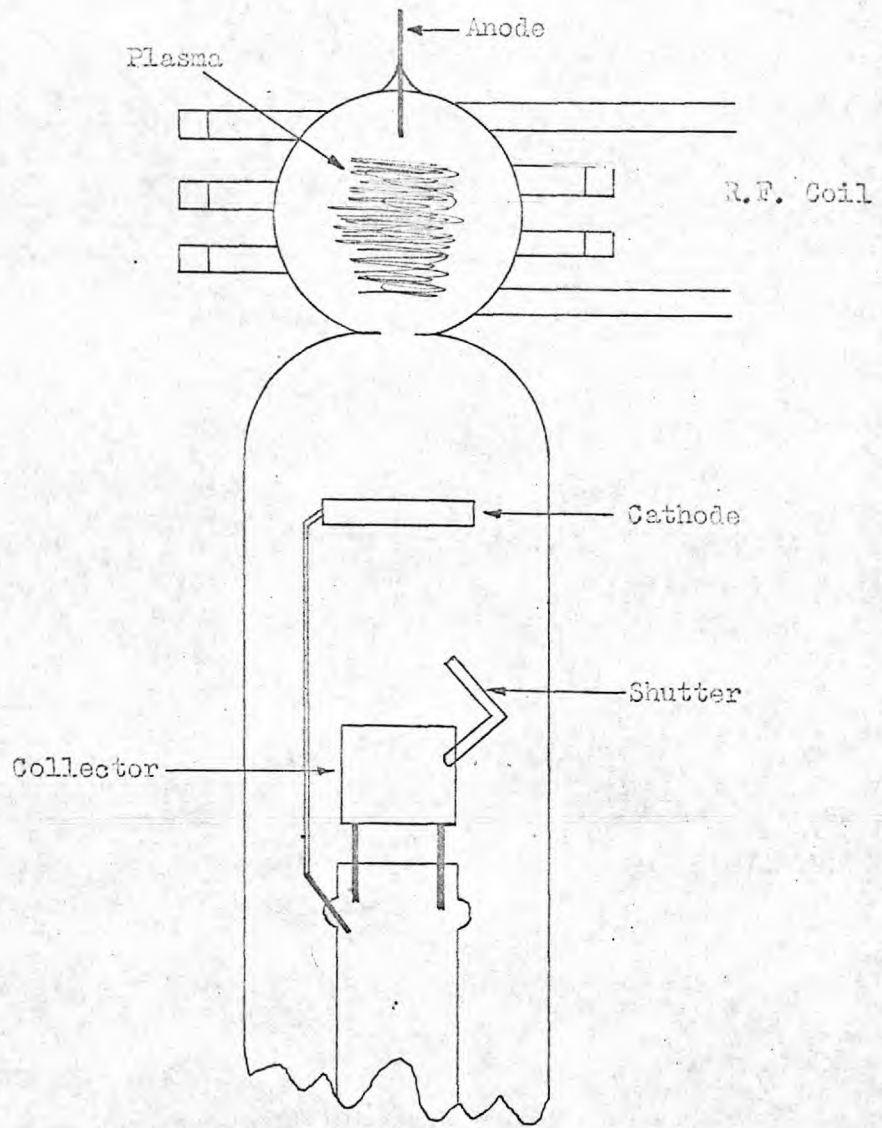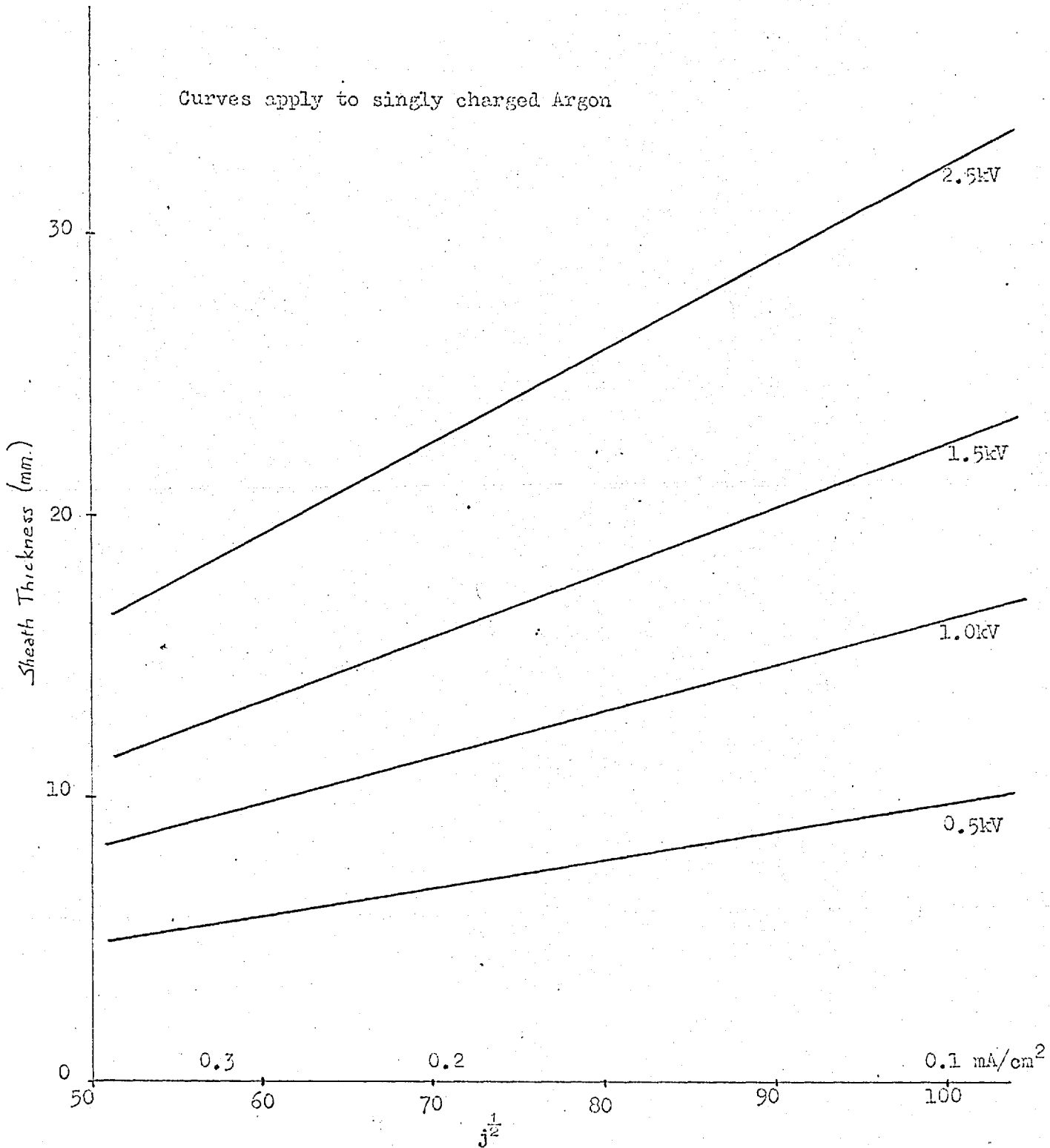R.F. Sputtering Apparatus (Gawehn,1963)

FIGURE 3.5

Sheath thickness as a function of ion current density for various target potentials.

Curves apply to singly charged Argon

Sheath Thickness (mm.)

$j^{\frac{1}{2}}$

(~5 cm. for thermal gas atoms, greater for fast moving
ions). Thus any ions finding themselves on the edge of the
sheath will be rapidly accelerated across the gap with very
little chance of collision. Hence angle of incidence effects
are reduced. Also, the incident ions will be monoenergetic
by the same reasoning, though their precise energy will depend
upon the potential difference between the anode and the edge
of the Langmuir sheath. Since the discharge can be maintained
at lower voltages than is necessary for glow discharges, the
probability of multiple ionisation is much reduced.

The advantage from the thin film growth point of view is that
there are very few collisions between sputtered atoms and
gas particles so that the energy of the sputtered atoms is
largely conserved; also deposition is no longer diffusion
rate dependent. One would therefore expect higher deposition
rates. A further feature is that the probability of gas atom
inclusion in the growing film is much reduced by operating
at lower pressures. Contamination can be reduced in glow
discharge sputtering by special techniques as will be des-
cribed below.

A further low pressure technique now gaining wider use
experimentally is to employ an external ion source and to
direct the ions at the target. Early attempts to use ion
sources were dogged by space charge complications, but with
the development of high density sources these difficulties
have been overcome. Ion current densities in excess of
$1mA/cm^2$ have been achieved.

3.2.3.1 Bias Sputtering (Maissel & Schaible, 1965)

In this technique, the growing film is biassed neg-
atively with respect to the anode. The film is con-
sequently subjected to continuous ion bombardment
during its growth. The ion energy is sufficient to
sputter contaminants from the surface and hence clean
the surface (the growing film is also sputtered to
some extent, so that the overall deposition rate is
less than that without bias). This technique is
especially useful when depositing in reactive gases
and Maissel and Schaible have shown the effects on
glow discharge sputtered tantalum films. The
resistivity of such films was found to be much
reduced when a bias of <-100V was applied, even when
oxygen was deliberately introduced as a contaminant.

Assymetric and a.c. sputtering is similar to bias
sputtering. In this case the role of anode and
cathode is periodically reversed so that in one half
cycle the target is bombarded while in the other
half-cycle the film is bombarded. A net transfer
of material from cathode to substrate is ensured by
having a larger current flowing to the target during
its negative half-cycle.

3.2.3.2 Getter Sputtering (Theurer & Hauser, 1965)

This technique employs a stainless steel secondary
enclosure within the main vacuum system. The elect-
rode system within the secondary enclosure is essent-
ially a diode arrangement. The discharge gas is
admitted to the main chamber but only finds its way

into the inner chamber by devious means through joints and other small inlets. The gas thus leaks into the chamber and because of the d.c. field inside a gettering action is set up and impurity atoms are gettered onto the walls of the chamber. In this way, Theurer and Hauser have been able to reduce the partial pressure of oxygen at the substrate to as low as 10^{-10} torr even with a nominal vacuum of 10^{-6} torr. Thus the deposited films have a very low impurity content without having gone to the trouble of obtaining a very low residual gas pressure. However, not all gases and target materials make efficient getter combinations, and also the technique is restricted to diode sputtering. It has therefore not been used to any great advantage.

In conclusion the type of system one uses depends very largely upon the results one wishes to obtain. For fundamental studies of the sputtering process the independent ion source is the most appropriate since it affords close control of the various parameters. For thin film growth, however, the method used depends upon the quality and type of film required.

3.3 SPUTTERING CHARACTERISTICS

Before discussing the theories of sputtering, it is relevant to consider the experimental results of the study of the phenomenon. Much of the reliable early studies of the sputtering process was carried out by Wehner (see review by Wehner, 1955)

and his co-workers using the mercury-pool cathode arrangement described above. The parameters which lend themselves to investigation are the following :

a)   Angle of incidence of the bombarding ions.

b)   Energy of the bombarding ions.

c)   Mass of the bombarding ions.

d)   Ion current density.

e)   Gas pressure.

f)   Target material and surface nature.

g)   Target Temperature

h)   Angular distribution of sputtered atoms.

i)   Velocity distribution of sputtered atoms.

j)   Charge carried by sputtered atoms.

Characterisation of a given sputtering experiment is most conveniently in terms of the sputtering yield. This is defined as the number of atoms ejected for each ion incident on the target. The variation of the yield as a function of the parameters a-g above gives information on the sputtering process. The parameters (h) and (i) are also dependent upon (a) - (g) and also characterise the process. They are also influential on the growth of thin films result - ing from sputtering.

3.3.1   Angle of Incidence

The effect of angle of incidence was first observed by Fetz (1942) who found that for a given material the sputtering yield increased with increased incidence angle away from the normal as shown in Fig. 3.6. Wehner (1960) has studied several metals bombarded by Hg^+ and A^+ ions. He has found that the effect is greater for Hg^+ than for A^+, i.e. higher incident ion mass. Generally, also the effect for a given

FIGURE 3.6

Variation of sputtering yield with angle of incidence for
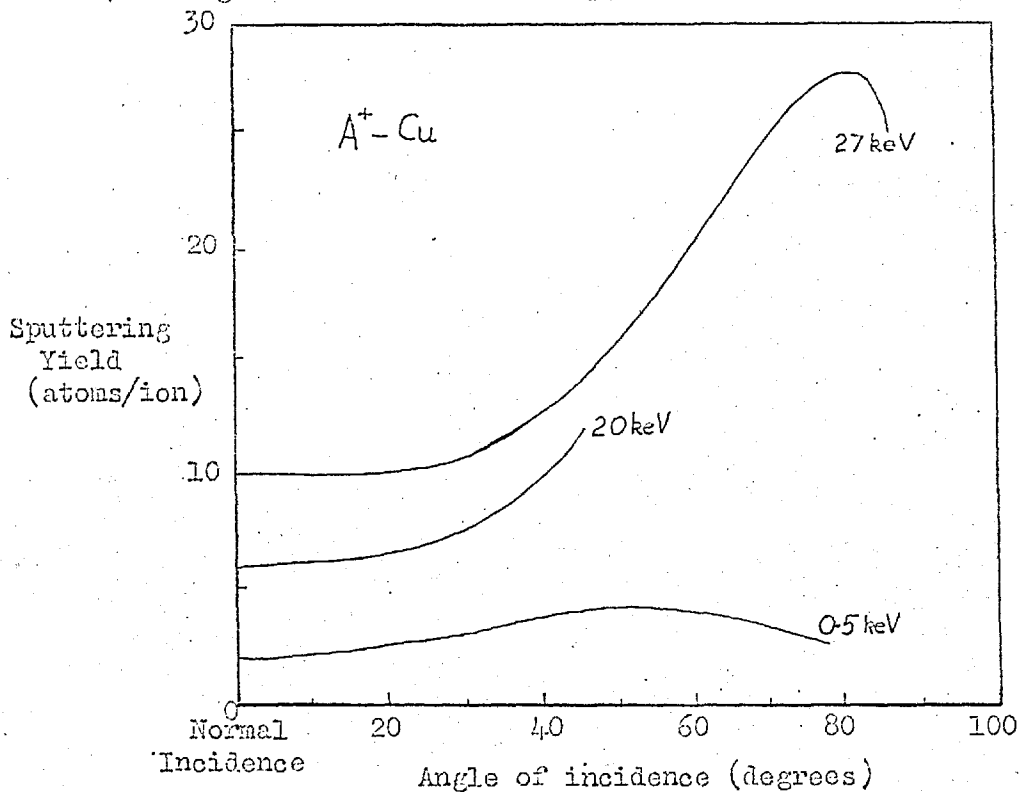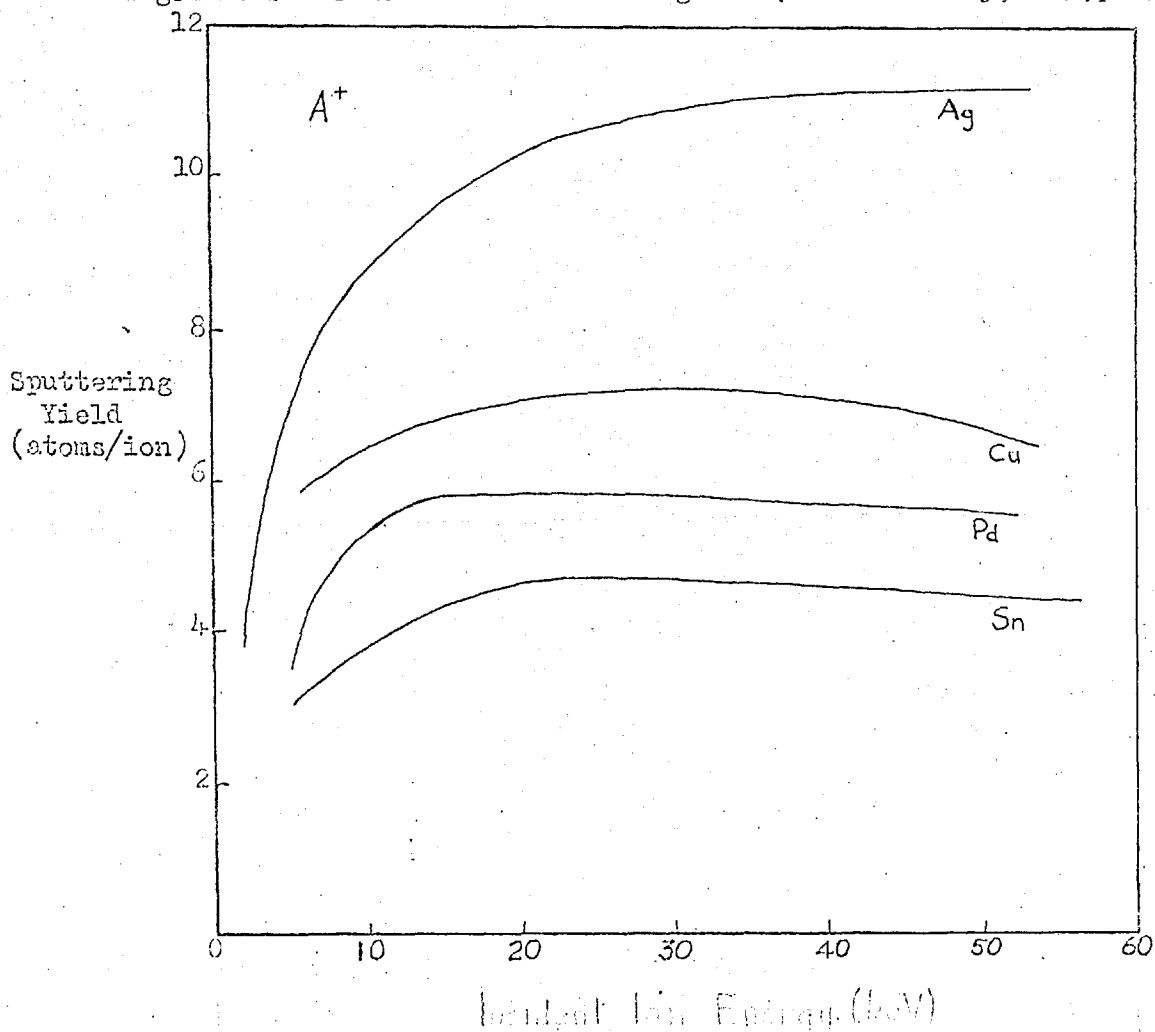27keV argon ions incident on copper. (From Kaminsky,1965,p.160)

FIGURE 3.7

Variation of sputtering yield with incident ion energy for
argon ions incident on various targets. (From Kaminsky,1965,p.158)

lattice type becomes larger with decreasing atomic weight, though at higher energies ($\sim$45keV) this is found not to be true. At low energy it is found that those materials with the highest yield show the least angular effect and vice-versa.

The effect of angle of incidence is observed in both poly-crystalline and single crystal targets, though in the latter it is modified by the lattice arrangement. Sputtering theory does not satisfactorily account for the effect, but Martynenko (1966) has attempted to formulate a theory for the case of single crystals based upon multiple collisions of ions with atoms in the crystal.

3.3.2 Incident Ion Energy

The effect of ion energy has been extensively studied and may be subdivided into two ranges 0-1 keV and 1-60 keV.

The object of the low energy investigations has been to establish the threshold energy, below which there is no ejection of atoms from the target. Workers using the glow discharge found that $M = a (V - Vo)$ where M = mass of material deposited on a collector, V = applied potential and a and Vo are constants, Vo being the threshold voltage. Careful measurement of the threshold using microbalance or radio-tracer techniques has shown the value to be similar for many different ion-atom combinations. Typically it lies in the range 10-40eV. However, the rate of increase of yield with increasing ion energy above the threshold shows marked differences. Koedam (1959) and Wehner & Medicus (1954) find that the yield (S) varies as E^2 at low energies ($<$100eV)

becoming linear at higher energies ($>100eV$). According to the model chosen to explain the process at low energies, various authors predict a yield dependence of $E^{\frac{1}{2}}$, E or E^2 each of which fits certain systems (Kaminsky 1965). It does not seem possible, therefore, to predict a general behaviour.

At higher ion energies, $>1keV$, the variation of yield with energy is more predictable. In general, the yield increases with increasing mass of ion and increasing energy, reaching a saturation value at very high energies. The saturation value is lower for lighter ions. The magnitude of the yield is found to increase as the d-shell fills within a given period of the periodic table, so that Cu, Ag and Au have the highest values. Curves showing the yield for various metals as a function of ion energy are given in Fig. 3.7.

When the incident ion or target atom is only weakly screened, i.e. low atomic number or very high ion energy, the ion-atom collisions are no longer hard sphere and it is not possible to predict readily the sputtering behaviour.

3.3.3   Ion Current Density and Gas Pressure

The dependence of the sputtering yield on ion current density has been found to be zero, (Almén & Bruce, 1961), provided the effects of secondary electron emission are taken into account and the target is very clean. This latter aspect of cleanliness can also account for the sometimes observed variation of yield with gas pressure. The effect is due to the contamination of the target surface by adsorbed layers of gas atoms, which have to be removed before the true yield may be attained.

3.3.4 Target Temperature

The effect that temperature has on the yield has been studied in detail by Nelson (1965) for several ion/atom combinations. He has shown that there is a steady increase in yield with temperature above a critical temperature ($\sim 800^\circ$K for Ag and Au). Below this temperature the yield does not vary.

3.3.5 Target Structure

The crystallographic orientation of the target plays a considerable part in sputtering. It has been found without exception that a single crystal target ejects atoms along certain preferred crystallographic directions. These are the close packed directions in the crystal. For a polycrystalline target, which is a collection of small randomly orientated single crystallites, the affect is smeared out to give a random ejection with uniform yield in all directions (neglecting angle of incidence effects). This is discussed at greater length below.

3.3.6 Charge Carried by Sputtered Atoms

There has been little quantitative analysis of the sputtered particles with regard to species and charge carried. Honig (1958) has attempted such a study using a mass spectrometer and has found that no less than 65 different species were ejected from a silver target bombarded by xenon at 300eV, many of which carried positive charge. However, he found that only approximately 1% of all sputtered particles carried a charge. The energy of the ionised particles is found to be of the same order as that of the neutral atoms, though Kistemaker and Snoek (1962) detected particles with much higher energy ($\sim$several keV) when ion bombarding at 10-15keV.

3.3.7 Angular Distribution of Sputtered Atoms

This topic has received much attention but the total experimental evidence for polycrystalline targets is somewhat conflicting. For thermal evaporation from a Knudsen type source a cosine distribution of atoms would result and experiments on sputtering have been concentrated on the proof or otherwise of such a distribution. Early results of Seeliger and Sommermeyer (1935) indicated a cosine distribution, independent of angle of incidence of the ions. However, Wehner et al (1960) subsequently showed this not to be true and observed an under-cosine distribution (i.e. greater proportion of particles ejected parallel to substrate) for low energy bombardment. Experiments at higher ion energies showed a transition from under-cosine to over-cosine distribution.

For single crystal targets, however, the situation is far different. As mentioned previously, preferential sputtering is found to occur along the close packed directions, <110> and <100> in fcc materials. If a collector is placed so as to pick up the sputtered atoms then a characteristic ejection pattern for the target is obtained. The pattern is found not to vary very much with angle of incidence of the ions, but is dependent on the index of the bombarded surface. A schematic of the ejection pattern from a (100) and a (111) plane in an fcc crystal is shown in Fig. 3.8. This phenomenon has been extensively studied (for example by Koedam (1959), Anderson and Wehner (1960), Nelson and Thompson (1961) for a variety of conditions of ion energy, target plane, ion and target species and in all cases a characteristic distribution results.

The interpretation of the various ejection patterns and their changes with ion energy has been largely based upon channeling and focusing mechanisms within the crystal. This is

FIGURE 3.8

Schematic ejection patterns for face-centred cubic metals.

[T01]   [011]   [110]   [101]

[001]

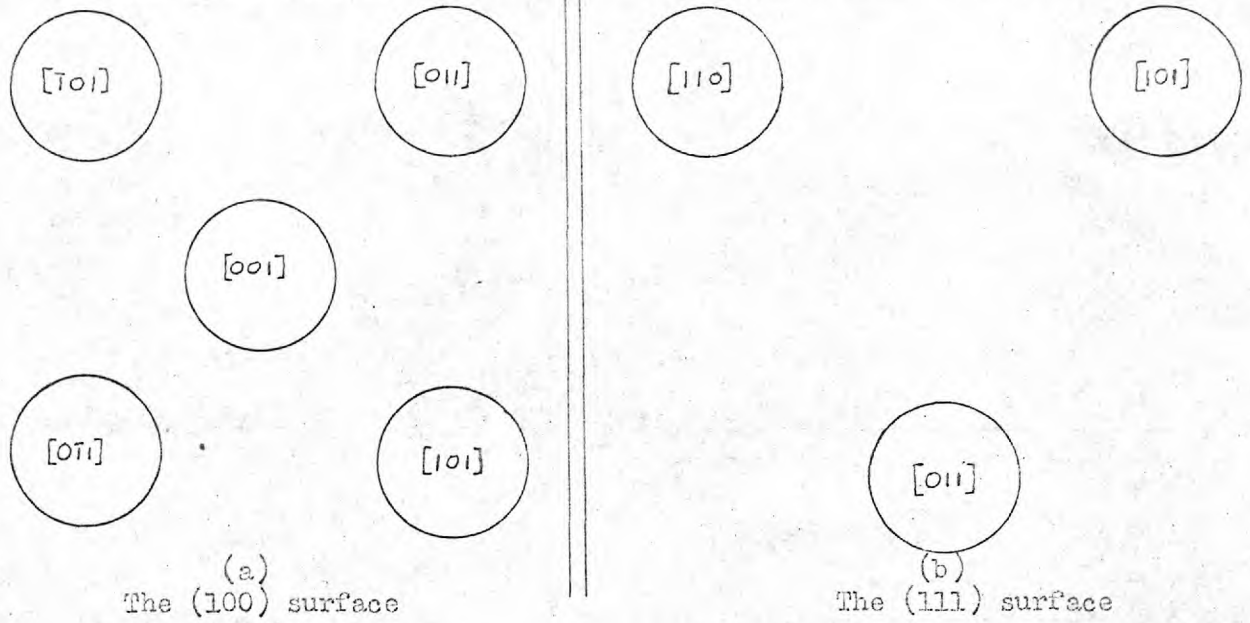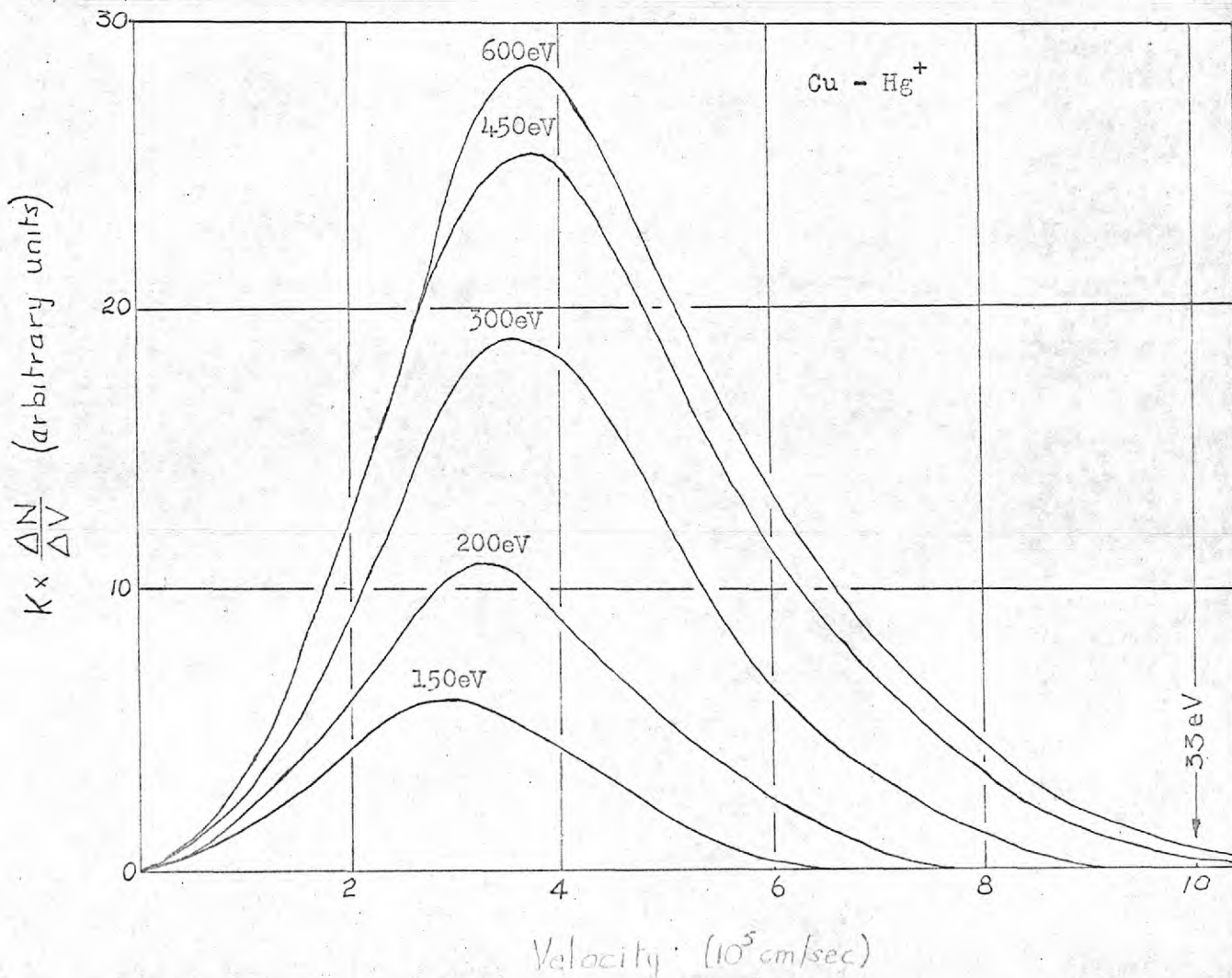[0T1]   [101]   [011]

(a)
The (100) surface

(b)
The (111) surface

FIGURE 3.9

Velocity distribution of sputtered atoms ejected at $0°$
from a polycrystalline copper target. (Stuart and
Wehner,1962)

Cu – Hg$^+$

600eV
450eV
300eV
200eV
150eV

33eV

$K \times \dfrac{\Delta N}{\Delta V}$ (arbitrary units)

Velocity (10^5 cm/sec)

mentioned in greater detail below.

3.3.8 Energy Distribution of Sputtered Atoms

The mean energy of sputtered atoms has been investigated by
various authors using different techniques. Wehner (1960)
employed a torsion balance and determined the forces exerted
on a collector. He found the mean energy $\bar{E}$ to be $\sim 3.6eV$ for
$300eV$ Hg^+ ions bombarding a copper target. Kopitzki (1961)
has made a study of a large number of metals bombarded by
$35keV$ Xe^+ ions. He found a periodicity in $\bar{E}$ similar to that
in the periodic table of the elements. Almén and Bruce
(1961) have studied bombardment of polycrystalline silver
with A^+ ions and they have shown that the mean velocity in
the direction normal to the target is 7.1×10^5 cm/sec.
(equivalent to $\sim 6eV$).

The study of the distribution of energy has been carried out
in detail by Stuart (1962) at low energies ($< 1keV$) and by
Thompson (1967) at high energy ($\sim 43keV$). Both methods are
based upon time of flight measurements. The significant
point to emerge from all the measurements of energy of the
sputtered particles is that the peak energy of ejection can
be several orders of magnitude higher than the energy of
evaporated atoms. In fact for an incident ion energy of only
$600eV$, copper bombarded by Hg^+ ions can have ejection energies
in excess of $30eV$. A plot of the energy distribution for
such a system is shown in Fig. 3.9. Thompson (1967) has
observed ejection energies up to $1000eV$ for high bombardment
energy. Stuart (1962) found that the mean energy of ejection
increased with ion energy, though the most probable value did
not alter very much within the range of his investigation

(150 - 600eV). The dependence upon angle of incidence was only slight.

For the case of single crystal targets, both Stuart and Thompson found increased energy of ejection along certain crystallographic directions, though the greatest energy was not necessarily along the close-packed directions. For 43keV bombardment of gold, Thompson found maximum ejection $\bar{E}$ along the <100> (93.5eV) followed by the <121> and the <110>. He explains his results on the basis of a) random cascades, b) focussing, c) channelling and d) thermal evaporation.

Although a knowledge of the energy distribution of atoms leaving the target is of fundamental importance when considering the mechanisms of sputtering, the point of interest as far as thin film growth is concerned is the energy of the sputtered atoms on arrival at the substrate. The next section is devoted to such a discussion in terms of the arrival energy relative to a thermal beam.

3.4 ENERGY OF ARRIVAL CONSIDERATIONS

It has been shown in the previous section by reference to several authors that the energy of ejection of sputtered atoms is significantly higher than that of evaporated atoms. In an investigation of the differences between deposition by sputtering and evaporation it is of interest to know the relative energy of atoms on arrival at the substrate. Because of possible collisions between sputtered atoms and gas atoms or ions, the energy distribution of the sputtered atoms may be modified. Clearly this is a function of the gas pressure for a given geometry. For the results to be of

interest from an energy viewpoint, we require to know what proportion of the sputtered atoms arrive at the substrate with an energy significantly greater than that of thermally evaporated atoms. For atoms having energy comparable to thermally evaporated atoms, the deposition will be fundamentally the same as it is in evaporation (considering energy only). An energy distribution for silver evaporated from an open source at $1800°K$ we will assume is Maxwellian with a most probable velocity of $\sim 3 \times 10^4$ cm/sec. Experimental evidence for Maxwellian distributions from evaporation sources has been given for potassium and thallium by Miller and Kusch (1955). A very small number will have velocities above 1×10^5 cm/sec. ($> 0.01\%$). On this basis the following calculation has been directed at establishing the numbers of sputtered atoms that arrive at the substrate with velocities above 1×10^5 cm/sec. For silver, this is equivalent to an energy of $\sim 0.6eV$.

As mentioned in a previous section, sputtered atoms are ejected in all directions from a polycrystalline target and a near cosine spatial distribution exists. For ease of calculation however only those travelling normally away from the target have been considered and it assumed that all colliding target atoms continue in a forward direction following collision. Velocity distributions for ejection normally from a polycrystalline target have been given by Stuart (1962) for the case of Cu bombarded with Hg^+ at energies up to 600eV. Their curves are approximately Maxwellian (see Fig. 3.9) but with a high energy tail; the most probable velocity is 3.5×10^5 cm/sec. (Mean velocity $\sim 4 \times 10^5$ cm/sec.) In the absence of velocity data for silver bombarded with argon at 3keV (as employed in our diode sputtering experiments) this velocity distribution has been employed. Certainly there appears to be little

change in most probable velocity with bombarding energy up to 600eV (Stuart 1962) and it seems probable that it will not vary appreciably up to 3keV. The high energy tail is certainly lengthened but Almen and Bruce (1961a) working at 45keV show that the mean velocity in the direction normal to the target is 7.1×10^5 cm/sec. indicating that relatively few atoms carry very high energy. There is thus no large rise in the most probable velocity with bombarding energy and it is therefore felt that the use of the Stuart and Wehner (1962) distribution can give useful information which will be not too far from the actual distribution behaviour.

The following calculations are for a parallel plate electrode system in which sputtered atoms leave one plate (the target) and travel towards the opposite plate. It is therefore based on a diode sputtering system in which the region between the plates is occupied by gas ions travelling towards the target, electrons travelling towards the anode, and gas atoms. Under the conditions of the diode sputtering experiments described in chapter 4, the highest ion current density employed was $\sim 125 \mu A/cm^2$ which corresponds to an ion impingement rate of $\sim 5 \times 10^{14}$ ions/cm^2/sec. The number of ions per unit volume assuming a velocity equivalent to 1keV is $\sim 5 \times 10^9$ ions/cc. For a gas at $300°K$, the number of molecules per unit volume is $\sim 5 \times 10^{14}$ cm^{-3}, so the ratio of atoms to ions is $\sim 10^5 : 1$. Collisions between sputtered atoms and discharge gas ions can therefore be neglected. Collisions between sputtered atoms and electrons would have virtually no effect a) because the relative masses are so different and b) because the particles would be moving in the same direction as the electrons.

To simplify the calculation, the gas is assumed to be stationary. This is a reasonable assumption since, for a Maxwellian distribution only 0.01% of the molecules have $V > 3\bar{V}$ where $\bar{V} = 4 \times 10^4$ cm/sec. whereas the sputtered atoms have $\bar{V}$ around 4×10^5 cm/sec.

If the sputtered atoms have velocities approaching that of the gas atoms, then the stationary gas assumption breaks down. However, it has already been decided to ignore sputtered atoms with velocities below 1×10^5 cm/sec., so the stationary gas approximation remains satisfactory.

For the purposes of computation, let the inter-electrode space be considered as being made up of n slabs of unit cross-sectional area, each of thickness δx arrayed one behind the other. If there are N gas atoms per unit volume then each slab contains $N.\delta x$ atoms which will present an area $N.\delta x.q$ to the impingeing beam, where q is the collision cross-section. The total collision area A presented by n slabs is then given by the binomial expression

$$A = 1 - (1 - N.\delta x.q)^n$$

Thus the number of impingeing atoms which pass through without collision is equal to the "free space" area, (1-A). The error in (1-A) depends upon the value of n. For an interelectrode separation of 10 cm divided into 100 slabs, at a gas pressure 10^{-2} torr, the error in calculating (1-A) is 6.5%. The error is proportional to $1/n$, so that for 500 slabs the error is only 1.3%. The error is due to the assumption regarding the numbers of atoms lying behind one an ther in the same slab.

Since we are interested in those particles with final velocities $\geqslant 1 \times 10^5$ cm/sec., regardless of what happens on the way to the substrate, it is possible for some particles to make more than one collision and still have a final velocity $>1 \times 10^5$ cm/sec. Some may make as many as 10 collisions before their velocity falls below the lower limit. It is therefore necessary to consider collisions in each slab, whence the larger fraction of atoms will continue with the same velocity and a small fraction will set out with a

velocity modified by the collision within the slab. If the fraction of atoms which have had collisions is plotted as a function of n, a set of curves is obtained whose shape and starting points depend upon the velocity on entering the slab and the position of the slab in which collision occurred.

Since the collision cross-section is a function of velocity this must also be taken into account. From thermal beam scattering, q varies as $v^{-2/5}$, assuming r^{-6} variation of potential with distance (Rothe et al 1959). Assuming this law, and if a value for the collision diameter at $0^{\circ}C$ is taken as $\frac{1}{2}(D_1 + D_2)$, where D_1 and D_2 are the molecular diameters of Ag and A respectively, the value of q as a function of velocity may be calculated.

The average fractional energy loss per collision, $\bar{f}$, by a molecule is given by Cravath (1930) for the case of two gases with Maxwellian distributions corresponding to temperature T, and T_2 respectively

$$\bar{f} = \frac{8}{3} \frac{M_1 M_2}{(M_1 + M_2)^2} (1 - \frac{T_1}{T_2})$$
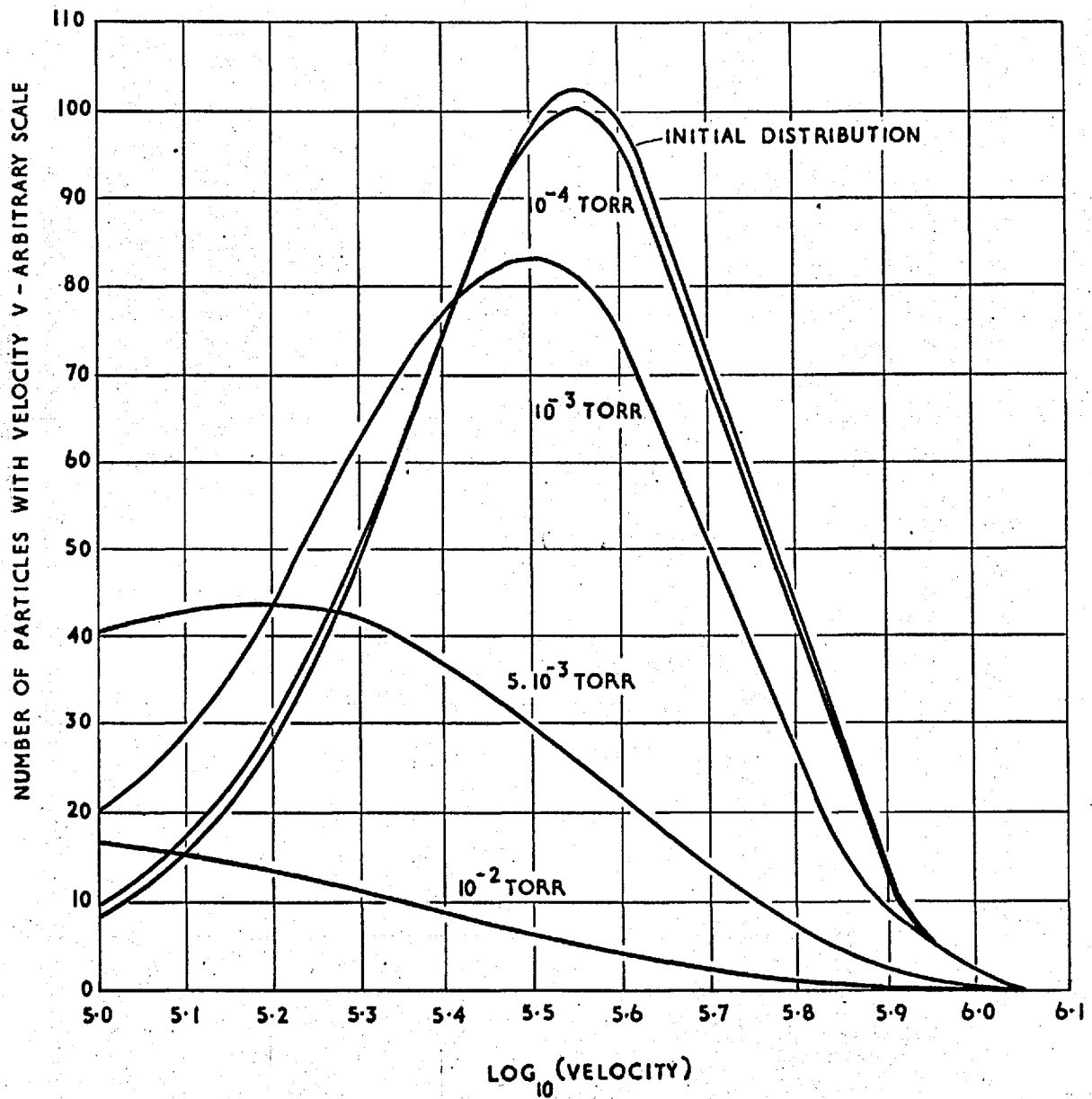
where M_1, M_2 are the masses of the colliding particles.

For the case of sputtered silver in argon, $T_1 < T_2$ and $\bar{f} \simeq 0.5$ hence the average fractional velocity loss by a silver particle is $1/\sqrt{2}$.

A computer programme was therefore written to calculate the fraction of atoms arriving at the substrate with velocities $> 1 \times 10^5$ cm/sec. using the curve given by Stuart and Wehner (1962) as a starting distribution. The results of the computation are given in Fig. 3.10 for various gas pressures and a target substrate separation of 10 cm. divided into 500 slabs. A value of 33.5×10^{-16} cm^2

FIG.3.10

CALCULATED VELOCITY DISTRIBUTION OF SILVER ATOMS
ARRIVING AT THE SUBSTRATE FOR VARIOUS ARGON GAS PRESSURES.

(CATHODE SUBSTRATE SPACING – 10 CM)

INITIAL DISTRIBUTION

10^{-4} TORR

10^{-3} TORR

$5 . 10^{-3}$ TORR

10^{-2} TORR

NUMBER OF PARTICLES WITH VELOCITY V – ARBITRARY SCALE

LOG_{10} (VELOCITY)

was assumed for the collision cross section, measured at $0^{\circ}C$, i.e.
a relative velocity of 4.10^4 cm/sec. The fraction of atoms arriving
at the substrate with velocities above 1×10^5 cm/sec. may be cal-
culated from the integrated areas of the distributions.

The results indicate that at a pressure of 1×10^{-2} torr, 15%
of all particles which set out with velocities $>1 \times 10^5$ cm/sec.
arrive at the substrate with velocities greater than this value.
Fig. 3.11 shows how the percentages change with gas pressure, for a
cathode-substrate spacing of 10 cm. The curves can be applied for
other spacings provided the pressure-distance product remains the
same. These figures represent maximum values since it has been
assumed that all particles continue in a forward direction following
collision, i.e. no back-diffusion.

There is thus a significant difference in arrival energy
between sputtered atoms and evaporated atoms, even at 10^{-2} torr.
At 10^{-3} torr and below, the difference is even more marked. This
difference may influence the growth behaviour in various ways which
will be discussed in chapter 6. If the energy of arrival is import-
ant one would certainly expect a difference between evaporated film
growth, sputtered film growth at 10^{-2} torr (diode sputtering) and
sputtered film growth at 10^{-3} torr and below (triode sputtering).

While the above results have been obtained for Ag in A, the
same curves may be applied for other systems provided the collision
cross-section is not widely different. For instance for Ge,
$q = 31.9 \times 10^{-16}$ cm^2 calculated from $\frac{1}{2} (D_1 + D_2)$ at $0^{\circ}C$, so the
above curves will be only slightly altered.

FIG.3.11

CALCULATED VARIATION OF % SILVER ATOMS ARRIVING AT SUBSTRATE WITH ENERGIES ABOVE 0·6eV AS A FUNCTION OF ARGON GAS PRESSURE.

(CATHODE-SUBSTRATE SPACING - 10 CM)

ARGON GAS PRESSURE TORR
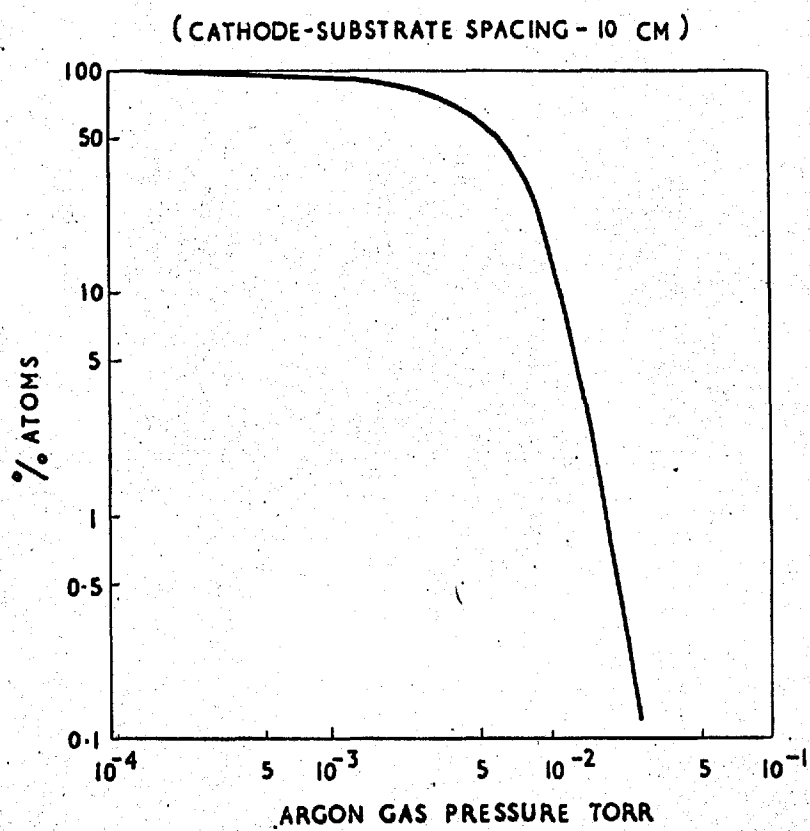
3.5 THEORIES OF SPUTTERING

Early models for the sputtering phenomenon were founded on the belief that the energetic ion beam produced a molten zone from which thermal evaporation took place. From the point of view of increased yield with increasing ion energy, such a theory was acceptable. However more sophisticated experiments of the types described in section33 proved such a theory to be false. For example, the effect of angle of incidence, the non-existence of a true cosine distribution law for ejected particles and the sometimes observed decrease in yield with energy could not possible be explained on an evaporation basis. The final proof of the falsity of the model was the previously discussed ejection energy of the sputtered material which corresponded to a source temperature of $\sim 50000^{\circ}K$. Thompson (1967) however has invoked a thermal evaporation process to explain a low energy part of their distribution curves.

Current sputtering models are based on collision processes within the crystal with a transfer of momentum initially from ion to atom and then from atom to atom. There are three types of possible interaction dependent upon the ion energy. 1) Rutherford collisions at very high energy (interaction through Coulombic repulsion of nuclear charges), 2) Weakly screened Coulomb collisions (partial screening by the electron clouds), 3) Hard sphere collisions (no penetration of the electron cloud). The boundary energy for each process depends upon the ion-atom pairing but for the inert gases upon metal targets, hard sphere collisions occur below ~ 100 keV. Most models have considered only this type of collision therefore.

One of the earlier modern theories of sputtering was due to Keywell (1955) based on a modification of neutron cooling theory. He considered successive "knock-ons" within the crystal until the

transferred energy became less than the displacement energy. He assumed that the number of sputtered atoms could be related to the number of displaced atoms, and was able to derive an expression for the sputtering yield which was a function of $E^{\frac{1}{2}}$. However, this function is found to be true for only part of the energy range. Rol et al (1960) advanced a theory in which they assumed that only the first collision contributed to the sputtering process and they neglected subsequent collisions. This resulted in a linear dependence of yield or energy. They claimed fair agreement with their own results but other authors found discrepancies over 20%. Also their theory fails to account for ejection patterns from single crystal targets in which successive secondary collisions are important.

The effect of the directional properties of a crystal lattice was introduced by Silsbee (1957) who showed that momentum may be focused along a line of atoms in a close packed direction. Provided the distance of closest approach in a head-on collision is greater than half the separation of atoms along a row, focussing will occur. Fig. 3.12 demonstrates the effect. Silsbee, and later Thompson (1963) defined an upper energy limit above which focussing could not occur. For the $\langle 110 \rangle$ direction in gold, Thompson (1963) obtained a figure of 280 eV for this energy. The proposed focussing mechanism of Silsbee was able to account for preferential ejection along $\langle 110 \rangle$ directions but could not account for the cases when $D > 4R$. Such directions are the $\langle 100 \rangle$ and $\langle 111 \rangle$ directions in fcc crystals.

Based on computer calculations, Gibson et al (1960) showed that when an atom moves at a small angle to say the $\langle 100 \rangle$ direction it experiences electrostatic forces due to a ring of four nearest neighbour atoms which tend to deflect the particle towards the axis before collision with the next atom in the $\langle 100 \rangle$ direction. This is known as assisted focussing and the ring of 4 atoms acts in a way

FIGURE 3.12

Schematic illustration of Silsbee focussing mechanism for momentum transfer along a line of hard spheres.
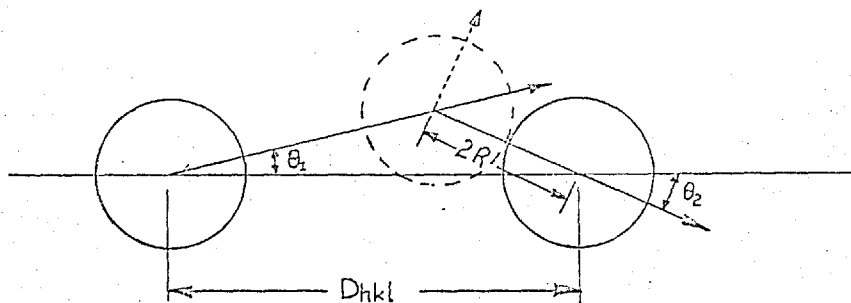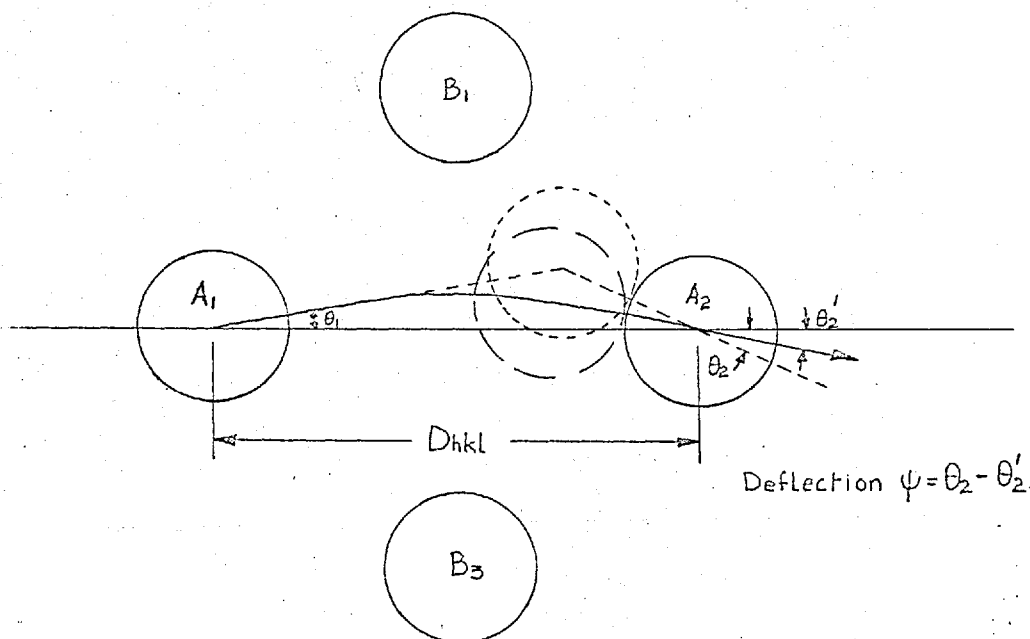

$$\frac{\theta_2}{\theta_1} = \frac{D_{hkl} - 2R}{2R} = \frac{D_{hkl}}{2R} - 1$$

Focussing condition $\theta_2 < \theta_1$ occurs when $\frac{D_{hkl}}{2R} - 1 < 1$

i.e. when $D_{hkl} < 4R$

FIGURE 3.13

Schematic illustration of assisted "lens"- focussing mechanism for propagation of momentum. (After Nelson and Thompson, 1961)

Deflection $\psi = \theta_2 - \theta_2'$

For atom moving at small angle to 100 direction in f.c.c. lattice, the focal length of atoms $B_1 B_2 B_3 B_4$ in (100) plane surrounding 100 direction is given by

$$f_{hkl} \simeq \frac{D_{hkl} \, (\theta/\psi)}{\sqrt{2}}$$

analogous to an optical converging lens. The effect is shown dia-
grammatically in Fig. 3.13. Thus it is possible for the collision
sequence to be propagated down the chain of $\langle 100 \rangle$ atoms even though
geometrically the Silsbee criterion is not satisfied.

The above theories explain with reasonable satisfaction the
observed ejection patterns formed from single crystal targets. They
do not however totally account for the energy distribution of part-
icles observed by Thompson (1967) at high bombardment energy. Also,
the range of ions in crystals can be greater than that predicted by
focussing mechanisms. This latter observation was suggested to be
due to the open-ness of the lattice, such that if a particle approach-
ed from the right direction it could pass along the open channels
between rows of atoms. In an fcc crystal such channels are formed
between $\langle 111 \rangle$ and $\langle 100 \rangle$ planes and also between $\langle 110 \rangle$ and $\langle 100 \rangle$
directions. The angle of approach must be very small ($<3^{\circ}$) or
the ion will rapidly lose energy by collision. It proceeds along
the channel by a series of very low angle glancing collisions and
for an 80eV ion the range may be $\sim 2500\overset{o}{A}$. This concept of channel-
ing has been successfully applied to the interpretation of ion
ranges in solids, of preferential ejection and of dependence of
sputtering yield on angle of incidence.

However, focussing and channelling only apply to directional
properties of sputtered particles. The energy distributions obtained
by Thompson (1967) show that even when focussed collision sequences
are not expected as in the $\langle 121 \rangle$ a high energy distribution is
observed. Such a distribution is consistent with a multiplication
of random collision cascades as in the case of radiation damage in
crystals. This occurs when there is no directional influence upon
the collisions, i.e. when the angle of collision is fairly high.

The process can be analysed in similar terms to those used by Keywell (1955) (neutron cooling). It is also possible to consider the cascade as a disturbance in an elastic medium with sound velocity. The model gives an E^{-2} dependence of sputtering yield in the range 10-10^4eV. Below 10eV surface binding energies become important and above 10^4eV the mean free path is long and certain basic assumptions are invalid. The model can successfully account for ejection patterns since, when the mean collision free path is approximately equal to the interatomic spacing, the cascade reaches the surface via a collision in the penultimate layer. There is thus a tendency for the surface/atom to move off in a direction close to that joining it to its nearest neighbours.

Thompson (1967) finds that random cascades and focussing sequences account for ~90% of the sputtering in most cases (bombarding energy ~43keV). He also finds that the mean energy of ejection where directional properties are observed are: $\overline{E} = 13.8$eV for $\langle 110 \rangle$, $\overline{E} = 93.5$eV for $\langle 100 \rangle$ and $\overline{E} = 47.4$eV for $\langle 121 \rangle$. Thus the highest ejection energy is for the case of assisted focussing. These figures refer to $\langle 100 \rangle$ ion bombardment.

3.6 SUMMARY

The above brief outline of the sputtering theories and the preceding section on experimental observations demonstrates that as a means of thin film deposition sputtering is unique. Its most outstanding feature is that the energy of sputtered atoms is very high and it might be expected that this will influence the growth of thin film. By using preferred ejection directions from a single crystal target it would be possible to deposit films under

known high energy conditions. This type of experiment has been performed by Chapman (1968) in an investigation into nucleation behaviour of gold films on rocksalt. The way in which the energy may manifest itself at the substrate is discussed in a later chapter. By suitable placing of substrates relative to the target, films may be grown under conditions where the only experimental variable is the energy of arrival. An investigation into single crystal target behaviour can be usefully applied to polycrystalline targets by simply summing the effect for different directions.

CHAPTER IV

EXPERIMENTAL APPARATUS AND PROCEDURE

4.1. VACUUM PLANT

Two types of vacuum plant were employed, both being standard

Edwards units. The first, an Edwards 12E3 unit, employed a 4 inch oil

diffusion pump backed by an oil rotary pump. A water-cooled chevron

baffle and a liquid nitrogen trap were incorporated in order to lower

the ultimate pressure and to reduce the amount of oil vapour reaching the

work chamber. With liquid nitrogen trapping the final pressure was

$< 1.10^{-6}$ torr. The work chamber was, for the diode work, a 12 in. diameter

x 14 in. high glass bell jar, of total volume 22 litres. For the triode

system a 12 in. diameter x 12 in. long Quickfit pipesection was used also

of total volume 22 litres. The closure was an aluminium plate. Seals

used were Viton 'A' O-rings or L-gaskets where applicable. An alternative

chamber used where water cooling of the target was deemed necessary,

employed a Quickfit 12 in. to 3 in. pipe reducer of total volume ~10 litres.

The cathode assembly acted as the 3 in. closure flange.

The second unit employed was an Edwards UHVM2, said to be capable

of 10^{-11} torr. It used a 2 in. mercury diffusion pump, backed by a 1"

mercury diffusion pump which in turn was backed by a liquid nitrogen cooled

sorption pump. A Peltier cooled chevron baffle and a liquid nitrogen trap

were again employed to prevent mercury reaching the work chamber. The work

chamber took the form of a 6-arm Pyrex cross, arm-diameter 3 in. manu-

factured by Quickfit. This was found to be the most convenient chamber for

the experiments at a low sputtering pressure. The total volume of the

chamber was 4.5 litres. The closure flanges for the chamber were of stain-

less steel or aluminium with Viton 'A' O-ring seals. It was probably due

to the porosity of the seals that the best pressure achieved ($\sim 10^{-8}$ torr) was considerably higher than the ultimate claimed for the unit. The unit incorporated a backing reservoir so that, where necessary, the backing pumps could be shut off. At a later stage in the work a 2 in. butterfly valve was added so that the pumps could be left under vacuum while specimens etc. were removed from the work chamber. This also required an extra sorption pump to re-evacuate the work chamber, prior to opening the butterfly valve. Pressure measurement was by means of a Pirani gauge in the $> 0.1\mu$ range and by an ionisation gauge (Mullard I-OG 12) at lower pressures. Gas admission to both the above systems was from a cylinder by way of a desiccant (Al_2O_3) through a fine control needle value (Edwards LS01). The gas used for all experiments was argon of 99.999% purity supplied by Air Products Ltd. Prior to admission the system was always evacuated to $< 1 \times 10^{-5}$ torr. No other measures were taken to further purify the gas. A mass spectrometer trace, using an AEI 29D18 head shows, in Fig. 4.1., that little or no water vapour was admitted to the system along with the argon. A maximum pressure of 4.10^{-5} torr was used to safeguard the spectrometer head. The A^{++} and A^{+} peaks can be seen in the lower trace, but the peaks lying above A^{+} are not identifiable. They appear to be spurious peaks introduced by the head itself.

4.2. DEPOSITION TECHNIQUES

4.2.1. Diode Sputtering

4.2.1.1. Apparatus and Circuit

The apparatus used for the diode sputtering work is shown schematically in Fig. 4.2. and Fig. 4.3(a). The vacuum system employed for all diode experiments was the Edwards 12/E3 unit described above. The system shown in Fig. 4.2. was used for early work but for all later studies where high rates might have been employed, the latter system was used since it incorporates water cooling . For diode sputtering, the target is made

FIGURE 4.1
(A)

MASS SPECTROGRAPH OF 12E3 SYSTEM EVACUATED FROM
ATMOSPHERIC PRESSURE TO $5 \cdot 10^{-6}$ TORR.
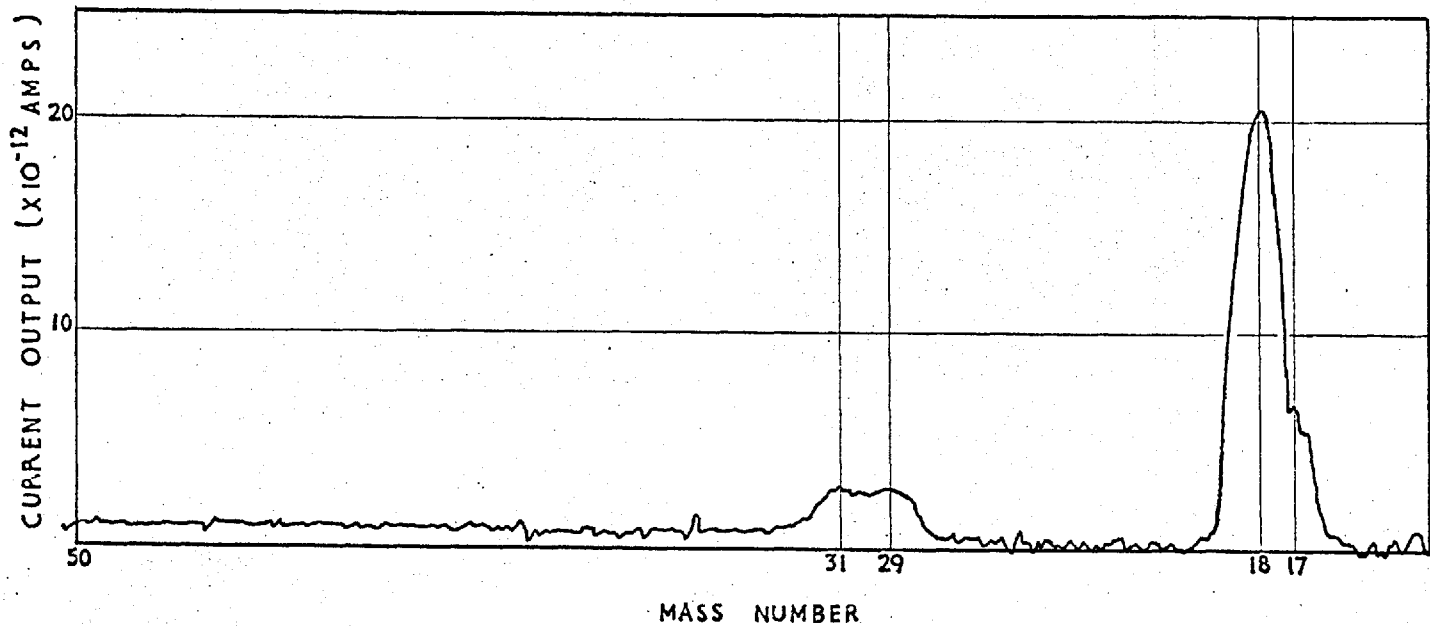
(B)

MASS SPECTROGRAPH OF 12E3 SYSTEM WITH ARGON GAS
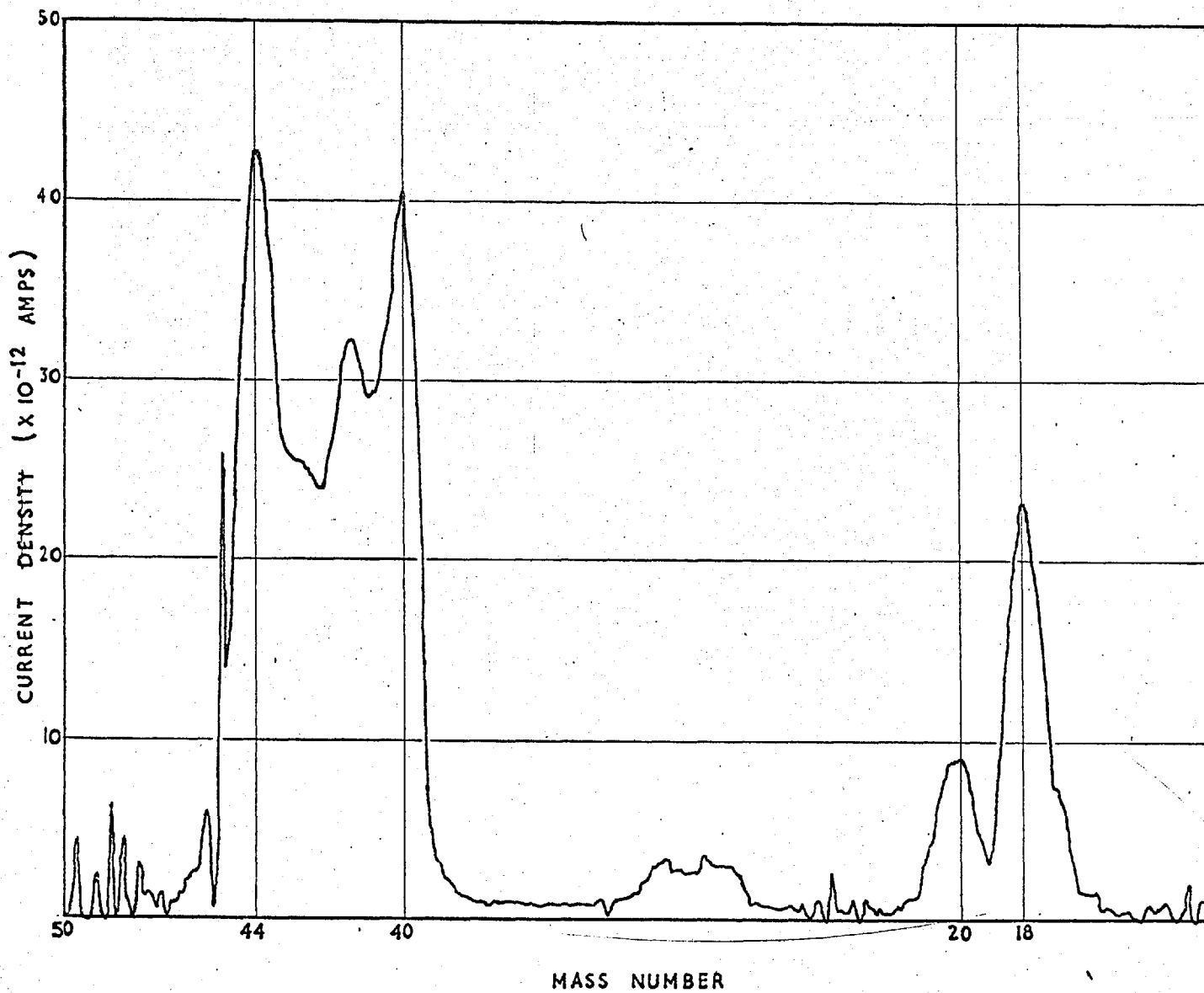ADMITTED THROUGH AL_2O_3. PARTIAL PRESSURE OF ARGON $4 \cdot 10^{-5}$ TORR.

FIGURE 4.2

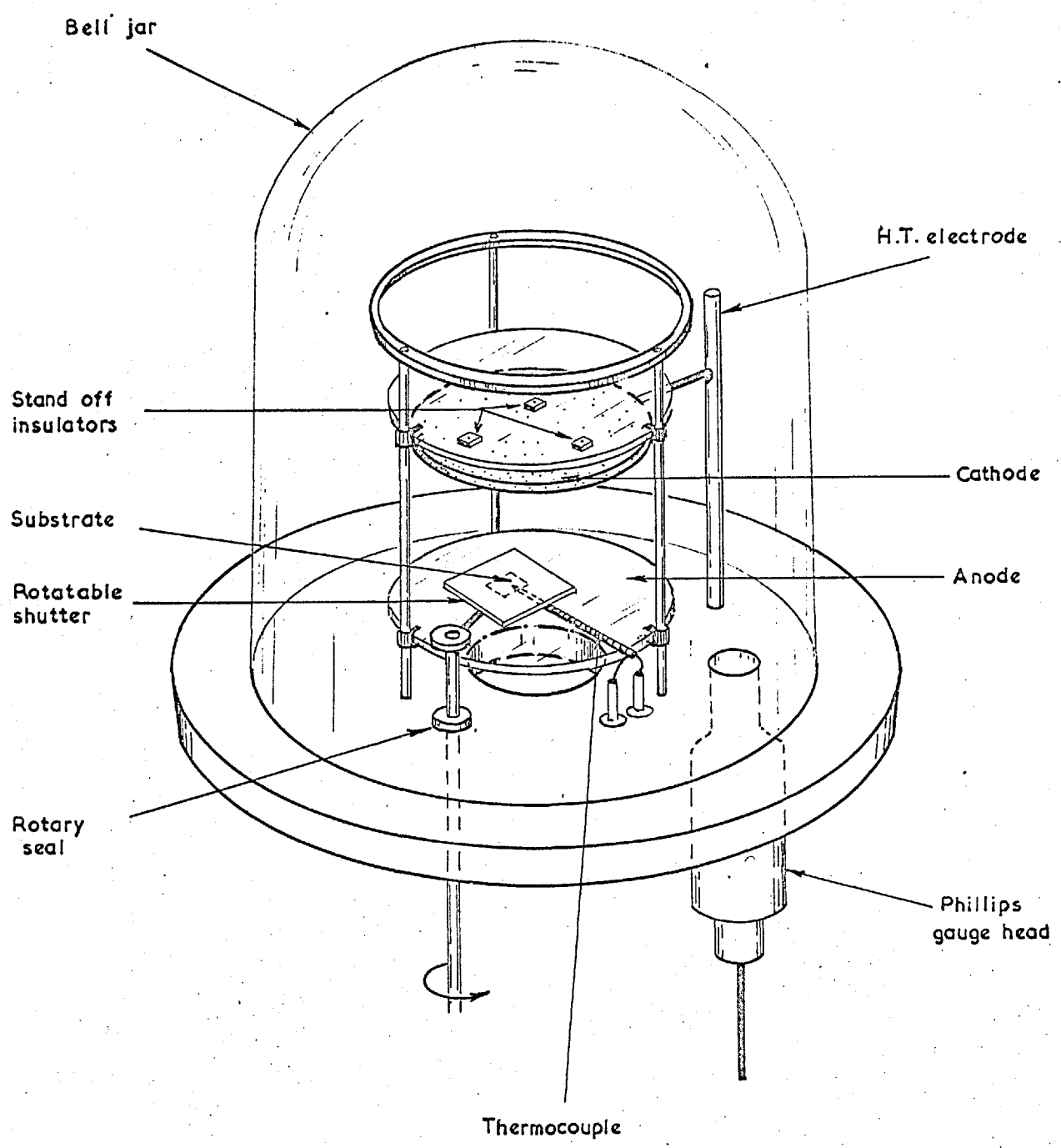System used for initial Diode sputtering experiments.

Bell jar

H.T. electrode

Stand off
insulators

Cathode

Substrate

Anode

Rotatable
shutter

Rotary
seal

Phillips
gauge head

Thermocouple

FIG. 4.3(a)

SPUTTERING SYSTEM FOR ROOM TEMPERATURE DEPOSITION WITH FACILITIES FOR WATER COOLING OF THE TARGET. (USED WITH 12E3 UNIT.)

Cooling water

In

Out

H.T shield

−3kV

Insulating screws (nylon)

Insulating stand offs

Screen to prevent discharges from unwanted regions. (Earth potential)

12″ to 3″ glass pipe reducer

Target

10 cm

Argon

Anode (Earth potential)

Substrate (or shutter system see text)

Baseplate
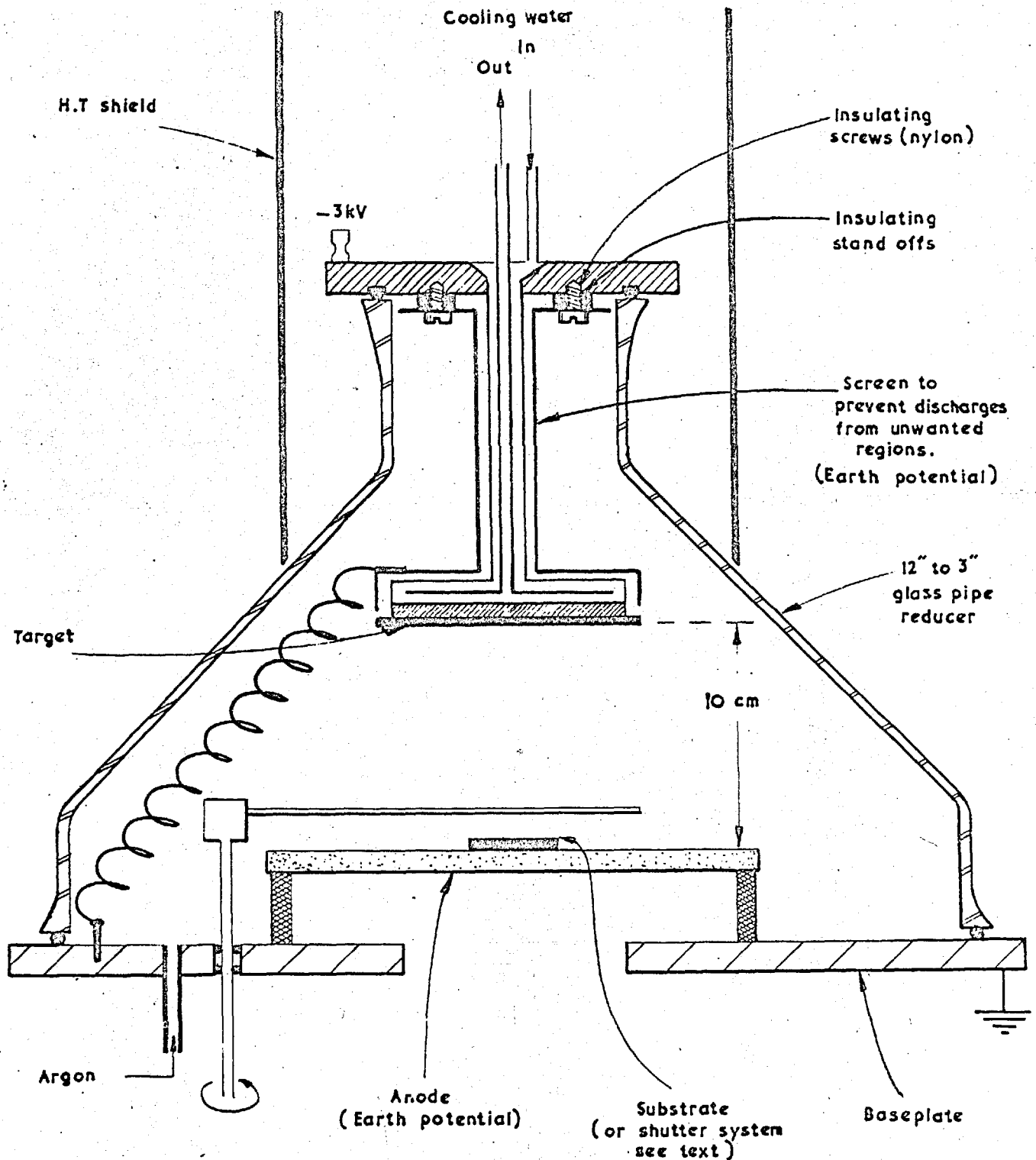
FIGURE 4.3(b)

Water-cooled target assembly used for
Diode sputtering.
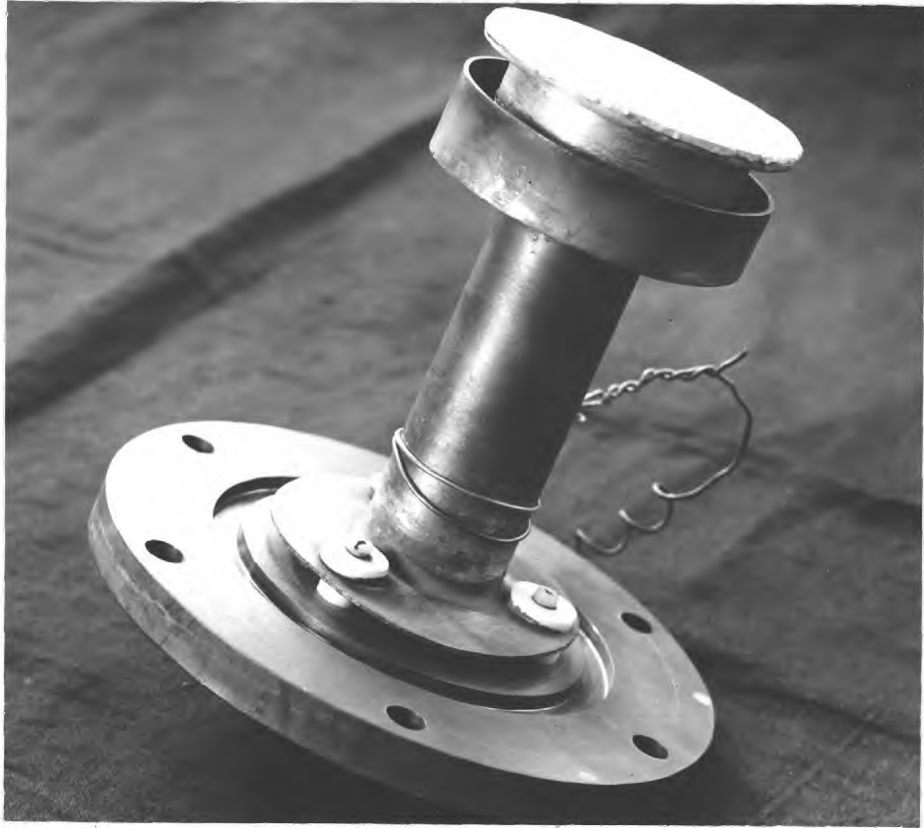
the cathode and the substrate is normally placed on the anode which is
at earth potential. The target was cemented to the aluminium cathode
using high conductivity epoxy resin (Johnson Matthey). The water cooling
ensured that the target did not rise much above $100^{\circ}C$ at any time, thereby
preventing the cracking of the epoxy. At normal ejection rates water
cooling was not necessary but the same unit was employed, thus maintaining
electrode geometry. A photograph of the target assembly is shown in
Fig. 4.3(b). Where cooling was necessary allowance had to be made for
the current carried by the water since the final water outlet was at
earth potential.

In order to ensure uniformity of the deposit, the target should
be considerably larger than the substrate. A diameter of 7.5 cm. was
chosen for all experiments. Specimen sizes were typically 0.5 cm. square
and the separation typically 10 cm. The electrode geometry was such that
the discharge always took place between cathode and anode, other earth points
being further away from the cathode or within the discharge dark space.

The circuit employed for diode sputtering is straightforward. It
consists of a high voltage transformer (5kV, 50mA) driving a full wave
rectifier the output of which is taken to the cathode and anode of the
system. The basic circuit is shown diagrammatically in Fig. 4.4. The
bridge rectifier used selenium diodes as these are better able to with-
stand peaks. A voltage of $\leqslant 3kV$ was applied to the target and the current
was varied by varying the gas pressure by means of a fine needle valve.
For diode sputtering a discharge gas pressure of tens of microns is
required in order to obtain currents of the order of 1mA.

Normally, for diode sputtering, the substrate is placed on the
anode at earth potential, but it is sometimes required that the substrate
should not be at earth potential. For instance, where it is required to

FIGURE 4.4

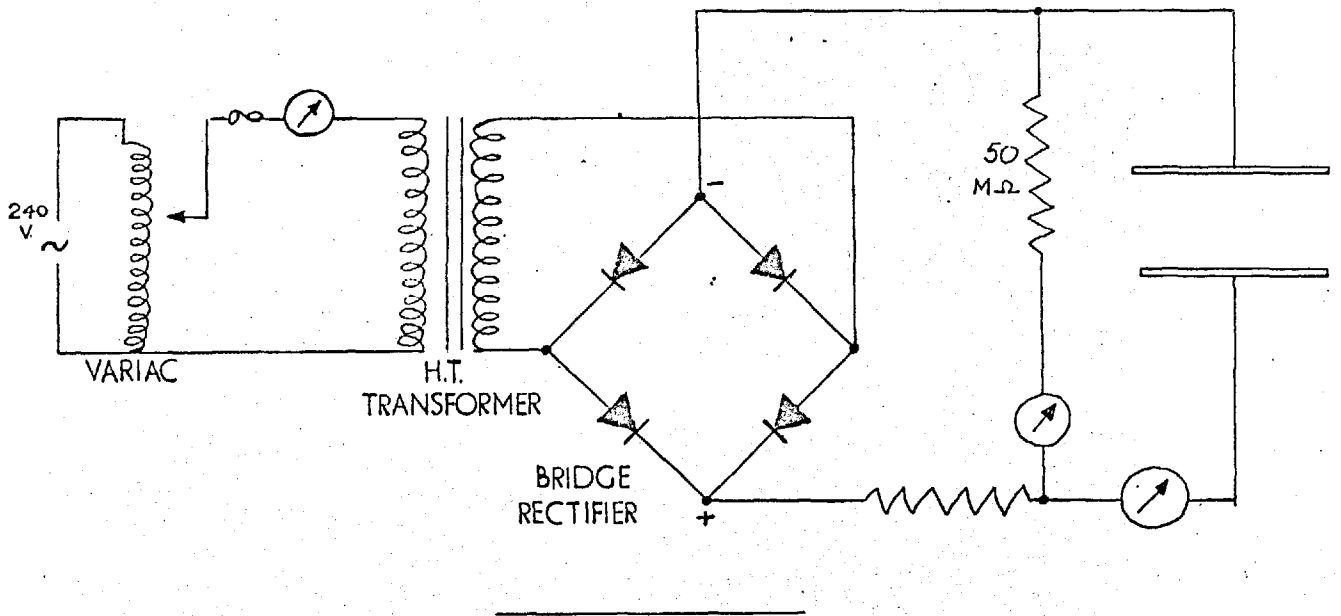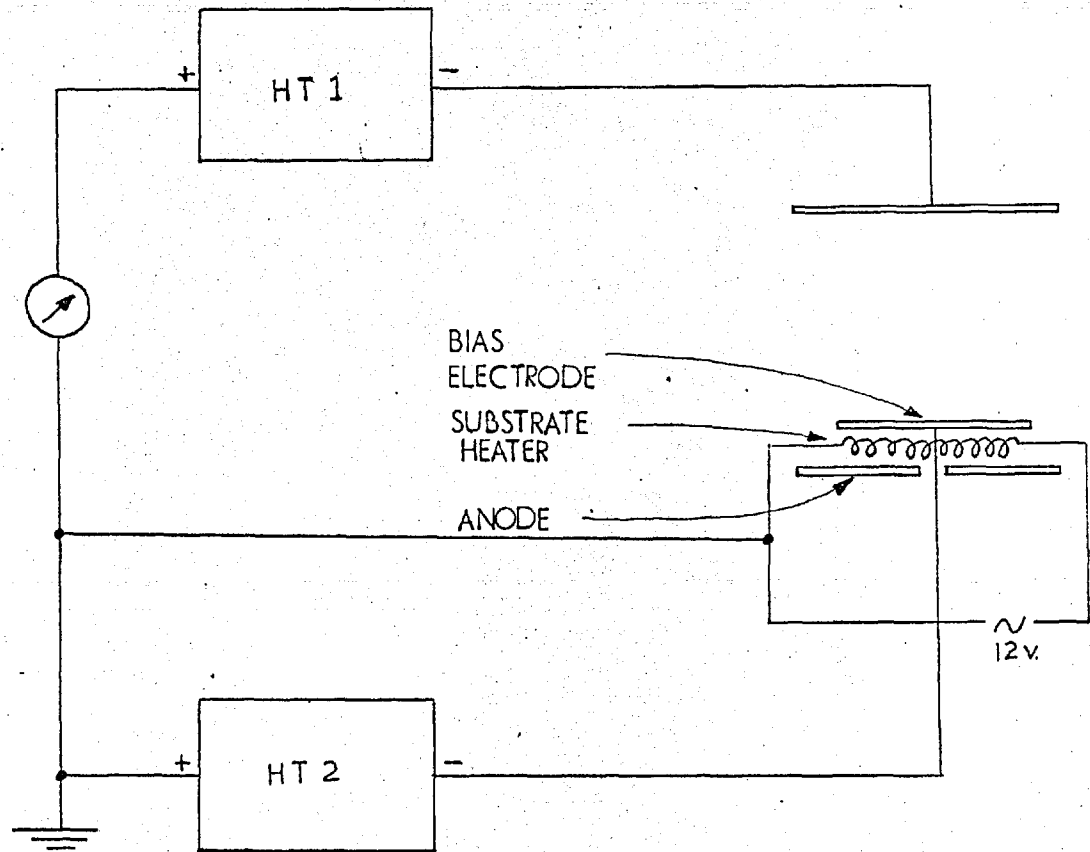Circuit used for the Preparation of Thin Films by Diode Sputtering.

FIGURE 4.5

Schematic circuit diagram for Bias Sputtering experiments in a

Diode System.

bombard the substrate with positive ions during deposition the substrate must be held at some negative potential with respect to earth. This technique is known as bias sputtering and the arrangement employed in these experiments is shown in Fig. 4.5. An auxiliary heater is also shown in Fig. 4.5. whereby the substrate may be heated to above room temperature. A negative potential was applied to the auxiliary electrode and the substrate surface was electrically strapped to it by way of a previously deposited gold land. The bias potential was provided by an auxiliary d.c. supply, capable of producing up to 10mA at 1kV.

4.2.1.2. <u>Successive Deposition</u>

Where it was necessary to deposit layers having different thick-nesses in the same experiment, a shutter system was required so that successive substrates could be exposed to the sputtered material. The two alternative methods used are shown in Fig. 4.6. Fig. 4.6(a) shows a simple withdrawal type shutter which could take a minimum of four substrates of size 10 x 5 mm. The number of substrates of a given size in this assembly is limited by the fact that material will deposit under the mask however close it is to the substrate. This is because atoms reach the substrate by a diffusion-controlled process so that some atoms may arrive almost at glancing angle. Substrates must therefore have a minimum sep-aration. Fig. 4.6(b) is a rotatable shutter, designed so that successive pairs of substrates could be exposed, followed by a complete covering of one set while the other set were being further treated, e.g. covered by carbon evaporation. The same substrate size and number limitation applies to this assembly. Both types of shutter were operated by an arm which was attached to a shaft passing through the baseplate by means of a rotary seal. In experiments where only a single substrate was being exposed, a simple shutter operating from the rotary shaft was employed.

FIGURE 4.6

Shutter Systems used for Successive Deposition in Diode Sputtering.

(A)

Actuating arm

(B).

Actuating arms
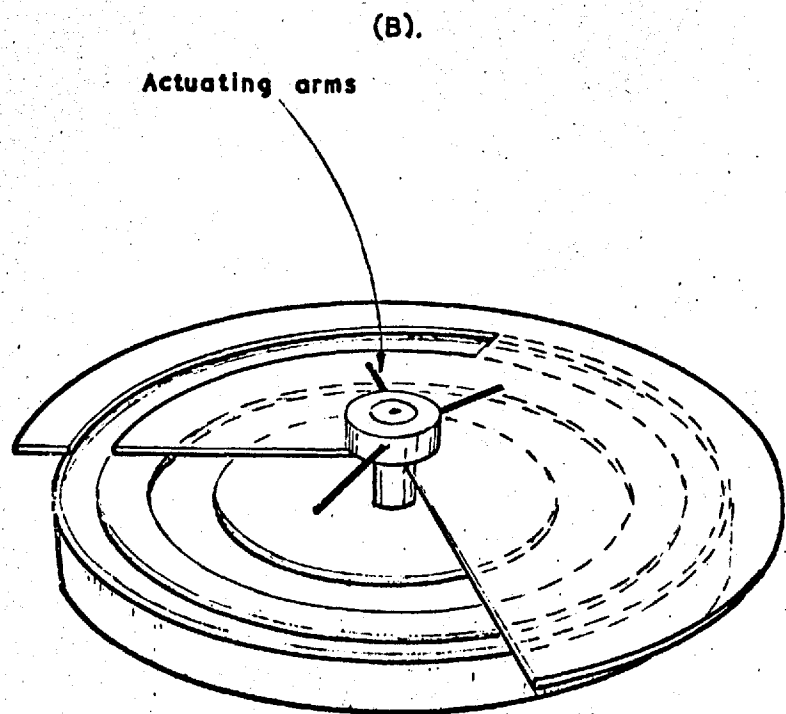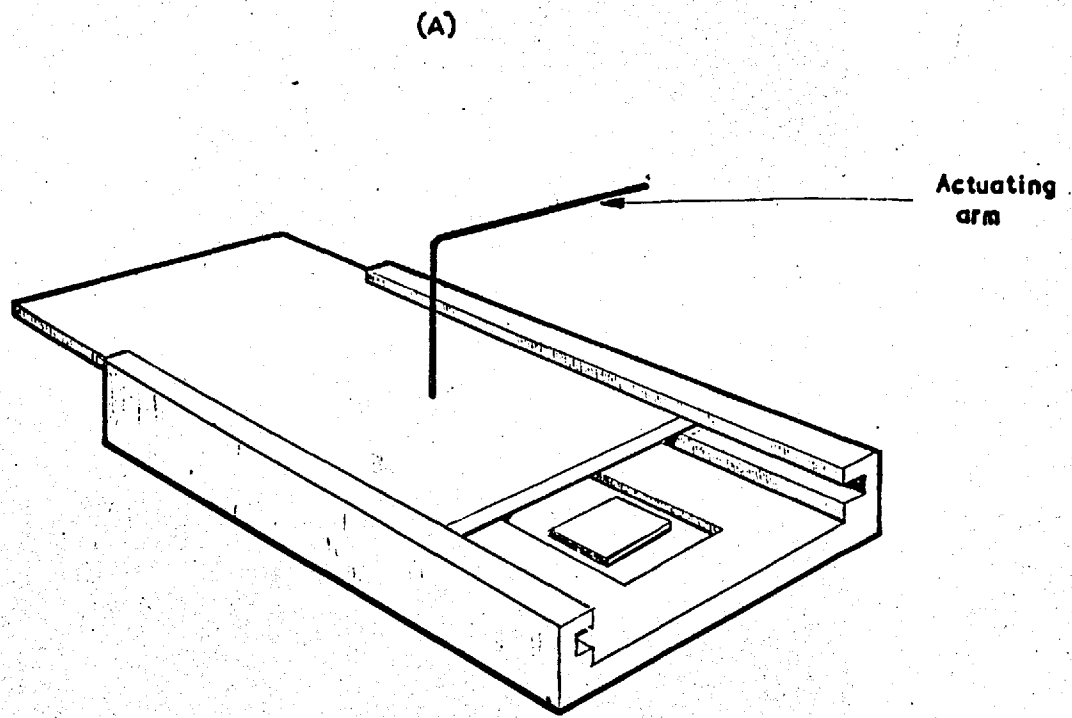
4.2.2. Triode Sputtering

The triode principle was fully described in the previous chapter and a schematic diagram of the system employed is shown in Fig. 4.7. The vacuum system was again an Edwards 12E3 unit as described above. For all experiments the residual gas pressure was $<2 \times 10^{-6}$ torr, and argon was admitted direct to the work chamber by means of a fine control needle valve. The apparatus constructed employed a spiral tungsten filament as the electron source. This was enclosed in a square section L-shaped tube, as indicated in Fig. 4.7, constructed entirely of stainless steel. In order to utilise the electrons produced more efficiently and to obviate the need for complex water cooling, an accelerating anode was placed in the position shown in the diagram. The optimum size of the aperture in the anode was determined empirically. The size finally chosen being 0.5 inches. The electrons were subsequently extracted into the sputtering region by the planar anode positioned as shown in the diagram. The mode of operation of this type of system has been described in Chapter 3.

The discharge was found to strike at a main-anode to filament drop of ∼100V and could be maintained at 60-80V drop. The actual values depended upon the accelerating anode potential which was adjusted to give maximum electron current. This was normally approximately +60V with respect to the filament. It was found possible to run the discharge with zero volts on the main anode but the ion current was lower than with finite volts. The discharge appeared to have been struck between filament and accelerating anode and ions diffused into the sputtering region where they were confined by the magnetic field. It was also possible for electrons to diffuse out of the source assembly and for ionisation to occur outside the assembly.

Fig. 4.8. is a schematic diagram of the circuit employed for all triode experiments. All D.C. power supplies were of the type used for the

FIGURE 4.7(a)

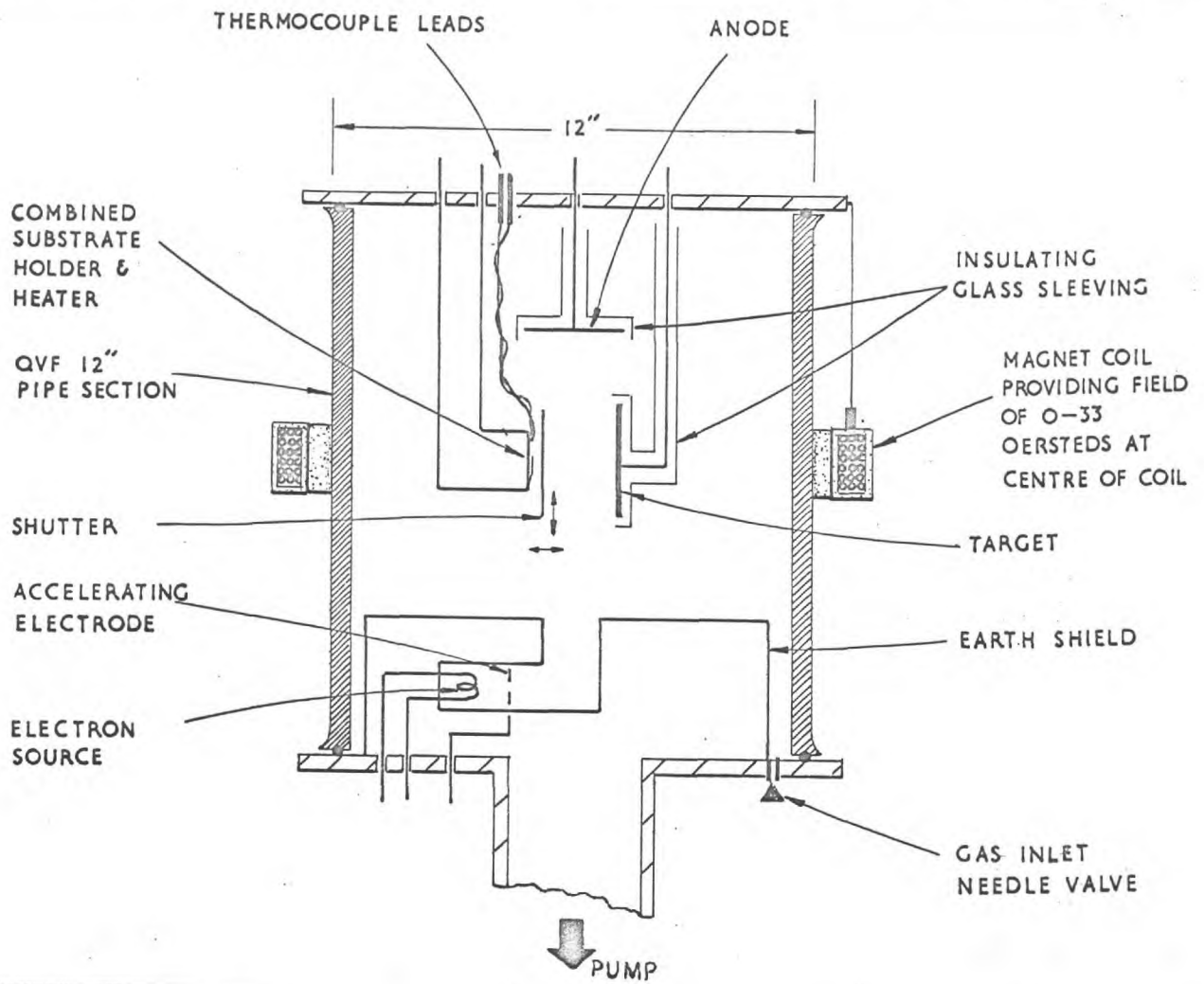SCHEMATIC DIAGRAM OF VACUUM ENCLOSURE COMPONENTS OF TRIODE SPUTTERING SYSTEM.

THERMOCOUPLE LEADS   ANODE

12"

COMBINED SUBSTRATE HOLDER & HEATER

QVF 12" PIPE SECTION

SHUTTER

ACCELERATING ELECTRODE

ELECTRON SOURCE

INSULATING GLASS SLEEVING

MAGNET COIL PROVIDING FIELD OF 0–33 OERSTEDS AT CENTRE OF COIL

TARGET

EARTH SHIELD

GAS INLET NEEDLE VALVE

PUMP

FIGURE 4.7(b)

General view of triode sputtering apparatus
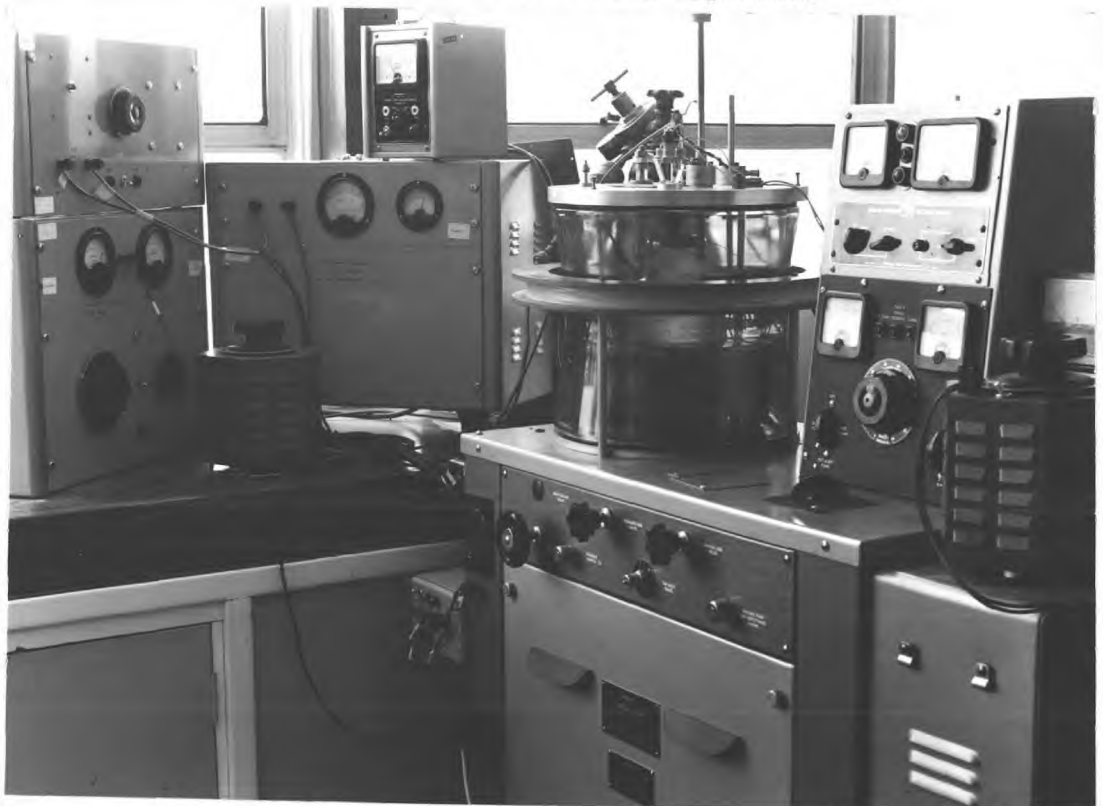
FIG. 4.8

SCHEMATIC CIRCUIT DIAGRAM FOR TRIODE SPUTTERING EXPERIMENTS.
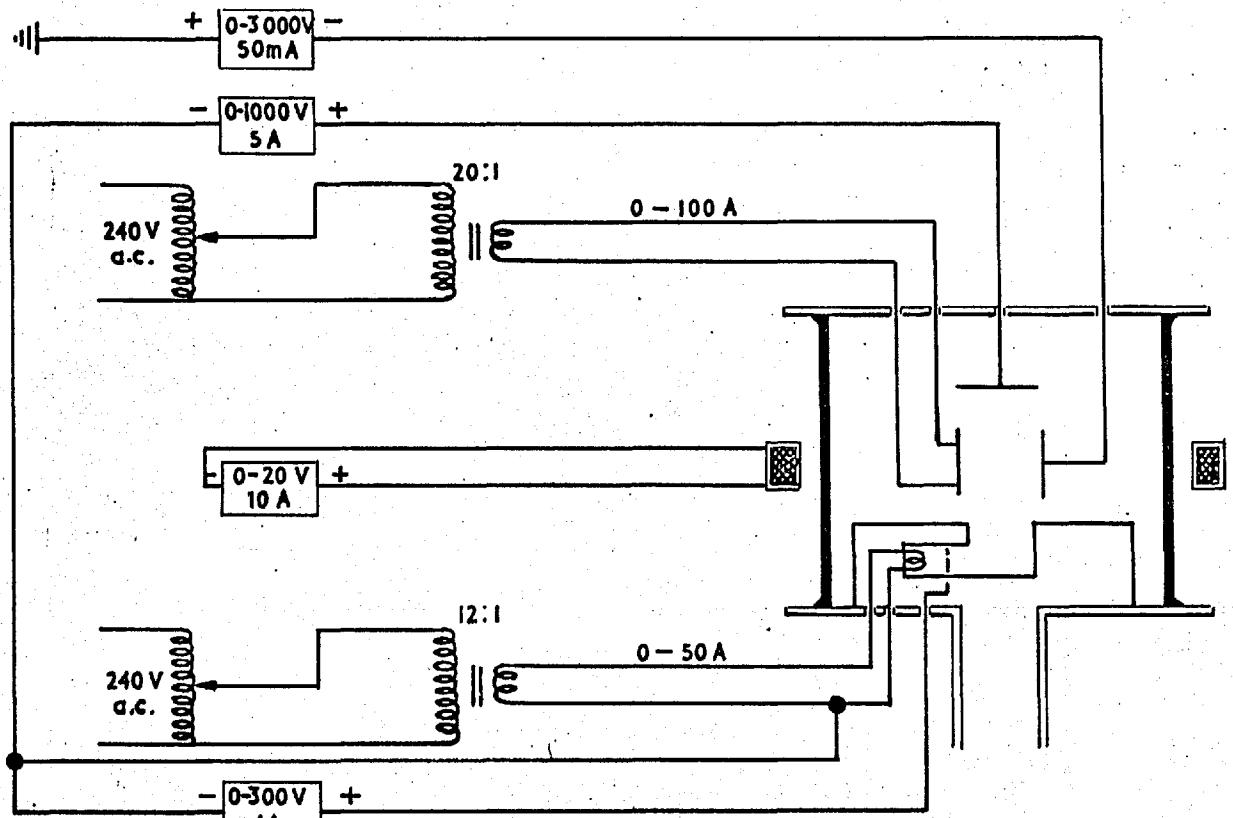
diode experiments as shown in Fig. 4.4. Full-wave rectification was
employed with no subsequent smoothing. Lack of smoothing is beneficial
in fact as it suppresses the tendency for arc breakdown (Hurwitt, 1968)
though such breakdown is unlikely anyway at the power levels used in these
experiments.

As in the case of diode sputtering the targets were 7.5 cm. in
diameter, fixed by conducting epoxy resin to a stainless steel aluminium
backing plate. At the power densities employed no water cooling was
necessary. The back surfaces of the anode and target, and also the support
rods, were shielded with Pyrex glass to prevent spurious discharges. The
substrate support and heater was placed opposite and parallel to the target
such that the main part of the electron beam passed between them. The
substrates generally were held at one edge by a Ta strip spot welded to the
heater strip so as to form a V-pocket and at the opposite edge by the
measuring thermocouple. A stainless-steel shutter, close to the substrate,
was operated from outside the system by way of a rotary seal. The substrate –
target separation was 5 cm. All the apparatus required for a deposition,
except for the electron source assembly was mounted on a 13 inch diameter
aluminium flange which acted as the top plate for the work chamber. This
enabled all the setting up to be done quite simply away from the vacuum
system.

4.2.3. Low-Pressure Sputtering

The vacuum system used for the low pressure sputtering work was
the Edwards UHVM2 unit described in Section 4.1. The discharge system is
similar in many respects to the triode system but can be operated at a
lower discharge gas pressure. The associated circuitry resembles that of
the triode system and is shown schematically in Fig. 4.9. which also shows
an elevation view of the work chamber. A plan view of the chamber is shown

FIG.4.9(a)

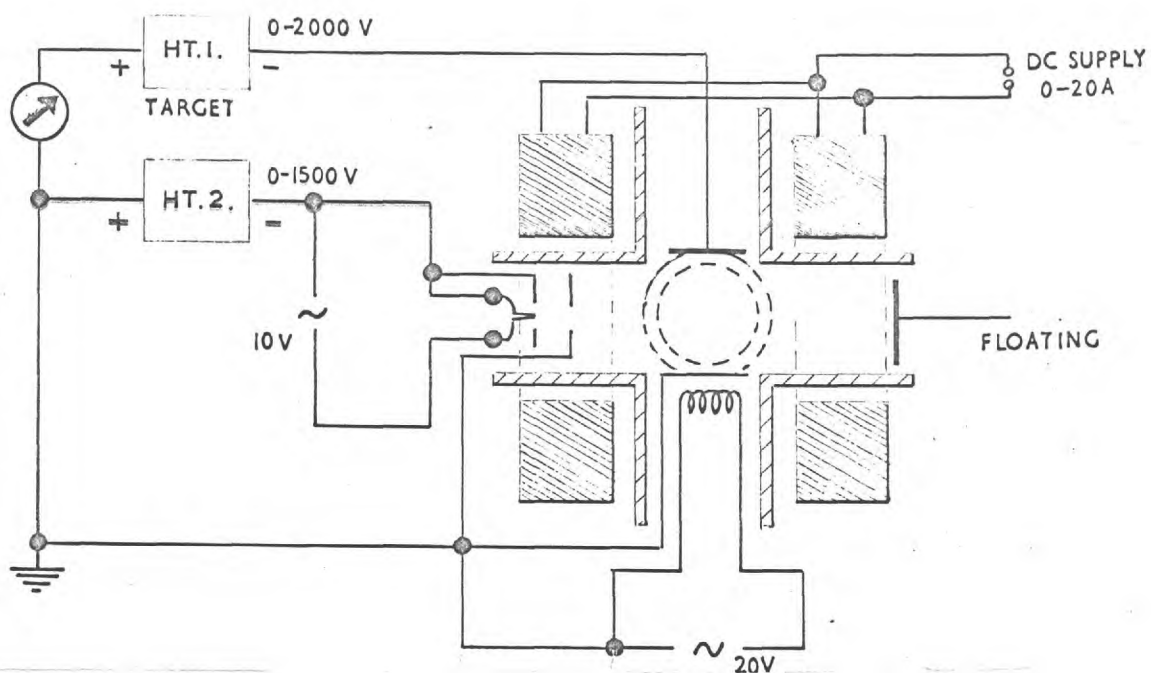SCHEMATIC CIRCUIT DIAGRAM FOR LOW PRESSURE SPUTTERING EXPERIMENTS.

FIGURE 4.9(b)

General view of low pressure sputtering system.

in Fig. 4.10. The electrodes and other inlets were introduced through
the stainless steel closure flanges, the seals being made with Viton
'O'-rings or with a cold setting low volatile resin ("Torr-seal",
manufactured by Varian Associates and recommended for vacuum work down
to 10^{-8} torr).

As in the case of triode sputtering, the principal parts of the
apparatus are the electron source and the magnetic field coil. In this
apparatus the electron source was based upon an electron microscope
tungsten hairpin filament, surrounded by a screen at the same potential.
Other potentials were tried but with detrimental results. An accelerating
anode at earth potential was placed in front of these. The complete
arrangement is shown in Fig. 4.11. The accelerated electrons entered an
essentially electrostatic field-free region where they were acted upon by
an axial magnetic field. The magnet coils were arranged in a near-Helmholz
arrangement so as to give a fairly uniform field at the centre of the cross.
The field could be varied to a maximum of approximately 600 oe at the
centre. The coils which were manufactured by Newport Instruments and had
provision for water cooling, were connected in parallel and a current of
15 amps was required for 600oe. They each consisted of 1,000 turns of
0.15" square section copper wire. Measurable ionisation could be produced
thus at gas pressures of <1 x 10^{-4} torr. though for useful ion currents a
pressure of ~ 2 x 10^{-4} torr was necessary.

In operation the accelerating field between filament and anode
was typically 500 V/cm. depending upon the ion current to be extracted and
the pressure in the system. The exact potential was varied to stabilise
the discharge. The closure flange at the end of the cross opposite to the
electron source acted as a reflector since it was allowed to float elect-
rically and so acquire a negative potential from the electron beam. Thus
the electrons made several traverses down the arms of the cross, being

FIGURE 4.10

SECTIONAL DIAGRAM OF LOW PRESSURE SPUTTERING SYSTEM.
(THE PUMPING SYSTEM AND IONISATION GAUGE HEAD
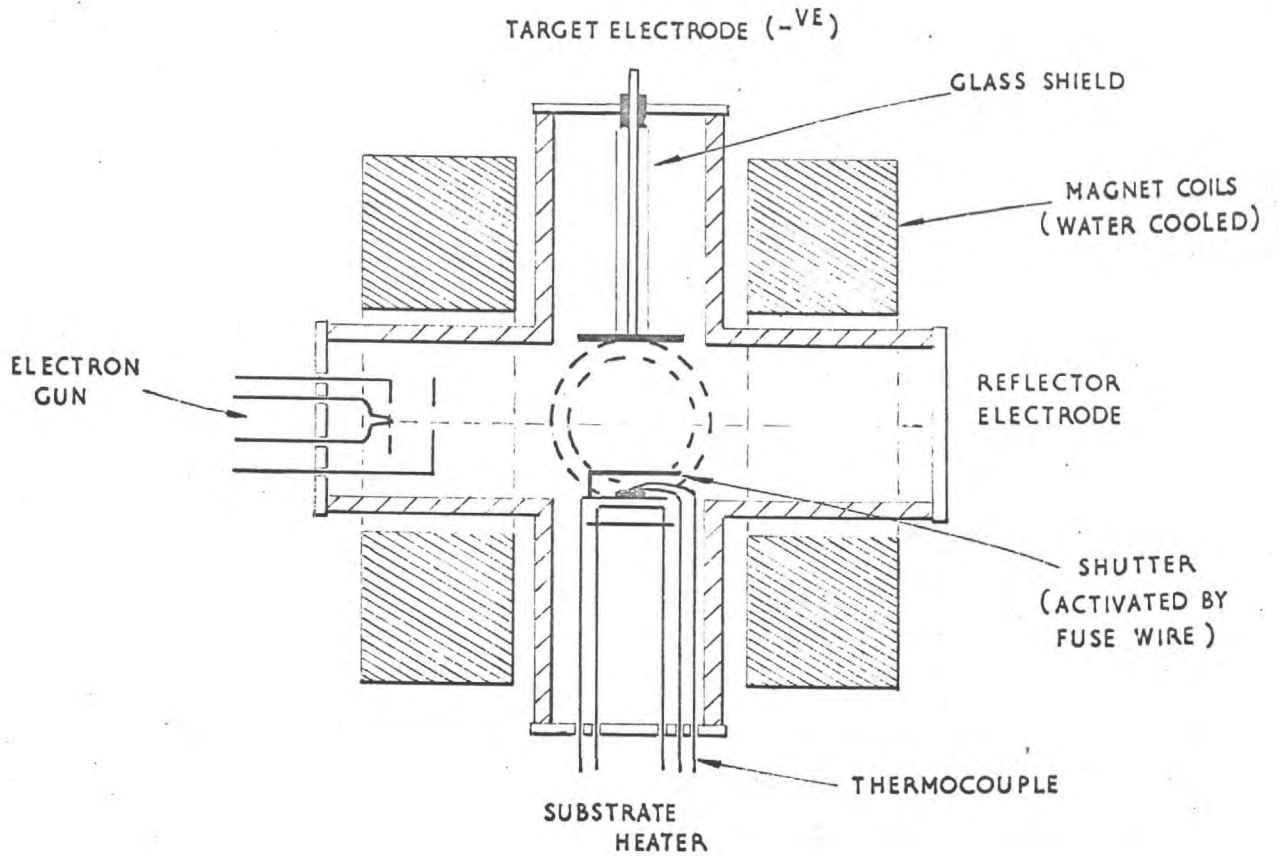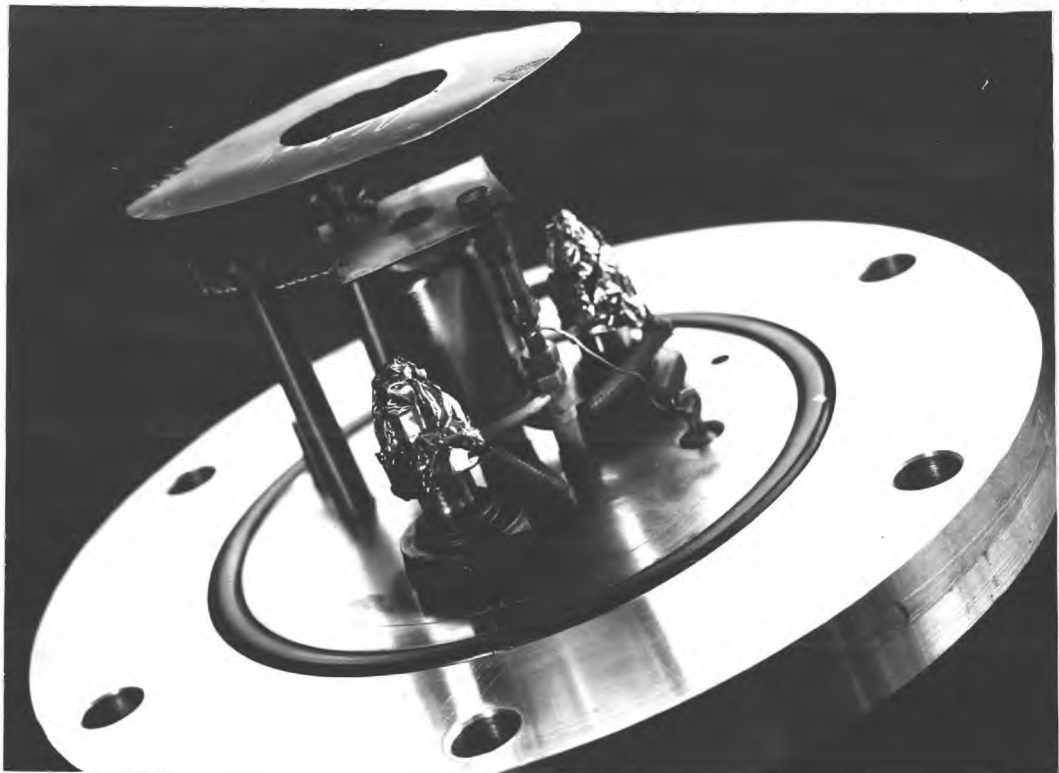### ARE ATTACHED TO ARMS ORTHOGONAL TO THE PLANE OF THE DIAGRAM).

TARGET ELECTRODE (-VE)

GLASS SHIELD

MAGNET COILS
(WATER COOLED)

ELECTRON
GUN

REFLECTOR
ELECTRODE

SHUTTER
(ACTIVATED BY
FUSE WIRE)

THERMOCOUPLE

SUBSTRATE
HEATER

FIGURE 4.11.

Electron source for low pressure sputtering system.

captured finally by the anode close to the source. The aperture of the anode was deliberately chosen large, approximately 1 inch, so as not to present too large a collection area. With the closure flange earthed the ion current dropped to a low value. The value of the accelerating voltage was limited because of the possible sputtering of electrode materials by positive ions. All H.T. electrodes were shielded but where this was not possible they were covered by tantalum foil, a low sputtering yield material.

The mode of operation was fundamentally the same as for the triode experiments discussed previously. The substrate, suitably mounted, was introduced into the system which was then pumped down to the residual pressure required. This was always $<2.10^{-7}$ torr. If necessary, the substrate was heated and the whole allowed to outgas at a temperature a few degrees above that finally required. The electron source filament was also heated to allow this to thoroughly outgas. After outgassing, the discharge gas was admitted slowly until the required discharge pressure was reached, generally 2×10^{-4} torr, at which point the discharge was struck by applying a suitable magnetic field along the axis of the electron source and a high potential to the filament relative to the anode. The stability of the discharge was a function of the operating parameters, particularly the electron density. The probability of ionisation depends upon the electron density so that the ion current which can be extracted also depends upon the electron density. In order to maintain a constant pressure in the experiments, the primary control of the ion current was the electron current varied by means of the filament current. The electron emission was temperature limited, the accelerating anode potential remaining constant wherever possible, it only being slightly varied to maintain stability. The preferred field was 500V/cm. The magnetic field was constant throughout the experiments at 400oe (i.e. 10A in the coils). This was found empirically to produce a visible ion beam of approximately 2 cm. diameter.

FIGURE 4.12

Variation of ion current with distance from visible ion beam.
Target voltage -1000V, target area 44 cm^2. Magnetic field
400 oe.
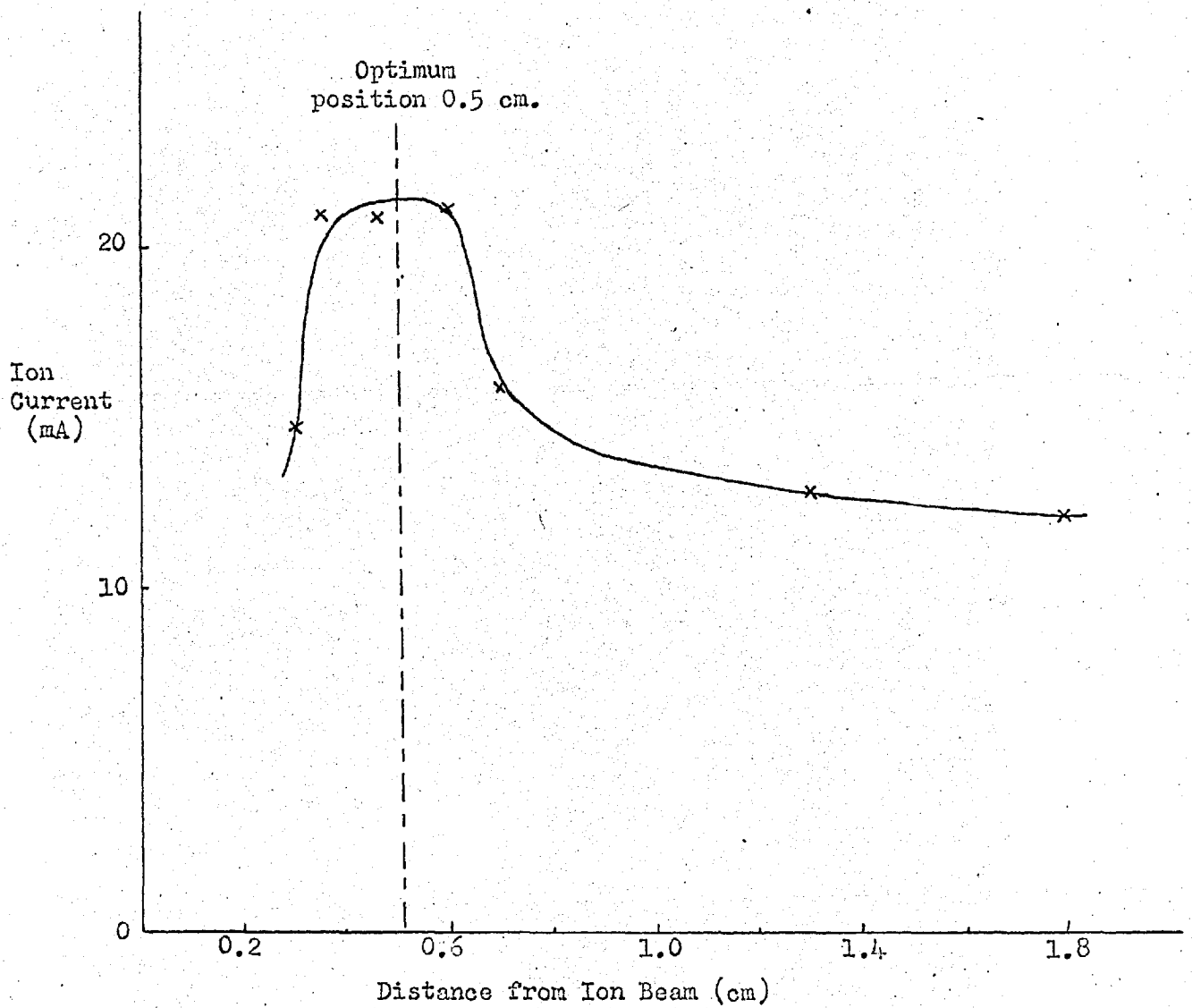
Once discharge and temperature stability had been attained, the target was negatively biased so as to extract ions from the plasma. The substrate shutter remained in position throughout the stabilising process. With a negative potential on the target, sputtering occurs at a rate determined by the ion current density. The ion current density extracted depends upon the discharge conditions and also the relative position of the target to the ion beam. The beam was approximately 2 cm. diameter and Fig. 4.12 shows a plot of ion current density as a function of distance of target from an arbitrary reference point (for varbus target potentials). The optimum target position was selected and maintained for all experiments. In this apparatus a 2.5 cm. target was generally employed and it was assumed that the current density was uniform over its area in all positions. This would not have been the case for a larger target.

As for the previous modes of sputtering, the target was sputtered for a finite time prior to substrate exposure, so that contamination was removed from the surface. The substrate shutter was then actuated to reveal the substrate which was then exposed for a time selected to give a pre-determined thickness. The time was based on previous calibration runs in which the thickness as a function of time was measured. Since, in this apparatus, the shutter was irreversibly actuated, the deposition was terminated by removing the bias from the target. The sub-strate was removed from the system, when it had cooled to $<30^{\circ}C$. The chamber was brought to atmospheric pressure by admitting argon.

The gas throughput of the system during deposition was controlled by the gas inlet and not by the pumping aperture as in the case of diode sputtering.

4.2.4. Evaporation

In order to compare sputtering and evaporation for thin film deposition it was necessary to deposit films of silver under controlled evaporation conditions. A high-vacuum system, custom built by Edwards Ltd. for the Allen Clark Research Laboratory was used for the deposition. A residual pressure of $<10^{-8}$ torr was easily achieved and deposition onto two NaCl substrates vacuum cleaved using a jig designed and reported by Stirland, 1967. Quartz-iodine-lamp substrate heating was employed in the manner described below in Section 4.4.2.2. Rate of deposition was stabilised before cleaving using a disc ratemeter, of a type described by Beavitt (1966). Rate control was by means of evaporant temperature. Evaporation was from a heated tungsten spiral positioned approximately 15 cm from the substrate. Using a shutter system it was possible to cover one substrate while continuing deposition onto the other. Following deposition an overlayer of carbon was deposited in the manner described below in Section 4.5. The substrates were removed from the system when their temperature had fallen to $25^{\circ}C$ and the system had been brought to atmospheric pressure by the introduction of air.

4.3. SUBSTRATE PREPARATION

4.3.1. Germanium

The material was provided as 1" diam. 178μ thick discs of n-type unpolished germanium. These were mechanically polished to $<\frac{1}{4}\mu$ diamond finished and ultrasonically degreased in iso-propyl alcohol. They were placed in position in the triode system which was then evacuated to $<2 \times 10^{-6}$ torr. The substrate temperature was then raised to $600^{\circ}C$ and held at this value for 5 minutes in order to remove oxide layers from the surface. Argon was then admitted to a pressure of 1.5×10^{-3} torr and a

discharge struck. Further cleaning of the substrate was thus accomplished by bombardment for 5 minutes. Following this cleaning process the substrate temperature was lowered to the required experimental value.

4.3.2. Mica, CaF$_2$ and NaCl

Fresh air-cleaved surfaces of these substrates were employed. The mica was cleaved using two strips of adhesive, one on either side of a sample which were then pulled apart to reveal a fresh surface. Alternatively, where small areas were required, cleavage was achieved using a pointed instrument to separate layers. Surfaces which had visibly obvious cleavage steps were rejected. Calcium fluoride, which cleaves on a (111) plane, was cleaved with a sharp blade, similar conditions for surface selection applying. Sodium chloride substrates were also prepared by cleaving with a sharp blade to reveal a fresh (100) crystal face. The energy required to cleave the NaCl substrates was considerably less than that required for CaF$_2$. Vacuum cleaving was also employed on NaCl in some experiments. These are detailed in the next chapter and the technique was to break a pillar of NaCl by means of a hammer. The exposed surface was relatively free of steps.

4.3.3. Single Crystal Sapphire (Al$_2$O$_3$)

Slices of sapphire ~1mm. thick were cut to give a (1$\bar{1}$02) face. These were highly polished to $<\frac{1}{4}\mu$ diamond finish mechanically, and ultrasonically degreased in iso-propyl alcohol. Bombardmet cleaning in the apparatus was also employed.

4.3.4. Glass

These substrates, used for monitoring purposes, were of borosilicate glass and were cleaned in a soap-solution followed by deionised water and iso-propyl alcohol.

4.4. SUBSTRATE TEMPERATURE CONTROL AND MEASUREMENT

4.4.1. Introduction

In all the experiments control of substrate temperature was essential as deposition temperature was an important parameter in the structural and electrical properties of the films.

In the case of diode sputtering there is a significant contribution to the substrate temperature from the discharge itself. A typical discharge power was 30W, capable of producing a temperature rise of 50°C in 30 mins. sputtering. Whether heating or cooling was required depended upon the power input to the system and the sputtering temperature required. A typical heating curve shown in Fig. 4.13 demonstrates schematically the possible requirements of an experiment. If temperature T_1 is required heating of the substrate is necessary throughout, but if T_2 is the required temperature cooling is required after an initial heating period. Generally the initial period was that during which the discharge stabilisation and target cleaning was carried out. The third temperature condition T_3 shows that cooling is required from the outset.

The same applies in the case of triode sputtering where the power input to the discharge in some cases exceeded 100W. Generally fairly high substrate temperatures were required so that heating was required throughout. In the case of low pressure sputtering, however, the power input to the discharge was only $\sim$5W and was confined to a narrow ion beam. Since the substrate was well outside the beam the contribution to substrate temperature was negligible.

4.4.2. Substrate Heating

Various types of heater were employed, the major prerequisite being that outgassing should be minimal. The following types were those used most extensively :

FIGURE 4.13

Schematic plot of Substrate Temperature as a function of
Sputtering Time for some arbitrary input power. T1, T2
and T3 are possible experimental substrate temperature
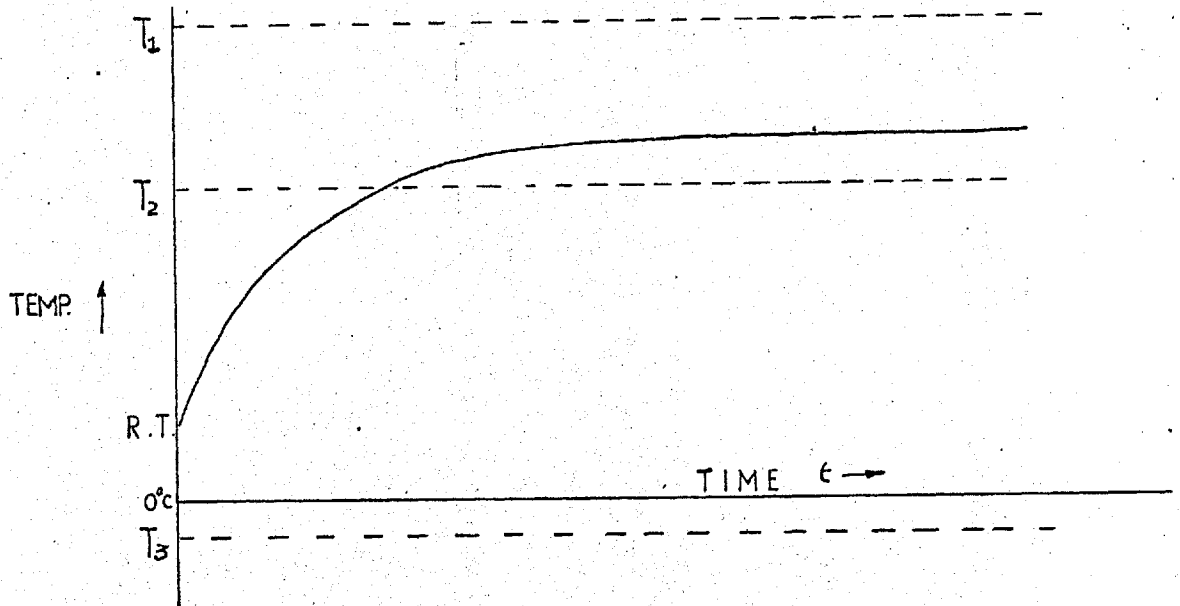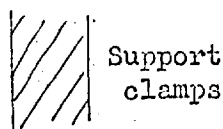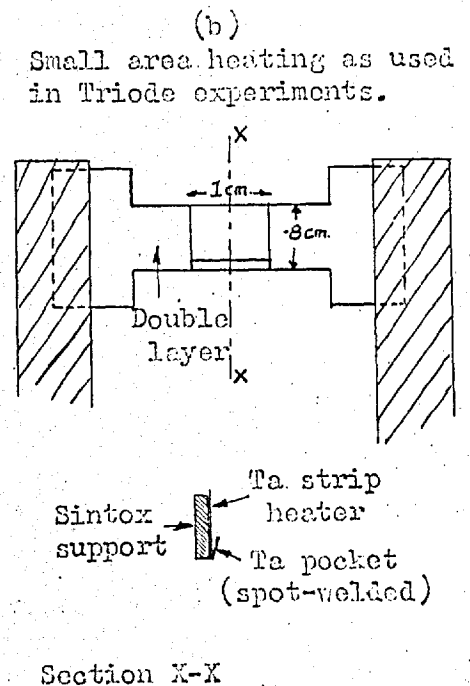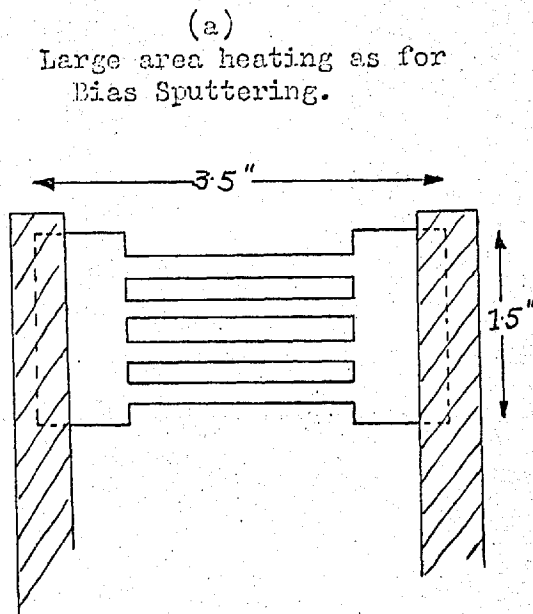requirements.

FIGURE 4.14

Two types of Tantalum strip heater used in the sputtering
experiments.

(a)
Large area heating as for
Bias Sputtering.

(b)
Small area heating as used
in Triode experiments.

Section X-X

4.4.2.1. Ta Strip Heaters

The heaters were of two main types.

a) Those which heated a substrate mounting, and

b) Those which doubled as a substrate mounting and heater.

The first type is illustrated in Fig. 4.14(a). This was designed to give uniform heating to a temperature of $\sim 250°C$ of an auxiliary table outlined in the figure. The system was primarily designed for bias sputtering and the table could be biassed independently of the main anode. The material used was .004" Ta with a double thickness at each end.

The second type of heater which was used for the deposition of Ge films in the triode system took the form of a Ta strip of thickness .004", width 1 cm. and "hot region" length 1 cm. The substrate was mounted directly onto this strip which to give rigidity was backed by a tile of Sintex 2.5 cm. x 1 cm. x .15 cm. The heater is illustrated in Fig. 4.14(b). The substrate temperature attainable using such a system was in excess of $700°C$.

Both the above types required outgassing for some time after installation.

4.4.2.2. Quartz Iodine Heaters

The use of Ta heaters was satisfactory from most aspects but where minimum outgassing was required as in the case of low pressure sputtering they were not so suitable. For this purpose quartz iodine lamps of the type used in projectors etc. proved very adequate. They had the advantage of being very clean, of requiring little power and of rapid interchangebility. Their radiated heat could also be quite readily focussed. Using a system of the type shown in the photograph of Fig. 4.15(a) temperatures of around $450°C$ could be achieved for a power input of $\sim 100W$. The arrangement shown in the figure was used in the low pressure system. An alternative system

FIGURE 4.15(a)

Quartz-iodine substrate heater with focussed reflector.

Substrate support

Shutter (fuse-wire operated)

Quartz-iodine projector lamp

Focussing reflector

Glass tubing
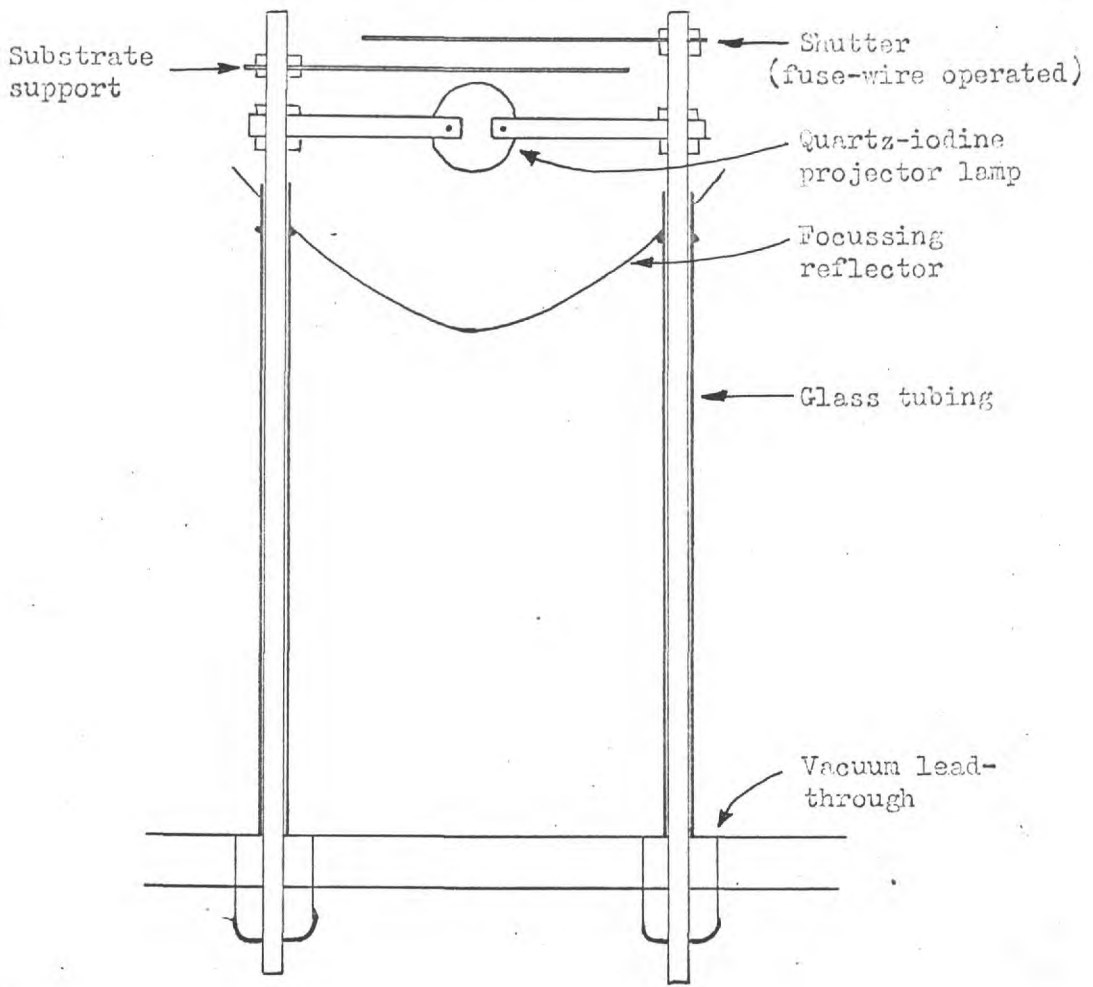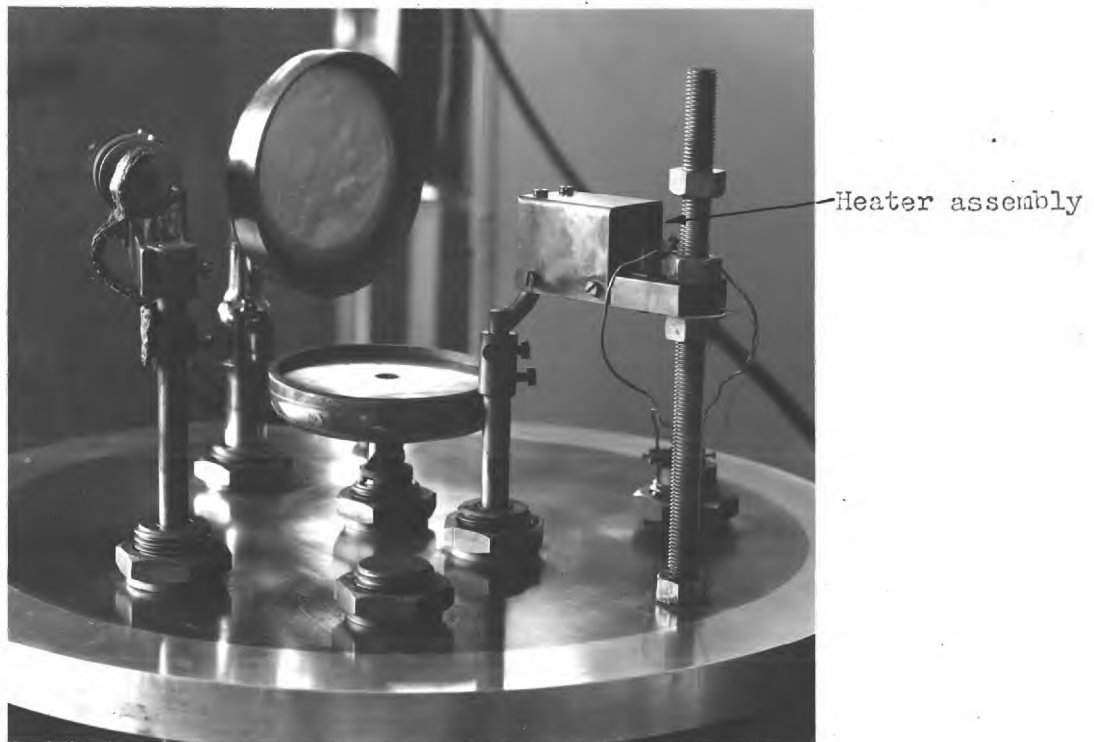
Vacuum lead-through

FIGURE 4.15(b)

Quartz-iodine substrate heater as used in Triode system.

Heater assembly

as used in the triode system during nucleation density measurements is shown in Fig. 4.15(b).

4.4.3. Substrate Cooling

One of the difficulties associated with heating or cooling a substrate is that of thermal contact. This is particularly so in the case of cooling when a constant heat source surrounds the substrate. The thermal contact between substrate and heat sink (coolant) is then of great concern. An exaggerated view of the situation is demonstrated in Fig. 4.16 The gaps must be filled with a conducting medium or a large proportion of the cooling capacity is lost. Several methods were employed as described below.

4.4.3.1. Cooled Mounting Methods

a)   Careful polishing of the cooled substrate mount. Not particularly successful since the substrate (NaCl) itself is stepped so that contact is not ensured.

b)   Filling the gap with vacuum grease. Rather messy and though all right in principle it was found difficult to remove air included in the grease.

c)   Pressure contact. This is unsatisfactory since only the area immediately under the pressure point attains a low temperature.

d)   Floating on a pool of mercury. This met with reasonable success and temperatures of -150°C were achieved on the substrate surface when liquid N_2 was passed through the cooling plate. The technique was to form a pool of mercury in a containing well and to float the substrate in this pool. On evacuating and cooling the plate on which the mercury pool resided, the pool froze with the substrate embedded in its surface. The drawback to the technique was that Hg

is a rather unwelcome contaminant in a sputtering system since it readily reacts with aluminium, gold etc. Its contamination effect was noticed markedly in a pair of experiments carried out at low temperature and the technique was, therefore, abandoned.

4.4.3.2. Total Enclosure Method

The alternative method of reducing the substrate temperature is to reduce the emission from surrounding surfaces. By totally enclosing the substrate, therefore, by a box whose temperature is low the desired result is achieved. Since the emitted radiation from a surface varies as T^4, a reduction to 77°K reduces the radiant heat by 200. A simple experiment in which the substrate was placed on a liquid nitrogen cooled plate and enclosed by an aluminium box resting on the cooled plate, showed that a substrate temperature within a few degrees of 77°K could be achieved.

Such a system as that described above cannot be employed for sputtering since the top of the enclosure must be open to allow deposition onto the substrate. Also the presence of a metal box would upset the discharge distribution. The technique therefore adopted was to totally enclose the whole sputtering assembly within a cooled vessel. A drawing of the assembly is shown in Fig. 4.17. It consisted of a stainless steel thin walled cylinder to which was brazed a close-wound copper coil. The bottom of the 'can' was spot welded to the cylinder and the substrate support and heater assembly was attached to this by way of insulated bushes of Pyrophyllite. The target was similarly attached to the top closure which was a push fit to the cylinder. The substrate support was a Ta strip which could be heated and the substrate temperature was controlled by adjustment of the heater current and the flow rate of liquid nitrogen was supplied under pressure ($\sim$5 p.s.i.) from a 25 l. vessel by way of a low thermal conductivity seal as shown in the figure. Using this

FIGURE 4.16

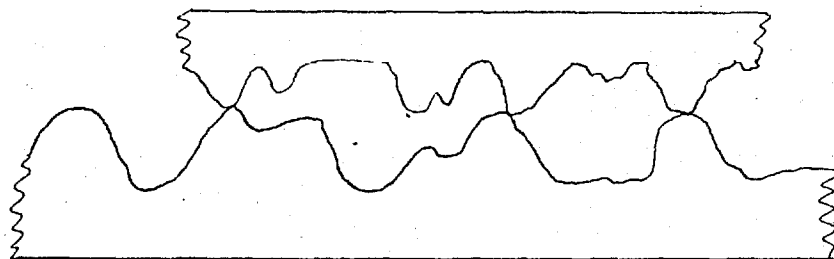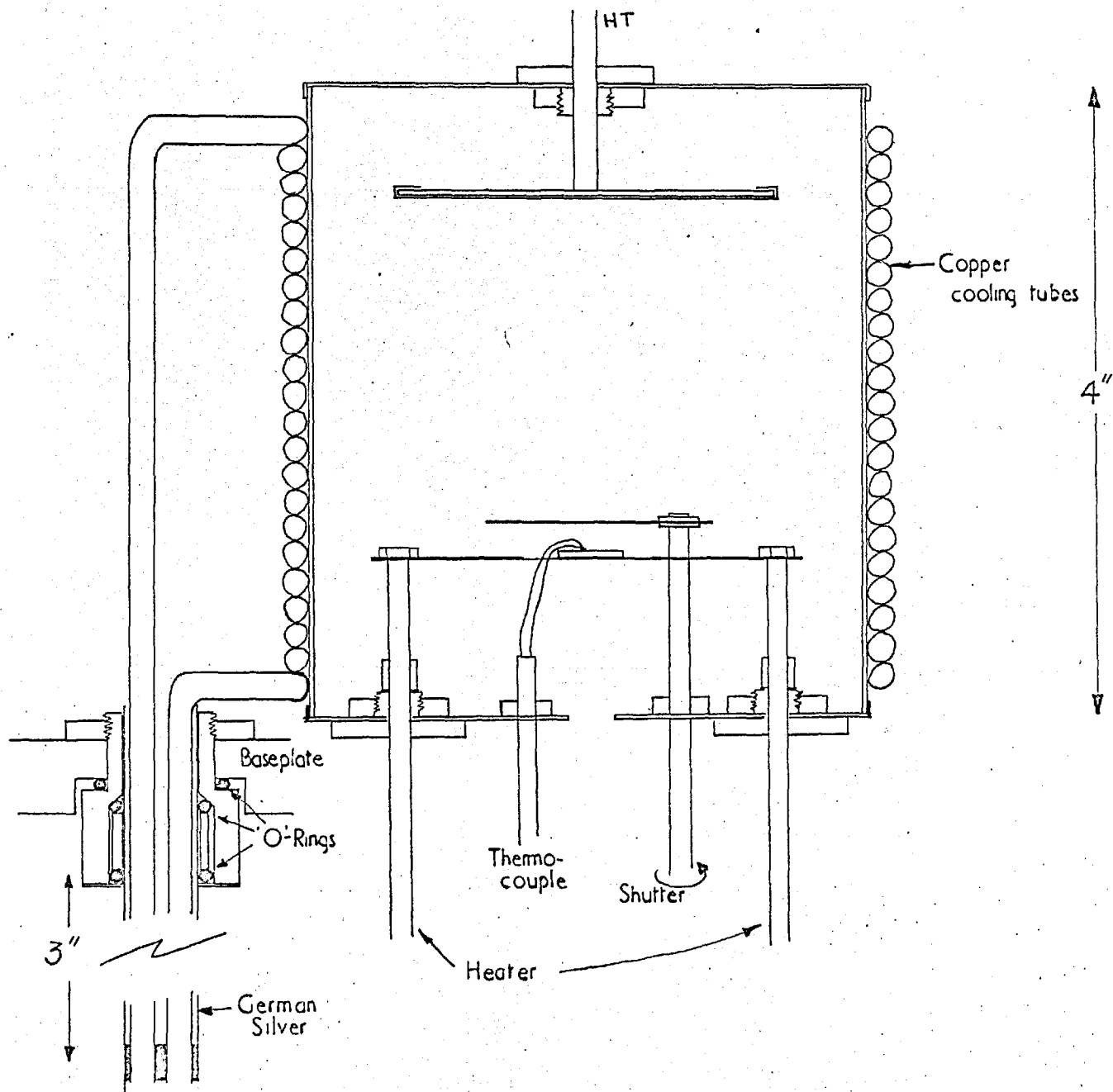Exaggerated view of contact between substrate and flat support.

FIGURE 4.17

Low Temperature Enclosure used for Diode Sputtering in the range -60°C to +25°C.   (Not to scale)

system experiments over the range -60°C to room temperature were carried out. The time lapse required to attain a steady substrate temperature was ~30 mins. from beginning nitrogen flow. Temperature could generally be maintained to $\pm$0.5°C near room temperature and $\pm$1°C near -50°C. In this assembly the target diameter was ~4 cm. and the target-substrate separation 8 cm. The pressure in the inner vessel was assumed to be the same as in the surrounding chamber. The rate of deposition as a function of current is shown in Fig. 4.18. Such a determination was made on a series of calibration runs using glass substrates. Measurement of thickness at temperatures from -50°C to +20°C showed the variation to be within the measuring accuracy of the instrument ($\pm$30Å).

In operation, temperature stability of the substrate was attained, in the presence of the discharge, before exposing the substrate. Film thickness was maintained the same for each experiment so that the deposition times were varied according to the rate curve given in Fig. 4.18. After deposition, the assembly was allowed to return to room temperature before removing the substrate.

Deposition at temperatures above 25°C were carried out in the normal diode system described earlier. A few experiments were carried out in the low temperature enclosure, employing heating only, and these were found to produce similar results to the normal system.

4.4.4. TEMPERATURE MEASUREMENT

In all the experiments, thin wire thermocouples were employed. Where the thermocouple was required to be springy in order to hold the substrate in place, as in the case of triode sputtering of Ge, Chromel/ Alumel was used. For low temperature work or for other instances where a very small contact area was required, Pt/Pt - 13% Rh was employed. The

FIGURE 4.18

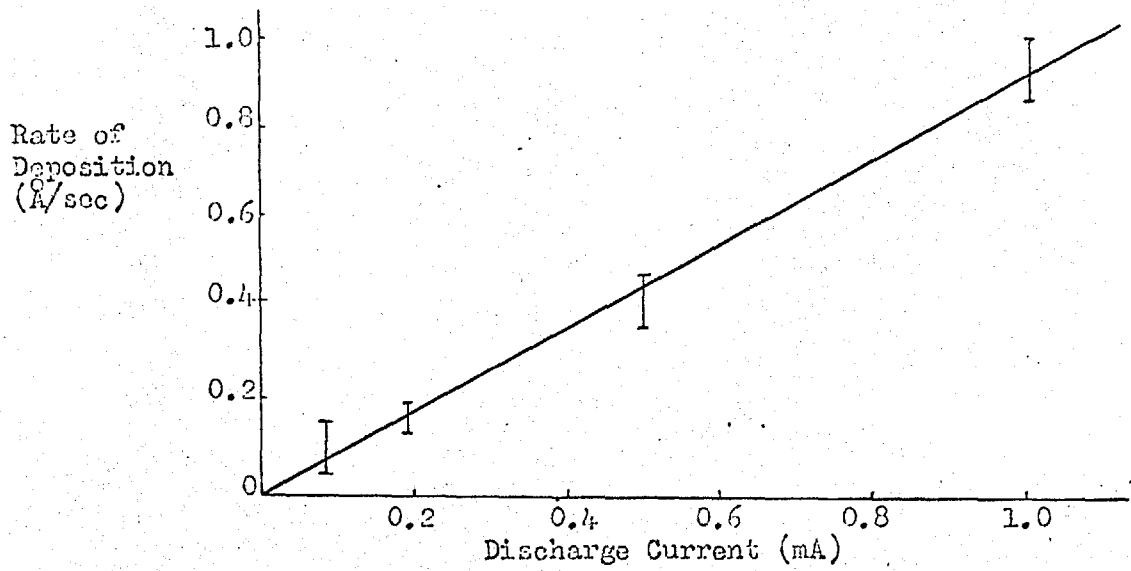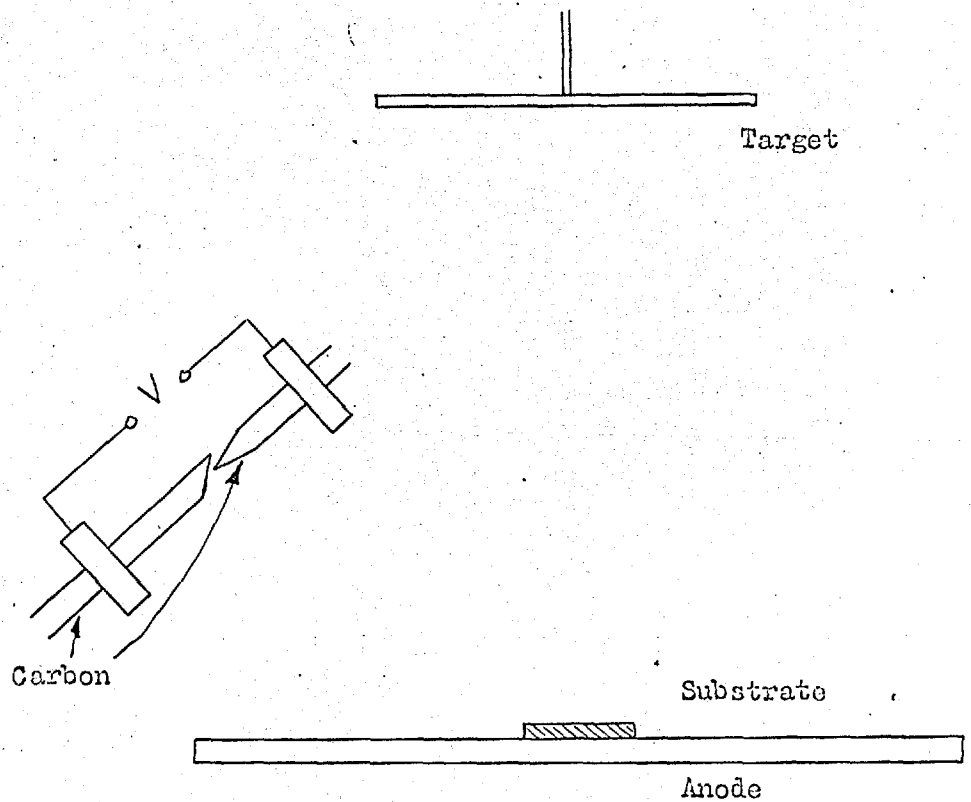Rate of Deposition as a function of Discharge Current for the Low Temperature Enclosure. (Target voltage— -3kV)

Rate of
Deposition
$(\overset{o}{A}/sec)$

Discharge Current (mA)

FIGURE 4.19

Schematic of the Carbon Evaporation jig used for Overlayer Deposition onto very thin Sputtered films.

Target

Carbon

Substrate

Anode

couples were formed by spot or ball-welding and were accurate to ±1°C.
Absolute temperature is not so important, however, as the reproducibility
of temperature conditions. The cold junctions were at ambient temperature
measured with a mercury thermometer. For determining the couple potential,
a potentiometer was used, measuring to an accuracy of 10µV. For the
measurement of high temperatures a temperature indicating millivoltmeter
was employed, accurate to ±10°C compared against the potentiometer.

4.5. OVERLAYER DEPOSITION

In cases where the deposited films were very thin, it was nec-
essary to deposit an overlay in order to support the film for examination
in the electron microscope. The most common method is to evaporate a layer
of amorphous carbon over the entire film to a thickness of ∿150Å. Such a
film does not systematically affect the electron beam and allows full
examination of the initial film. This technique was employed where nec-
essary in these experiments and a diagrammatic representation of the jig
for a simple case of diode sputtering is shown in Fig. 4.19. Shielding
of the source from the target was essential to prevent contamination of
the target.

In one series of experiments it was required to deposit an overlayer
of nickel rather than carbon and this was carried out by replacing the
carbon source by a heated tungsten spiral. The spiral was loaded with
nickel wire and on heating the nickel was evaporated onto the substrate.
Rate of deposition was not critical and was ∿15Å/Sec. Shielding of the
target from the evaporant was again important.

4.6. THICKNESS AND RATE DETERMINATION

The apparatus used to measure the film thickness was a Talysurf
surface probe. The principle is illustrated in Fig. 4.20 and typical

FIGURE 4.20

Principle of operation of Talysurf surface profile
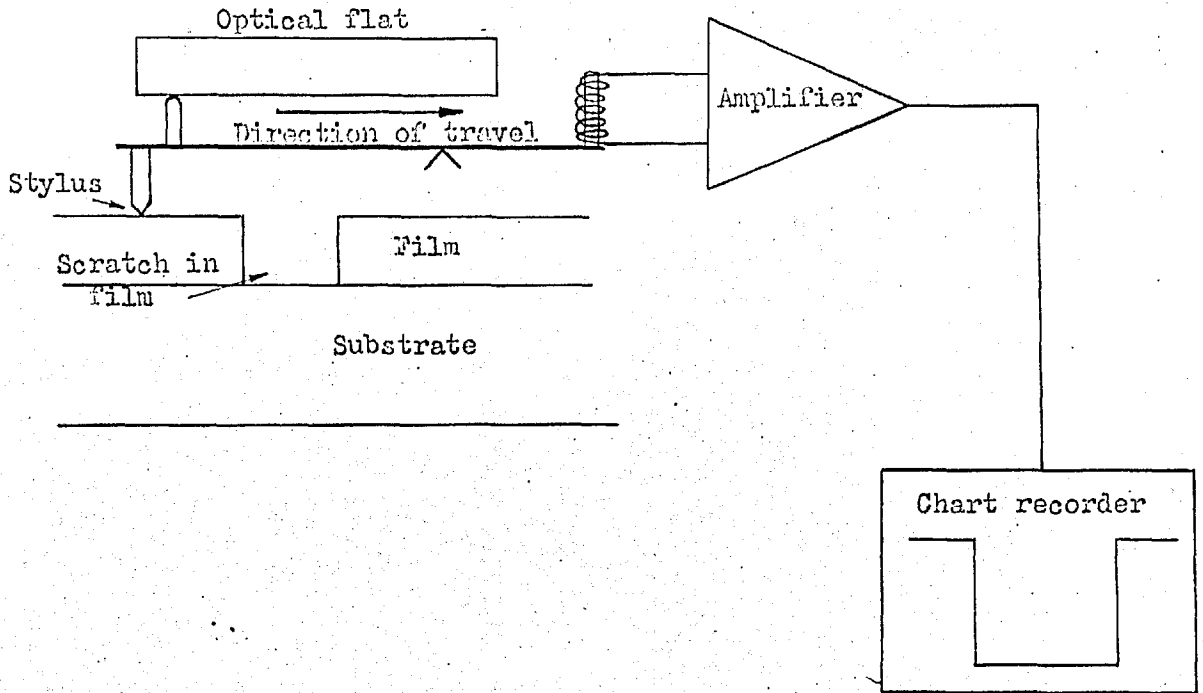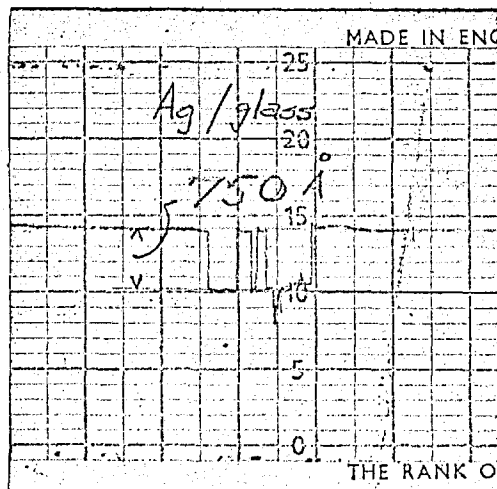measuring instrument.

FIGURE 4.21

Typical surface profile obtained from a scratch in a
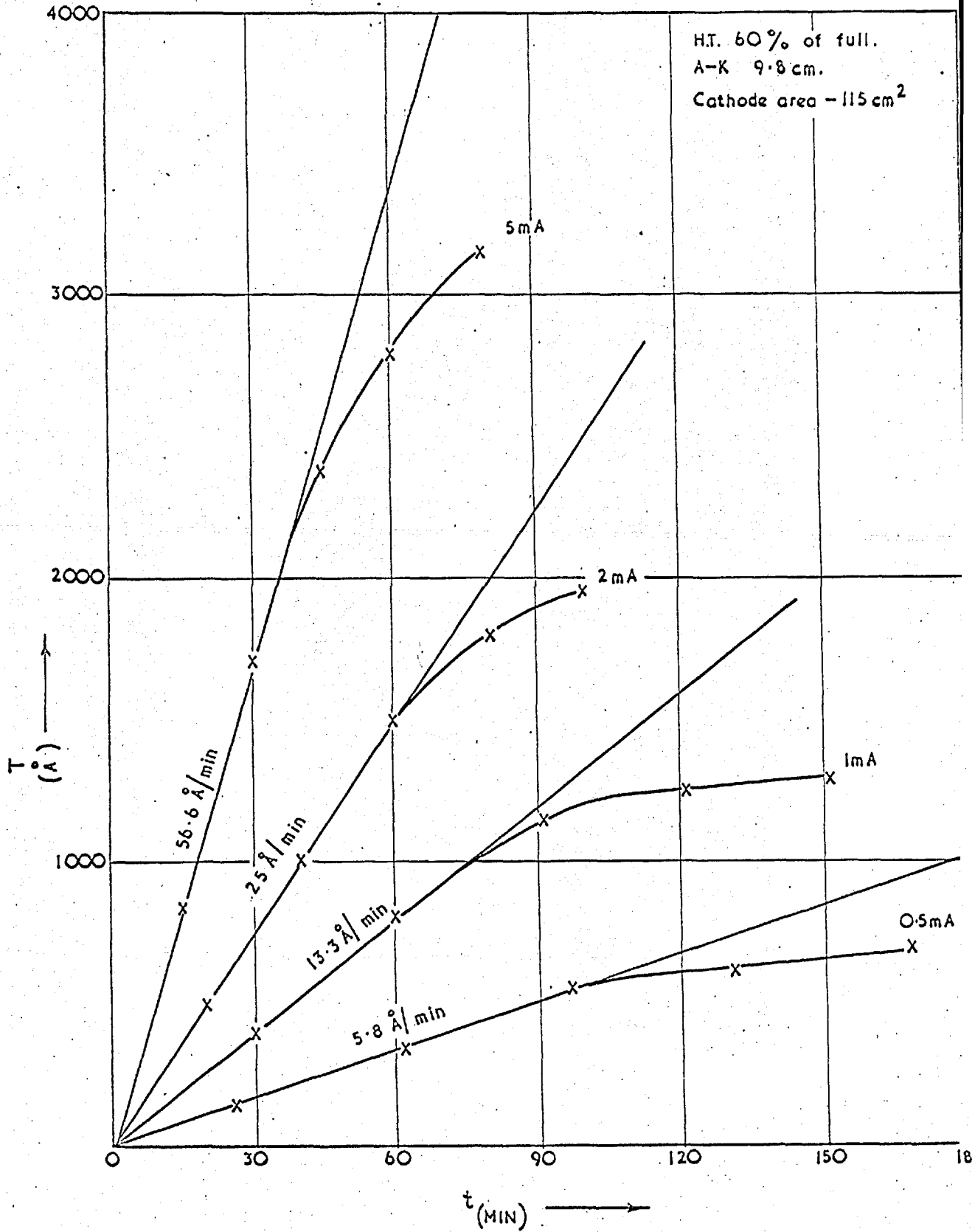silver film grown on a glass substrate.

surface profile traces are shown in Fig. 4.21. The trace is derived by detecting and amplifying an out-of-balance current in an a.c. bridge. The probe stylus is attached by way of a lever to the slug core of an inductor and the movement of the core varies the inductance and hence the current. The accuracy claimed for the instrument is $\pm20\overset{o}{A}$ (Campbell & Blackburn 1961) though the accuracy in practice was determined by the thickness of the drawn line. The reference for the surface probe was an optical flat. Calibration of the instrument is by way of prepared standards.

The method was to produce a step in the film over which the stylus could traverse. In the case of soft films on hard substrates (e.g. Ag on glass) scratches could easily be made in the film to produce the step. For harder films, which could not be scratched readily, the technique was to mask off a part of the substrate thus producing a step. In cases where the substrate was itself easily scratched, e.g. NaCl, mica, measurement of thickness was totally unreliable. In such cases thickness was determined from a film grown, either concurrently or during a similar experiment, onto glass. It is realised that such a method assumes equal condensation co-efficients for each type of substrate but for thicker films ($\geqslant 200\overset{o}{A}$) on which the measurements were made, the assumption is probably valid since it involves deposition of like on like. A plot of thickness as a function of time for silver films on glass in the diode system is shown in Fig. 4.22. The divergence from linearity at the extremes of the curves was thought to be due possibly to charge effects in the film. Experiment proved this to be partly true. However, all subsequent experiments, operated on the linear part of the curves. Rate of deposition was, therefore, determined by the division of total film thickness by total deposition time. Extrap-olation to lower thicknesses was assumed linear. The rate of deposition is proportional to the ejection rate from the target which is in turn dependent upon the number of incident ions, i,e. total current.

FIGURE 4.22

THICKNESS $(T)/$ TIME (t) CURVES FOR Ag SPUTTERED ON GLASS SUBSTRA

H.T. 60% of full.
A-K 9·8 cm.
Cathode area — 115 cm^2

5 mA

2 mA

1 mA

0·5 mA

56·6 Å/min

25 Å/min

13·3 Å/min

5·8 Å/min

T $(\overset{\circ}{A})$

4000

3000

2000

1000

0   30   60   90   120   150   18

t (MIN)

CHAPTER V

RESULTS OF STRUCTURAL STUDY

5.1. INTRODUCTION

This chapter documents the results obtained from films sputtered onto various substrates under a variety of conditions. Films were grown in one-off experiments except in the case of the study of film structure with thickness where sequential deposition was employed in a single run. Results of evaporated silver films grown for island density measurements are also given.

For the case of semiconductor films, only the structural results are described in this chapter. The galvanomagnetic properties of the films are given in Chapter 7.

The first part of the work, on metallic films, concentrated on the parameters influencing epitaxial growth. In the light of such investigations and following the energy distribution calculations detailed in Chapter 3, attention was turned to the more practical aspect of semiconductor films.

5.2. METALLIC FILMS

The material chosen for deposition was silver. Being an f.c.c. metal its crystal structure was of a simple nature and well understood and recognisable. Its orientation effects have been fairly extensively studied by evaporation techniques. The material was obtained as fine foil (.004" thick) silver from Johnson Matthey and was attached to the cathode using conducting epoxy resin (silver-loaded Araldite). For the gold experiments .005" foil of 99.98% purity was obtained.

5.2.1.   The Variation of Crystal Structure with Substrate Temperature and Rate of Deposition

Films were grown in the diode system, the mode of operation being as described in Chapter 4. Water cooling of the target was not necessary at the power levels employed. The rate of deposition was varied over the range 0.02Å/sec. to 2.0Å/sec. and the substrate temperature varied from -40°C to +80°C. Initial experiments carried out at around +30°C showed the films to be epitaxial. This fact determined that further experiments should be carried out at much lower temperatures. Determination of epitaxial temperature per se, i.e. the temperature below which the film is disoriented and above which it is oriented, is impracticable and unrealistic. The purpose of these experiments therefore was to span, as widely as was reasonable, the epitaxial temperature.

The results are shown in Figure 5.1, which is a plot of the deposition rate, R Å sec^{-1} as a function of the reciprocal of the absolute temperature. The points are plotted to represent the deposition conditions and the resultant film crystallinity. A boundary region may be drawn on the plot on one side of which the films were found to be epitaxial whilst on the other side the films were polycrystalline in nature. The films studied in this experimental series were all 200Å - 500Å in thickness. As in the case of evaporation, the conditions for epitaxy are low deposition rate and/or high substrate temperature. It is evident, however, that the substrate temperature required for a given rate to produce epitaxy is considerably less than that required for evaporated films. This is shown by comparison with the results of Sloope and Tiller on similar films grown by evaporation, shown by the straight line in Fig. 5.1. The slope of these lines and the possible implications are discussed in the next chapter.

FIGURE 5.1

The orientation dependence of Diode sputtered Silver on Rocksalt as a function of deposition rate and substrate temperature. Film thickness 200-300Å.
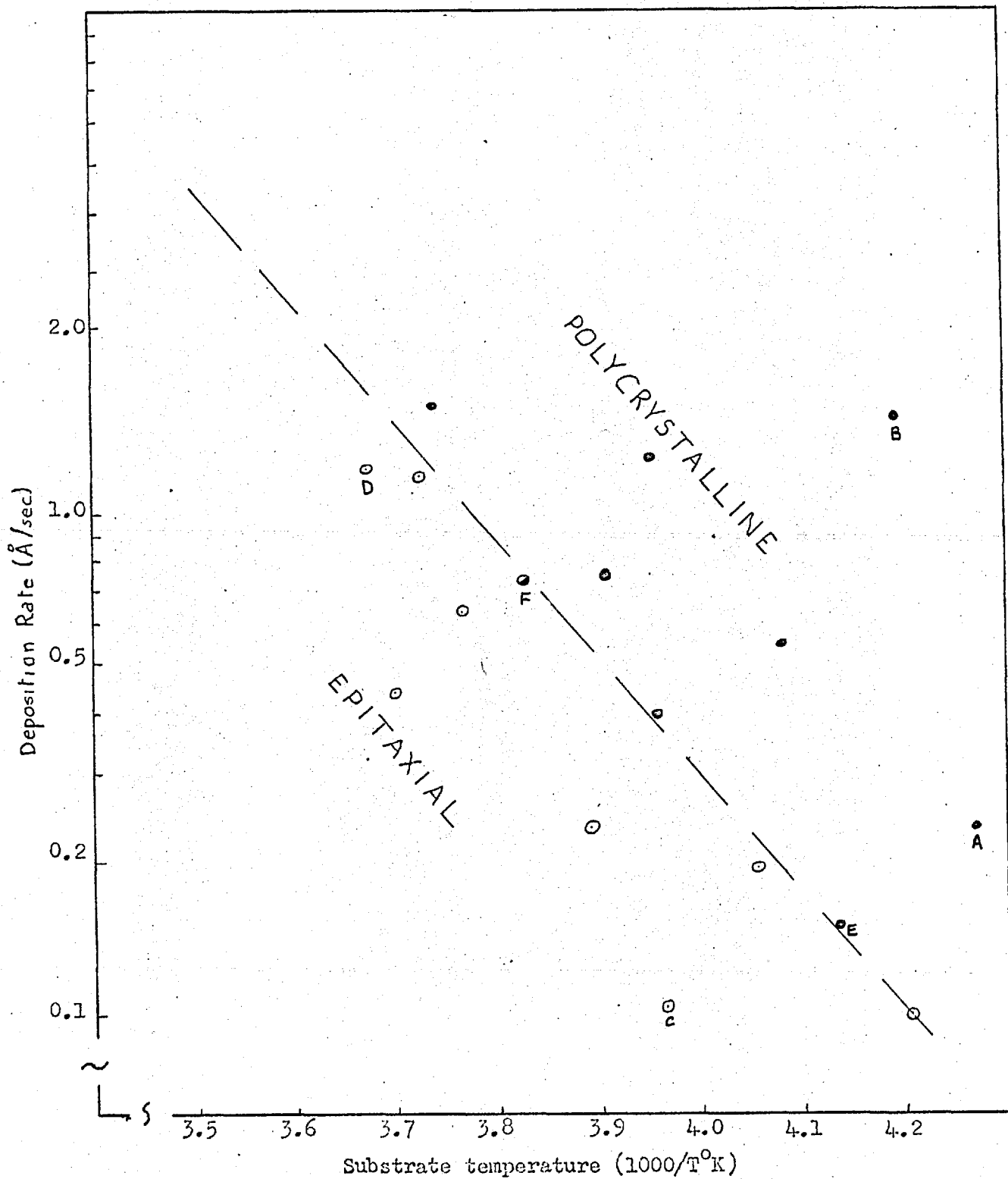
In Figures 5.2 - 5.7 are shown micrographs and diffraction patterns giving
rise to the points A - F in Fig. 5.1. The micrographs for each film are
very similar and are therefore shown for one or two films only. The diffraction
patterns were obtained by selected area diffraction at an electron energy
of 100 keV. Figure 5.4(b) is a low magnification micrograph showing Bragg
contrast contours. These indicate the extent of the perfection of the film
since the extinction required to produce these can only result from constant-
phase diffraction. The electron diffraction results shown in the figures
indicate the orientation changes and the difficulty in assessing the orient-
ation when close to the boundary conditions.

5.2.2. The Variation of Crystal Structure with Film Thickness

In order to investigate the variation of structure with thickness it was
necessary to produce films of varying thickness during the same pump-down
cycle. This required the use of a special type of shutter as described in
Chapter 4.

The rate of deposition was chosen initially to be 0.25Å /sec. which would
yield an epitaxial 200Å film at $>250°K$ as shown in Fig. 5.1. Deposition
times of $\frac{1}{2}$, 2 and 8 minutes to give nominal thickness values of 7, 30 and
120Å. Following deposition of the silver, carbon was evaporated over the
surface so that the films could be examined in the microscope.

The results of the initial experiments with carbon backing only, are shown in
the micrographs and diffraction patterns in 5.8. - 5.10. These show that 7Å
and 30Å films were made up of discrete islands virtually circular in shape
and reasonably uniform in distribution. Use of these results is also made in
the island density experiments described later. The diffraction patterns
clearly show an increase in the degree of orientation with increasing thick-
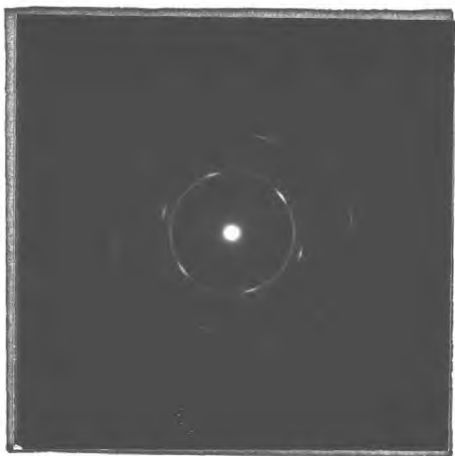ness..

Fig. 5.2(a) D.P. Point A in
Fig. 5.1.
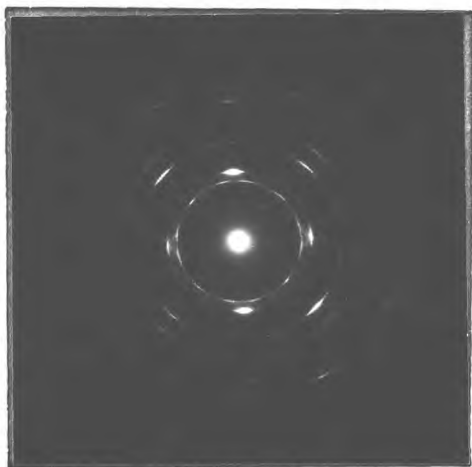

Fig. 5.2(b) Electron micrograph.
Magnification 20000x.
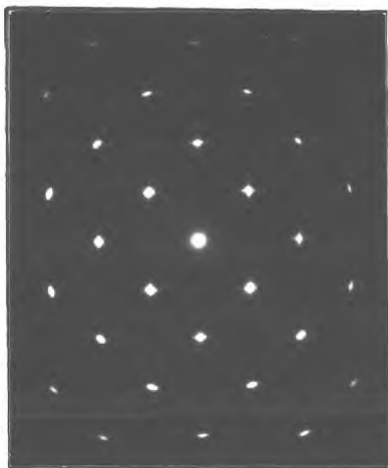

Fig. 5.3. D.P. Point B in Fig. 5.1.
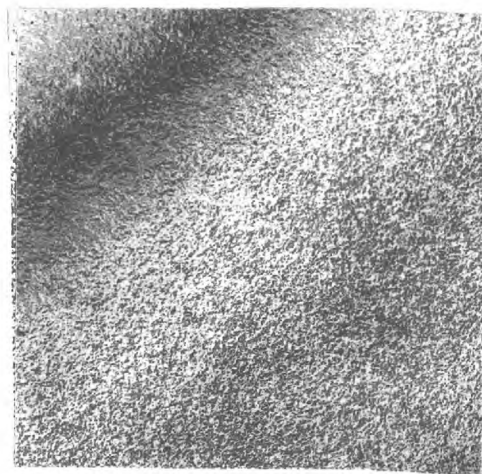

Fig. 5.4(a) D.P.
Point C in Fig. 5.1.

Fig. 5.4(b) Electron micrograph.
Mag^n. 4000x.

Fig. 5.2 - 5.4 Ag/NaCl prepared by diode sputtering. Growth conditions
as indicated.

Fig. 5.5(a) D.P.
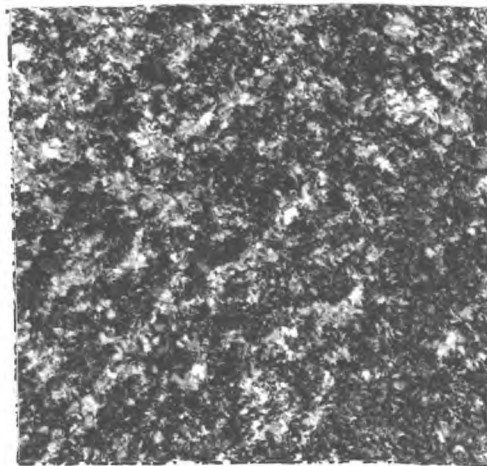   Point D in Fig. 5.1.

Fig. 5.5(b) Electron micrograph.
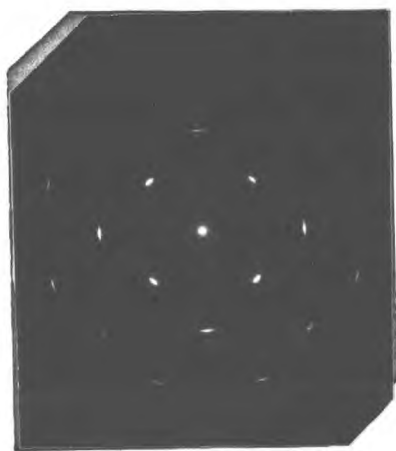   Mag^n. 20000x.

Fig. 5.6. D.P.
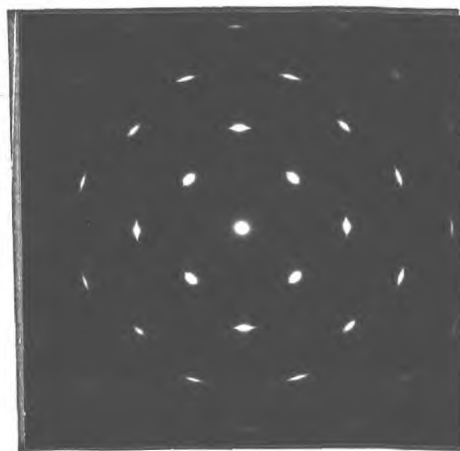   Point E in Fig. 5.1.

Fig. 5.7. D.P.
           Point F in Fig. 5.1.

Fig. 5.5. - 5.7 Ag/NaCl prepared by diode sputtering. Growth conditions
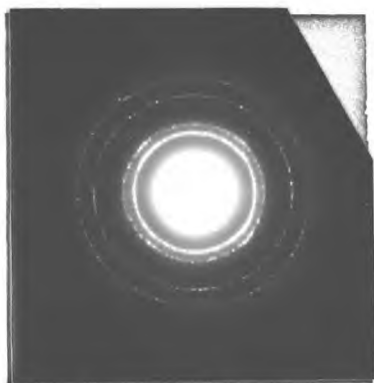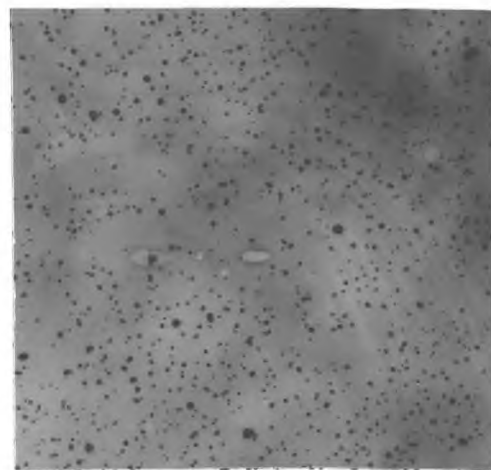as indicated.

Fig. 5.8(a) D.P.
Thickness 7Å

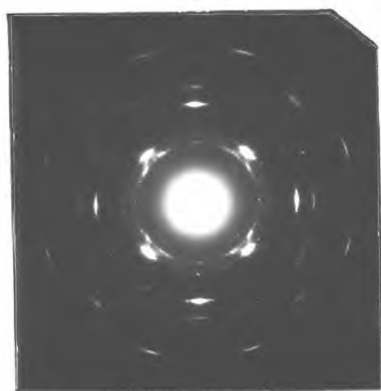Fig. 5.8(b) Electron micrograph.
Mag^n. 20000x.
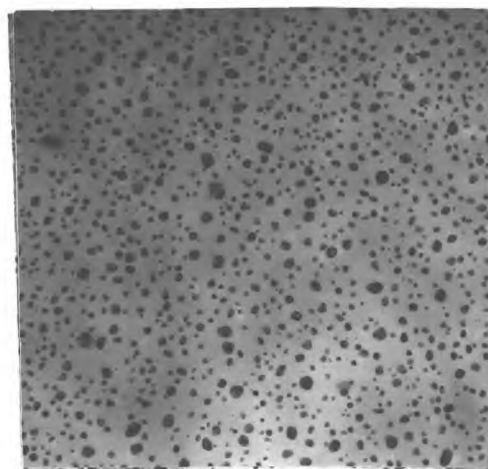Thickness 7Å

Fig. 5.9(a) D.P.
Thickness 30Å

Fig. 5.9(b) Electron micrograph.
Mag^n. 20000x.
Thickness 30Å.
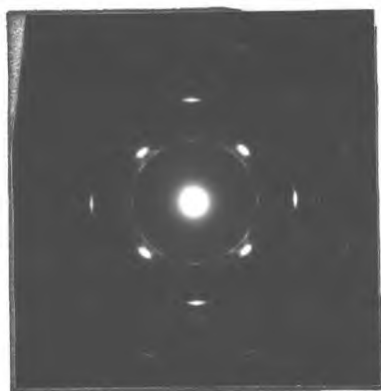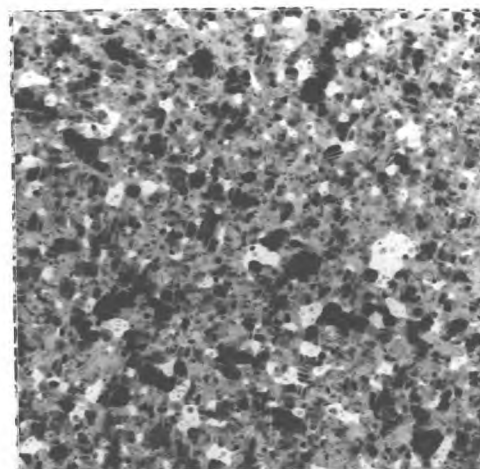

Fig. 5.10(a) D.P.
Thickness 120Å

Fig. 5.10(b) Electron micrograph.
Mag^n. 20000x.
Thickness 120Å

Fig. 5.8 - 5.10 Ag/NaCl prepared by diode sputtering. Carbon backing only. Thickness as indicated. Rate 0.25 Å/sec. Temperature 300°K.

Matthews (1963) has found a similar effect in evaporated films of gold on rocksalt and he explains it in terms of rotation of the smaller crystallites with respect to the larger ones so as to be in parallel or twin orientation with them.

In order to check whether crystallite rotation during the stripping operation or even loss of crystallites during the same process, (Stirland 1966), was responsible for the observed effects, a layer of nickel was evaporated over the silver. This has the effect of fixing the silver in position after deposition so that subsequent rotation is prevented. Films of silver were deposited at 0.12Å sec^{-1} to produce layers of 7Å to 115Å. The lower rate was due to the introduction of the nickel evaporation jig, and did not alter the purpose of the experiment. The jig was approximately 5cm. from the substrates and evaporation of 150Å at $\sim 30\text{Å}$ sec^{-1} was found sufficient. Following Ni evaporation an overlayer of carbon was evaporated though this was not strictly necessary.

The results of the nickel-backed experiments are shown in the micrographs and diffraction patterns of Fig. 5.11 a - d. The micrographs consist almost entirely of nickel as would be expected. It is interesting to note, however, that the nickel island size tends to increase with increasing silver thickness, suggesting that the nickel would prefer to nucleate on a silver rather than a rocksalt surface. A similar effect has been noted for nickel overlayers on CuMn films (Campbell - Private Communication). In the micrograph of 5.11(b) the dark spots are due to contamination which could not be identified. The dark-field image shown in Fig. 5.11(c) was obtained by placing the objective aperture over a (220) silver spot; no tilting of the electron gun was employed so in consequence the image-forming beam was not axial through the lens system. This gives rise to streaking of the bright spots on the dark field micrograph, due to lens aberration. These spots are those silver
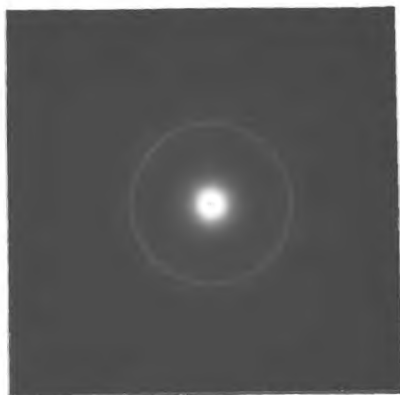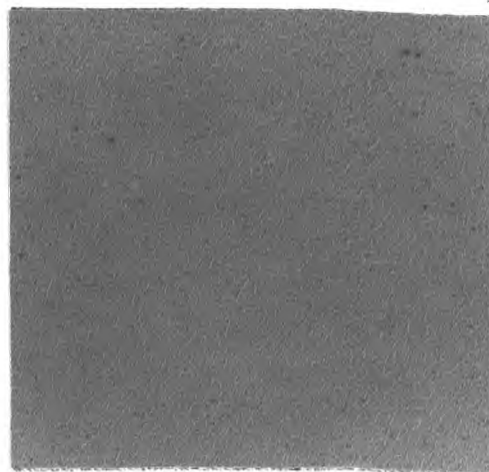
D.P.   Electron micrograph. Mag^n. 20000x.

(a) Thickness 7Å
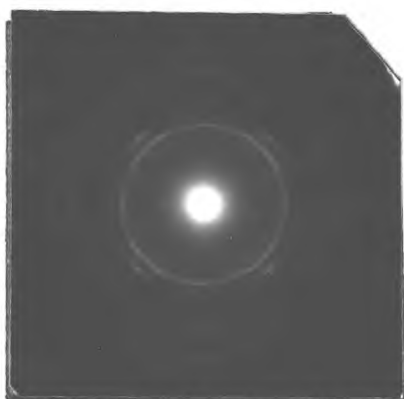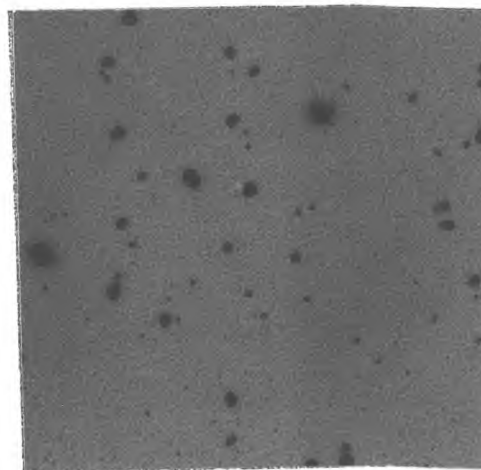
D.P.   Electron micrograph. Mag^n. 20000x.

(b) Thickness 14Å

Fig. 5.11(a) and (b) Ag/NaCl prepared by diode sputtering. Nickel
overlayer followed by carbon. Silver deposition rate 0.12Å/sec.
Temperature $\sim$300°K. Nickel rate $\sim$30Å/sec, thickness $\sim$150Å. Silver
film thickness as indicated.

D.P.
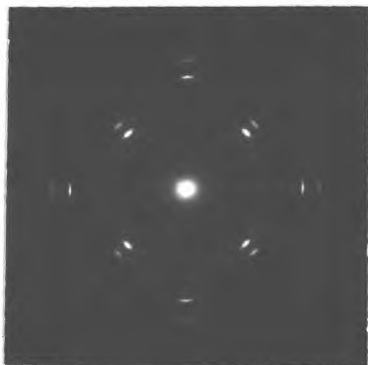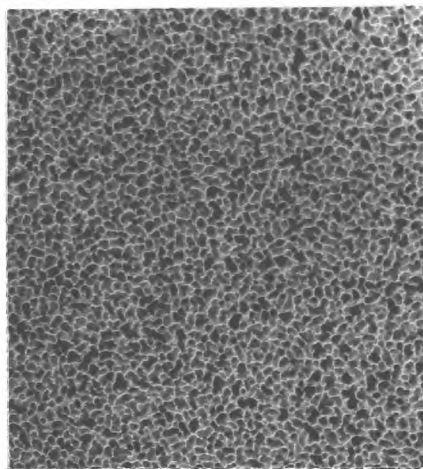
Electron micrograph.
Mag^{n}. 20000x.
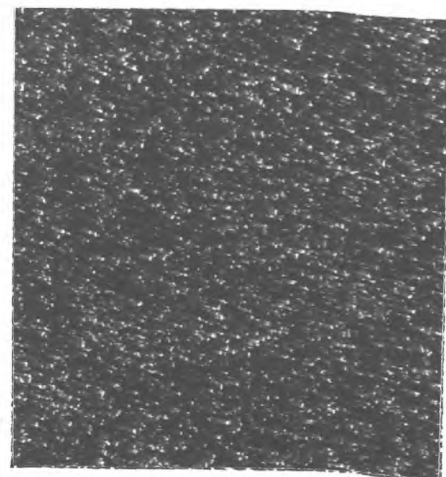
Dark field electron
micrograph of same area.

(c) Thickness 58Å

D.P.
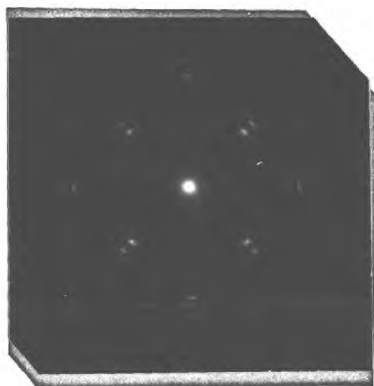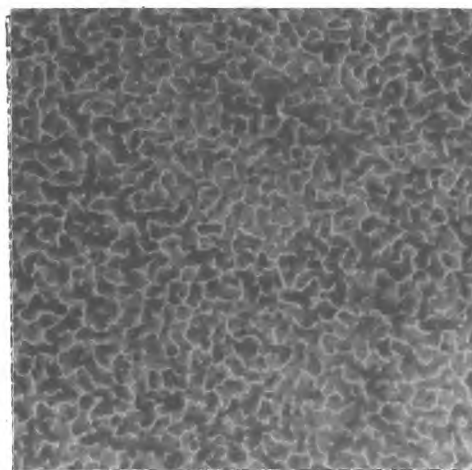
Electron micrograph. Mag^{n}. 20000x.

(d) Thickness 115Å

Fig. 5.11(c) and (d). Ag/NaCl prepared by diode sputtering. Nickel
overlayer followed by carbon. Silver deposition rate 0.12Å/sec.
Temperature ~300°K. Nickel rate ~30Å/sec, thickness ~150Å. Silver
film thickness as indicated.

crystallites whose planes are contributing to the (220) diffraction spot chosen and they give an indication of the distribution of the silver on the surface. At lower thicknesses there was insufficient silver to give a suitable image.

The diffraction patterns associated with these micrographs are composite, consisting of silver and nickel. As silver has the larger lattice parameter, its reciprocal lattice vector will be smaller. Both materials are f.c.c. so that the two patterns are identical except for spacing. Owing to the ratio of lattice parameters it so happens that the reciprocal lattice radius of the (200) silver group is the same as that for (111) nickel. It is thus not easily possible to identify characteristics from the (200) silver spots unless there are no (111) nickel spots or rings present,i.e. unless the nickel is perfectly epitaxial. The (220) silver ring, however, is not obscured by nickel. Observing this ring, it can again be seen that there is a marked increase in the single crystallinity of the silver deposit with increase in thickness. It is also observed that the orientation of the nickel overlayer follows that of the silver. At increasing thickness, a spot pattern emerges for the silver deposit. This can be seen clearly in the case of the (220) spots and also for the (200) spots, which can be identified by the presence of streaking from the primary diffraction spots at (200) to the double diffraction spots on the (111) silver ring. At the highest thickness in the series, 115Å, a completely single crystal pattern is observed. From the micrographs of the thinner films in this series, there is no evidence of "graininess", as was observed for the carbon only films. This may suggest that particles were being lost in the latter case, during the stripping operation.

The implications of these results will be discussed in the next chapter, but the mechanisms which may lead to the effect have been discussed earlier in Chapter 2.

5.2.3. Bias Sputtering

In the experiments from which the above results were obtained, the substrate was placed on the anode, whose potential was zero, i.e. earth potential. There is thus no bombardment of the substrate by positive ions. Maissel and Schaible (1965) however, observed an increase in the purity of sputtered tantalum if a negative bias was applied to the substrate during deposition. It was proposed that the resultant bombarding ion beam removed contaminant oxygen from the substrate surface, thus decreasing the probability of formation of tantalum oxide. On the basis of this hypothesis, it was thought likely that, since clean conditions have been found by many observers to be influential in promoting epitaxy, bias sputtering should enhance epitaxial growth.

The apparatus used was that described in the previous chapter (Section 4.2.1.2.), in which the substrate surface was strapped to a negatively biassed auxilliary electrode by way of an evaporated gold land and a phosphor-bronze clip. The bias was varied in 100V steps from zero to -300V. The deposit material chosen for this experiment was gold rather than silver. The use of silver would have necessitated cooling of the substrate at the deposition rate employed. The effect with gold was expected to occur at temperatures above room temperature, since the epitaxial temperature for gold at the rates employed is some $100^{\circ}C$ above that for silver. The rate of deposition employed was 0.42Å/sec., determined from calibration experiments as described in Chapter 4. The substrate temperature for each series was varied from $25^{\circ}C$ to $120^{\circ}C$, and the film thickness was kept approximately constant at 250Å.

The results of the experiment are shown in Fig. 5.12a - d, which is a series of selected area diffraction patterns for films grown at $80^{\circ}C$ at varying bias potential.
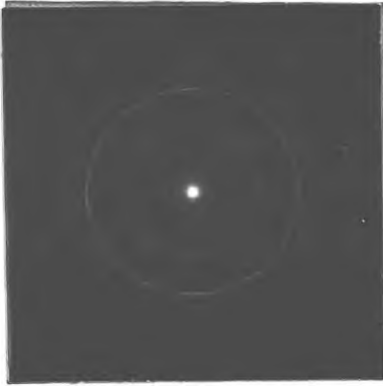
(a) Bias potential 0V
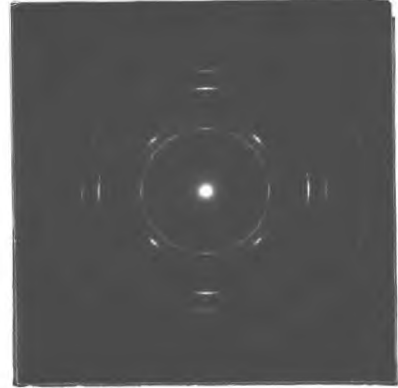
(b) Bias potential -100V
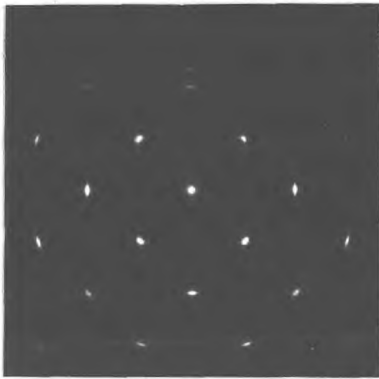
(c) Bias potential -200V

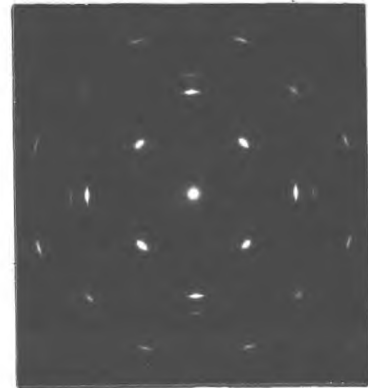(d) Bias potential -300V

Fig. 5.12 Au/NaCl prepared by biassed diode sputtering. Film thickness 250Å. Substrate temperature 353°K. Rate of deposition 0.42Å/sec. Bias potential as indicated.

The results clearly show that the application of a bias potential changes the orientation of the deposit. Whereas the film grown at zero bias shows very little preferred orientation, that grown at -100V bias is highly preferred. For a bias of -200V the film is virtually epitaxial, arcing of the spots only becoming apparent for the higher index planes. It is observed that application of a higher bias (-300V) shows a trend to disorder again. In this case it is thought that physical damage to the growing film is induced by the energetic ions. At -200V the energy is thought to be insufficient to damage. The energy may be sufficient to re-arrange or to clean the substrate. This is discussed more fully in the next chapter. The measured ion current density for these experiments was $\sim 20 \mu A/cm^2$ ($\sim 10^{14}$ ions/cm^2/sec.). The results presented in Fig. 5.12 were observed for each temperature employed, the extent of the effect being slightly varied owing to the contribution of substrate temperature to epitaxy, per se. The substrate temperature required for epitaxy at 0.42Å/sec. with zero bias was not precisely determined, but a film grown at 220°C and zero bias was found to be epitaxial. It should be noted that this temperature is well below that quoted in the literature for epitaxial growth of an evaporated gold film (~ 270°C). This is in keeping with the results obtained for diode sputtered silver.

5.2.4. Island Density Measurements

One of the essential features of the Rhodin-Walton-Lewis theory of nucleation (Chapter 2) is the establishment of, in the early stages of nucleation, a saturation density of islands. As discussed in Chapter 2, this number is a function of nucleation rate and substrate temperature. In order to give an indication of the relevance of this theory to the case of sputtering, it was necessary to perform experiments in which the island density could be established. Since comparison with evaporation was essential, films of silver were grown on rocksalt, as described in Chapter 4. It was necessary to perform these experiments since all the Lewis experimental evidence was for gold on rocksalt.

Films were prepared by evaporation at a constant rate (0.1Å/sec. - the lowest rate compatible with sputtering deposition rate) for 70 and 140 seconds, to give films of nominally 7Å and 14Å. A pair of films of these thicknesses were grown for three substrate temperatures, 65°C, 90°C and 120°C. Time did not allow for a complete plot of island density as a function of time for each temperature. It was assumed that the density was at saturation. Jordan (private communication) had previously found for gold on rocksalt that saturation had been reached by ~10A°.

Similar films were also grown by diode and triode sputtering using the apparatus shown in Fig.4.15b.The diode arrangement was rather unconventional but was used in this way to preserve as nearly as possible the same geometrical arrangement for both triode and diode experiments. The system was calibrated in each case prior to the experiments to give a deposition rate of 0.1Å/sec. The target potential was-1500V. The substrates were vacuum cleaved, and were heated by a quartz-iodine lamp. In the jig used, it was only possible to deposit onto one substrate per pump-down cycle. The deposition time was 120 secs. to give a nominal film thickness of 12Å.

In all the above experiments, carbon was evaporated over the deposits to facilitate electron microscope examination. The island density was obtained by counting an area of the resultant micrograph, at a known magnification. On some deposits, counting was hampered by loss of particles during the film removal process. However, the presence of particles was distinguishable from the depressions left in the overlaying carbon. Wherever possible counts were taken from more than one area of a given deposit, and an average value taken.

The results of these experiments are shown in Fig. 5-13 which is a plot of saturation island density ($\log N_S$) against reciprocal temperature; (c.f. the method of Lewis in Chapter 2). The feature of the results is that there appears to be no difference between evaporated and sputtered deposits, diode

FIGURE 5.13

Variation of saturation island density with substrate
temperature for Ag grown on NaCl by evaporation and by
diode and triode sputtering.
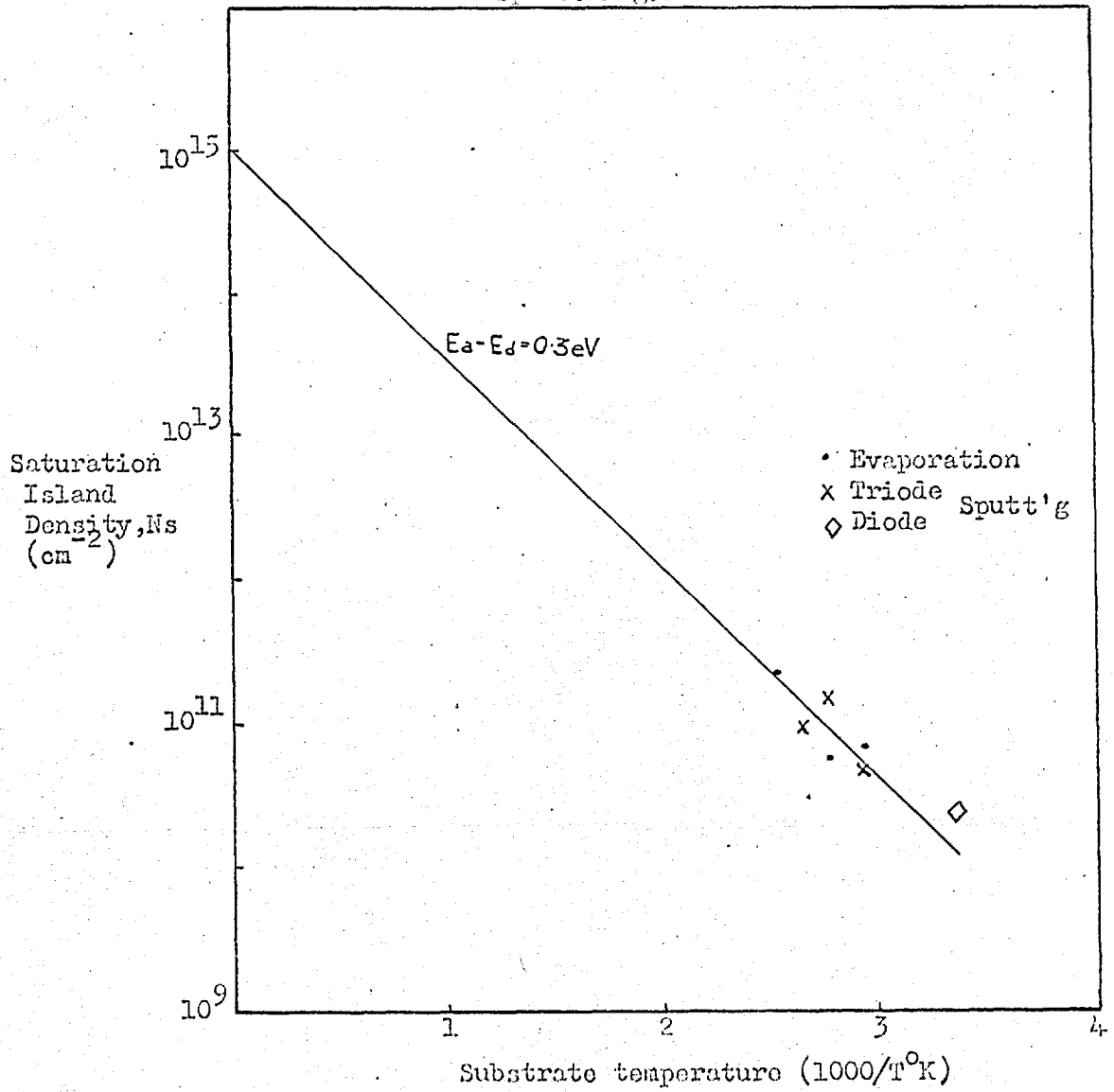
or triode. The points appear to lie on a straight line which passes through $N_S = 10^{15}$ (this is N_O according to the Lewis theory). The slope of the line is 0.3eV, however the slope is fairly insensitive to changes in N_S of an order of magnitude. Also plotted on the graph is a point obtained at room temperature for diode sputtered silver in the experiments designed to study the variation of structure with thickness. The implications of this curve are discussed in the next chapter.

5.3. SEMICONDUCTOR FILMS

The results obtained from sputtering of metals showed that epitaxial films could be grown at low substrate temperatures. The possibility of the extension of this observation to the epitaxial growth of semiconductor films was interesting. Semiconductor devices in which diffusion areas had previously been prepared, would not have those diffusions affected by the overgrowth of an epitaxial layer. Also, if layers of various dopant concentrations could be grown epitaxially at low temperatures, sharp junctions could be prepared. This would prove particularly useful at high frequencies. Present methods of growth, e.g. vapour phase deposition, require high substrate temperatures where diffusion does take place, so precluding sharp interfaces.

The growth of semiconductor films was therefore investigated with the results obtained from the growth of metal films influencing the investigation. The material chosen for the most detailed part of the study was germanium. Attempts were made with silicon, but oxidation proved troublesome in the early experiments. The same trouble did not exist for germanium.

5.3.1. Germanium Films

The germanium target used for the majority of experiments was 7.5cm. diameter disc, 3mm. thick, supplied in polycrystalline form by Haldor Topsoe of Denmark.

The discs were mounted, using conducting epoxy, to a backing plate of aluminium. Water cooling was found not to be necessary at the power levels used except in the case of diode sputtering. The substrates generally employed were either $\langle 111 \rangle$ germanium slices, or $\langle 111 \rangle$ Cr-doped GaAs (semi-insulating). These were prepared as detailed in Chapter 4. Single crystal Al_2O_3, ($1\bar{1}02$) face, was also employed, mainly for electrical investigation but a structural study was also necessary and was therefore carried out. Early investigation in the diode system employed various substrates, as detailed below.

5.3.1.1. Diode-Grown Films

Germanium films were grown by diode sputtering using exactly the same experimental arrangement as was employed for metallic sputtering. A number of films were grown on air-cleaved rocksalt surfaces at temperatures up to 400°C. The deposition rate (determined from a glass monitor slide) was $\sim 0.7\overset{\circ}{A}/sec$. On examination of these films in the electron microscope, they were found to be amorphous with some crystallinity appearing in the films grown at higher temperatures. However, consideration of the vapour pressure of NaCl at the highest temperatures indicated that the loss rate of NaCl from the surface was of the same order as the deposition rate of germanium. Thus deposition was occurring onto a continuously changing surface.

Single crystal calcium fluoride proved to be a more stable substrate and one which had been used by other investigators growing films by evaporation (for example, Sloope and Tiller, 1966). A cleaved $\langle 111 \rangle$ surface was employed and deposition at temperatures ranging from 350°C to 550°C and rates of 0.9 to $1.4\overset{\circ}{A}/sec$. The rates were difficult to measure, either on the substrate or on a quartz monitor and extrapolation from only two successful measurements was therefore made. The resultant films when examined by glancing angle or transmission diffraction showed increasing orientation with substrate temperature; however single crystal films were not observed at the highest substrate temp-

erature employed. This temperature (550°C) was the highest attainable with the tantalum strip heater being used. The results, while not being conclusive, did show the expected trend, i.e. increasing epitaxy with increasing temperature and/or decreasing deposition rate. Figure 5-14 shows the diffraction pattern obtained from a film grown at 515°C and a rate of 1.12Å/sec. The films were generally rather poor in quality and this diffraction shows the best that was obtained.

Since the results of bias sputtering of metal films showed epitaxy to be enhanced by application of a bias, a similar technique was employed for germanium on CaF_2. A bias of - -200V was applied (this being the bias found to be the optimum for the metal films) and films were grown at temperatures ranging from 250°C to 500°C and estimated rates from 0.7 to 1.4Å/sec. The results obtained did not show the dramatic improvement observed for gold or rocksalt. Figure 5.15 shows a series of glancing angle diffraction patterns which indicated an inprovement in the orientation with temperature. The rate was kept constant for this series, i.e. 1.1Å/sec. - the same as for the zero-bias result of Figure 5.14.

The above results, while following the expected trend, were not epitaxial at as low a temperature as was hoped. In view of the calculations described in Chapter 3, it was decided to investigate the deposition of semiconductor films by triode sputtering.

5.3.1.2. Triode-Grown Films

Films of germanium were grown using the triode sputtering technique on (111) and (110) germanium, the cleavage plane of CaF_2, mica, amorphous quartz and single crystal (1$\bar{1}$02) sapphire. The preparation of the substrates prior to deposition, and the deposition technique are discussed in the previous chapter. Since it is difficult to remove the films from the substrates following deposition, glancing angle electron diffraction was used throughout for film examination.
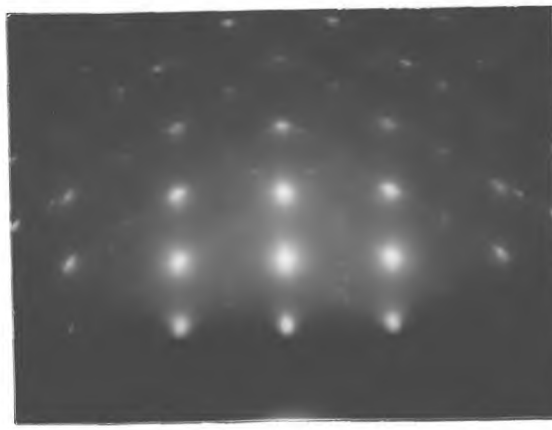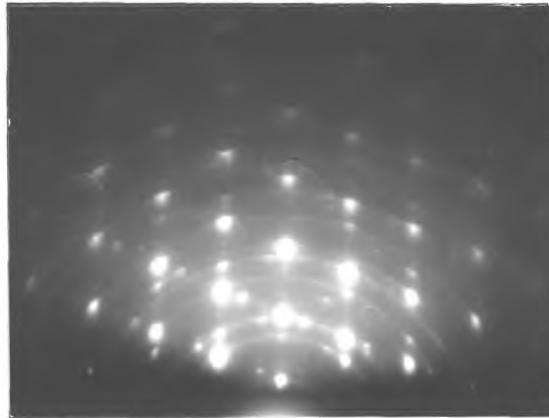
Fig. 5.14. Ge/CaF$_2$ grown by diode sputtering. Deposition rate 1.12Å/sec. Substrate temperature 515°C.

(a) Substrate temperature 295°C

(b) Substrate temperature 410°C

(c) Substrate temperature 490°C

Fig. 5.15 Ge/CaF$_2$ grown by biassed diode sputtering. Deposition rate 1.1Å/sec. Bias potential -200V. Substrate temperature as indicated.

Film deposition at several ion current densities was studied and it was found that the deposition rate in all cases decreased with increasing substrate temperature.

5.3.1.2.1. Ge/(111) Ge

Figure 5.16 represents the results for Ge deposited on (111) Ge for ion current densities ranging from 40 - 300 μA/cm^2, as a plot of growth rate versus substrate temperature. Distinction is also made on the graph between single crystal, polycrystalline and amorphous films, as judged by electron diffraction. A boundary can be drawn between each region as shown, and also between twinned and non-twinned single crystals. These distinctions between the regions of crystallinity are, by their very nature, ill-defined. An exact transition clearly does not occur. The results show, however, that the temperature at which epitaxial films may be grown is rate dependent and is lower for lower rates. The significance of the rate and temperature effects on epitaxy in the triode system is discussed in the next chapter. Typical diffraction results are shown in Fig. 5.17 - 5.20 for Ge or (111) Ge, for four current densities.

The patterns correspond to the points indicated on each growth curve in Fig. 5.16. Some of the results do not show up very clearly in a photographic print, particularly the amorphous stage where the diffraction pattern consists of a very bright central region with two diffuse bright bands fairly close to the centre. The diffraction patterns do, however, clearly show the increase in film perfection with increasing temperature or decreasing rate.

Comparison of the triode results with those from diode or biassed-diode depositions shows that at similar conditions of rate and temperature, the triode-grown films are more oriented. However, more rigorous pre-deposition cleaning of the substrate was employed in the triode experiments.

FIG 5.16

THE GROWTH & ORIENTATION DEPENDENCE ON SUBSTRATE TEMPERATURE FOR Ge FILMS ON <111> Ge SUBSTRATES
FOR VARIOUS ION CURRENT DENSITIES. TARGET POTENTIAL-1500V; TARGET/SUBSTRATE SEPARATION, 5cm TARGET DIAMETER 7·5 cm

● SINGLE CRYSTAL UNTWINNED
○ "   "   TWINNED
△ POLYCRYSTALLINE
□ AMORPHOUS

SUBSTRATE TEMPERATURE °C

GROWTH RATE Å/Sec

40μA/cm²   100μA cm²   200μA/cm²   300μA/cm²
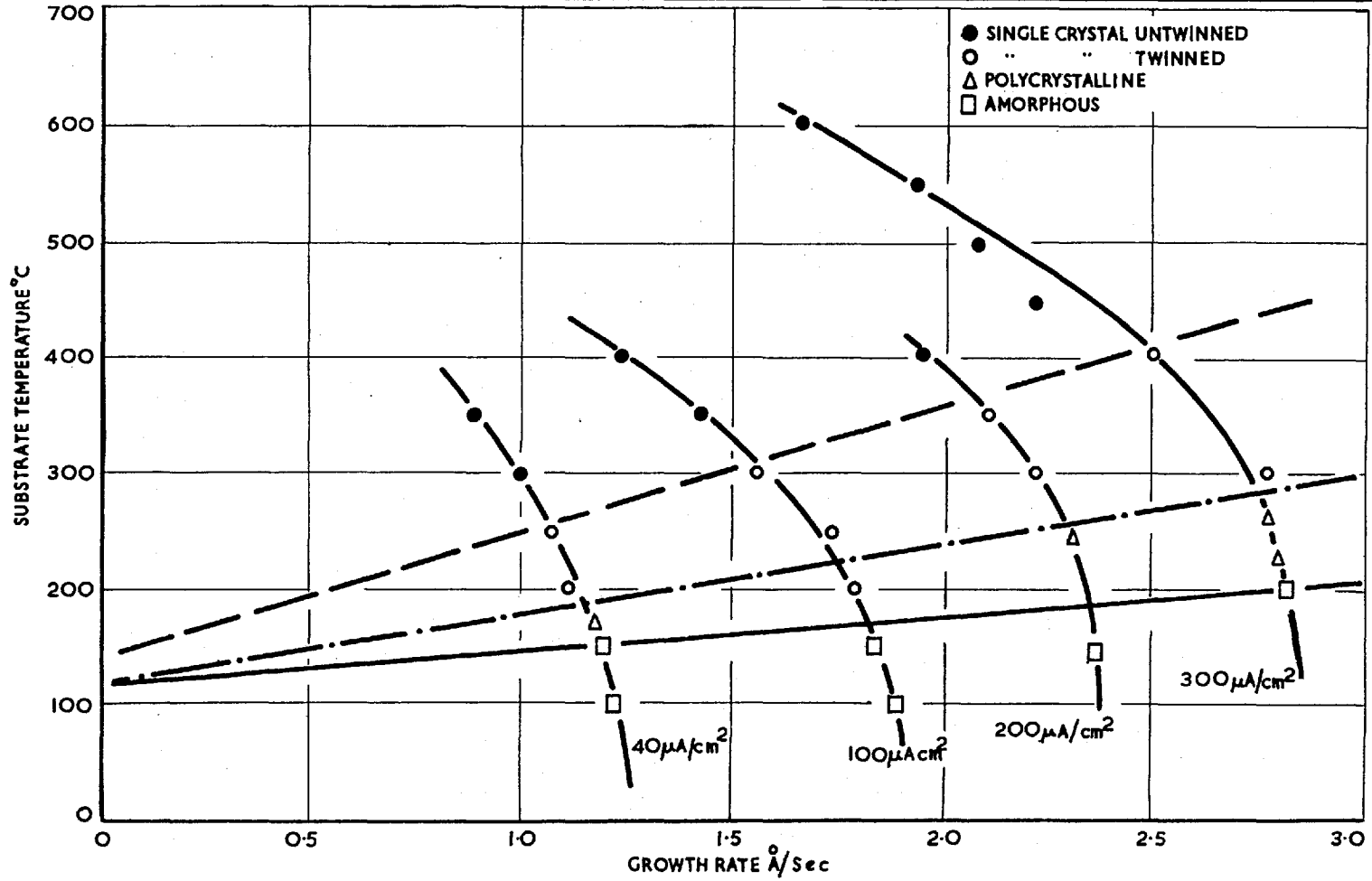
(a) Substrate temperature 150°C
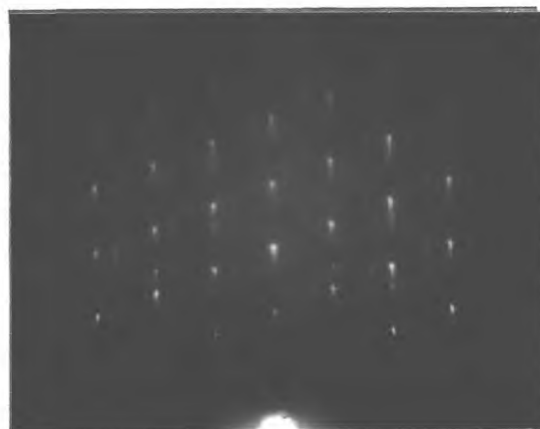
(b) Substrate temperature 200°C
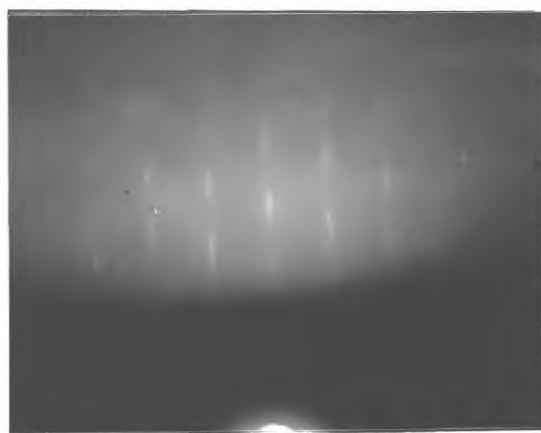
(c) Substrate temperature 300°C
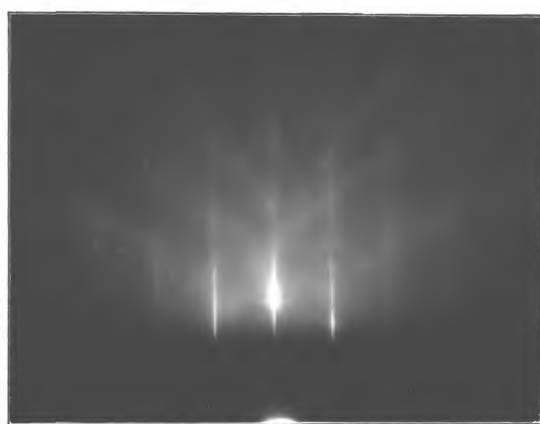
(d) Substrate temperature 450°C

Fig. 5.17 Ge/(111)Ge grown by triode sputtering. Target current density 40 μA/cm^2. Substrate temperature as indicated.
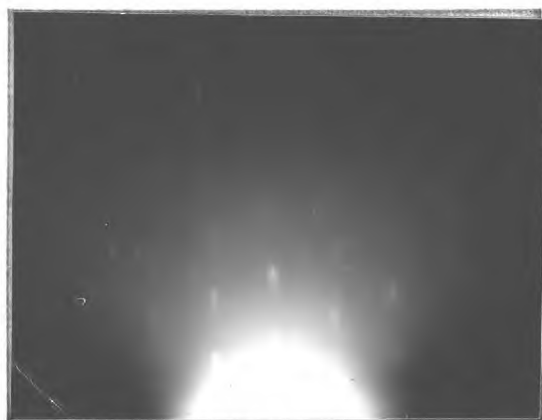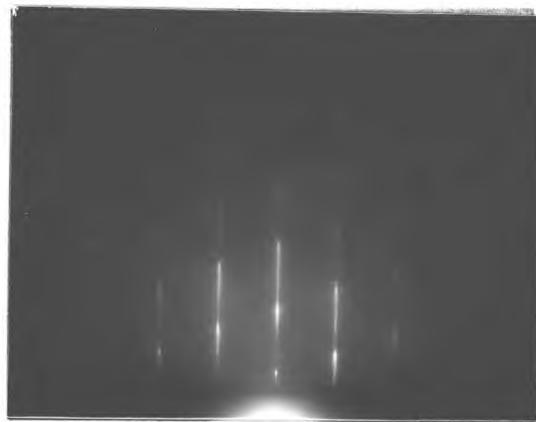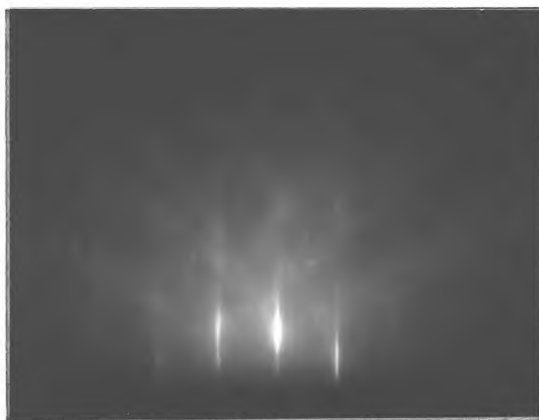
(a) 250°C

(b) 350°C

(c) 450°C

Fig. 5.18 Ge/(111)Ge grown by triode sputtering. Target current density 100 µA/cm^2. Substrate temperature as indicated.

(a) 250°C

(b) 350°C

(c) 450°C

Fig. 5.19 Ge/(111)Ge grown by triode sputtering. Target current density 200 µA/cm^2. Substrate temperature as indicated.

(a) 300°C

(b) 400°C

(c) 500°C

Fig. 5.20 Ge/(111)Ge grown by triode sputtering. Target current density 300 μA/cm^2. Substrate temperature as indicated.
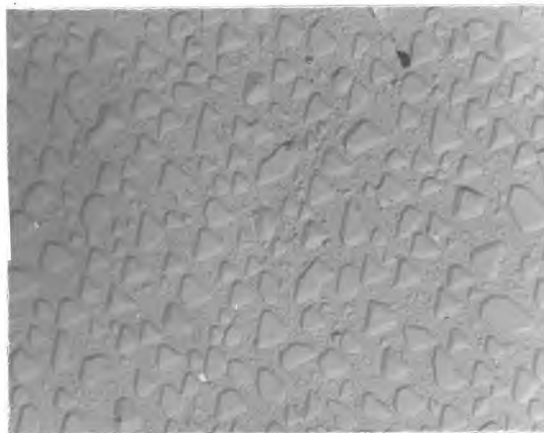
Fig. 5.21. Carbon replica obtained from a Ge film grown at 400°C on (111)Ge at a rate of 1.1Å/sec. Thickness 200Å.

Since it was not possible to remove the film from the substrate for electron microscopic examination, a replica of the surface was made using a Pt/C shadowing technique. This is described in the previous chapter. A replica obtained from a film grown at 400°C or (111) Ge at a rate of 1.1Å/sec. is shown in Figure 5.21. The growth is similar to that observed for silicon grown on silicon by vapour phase deposition (Booker and Joyce, 1966), i.e. large triangular shaped islands. The density of those islands with crystallographic shape is found to be $\sim 5 \times 10^8 \text{ cm}^{-2}$. This is an order of magnitude greater than the highest observed by vapour phase deposition of Si on Si (Joyce and Bradley, private communication). The part of the substrate which was protected from the depositing atoms during growth was observed to be virtually featureless, apart from a few polishing scratches.

The number of replication experiments carried out did not allow identification of the inclined planes of the truncated tri-pyramids. However, certain planes could be eliminated from considerations of estimated island thickness. This estimate is obtained by measuring the length of the inclined plane projected on the interface plane and calculating the height from the known angle between the planes. The interface plane is assumed to be (111) and if the inclined planes are also (111) then the calculated island thickness of the islands is $\sim 3000\text{Å}$.

Since the expected "film" thickness derived from the deposition conditions is 200Å, such a calculated thickness is extremely unlikely. However, if the planes are assumed to be (311), as has been suggested for Si or Si then the calculated island thickness is 700Å. A surface coverage of one third is estimated from the micrograph, thus giving an overall "film" thickness of $\sim 230\text{Å}$. More detailed studies are obviously required to establish this beyond doubt.

Very little evidence of double-positioning (inversion) as observed by Booker
and Joyce, has been observed in the replicas obtained. Such inversion would
lead to twin formation. In the film from which Fig. 5.21 was taken, no
twinning was observed by electron diffraction.

5.3.1.2.2. Ge/(110) Ge

Films were also grown by identical techniques on (110) germanium substrate
faces. The study was not so extensive as for growth onto (111) Ge. The
results from films grown at 30 $\mu A/cm^2$ are shown in Figure 5.22. The films
are polycrystalline with preferred orientation, the preferred orientation being
(110) deposit $/\!/$ (110) substrate. The trend is the same as for the (111) grown
films, i.e. increased orientation with increasing temperature. Comparison of
these results with Figure 5.20 show that the epitaxial temperature is lower
for (111) growth than for (110), probably due to differences in the surface
atom arrangement and the energetics of the system. Figure 5.23 is a diffract-
ion pattern from a film grown at 20 $\mu A/cm^2$ at $400^\circ C$. This can be compared
with Fig. 5.19 giving the same conclusions as for the films grown at a faster
rate, i.e. higher orientation for higher substrate temperatures/low deposition
rates.

5.3.1.2.3. Ge/CaF$_2$

In order to compare the results of films grown by sputtering with those obtained
by other workers employing evaporation, (e.g. Sloope and Tiller, 1965; Krikorian
and Sneed 1965), films were grown on the cleavage face of CaF_2 - (111). It was
hoped that these films might also prove useful for electrical measurements, but
unless the films were ~1μ thick, cleavage steps in the surface (up to 1000Å in
depth) were found to preclude such use.

Direct measurement of film thickness was not possible so the thickness was
assumed to be the same as for growth onto Ge substrates. The results for films
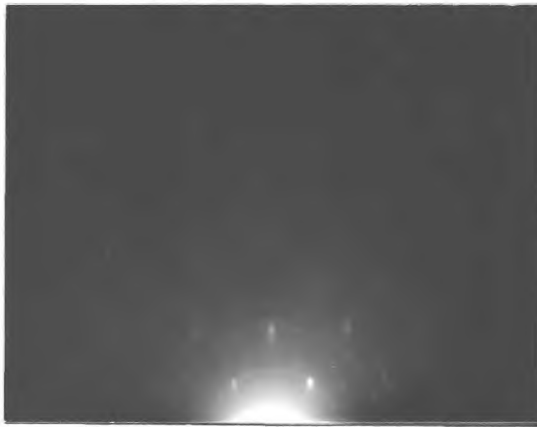
(a) 350°C   (b) 500°C
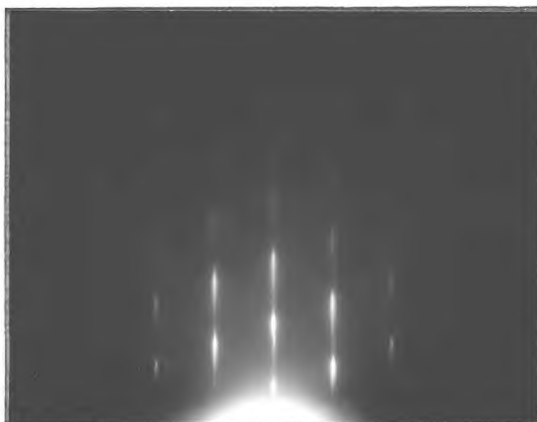
Fig. 5.22 Ge/(110)Ge grown by triode sputtering. Target current density 300 μA/cm^2. Substrate temperature as indicated.
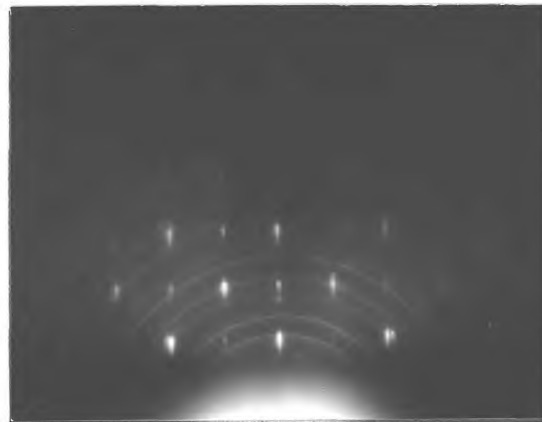
Fig. 5.23 Ge/(110)Ge grown by triode sputtering. Target current density 200 μA/cm^2. Substrate temperature 400°C.

(a) 200°C

(b) 300°C

(c) 400°C
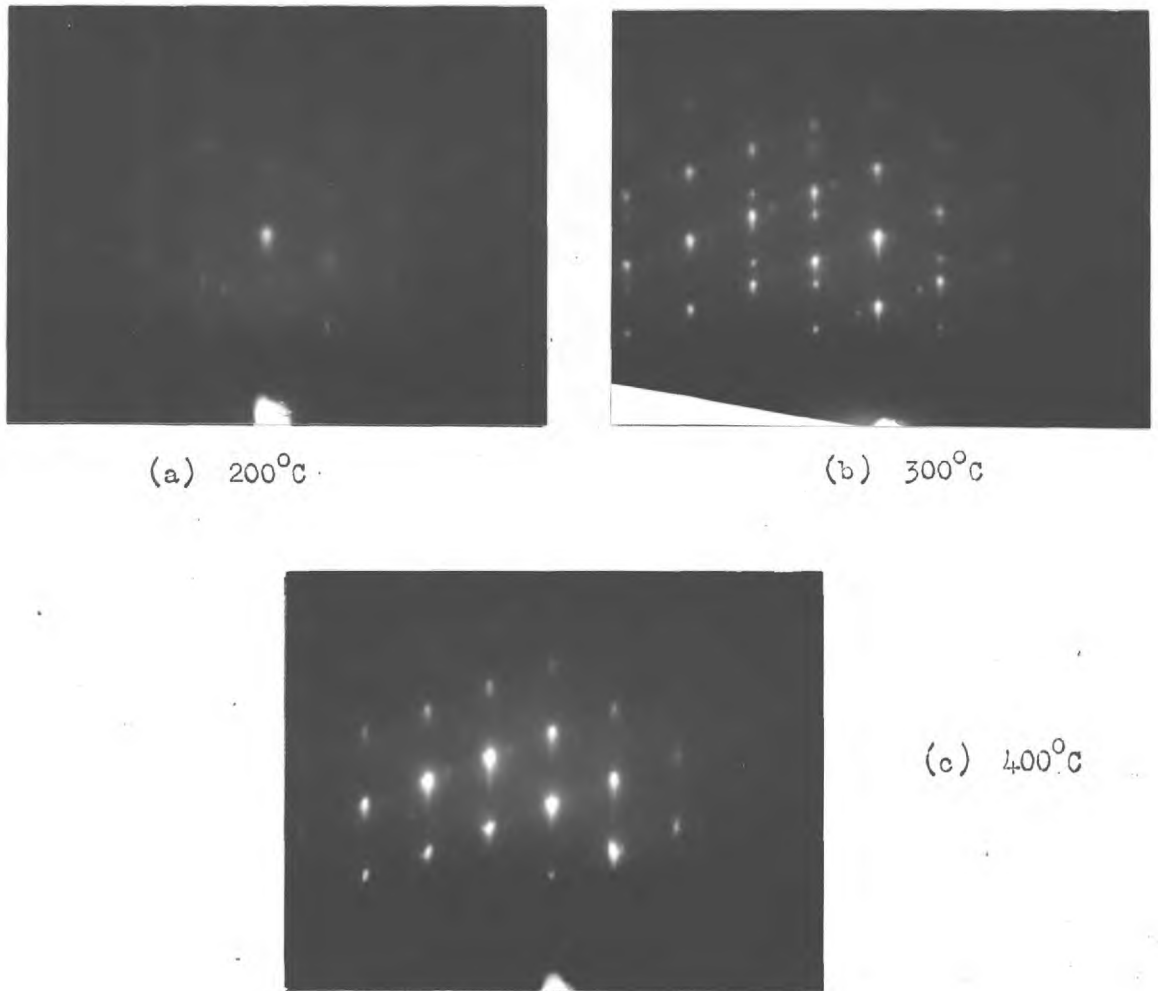
Fig. 5.24 Ge/CaF₂ grown by triode sputtering. Target current density 100 μA/cm². Substrate temperature as indicated.
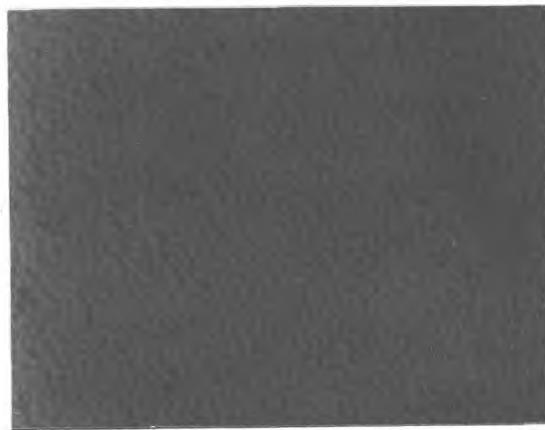
Fig. 5.25 Carbon replica obtained from Ge film grown on CaF₂ at 400°C and a rate of 1.1Å/sec. Thickness 65Å. (From Fig. 5.24(c))

grown at a current density of $100 \mu A/cm^2$ are shown in Fig. 5.24 for a series of substrate temperatures. Fig. 5.25 is a replica taken from the film whose diffraction pattern is shown in Fig. 5.24(c). The island density, $5 \times 10^9 cm^{-2}$ is an order of magnitude greater than that for Ge on Ge, though it is still two orders of magnitude less than that for metals on rocksalt.

Comparison of the results with those given in Section 5.2.1.1. shows that the temperature required for epitaxial growth on CaF_2 is lower for triode sputtering than for diode sputtering, even if biassing is employed in the latter case.

5.3.1.2.4. Ge/mica and Amorphous Quartz

In order to provide a "step-free" substrate, films were deposited on air-cleaved mica, but only partial orientation could be obtained. Temperatures up to $400^\circ C$ were used with an ion current density of $50 \mu A/cm^2$ (producing a deposition rate of approximately $0.8 \overset{\circ}{A}/sec.$ at room temperature and $0.1 \overset{\circ}{A}/sec.$ at $400^\circ C$). Muscovite mica was employed as the substrate but this material was found to exfoliate above $450^\circ C$.

Deposition onto amorphous quartz was also carried out, since Wolsky et al (1965) had reported that all his electrical measurements were carried out on films grown onto this material. Wolsky found some preferred orientation to occur. Deposition in the triode system using exactly the same techniques as for other substrates, showed that some preferred orientation could be observed at temperatures above $200^\circ C$, but in general the films were not as well oriented as the films grown on mica.

Since it did not prove possible to grow highly oriented films on either of the above substrates, further study was halted. It was felt that to correlate electrical properties with structural characteristics, amorphous, polycrystalline and epitaxial films grown on the same type of substrate were needed.

5.3.1.2.5. Ge/Al$_2$O$_3$

In order to fulfil the above requirements, a crystalline substrate which could be obtained in a polished form and withstand reasonably high temperatures was necessary. For electrical measurements, an insulating substrate was preferable. Single crystal Al$_2$O$_3$ was therefore employed, the index of the polished face being (1$\bar{1}$02). This plane is the one employed most successfully for epitaxial growth of Si on Si.

Since the main purpose of the investigation was to be an examination of electrical properties, films were grown at a single ion current density (200 μA/cm^2). The growth curve is shown in Fig. 5.26. and all films for electrical examination were grown according to this curve. The diffraction patterns shown in Fig. 5.27 (a) to (c) are for three films grown at increasing temperature and again show increasing orientation with increasing temperature and/or decreasing rate. The temperature at which the poly-crystalline ring pattern gave way to a spot pattern was ~425°C. The spot pattern was not of single orientation but consisted of a mixture of two or three orientations. The temperature of 425°C cannot be considered strictly as the epitaxial temperature for these conditions. It will be referred to in Chapter 7, in discussing the relationship between electrical properties and structure, as the "ordering temperature". The diffraction patterns show the films to have a lot of twinning and double diffraction effects.

5.3.1.2.6. Ge/(111)GaAs

Since electrical measurements were not possible without complicated analysis of the results, on Ge films grown on Ge substrates, it was felt desirable to deposit onto a semi-insulating material of very similar crystal structure. This was to verify that it was reasonable to make some correlation between general structural results for Ge on Ge and electrical results obtained from Ge on Al$_2$O$_3$. Semi-insulating (Cr-doped) GaAs was available

FIGURE 5.26

Growth rate dependence on substrate temperature for Ge films

on $\langle 1\bar{1}02 \rangle$ Al$_2$O$_3$. Discharge conditions same as for Fig. 5.16.
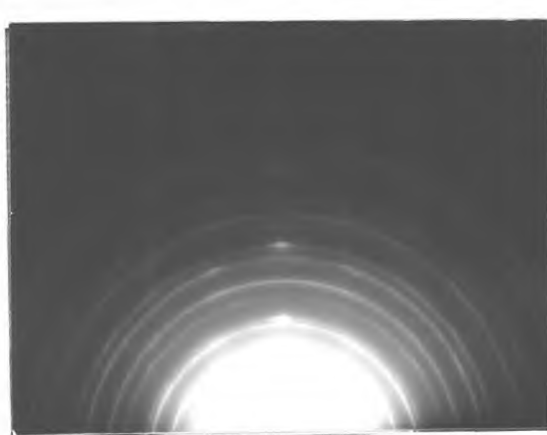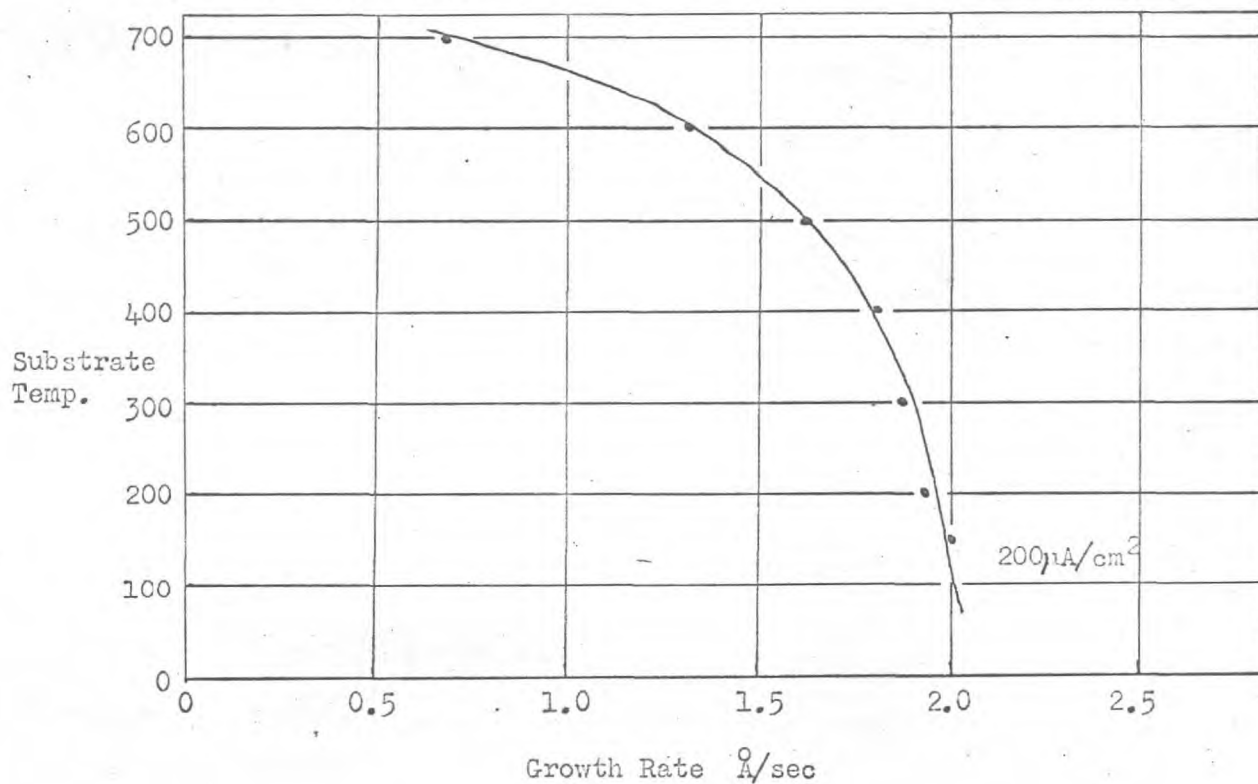
(a) 350°C
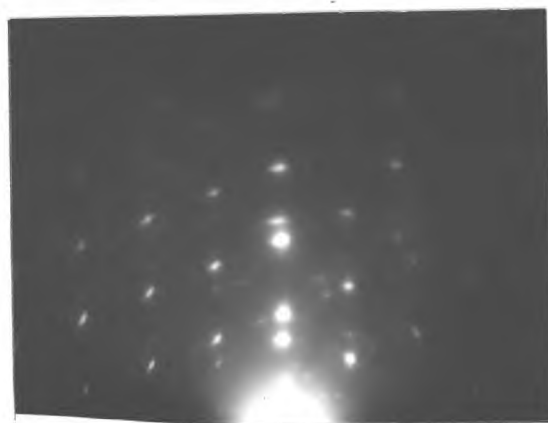
(b) 450°C
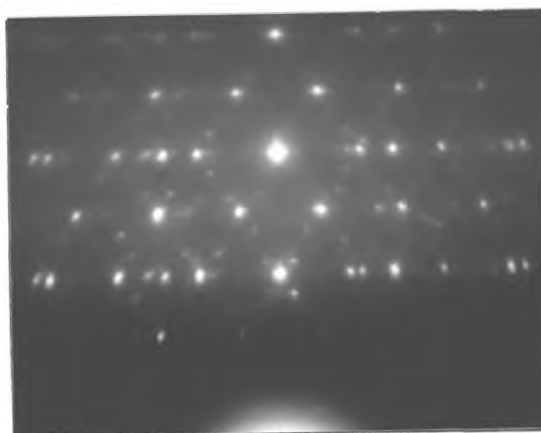
(c) 400°C

Fig. 5.27 Ge/(1$\bar{1}$02)Al$_2$O$_3$ grown by triode sputtering. Target current density 200 μA/cm^2. Substrate temperature as indicated.

and suitable, and films were therefore grown on cut and polished (111)

surfaces of this material. Growth curves were not established, but similar

current densities gave similar rates as for Ge on Ge or Al_2O_3. The films

were epitaxial under conditions similar to Ge on Ge. Glancing angle

diffraction patterns are shown in Fig. 5.28, and may be compared with

Fig. 5.19. The electrical results given for these films in Chapter 7 were

very similar to Ge/Al_2O_3, which was some justification for the use of Al_2O_3

substrates.

5.4. LOW PRESSURE SPUTTERING

5.4.1. General

Concurrent with the examination of elemental germanium films, it was

felt desirable to examine compound films. For the reasons discussed in

Chapter 3, sputtering affords the possibility of growing compound films of

known composition directly related to the composition of the starting

material.

The apparatus used for these experiments was the low pressure type

described in Section 4.2.3. of Chapter 4. Calculation of the effect of

residual pressure on energy attenuation of the ejected target atoms,

described in Chapter 3, showed there to be little difference between low

pressure (10^{-4} torr) and triode (10^{-3} torr) sputtering. The advantage of

the low pressure system lies in the reduced rate of arrival of unwanted

species at the substrate. Gas entrapment should therefore be reduced.

However, the differences were thought to be few between films grown in the

two types of system. As a test for this, a germanium film was grown on

($1\bar{1}02$) Al_2O_3 under similar rate and temperature conditions to those pertain-

ing to a film grown under triode conditions. The diffraction pattern of

Fig. 5.29 from a film grown at $500°C$ and $0.8\text{Å}/sec.$ indicates if anything a

slightly higher degree of perfection than was obtained from triode sputtering.
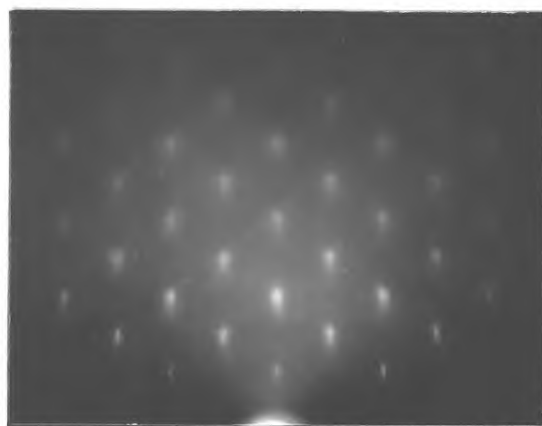
(a) 250°C
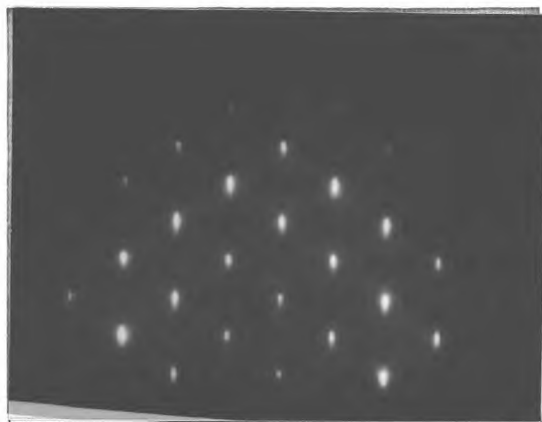
(b) 350°C
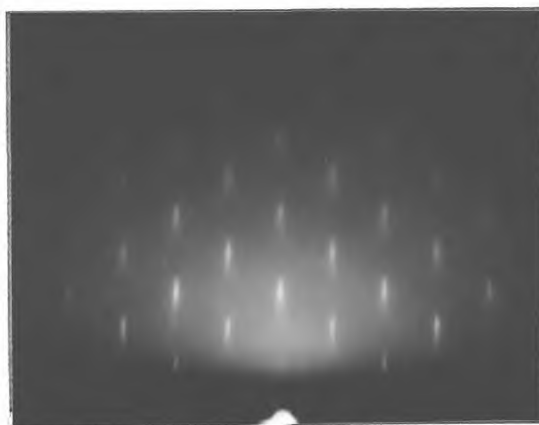
(c) 400°C

Fig. 5.28 Ge/(111)GaAs grown by triode sputtering. Target current density 200 µA/cm². Substrate temperature as indicated.
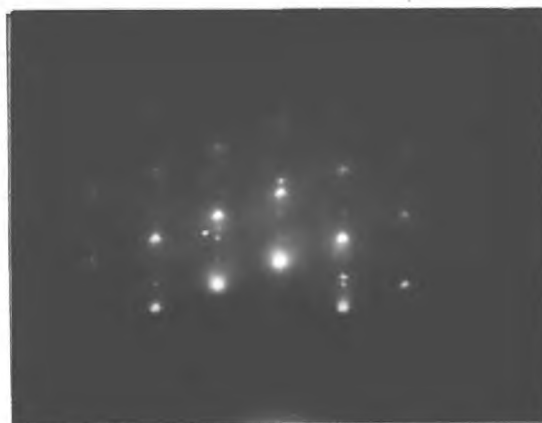
Fig. 5.29 Ge/(111)Ge grown by low pressure sputtering. Deposition rate 0.8Å/sec. Substrate temperature 500°C.

Time did not allow a fuller investigation to compare the two techniques,
since the exercise was intended to study the feasibility of compound semi-
conductor deposition.

5.4.2. Compound semiconductors/various substrates

Films of InSb, GaAs, Bi_2Te_3, PbTe and Cd_3As_2 were deposited onto
substrates of MgO, NaCl, CaF_2, glass and mica. All the materials sputtered
very readily and Table 5.1. shows the rates obtained for each material
sputtered onto glass with the conditions indicated.

TABLE 5.1.

	Substrate Temp. °C	Ion Current Density mA/cm^2	Target Pot[1] Volts	Rate Å/sec.
InSb	50-325	0.1-1.5	1,000	0.13-2.5
GaAs	250-340	1	1,000-1,500	1.3 -1.67
Cd_3As_2	25- 80	0.5-2.0	1,000	0.37-1.25
PbTe	200-300	1	1,500	1.7 -4.3
Bi_2Te_3	100-200	0.5	1,500	5.0 -7.1

The electron diffraction results from films grown on NaCl or MgO
show that films can be grown whose structure and composition is that of
the starting material. Typical diffraction patterns are shown for each of
the above compounds in Figs. 5.30 to 5.34. The patterns for InSb and GaAs
were obtained in the electron diffraction camera. They are therefore
general area patterns but for plate measurement they are more accurate.
For InSb, the results show the pattern to be due entirely to the compound
material of the correct lattice spacing (aluminium was used as the standard
reference to obtain the camera constant). In the case of GaAs, which was
polycrystalline, at all temperatures, there are a number of other unidentifi-
able lines in addition to those due to GaAs which may possibly be double
diffraction effects. They are not due to any oxide or to free Ga or As,
ascertained by measurement of the diffraction plate.
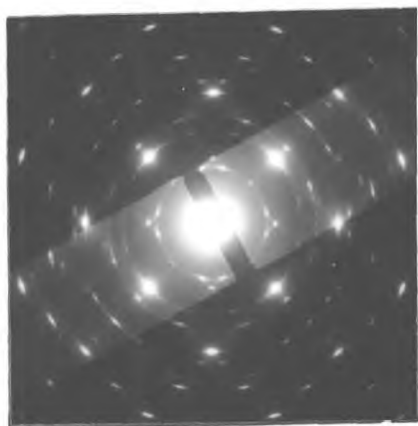
Fig. 5.30 InSb/NaCl grown by low pressure sputtering. Substrate temperature 350 °C. Rate ~ 1·2 Å/sec
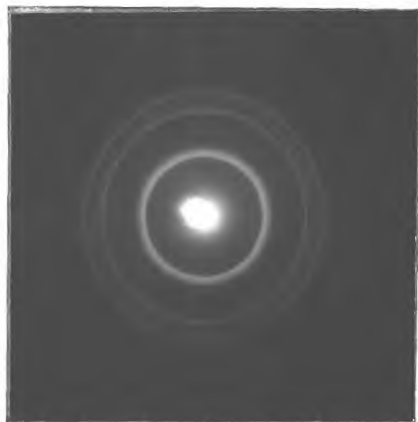
Fig. 5.31 GaAs/MgO grown by low pressure sputtering. Substrate temperature 400 °C. Rate ~ 1·5 Å/sec
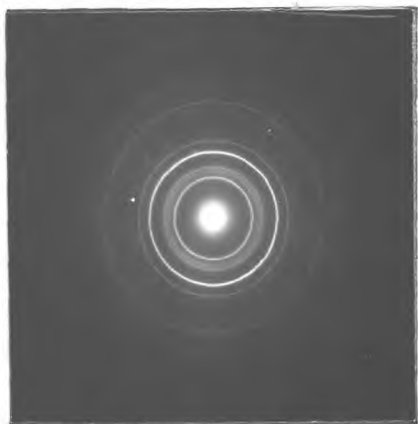
Fig. 5.32 Cd$_3$As$_2$/glass grown by low pressure sputtering. Substrate temperature 75°C. Rate ~ 0·8 Å/sec
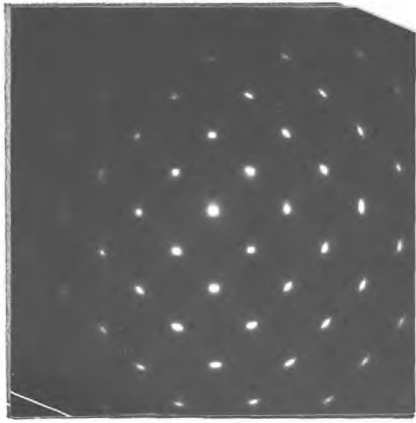
(a) D.P.
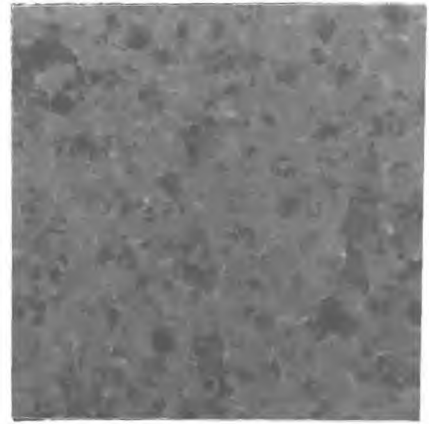
(b) Electron micrograph.
Mag^n. 20000x.

Fig. 5.33 PbTe/NaCl grown by triode sputtering. Substrate
temperature 200°C.
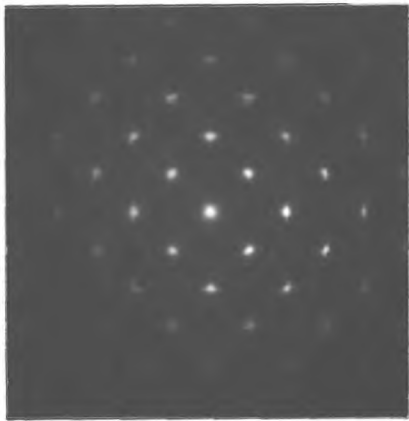
(a) Substrate temperature 100°C
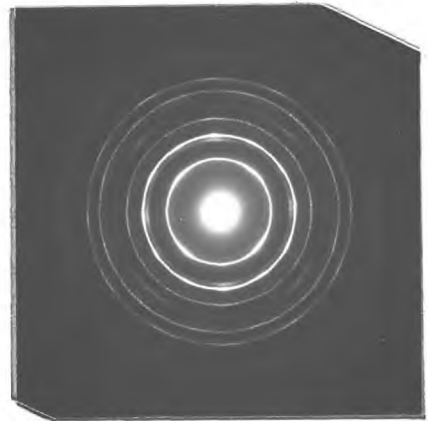
(b) Substrate temperature 200°C.

Fig. 5.34 Bi$_2$Te$_3$/NaCl grown by triode sputtering. Substrate
temperature as indicated.

The high volatility of the components of Cd_3As_2 led to a maximum temperature at which films could be deposited. There were visible differences between films grown above and below $100^\circ C$. Above $100^\circ C$ the films were translucent and milky whereas below $100^\circ C$ they were metallic and opaque. Measurement of film resistance on the two types of film showed that of the high temperature film to be several orders of magnitude higher (20 M ohm as compared to 200 ohm). Because of this temperature limitation epitaxial films could not be grown on mica. In all cases, for mica and glass substrates, the films were polycrystalline or amorphous.

Lead telluride readily formed an epitaxial layer when deposited on rocksalt, as it also does by evaporation. The degree of perfection increased with temperature as would be expected. Again there was no evidence in the diffraction patterns of free Te or Pb. Bismuth telluride, as Table 5.1. indicates, had a very high deposition rate. Even at these high rates the resultant films showed preferred orientation when grown on rocksalt. The perfection seemed to be greater at $100^\circ C$ than at $200^\circ C$ but, since Bi is fairly volatile at the latter temperature and the growing film therefore unstable, this is perhaps not surprising. At $250^\circ C$ no film was found on the substrate even after prolonged sputtering.

CHAPTER VI

DISCUSSION OF STRUCTURAL RESULTS

6.1. INTRODUCTION

This Chapter is devoted to a discussion of the structural results detailed in Chapter 5. Following a discussion of the contribution of the sputtering environment to the growing film, the effects of arrival energy are discussed and evaluated. A model is proposed in terms of the possible effects of direct impingement of energetic sputtered particles on growing islands. The most likely sources of energy are then discussed. The results are evaluated in terms of the experimental conditions and the proposed model. Comparison is drawn between these results and those of other investigators.

By far the most detailed study of the phenomenon of epitaxy has been carried out on films prepared by vacuum evaporation. This was mentioned in Chapters 1 and 2 and the references cited therein contain an adequate discussion of the early work on the subject. It is intended therefore to discuss only the more recent work here, particularly that which has the most relevance to sputtering.

Since the work of Bassett (1960) and others showed the early stages of growth to be an island structure (see Chapter 2), work has centred around the investigation of the initial nucleation of materials onto a variety of substrates (generally NaCl) in an attempt to establish a relationship between the rate, temperature and energy relevant to the experimental conditions. The theories which have met with most experimental success are detailed in Chapter 2.

The following discussion is confined to the growth of thin films by sputtering and a comparison where applicable to similar films grown by evaporation.

6.2. FEATURES SPECIFIC TO SPUTTERING

As has already been emphasised, the energy of ejection of sputtered particles is very much greater than the energy of thermally evaporated atoms. This energy may be attenuated by collision of the sputtered atoms with gas molecules as shown in Chapter 3, the degree of attenuation depending upon the discharge gas pressure. Also of extreme importance is the effect of charged particles on the nucleation and/or growth of the sputtered film. A number of authors have shown electrons to have a significant effect on the crystalline perfection of epitaxial films, particularly when deposited on rocksalt. It has been the purpose of the present work to examine films grown under conditions of varying energy and charge in an attempt to separate the two effects.

In the diode system, there are as many electrons bombarding the anode surfaces as there are ions bombarding the target. At the current densities employed in these experiments ($\sim100\mu A/cm^2$) the electron flux was therefore $10^{14} - 10^{15}/cm^2$ at energies up to 3keV. The effect of energy of arrival of the sputtered particles is shown from Chapter 3 to be the least for this system though still significant in comparison to evaporation. In the case of bias-diode sputtering the electron bombardment of the substrate is supplemented by positive ion bombardment.

In triode sputtering however, direct bombardment of the substrate by energetic electrons is very much less since the substrate and its support are introduced as an earthed probe into a discharge potential of not more than 60V. Also with the presence of an axial magnetic field to constrain the electrons away from the chamber walls, the effect is further reduced. The current density measured at the substrate was found to be not very informative since, depending upon the discharge conditions, there could be a net flow of ions or electrons to the substrate. Generally, however, with a discharge present and sputtering occurring the current density was $\sim1\mu A/cm^2$, i.e. $10^{12} - 10^{13}$ electrons/cm^2 net.

Thus the conditions were those of low density, low energy bombardment. The arrival energy of the sputtered particles however, was extremely significant. At the pressure used in the normal triode system ($\sim 1.10^{-3}$ torr) a large proportion of the ejected atoms arrive at the substrate with little or no energy attenuation. It is thought then that, rather than dealing simply with the same processes in each system, one being at a lower pressure than the other, there are two distinct mechanisms operating. The two mechanisms may be reconcilable in terms of Rhodins active site theory, discussed in Chapter 2. Bias sputtering probably combines both mechanisms.

The effect of charged particle bombardment on a surface has been widely studied in relation to its effect on a film growing on the surface. In extreme cases of electron bombardment of a rocksalt surface by electrons - as in the case of electron microscopy, the surface is completely dissociated. The effects of low energy electron irradiation of alkali halide surfaces and the modification of epitaxial nucleation and growth have been demonstrated by Stirland (1967) and Rhodin et al (1968) and are discussed in Chapter 2.

6.3. ARRIVAL ENERGY EFFECTS

The arrival energy of the sputtered atoms can manifest itself in various ways. Energetic particles may (1) penetrate the lattice upon which they impinge, (2) cause local heating of the substrate by energy transfer, (3) directly impinge upon islands or groups of atoms of the growing film thereby transferring energy to that group and (4) directly impinge upon contaminant atoms so as to dissociate them from the surface.

6.3.1. Lattice Penetration

Penetration can occur either by direct displacement of a lattice atom into a vacancy or interstitial position or by way of open channels in the lattice. In order to displace an atom from its lattice position into an interstitial position a bombarding particle must transfer energy of the order of the displacement energy. For most materials this is 20-30eV. At a deposition

rate of $0.1\overset{\circ}{A}$/sec., the number of atoms arriving per square centimetre of substrate per second is $\sim 10^{14}$. If the number with energy above 20eV is only 0.1%, the density of such at the substrate is 10^{11}/cm^2/sec. This figure is of the same order as the observed island density in films grown on rocksalt. In the case of diode sputtering in which considerable collision occurs between target and substrate, the ratio of high energy particles (i.e. $>$28eV) is $\sim$0.1%, deduced from the attenuation curves of Chapter 3. Thus there is a distinct possibility of lattice penetration by displacement even for the case of diode sputtering. In the case of triode sputtering operating at reduced pressure, the proportion of high energy ($>$28eV) particles is $\sim$1%, deduced from the same curve. The probability of lattice penetration is thus greater. There is at present insufficient evidence to show that penetration does occur in the sputtering environment though it is claimed to be shown by Chapman (1968) using highly energetic sputtered particles from a single crystal target.

The second means of penetration is by way of open channels in the lattice exposed to the sputtered particles. The range of penetration will depend upon the ratio of size of the lattice atoms and bombarding atom. If the ratio is favourable, penetration could be long range. If the bombarding atom is larger than the channel upon which it is incident, it may be possible for the lattice atoms to be displaced by a small amount in order to let the bombarding atom through. Thus the range of penetration will depend upon the incident energy. For a simple cubic lattice, channels exist along the $\langle 001 \rangle$ and there are as many channels as lattice rows. For the case of a bombarding atom of the same diameter as the lattice atom the displacement of each atom is approximately 0.3 times the lattice parameter. The energy required to displace a lattice atom by only $0.3a_o$ is approximately half the displacement energy. Thus there is a real possibility of lattice penetration by sputtered atoms to be at least the depth of one atom layer by this process. This form of penetration is of crystallographic regularity and may give rise to local nucleation centres, as discussed by Rhodin (1968).

6.3.2. Local Heating of Substrate

When an energetic particle strikes a surface, it may transfer some or all of its kinetic energy into lattice vibrations in the substrate. The vibrations will decay with time and with distance from the point of impingement. This type of mechanisms has been investigated by Nelson (1965) in relation to sputtering and is known as the "thermal spike." Nelson showed that for 45keV argon ions bombarding a gold surface, the radius of the thermal spike, or hot region, is $\sim 100\text{Å}$. The lifetime and temperature of the spike are given as $\sim 10^{-11}$ secs. and $\sim 600°C$ respectively. If Nelsons results can be extrapolated to lower energies (10-100eV), typical of sputtered species, the thermal spike region would be expected to be very small. In nucleation theory the typical lifetime of single atoms is 10^{-11} secs. and for pairs of atoms $\sim 10^{-8}$ secs. For local heating of the substrate to be of importance, temperature changes of $\sim 50°C$ would be necessary, which cannot be envisaged for incident energies of only 10-100eV. It is therefore concluded that this type of mechanism plays no part in the film growth. Experimental support for this conclusion was obtained using a fine wire thermocouple to detect temperature rise. At the rate of deposition used ($10^{14} - 10^{15}$ atoms/cm^2/sec) no temperature increase was observed above that due to the discharge itself. This was found to be true for all sputtering modes employed.

6.3.3. Direct Impingement onto Growing Islands

Clearly, at an island density of $\sim 10^{11}$ per cm^2 and an atom arrival rate from the target of $\sim 10^{14}$ per cm^2 per sec, there is a finite probability of direct impingement. The outcome of the impingement depends upon the distribution of the kinetic energy of the sputtered atom through the growing atom cluster. When the cluster is very small, the probability of it being struck is very small also but the result would be one of total destruction of the cluster.

The rate of increase of island size can be approximately determined from nucleation theory. For the case of nucleation on rocksalt, the capture rate

of single atoms by a cluster is initially $R(^{Ma}/No)$ where R is the impingement
rate, Ma is the catchment area (defined in Chapter 2) and No is the equilibrium
number of sites. This assumes growth by surface migration only and is also
only true for the case of non-saturated nucleation. For rates of impingement
of $\sim 10^{14}$ atoms/cm^2/sec. ($\equiv 0.1$Å/sec.) at $T = 400^\circ$K the capture rate is $\sim 10^3$
atoms/sec. The number of atoms increases linearly until the capture areas over-
lap at which point, due to competition for atoms, the capture rate decreases.
When the island size becomes significant the capture area for each island and
hence the capture rate, will increase with island size. Eventually coalescence
will occur and the rate of coalescence will be size dependent (Pashley 1965).
A plot of the number of atoms per island as a function of time will yield a
curve of the form shown in Fig. 6.1. The projected area of the islands will
follow a similar curve Fig. 6.2. but the actual shape of the curve is more
difficult to determine since it depends upon the three-dimensional shape of the
islands - i.e. whether the islands are hemi-spherical or plate-like. As the
island increases in size atoms will also be added by direct impingement from the
beam. This will modify the shape of the curve for large values of t but will
not affect the general argument. More important is the energy transferred from
the impinging atom to the atoms in the island.

The mean energy of the sputtered beam is $\bar{E}$ ev per atom. Stuart (1962) and
others have shown this to be ~ 5eV. If the deposition rate is R atoms/cm^2/sec.
(assumed equal to the ejection rate) the energy input to the receiver surface
is $\bar{E} \times R$ eV/cm^2/sec. The energy input per island is $\bar{E} \times R \times A$ eV/sec., where
$A = \pi r^2$ = the "island" area (r = collision radius of atom on island). There
are two regions of interest in this problem. Initially, when the probability
of collision is small, the number of atoms per island is also small. Thus when
a collision does occur the island will suffer severe damage and will probably
be destroyed. The probability of collision is given by :

$$P_i = A_i \times R \times T_i \quad \text{where } A_i = \text{Area of island size i}$$
$$T_i = \text{Lifetime of island size i.}$$

FIGURE 6.1

Variation of Number of Atoms per Island as a function of
Time for atoms condensing on a smooth substrate.
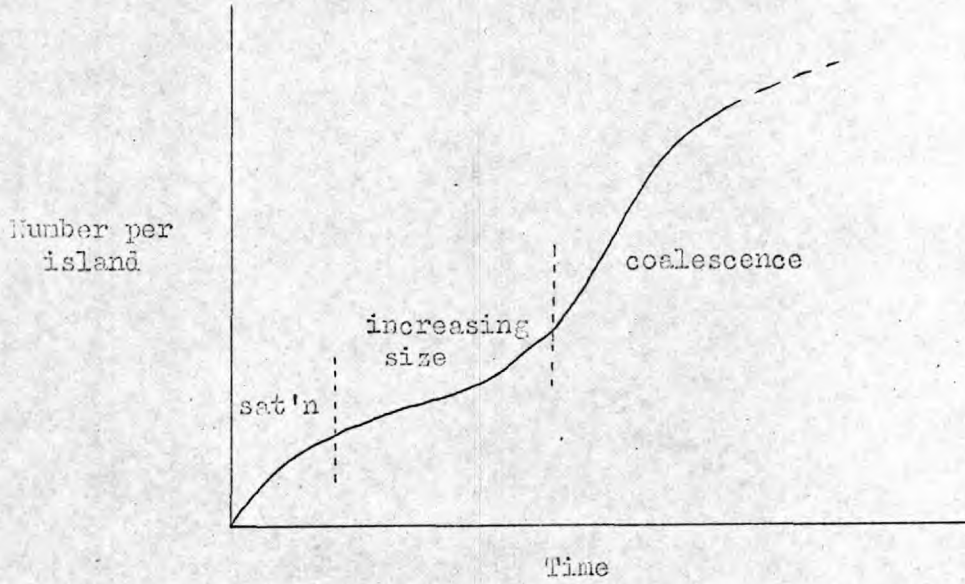
FIGURE 6.2

Variation of Projected Area of Island as a function of
Time for atoms condensing on a smooth substrate.
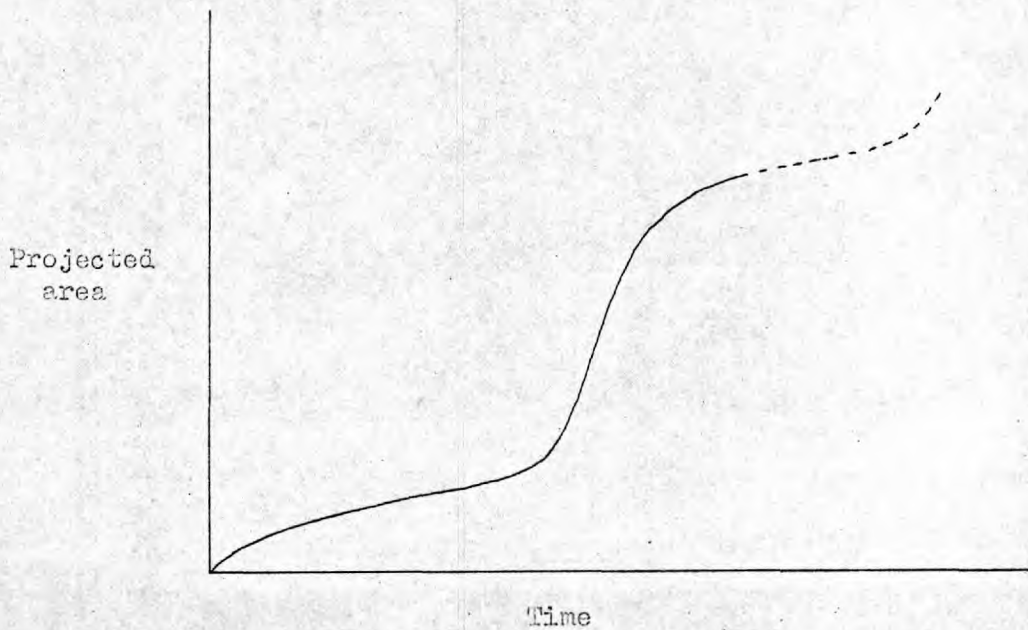
Assuming $R = 10^{14}$ atoms/cm^2/sec., the probability can be evaluated for islands of various size.

When $i = 2$ its lifetime is $\sim 10^{-8}$ secs (Chapter 2) giving a value of P_i of $\sim 10^{-9}$. Thus normal nucleation can proceed with only a very small number of islands being destroyed by direct impingement.

When $i = 10$, the lifetime is long (approximately given by the inverse of the capture rate, $\sim 10^{-3}$ sec). The probability is $\sim 10^{-3}$ which means that one island in 1,000 will receive a pulse of energy $\overline{E}$. The energy per atom is $\sim 0.5eV$ - sufficient to destroy the island. Thus the number of islands of size $i = 10$ is reduced by 0.1%.

At $i = 100$, the lifetime again approximates to 10^{-3} secs. giving a value of $P_i \sim 10^{-2}$. The energy per atom is only 0.05eV which is unsufficient to destroy the island but it may be sufficient to damage the island, due to variations in atomic binding with position within the island.

Thus as the island size increases the probability of it being struck by an impinging atom increases. Initially the probability is very low and nucleation and growth can proceed to the stage where the probability becomes appreciable and may result in the loss of islands by destruction. The number of islands of a given size will thus be less than that if the impinging beam were of low energy. At still larger island size, the probability is increased, almost to unity, and the energy per atom falls to a value too low to cause dissociation though atomic displacement may occur leading to defects.

The second region of interest is due to the relatively small energy required to move an island as a whole in relation to the substrate. Evidence for rotation has been given by Pashley (1965) and also Matthews (1965). Thus, taking the above arguments a stage further, the energy perisland will increase with island size. The energy required to cause an island to rotate is difficult

to estimate but one might expect it to be fairly large initially, when atoms are located in potential troughs in the substrate. As the number of atoms in the island increases the atoms will tend not to sit in potential troughs. If it is proposed that epitaxial island orientations are the low energy states then the island will tend towards this state. At large island sizes the lowest energy state of the island may not be the epitaxial state. This is because the misfit is such that, while some atoms may be in an epitaxial state other atoms are not with the net result that the energy is not a minimum. The proportion of islands receiving a pulse of energy increases with island size as the probability of collision goes up. As indicated above, at $i = 10$ the number of islands directly impinged upon is only 0.1%. At $i = 1000$ approximately 1 in 5 will be struck. This is an island diameter of $150\overset{\circ}{A}$. It may be concluded that reorientation of the growing islands will occur and may be significant in promoting epitaxial growth. The condition is that in which the probability of an island of radius r being struck by an energetic particle is a function of the rate of arrival of the energetic particles and the lifetime of the island of radius r. Figure 6.3. is a plot of the mean energy per island as a function of island radius. The mean energy per island is defined as

$$E_{MEAN}(r) = \frac{\text{No. of islands of size r receiving energy, } \overline{E} \times \overline{E}}{\text{Total number of islands of size r}}$$

Also plotted is the energy required to move the island relative to the substrate. This will tend to decrease at first and then increase as the island becomes very large. The shape of the curves in the figure is for illustration purposes only.

The interpretation of figure 6.3. should be that as the island size increases, the proportion of islands receiving sufficient energy to move to an epitaxial position increases. The overall orientation of the film would thus be expected to be initially polycrystalline at a given rate becoming increasingly epitaxial as the thickness increases. The results shown in Figs. 5.8. - 5.11. show that orientation does indeed improve with thickness.

FIGURE 6.3   164

Variation of Mean Energy per Island as a function of
Island Radius for Atoms condensing from a Sputtered beam.
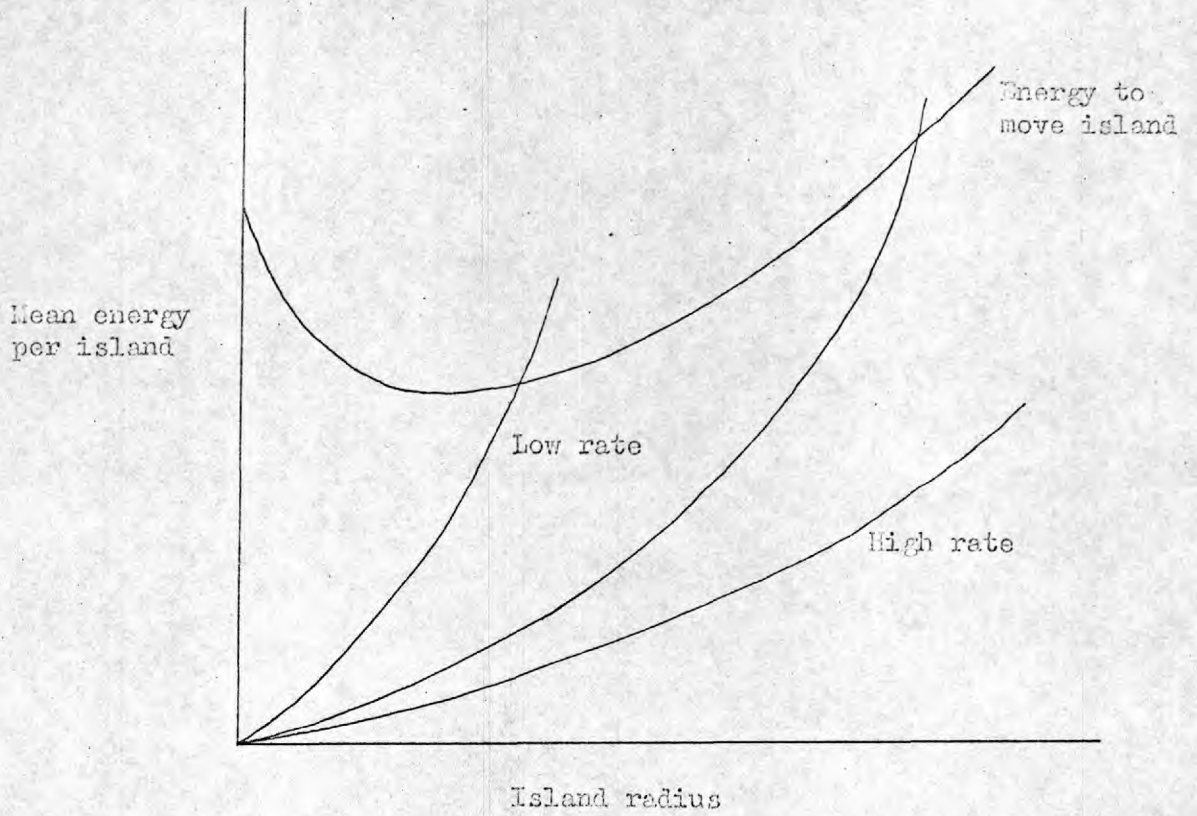
6.3.3.1. Rate Dependence

The effect of increasing rate of deposition is to both increase the energy density at the growing film and to decrease the lifetime of the island of radius r. Since the capture area increases with island size, the capture rate will also increase at a rate faster than linear. The effect of increasing deposition rate is thus to displace the energy per island curve in Fig. 6.3. towards high island radius, as shown. In extreme cases, the probability of the island of size r receiving sufficient energy to move to an epitaxial position may be zero, i.e. the film is growing too rapidly. At low rates, the mean energy per island is higher and the islands have a higher probability of moving to an epitaxial position. Low rate behaviour is a little more difficult to predict since other mechanisms such as contamination, re-evaporation etc. become involved. However, from the above argument it would be expected that at low rates the epitaxy would be observed in thinner films.

6.3.3.2. Temperature Dependence

The effect of temperature is of secondary importance in the above argument. Its main effect is to determine the initial orientation during the nucleation stage. At the temperatures employed in sputtering the nucleation is largely non-epitaxial. The effect of substrate temperature would be greatest at the nucleation stage in determining the lifetimes of clusters of a certain size. At the later stages the contribution of temperature to the energy required for island motion is small. However, if the initial nuclei are in epitaxial positions, the probability of the resultant film being epitaxial is greater. High substrate temperatures will also encourage the annealing out of defects. It is thus seen that epitaxy will be enhanced by increasing the substrate temperature but the mechanism is not that normally associated with epitaxy by evaporation.

The above model therefore accounts for the observed trend of increasing orientation with increasing thickness, increasing substrate temperature and decreasing rate. It is proposed therefore, particularly for the systems in which there is little attenuation of the particle energy between source and substrate, that epitaxy by sputtering is fundamentally a growth phenomenon.

The effect of direct impingement onto groups of contaminant atoms is discussed below in Section 6.6.

6.4. SOURCES OF ENERGY

The above discussion assumes the impingement of energetic particles onto the growing islands. There are several possible sources of energy and the relative importance of each type is dependent upon the probability of their occurence.

(a) Energy from the sputtered beam.

Already this source of energy has been widely discussed. The energy distribution of the sputtered particles is a "long-tailed Maxwellian" with a mean energy of 5-10eV and a maximum energy of up to 50eV. The maximum is dependent upon the incident ion energy and may be several hundreds of electron volts at ion energies of 50keV. However, at the ion energies employed in these experiments (1.5 - 3keV), 50eV is thought to be a reasonable estimate. The figures employed in the section above are based on $\overline{E}$ = 5eV, though clearly the argument is to orders of magnitude only. The effect of attenuation by the gas environment is fully discussed in Chapter 3.

(b) Recombination Energy

In the presence of a glow discharge, be it thermally assisted or not, the ions in the region of the substrate do not experience high accelerating fields away from the substrate. There is thus a probability of ions, moving with thermal velocities, bombarding the substrate and the growing film. The

thermal energy of these ions would not of itself produce any effects such as those described above. However, if an ion were to recombine with an electron at the substrate or, more importantly at a growing island, then the ionisation energy would be given up to the island. The flux of thermal ions is $\frac{n\bar{V}}{4}$ per unit area per second. For argon gas at 10^{-3} torr there are $\sim 10^{15}$ atoms/cm^3. Calculation has shown (Chapter 3) that the ratio of gas atoms to gas ions is $\sim 10^4$:1. Thus there are $\sim 10^{11}$ ions/cm^3. Assuming a mean thermal velocity of $\sim 4.10^4$ cm/sec. this results in a flux of 10^{15} ions/cm^2/sec. at the substrate. There is also, in the diode case, a flux of electrons bombarding the substrate of similar magnitude. It would be reasonable to expect therefore that there will be charge recombination. The extent of the recombination however is difficult to determine. Recombination within a growing island relies upon the island being negatively charged. The probability of the island being negatively charged is not easily calculated but is expected to be fairly low. Thus the effect due to recombination is not thought to be of major importance. This view is supported by the fact that in triode sputtering the ions and electrons are constrained by the magnetic field so that the flux of ions and electrons at the substrate is much reduced, yet epitaxy is still promoted at lower temperature.

(c)   Metastable States

In a glow discharge environment, there is a distinct probability of there being a large number of excited but not ionised atoms of the discharge gas. These are non-charged particles which have an excitation life-time and their energy is in the form of potential energy. They may decay on the substrate giving up this energy to the substrate lattice or to the growing film. The excitation energy for the metastable state of argon is ~ 11eV - clearly sufficient to affect the growth. The number of metastables can be calculated from the probability/of excitation which is a function of the excitation cross-section. The flux of metastables towards the substrate may be of the same order as the sputtered atoms. However, owing to their short life the number actually

reaching the substrate and giving up their energy is much lower. Work is at present in progress (Cozens 1968) in order to determine the precise effect of metastable states in growth by sputtering.

(d)   High Energy Neutrals

The concept of high energy neutrals is based upon energy exchange whereby an energetic charged particle transfers its energy by exchange interaction with an uncharged particle. There is some evidence to show the existence of such particles in the sputtering environment (   ) but it would be expected that the energy of the particles, which may be as high as 1000eV, would cause severe damage in the growing film or the substrate itself. Thus while recognising the existence of the mechanism, its application to the process of film growth must be treated with caution, since insufficient is known about the relative numbers and the energy distribution of these particles.

6.5.   DISCUSSION OF RESULTS

The characteristics of the various methods of deposition can be summarised as follows :

(a)   Diode   —   High gas pressure, therefore attenuation of energy
                                by collision.
                                High flux of energetic electrons at substrate.
                                High thermal ion flux.

(b)

       Triode and low —   Low gas pressure, therefore sputtered particle energy
       pressure   virtually unattenuated..
                            Magnetic field reduces electron and ion flux at
                            substrate.

(c)   Biassed Diode —   As normal diode, plus relatively high flux of energetic
                           positive ions at substrate.

6.5.1. Semiconductor Films

The results given in Chapter 5 show that for the case of germanium grown on germanium the epitaxial temperature is lower by triode than by diode sputtering. Indeed epitaxial films could not be grown by diode sputtering below about 550°C. A good deal of work on the growth of diode sputtered germanium films has been carried out by Krikorian and Sneed (1965). An interesting fact to emerge from their work is that, for a given growth rate, the epitaxial temperature decreases with increasing bombarding ion energy. High incident ion energy increases the number of high energy sputtered particles thus increasing the possibility of island movement due to direct impingement. Secondly decreasing current decreases the epitaxial temperature. Since the means of lowering the current was to lower the gas pressure, the result was to lower the degree of attenuation of the sputtered particles. Krikorian and Sneed observed that none of their sputtered films were epitaxial, for a given rate of deposition, at a lower substrate temperature than those grown by evaporation. This would seem to contradict the hypothesis of the energy being the important factor since evaporated atoms are of low energy. Krikorian concludes that it is the gas pressure at deposition which is important. However, the triode results show that a lower epitaxial temperature can be obtained even at a gas pressure of 1μ. Also, Winters and Kay have shown that in fact the percentage gas incorporation in a growing film decreases with increasing gas pressure. This unexpected result contradicts Krikorians conclusion that the epitaxial temperature is a function of gas pressure per se. The point about Krikorians work is that epitaxy is enhanced by increasing the arrival energy at the substrate. The apparent anomaly of the lowest epitaxial temperature occurring for evaporated atoms may possibly be explained in terms of the residual pressure, i.e. contamination. The evaporation pressure was $\sim 10^{-8}$ torr while for sputtering it was only $\sim 10^{-6}$ torr. Fig. 6.4. shows the results described in Chapter 5 superimposed on the curves given by Krikorian. It is clear that evaporation is not the ultimate even

FIGURE 6.4 170

Variation of Epitaxial Temperature with Deposition
Rate for Ge grown on (111) Ge surface by Evaporation
and Diode Sputtering (Krikorian and Sneed,1965) and Triode
Sputtering.
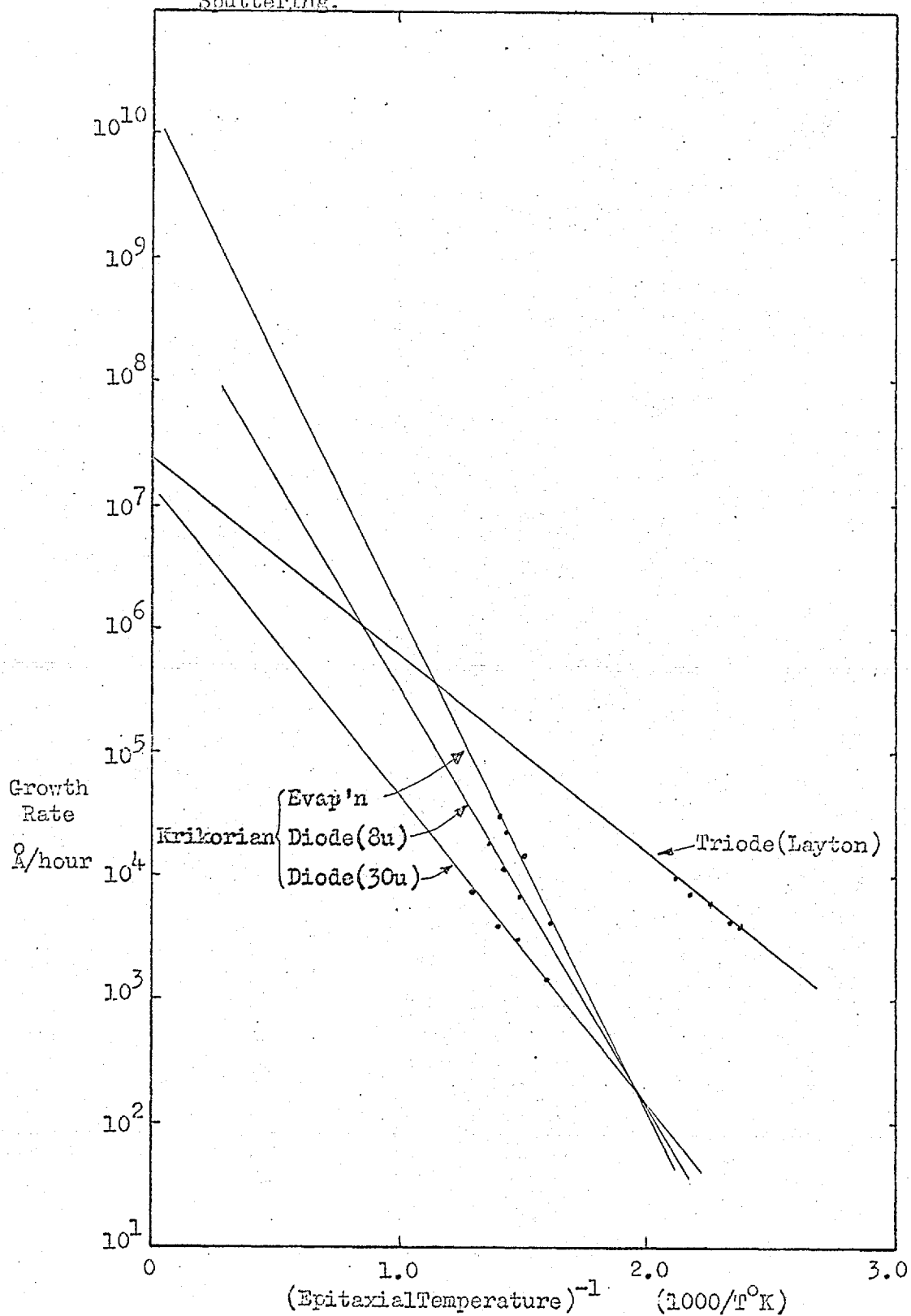
though it is a lower background pressure. The activation energy for epitaxy, defined by Krikorian as the slope of the lines in Fig. 6.4 is lower in the case of triode sputtering than for all others. This would imply that, since the activation energy is defined in terms of substrate temperature, energy is supplied from another source in order to overcome the epitaxial energy barrier. However this again disagrees with Krikorians findings that the activation energy is lower for higher discharge gas pressures since high pressures would result in lower energy of arrival at the substrate. There appears to be consistent discrepancy between the results obtained for diode and triode growth of germanium films which leads one to the conclusion that there are different mechanisms at work in the two cases. In the diode case, the arrival energy is probably not so important. The effect of charge has to be considered as mentioned previously though its precise effect on a semiconductor surface is difficult to analyse. Also the precise nature of the surface is unknown. Both germanium and silicon readily form an oxide which can only be removed by heating the substrate to well above the deposition temperature ($\sim 650^{\circ}C$ for germanium). The oxide growth is certainly dependent upon the background and discharge pressure (i.e. oxygen content of the atmosphere) and may conceivably account for Krikorians results. There appears to have been no provision for removal of the oxide prior to deposition in Krikorians work.

The results reported here for triode sputtering have been substantiated by Wolsky et al (1967, and private communication) who find their growth points fit precisely on the curves shown in Fig. 5.16 of Chapter 5. Both the present experiments and those of Wolsky do not confirm the findings of Krikorian that there is a triple-point in the growth of germanium films. In all cases increasing from low to high deposition temperatures yields films of all three crystalline phases, i.e. amorphous, polycrystalline and single crystal.

Germanium films, grown by evaporation have been studied by Sloope and Tiller (1965, 1966) both on $\langle 111 \rangle$ germanium and CaF_2 substrates. They find that

for CaF_2 a substrate temperature of at least $450^\circ C$ is required for epitaxy. They also disagree with the triple point findings of Krikorian. However, the epitaxial temperature is lower than that observed in the present diode work which supports Krikorians observations. It must be said however, that the work reported herein on CaF_2 substrates was very limited. The results obtained again showed the need for triode sputtering.

The structural results of the triode sputtering of germanium onto $\langle 111 \rangle$ germanium described in Chapter 5 and represented graphically in Fig. 5.16 demonstrate the relationship between film crystallinity, growth rate and substrate temperature. As has already been shown, the epitaxial temperature at a given deposition rate is considerably lower for triode grown films than for any other means of deposition. It is concluded from these results that the energy of arrival is playing a significant role in the growth possibly by way of the mechanism described in Section 6.3.3. It is noted that there are two single crystal regions distinguished by the presence of extra diffraction spots due to faults such as stacking faults and twinned regions in the film. It is observed that the faults are reduced at higher growth temperatures. This would indicate that the faults are growth induced and are not continuations of faults in the substrate lattice. At lower rates of deposition, the "fault free" films are formed at a lower temperature consistent with normal annealing kinetics of defects. This is consistent with the model proposed in the earlier section since lower rates would result in islands of a given size having a longer lifetime thus allowing defects caused by incidence of energetic atoms to grow out before the island increases in size, freezing the defect in. It is impossible however to completely remove all defects since the rate of growth of islands is such that, owing to lattice misfit, there are faults included due to coalescence which do not have sufficient time to anneal out.

6.5.2. Metal Films

The results of the diode sputtered silver films show that the epitaxial temperature is considerably reduced by sputtering. The points plotted in Fig. 5.1 indicate that the growth behaviour for epitaxy is the same as for evaporation, i.e. the epitaxial temperature decreases with decreasing deposition rate. The computer analysis of energy attenuation was carried out as a result of these observations and showed that the energy of arrival was greatly reduced at pressures greater than 10^{-2} torr. Since deposition rate was controlled by the ion current which was in turn directly related to gas pressure, the energy attenuation was a function of deposition rate. By using Fig. 3.11 of Chapter 3 a curve of the percentage of atoms arriving with energy >0.6eV could be plotted as a function of deposition rate. This curve is shown in Fig. 6.5. It shows that the percentage drops rapidly above a deposition rate of 0.5Å/sec. The results shown in Chapter 5 however indicate that the relationship between epitaxial temperature and deposition rate does not alter drastically above 0.5Å/sec. as would be expected if arrival atom energy were responsible for the epitaxial growth in this case. It would be expected that the curve would revert to that for films grown by evaporation. That this does not occur can lead to two possibilities - one that there is some other source of energy, or alternatively, that the existence of energetic electrons at the surface is having some effect. For KCl substrates it has been shown that there are mechanisms which will yield Cl^- ion vacancies in the surface of the KCl (Klick, 1960 and Hersch, 1966). As has been discussed in Chapter 2, Rhodin et al (1968) have suggested that originally the metal atom occupies the Cl^- vacancy and that when four more atoms have joined it, the lowest energy state is that of (100) (110) $Ag//$(100)(110) NaCl. The effect of the electrons is thought to be at saturation (since there are $\sim10^{15}$ electrons/cm^2/sec. at energies up to 3keV) so that the relationship between rate and temperature would follow a normal growth curve, i.e. higher rates, shorter lifetimes of clusters. One must be careful in attributing too much significance to the slope of the line in Fig. 5.1. since it was subsequently shown that the epitaxy was thickness dependent. However the slope of the line (~0.3eV) is of the

FIG. 6.5

CALCULATED VARIATION OF % SILVER ATOMS
ARRIVING AT SUBSTRATE WITH ENERGIES ABOVE 0·6eV
AS A FUNCTION OF DEPOSITION RATE.

(CATHODE-SUBSTRATE SPACING 10 CM)
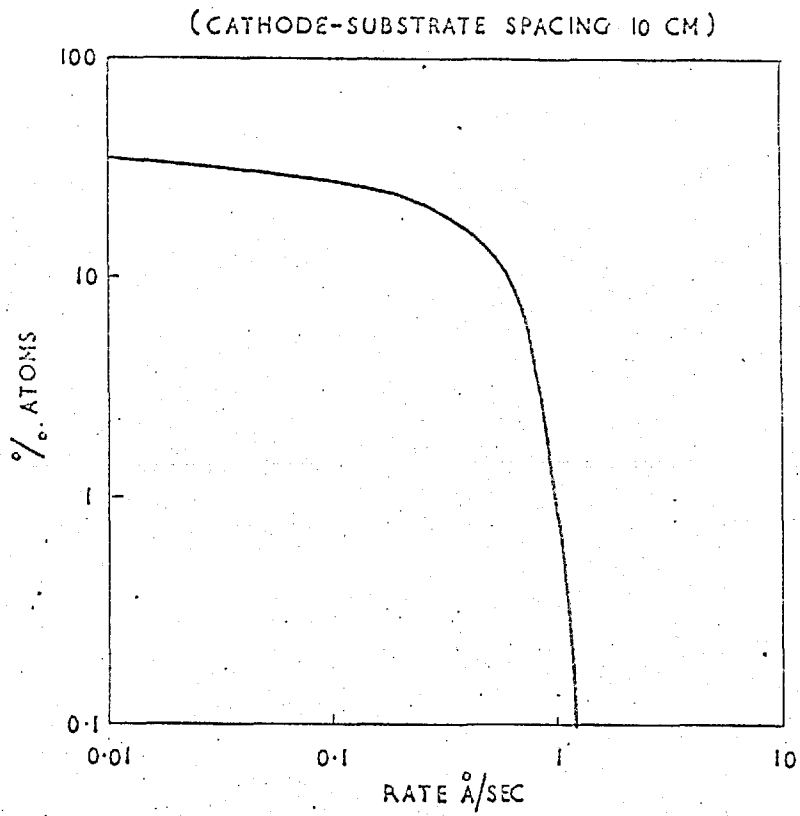
same magnitude as the energy required to move an atom from one site to another,

or indeed to move a group of atoms from one position to another (re-crystallisation).

6.5.3. Bias Sputtering Results

The observation was made that the epitaxy of gold on rocksalt was enhanced by application of a bias of -200V with respect to the plasma. The models discussed in previous sections are considered to be of direct application to the case of biassed growth. Since the bombarding particles are of high mass, high energy and are charged, the energy transfer to the growing film would be significant. The flux of the incident ions is of the same order as the sputtered atoms but their energy may not be as high as the bias potential value. This is due to collisions between ions and neutral gas atoms and also repulsion forces due to image charge existing in the metallic islands, since they are insulated from the electrode by the substrate, at least initially. Thus the precise nature of the bombarding ions are not known. However the result of the bombardment is consistent with the arguments outlined earlier. At low bias potential, the energy transfer, whether it be to the growing film or to the surface contaminants, is effective but insufficient to produce an oriented overgrowth. At high bias potential, the energy transfer is sufficient to damage the film, the damage not having sufficient time to anneal out.

The effect of charge might be supposed to be entirely analogous, with that of electron bombardment, the only difference being the sign of the charge.

The growth of germanium films under similar bias conditions did not have the same degree of improved orientation. The reason for this is not clear but it is possible that the energy transfer was insufficient to remove contaminants from the surface of the Ge substrate. The surface was almost certainly largely oxide since no measures were taken to pre-clean the surface prior to deposition in the diode experiments.

6.6. CLEANING EFFECT OF ENERGETIC ATOMS

The effects of cleanliness of the substrate on epitaxy has been demonstrated for the metal/rocksalt system by several authors. It has been clearly shown (e.g. Ogawa, 1963) that when the substrate is contamination free, i.e. ultra-high vacuum and cleavage in vacuum, the observed orientation of the deposit is predominantly (111). Matthews (1965) has shown that in very thin deposits the preferred orientation was parallel to the salt lattice whether the surface was contaminated or not. He concludes that it is in fact the relative growth rate of the (111) and (100) orientations which determine the final orientation of the thicker layer. On very clean surfaces the (111) nuclei grow rapidly, swamping growth of (100) nuclei. The succeeding mechanism of coalescence of large (111) nuclei with (100) nuclei leads to the (100) nucleus rotating into twin orientation of the (111). On a contaminated surface it was found that the (100) nuclei were more numerous than the (111) nuclei. On coalescence the grain boundary migrates through the (111) nucleus leading to its elimination. An alternative mechanism is the rotation of smaller (111) nuclei into twin orientation with the (100) nuclei. The existence of these twins of which there are four equal energy planes, are consistently observed in f.c.c. metals grown on aircontaminated rocksalt. Matthews therefore concludes that it is the number of (100) nuclei formed on the substrate surface which is important. At high nucleation rates, coalescence occurs at an earlier stage thus precluding the (111) nuclei from outgrowing the (100) nuclei. Matthews has also shown that the essential contaminant is moist oxygen. The exact mechanism for the increased nucleation density of (100) nuclei has not been made clear. It is possible that there is charge exchange between the substrate ions and the contaminant which leads to preferred (100) nucleation sites.

The argument applied to the case of sputtering may be in terms of substrate cleaning or in terms of supplying the energy required for migration of grain

boundaries or nuclei rotation. In the results shown in Chapter 5 for silver on rocksalt, there was no evidence for (111) orientation at any stage. Since all the experiments were carried out on air-contaminated substrates it is to be expected that the (100) phase would predominate. The arrival energy of the sputtered atoms may have been responsible for removing loosely bound contaminants from the surface while being insufficient to remove strongly bound contaminants such as water or oxygen. The removal of loosely bound contaminants would facilitate surface migration while the presence of water or oxygen contamination would aid nucleation of (100) at those sites. This would be consistent with a lowering of the epitaxial temperature and also the observation of twinning on the (111) planes. This hypothesis suggests a good deal of future work which is discussed in the final chapter.

The need for clean surfaces in the case of semiconductor films grown on like substrates (homoepitaxy) has been demonstrated by Widmer (1967). He has obtained epitaxial Si films on Si at $520^{\circ}C$ by evaporation in ultra-high vacuum of 10^{-10} torr, the surfaces being carefully pre-cleaned. The emphasis in the case of Si on Si, or Ge on Ge, is on the removal of the oxide layer which forms even at relatively high vacuum. In the case of sputtering the energy of the sputtered atoms may be sufficient to remove the oxide in which case, provided the rate of formation does not exceed the rate of removal, surface cleaning will take place. More precise investigation, possibly using LEED apparatus, is required.

The results of the nucleation density measurements would seem to indicate that for the case of diode and triode sputtering, the density of islands is not significantly greater than the density of islands formed by evaporation. The curve shown in Fig. 5.13 in Chapter 5 indicates that the points all correspond to incomplete condensation, defined in chapter 2. It was not intended in these experiments that they should substantiate any particular theory. The main

purpose was to determine whether the island density was larger than for evap-
oration, since Matthews proposed that high nucleation density led to lower
temperature epitaxy, as discussed above. The conclusion from the results
must be therefore that there is no difference in the nucleation behaviour of
sputtered and evaporated films, insofar as numbers are concerned. It should
not be concluded however, that the ratio of (111) nuclei to (100) nuclei is
the same in all cases. In order to establish this ratio under the various
conditions of deposition, experiments of a similar nature to those of Matthews
(1965) are necessary.

CHAPTER VII

ELECTRICAL PROPERTIES OF SPUTTERED

SEMICONDUCTOR FILMS

7.1. INTRODUCTION

Preceding chapters have dealt with the structural aspects of the growth of thin films on a variety of substrates. However, in the case of semiconductors it is important that the electrical properties of the films also be examined since a good deal of information with regard to structure can be obtained in this way. When examining a film by electron diffraction, only a very small area of the film is subjected to the beam of electrons, which are of very high energy (75-100 keV). Scattering centres such as impurities, grain boundaries etc., do not have a profound effect on the resultant diffraction image because of their relatively low density. When, however, one tries to pass a current along the length of the film, the effect of the scattering centres becomes more evident and more can therefore be learnt of the detailed structure. It is the purpose of this chapter, therefore, to describe the galvanomagnetic properties of the semiconductor films as well as the structural properties. Since the germanium substrates used for much of the structural study are themselves conducting, the interpretation of galvano effects from films grown on such is extremely complex. Insulating substrates (Al_2O_3) were therefore employed for all electrical measurements. Semi-insulating (Cr-doped) GaAs was also employed in a number of cases to further observe the effect of crystallinity on the electrical properties. However, these films turned out to be largely degenerate so that direct comparison was not justifiable.

The electrical results are discussed in terms of possible scattering mechanisms, particularly in relation to the structural properties of the films.

7.2. ELECTRICAL EXAMINATION

Electrical assessment of the layers was made using a conventional geometry Hall effect technique. The substrates were, where possible, in the form of rectangular slices of length to width ratio 3:1. Electrical contact to the film was made using indium solder and silver wire (~5 thou diameter). A five point method was employed; the circuit and the sample geometry is shown in Fig. 7.1. All measurements were in terms of voltage, as indicated by the circuit, which were measured using a Solartron 1450 digital voltmeter. A low current ($25\mu A$) was used to reduce heating effects and the magnetic field was produced by a permanent magnet giving a field of 3170 oe. Measurement over a temperature range $77-293^{\circ}K$ was accomplished by sealing the specimen in a copper can in liquid nitrogen and allowing the nitrogen to boil off. Measurements were carried out during the decrease and increase temperature cycle to eliminate any problem due to temperature differences between specimen and thermocouple. The thermocouple used was copper-constantan. In general, four measurements of each parameter were taken, for two directions of current flow and two directions of magnetic field. An average value was then used for calculation. To calculate values of resistivity, the film thickness is required and this was measured using a Talysurf instrument (as described in a previous chapter).

In cases where the specimen geometry was less than 3:1 corrections have to be made to allow for the shorting effect of the end contacts. A curve given by Putley (1960) was used and all values of mobility etc. given in the results are corrected on the basis of this curve.

7.3. RESULTS

7.3.1. Ge/Al$_2$O$_3$

Films of Ge were grown on alumina at substrate temperatures ranging from room temperature to $600^{\circ}C$, and rates ranging from $1\overset{o}{A}/s - 5\overset{o}{A}/s$. In all cases the thickness was measured of the actual films, not of a monitor. The curve shown in Fig. 5.26 represents the growth conditions. The results

FIG 7.1

CIRCUIT AND ELECTRODE GEOMETRY FOR HALL EFFECT MEASUREMENTS
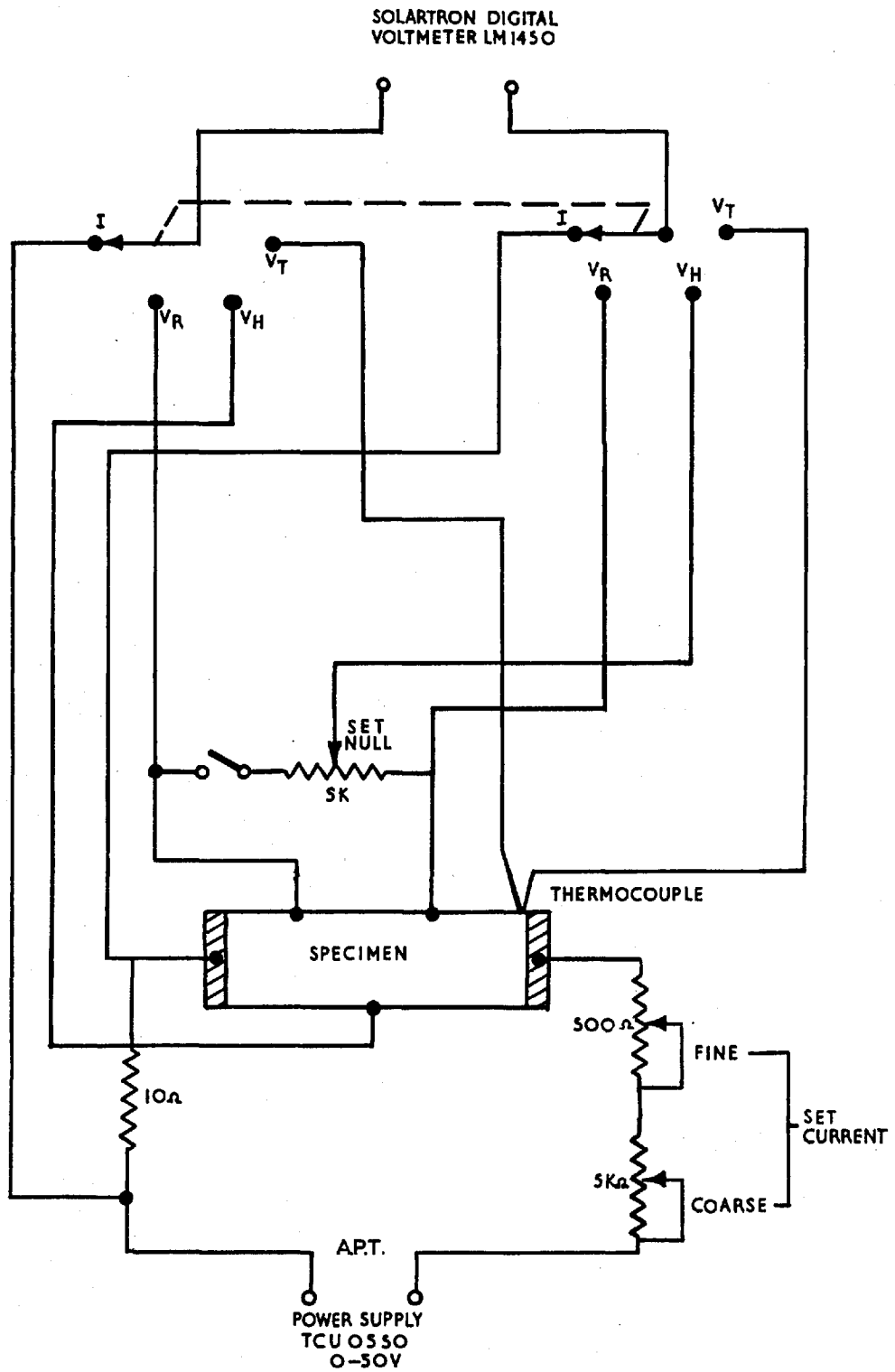
of the electrical measurements on a number of films are plotted in Figures
7.2. to 7.9. These show Hall mobility, μ_H, Hall coefficient, R_H, conductivity
σ or resistivity, ρ, and carrier concentration. $\frac{1}{R_H|e|}$, as functions of the
measuring temperature T_M or deposition temperature T_D. The films in all cases
were p-type, determined by the hot-probe method. Only a few films were measured
over the full temperature range $77^{\circ}K$ to $293^{\circ}K$. All films were measured at $77^{\circ}K$
and at $293^{\circ}K$.

The plot of μ_H against $1/T_M$ (where T_M is the measuring temperature) shows
that for films grown at low substrate temperatures, the room temperature mobility
is greater than the value at $77^{\circ}K$. High substrate temperatures however, show
the reverse to be true. If the mobilities are plotted as a function of the
deposition temperature, as shown in Fig. 7.6. then the region in which the change-
over takes place can readily be seen. This change is found to occur at approx-
imately the ordering temperature previously referred to in Chapter 5.

Curves showing the variation of the Hall coefficient, the conductivity
and the concentration of excess carriers as a function of deposition temperature
follow the expected trend, i.e. higher temperatures yield more nearly intrinsic
films. (The films are extrinsic over the temperature range measured. This is
discussed in a later section).

7.3.2. Ge/GaAs

In order to investigate whether the substrate was having a profound effect
upon the measured galvanomagnetic properties of the Ge layers, it was desirable
to measure some layers grown on a substrate very similar to that of germanium.
Suitable high resistivity (Cr doped) GaAs substrates were therefore obtained and
Ge layers sputtered onto them using the triode system. The electron diffraction
results are described in Chapter 5 showing that the films grown at $350^{\circ}C$ and
above gave a good spot pattern indicative of epitaxial growth. The films grown
at $300^{\circ}C$ were not so perfect. These results were similar to Ge on Ge.

FIG 17.2

THE VARIATION OF HALL MOBILITY μ_H, WITH MEASURING TEMPERATURE, T_M FOR Ge FILMS GROWN ON < ITO2> Al$_2$O$_3$
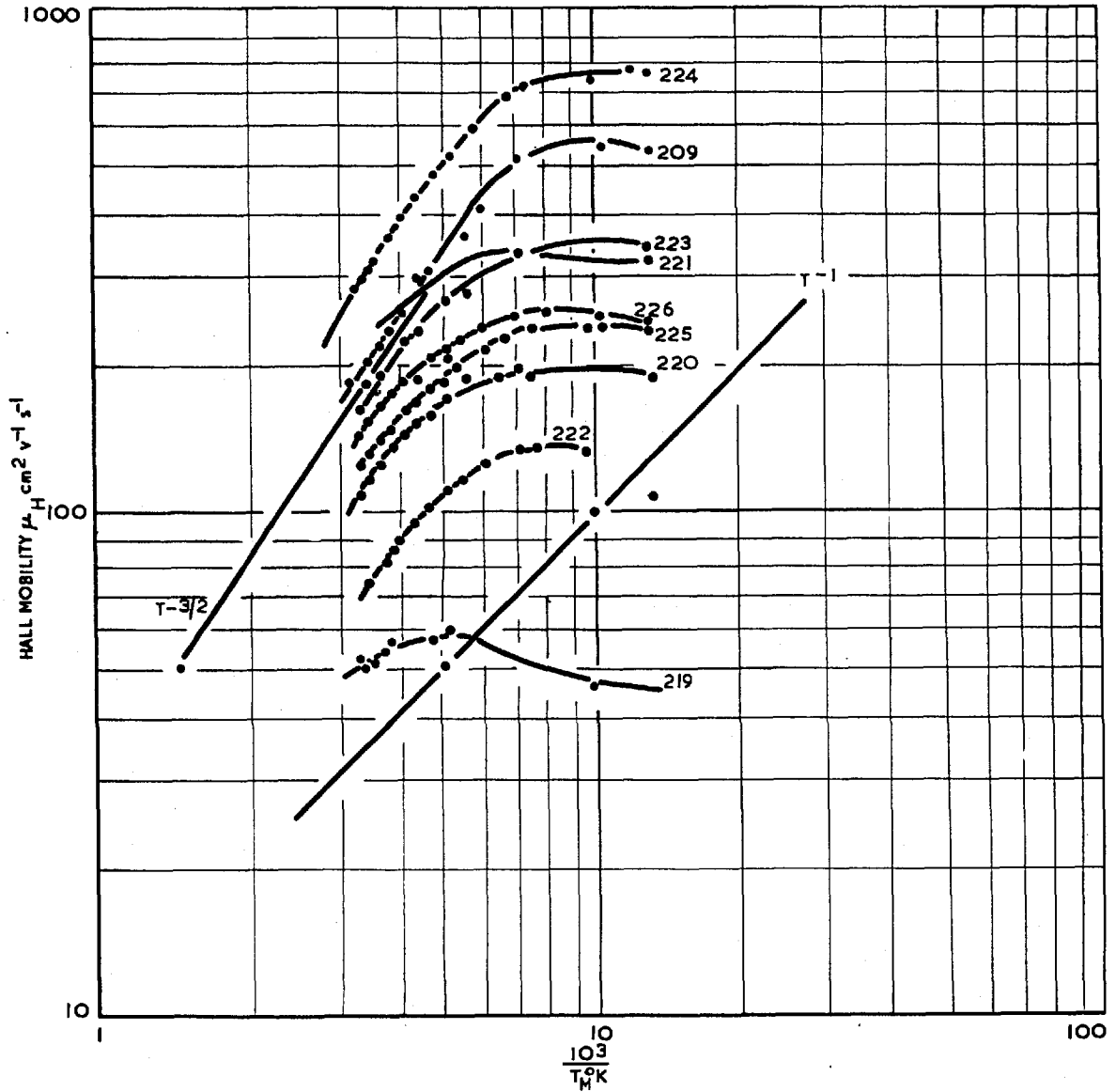
FIG ■ 7.3

THE VARIATION OF HALL COEFFICIENT, R_H, WITH MEASURING TEMPERATURE, T_M, FOR Ge FILMS GROWN ON <ITO2> Al_2O_3.
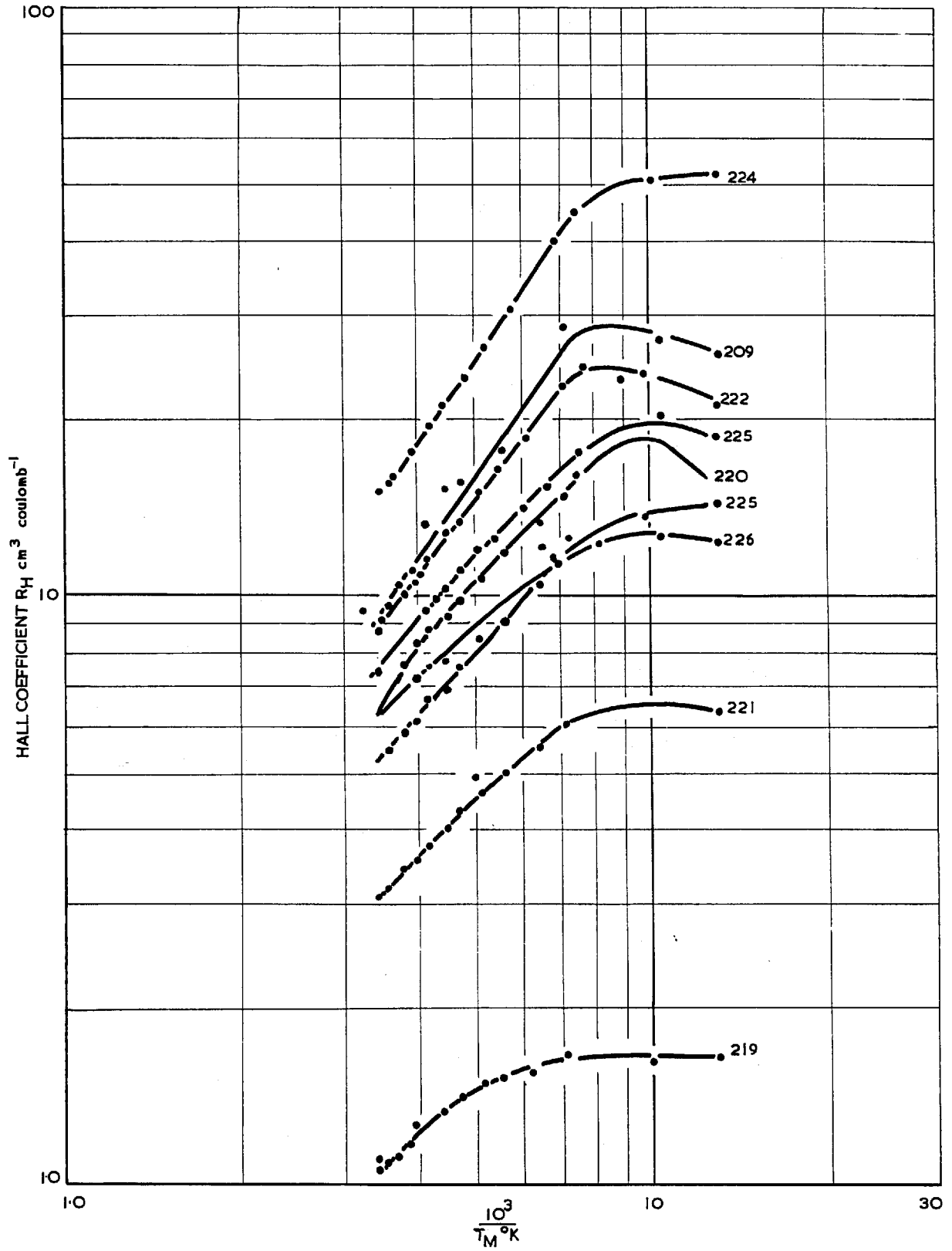
FIG 7.4

THE VARIATION OF CONDUCTIVITY, σ, WITH MEASURING TEMPERATURE, T_M FOR Ge FILMS GROWN ON <1TO2> Al_2O_3.
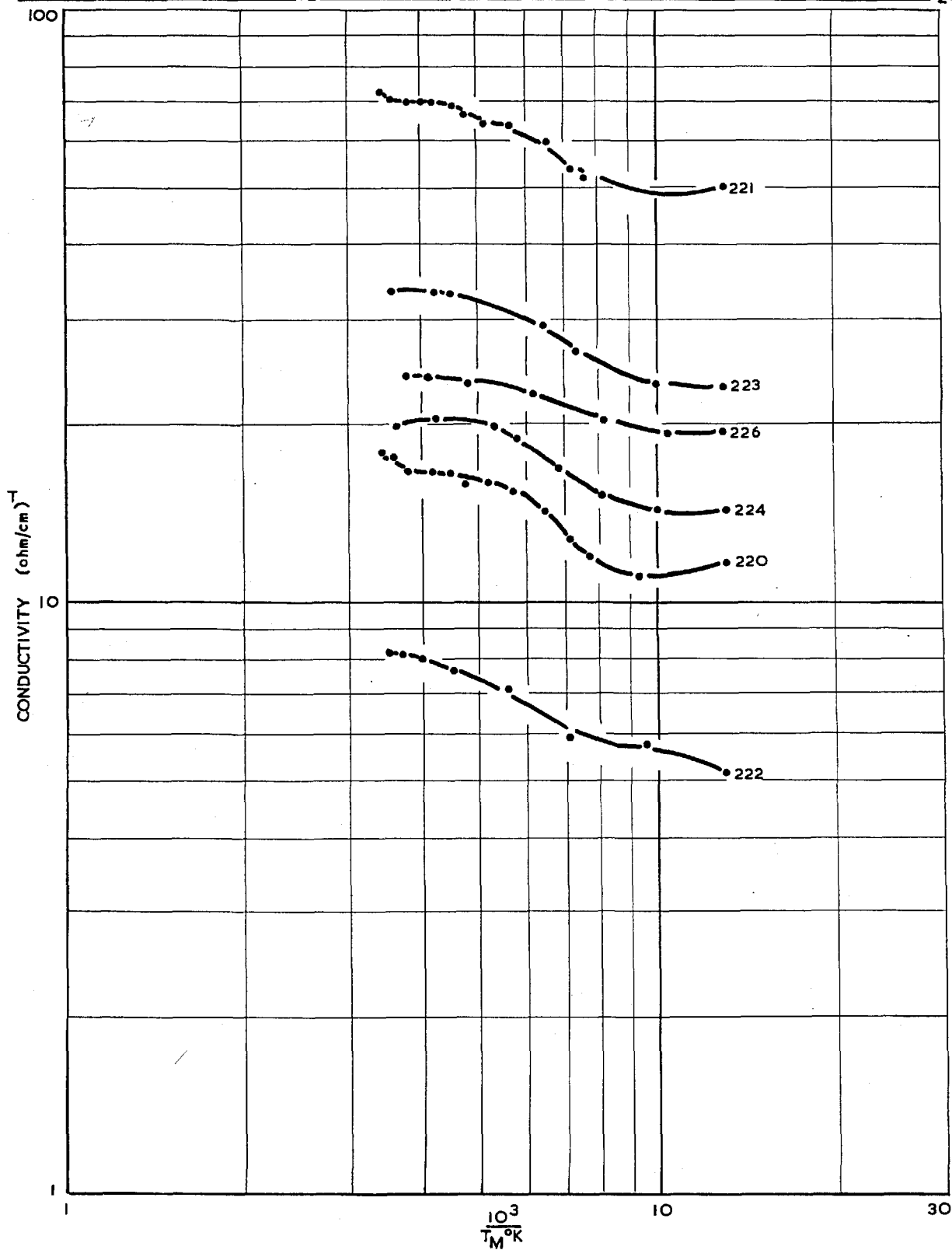
FIG 7.5
THE VARIATION OF MAJORITY CARRIER CONCENTRATION $1/R|e|$
WITH MEASURING TEMPERATURE, T_M FOR Ge FILMS GROWN ON <ITO2>Al$_2$O$_3$
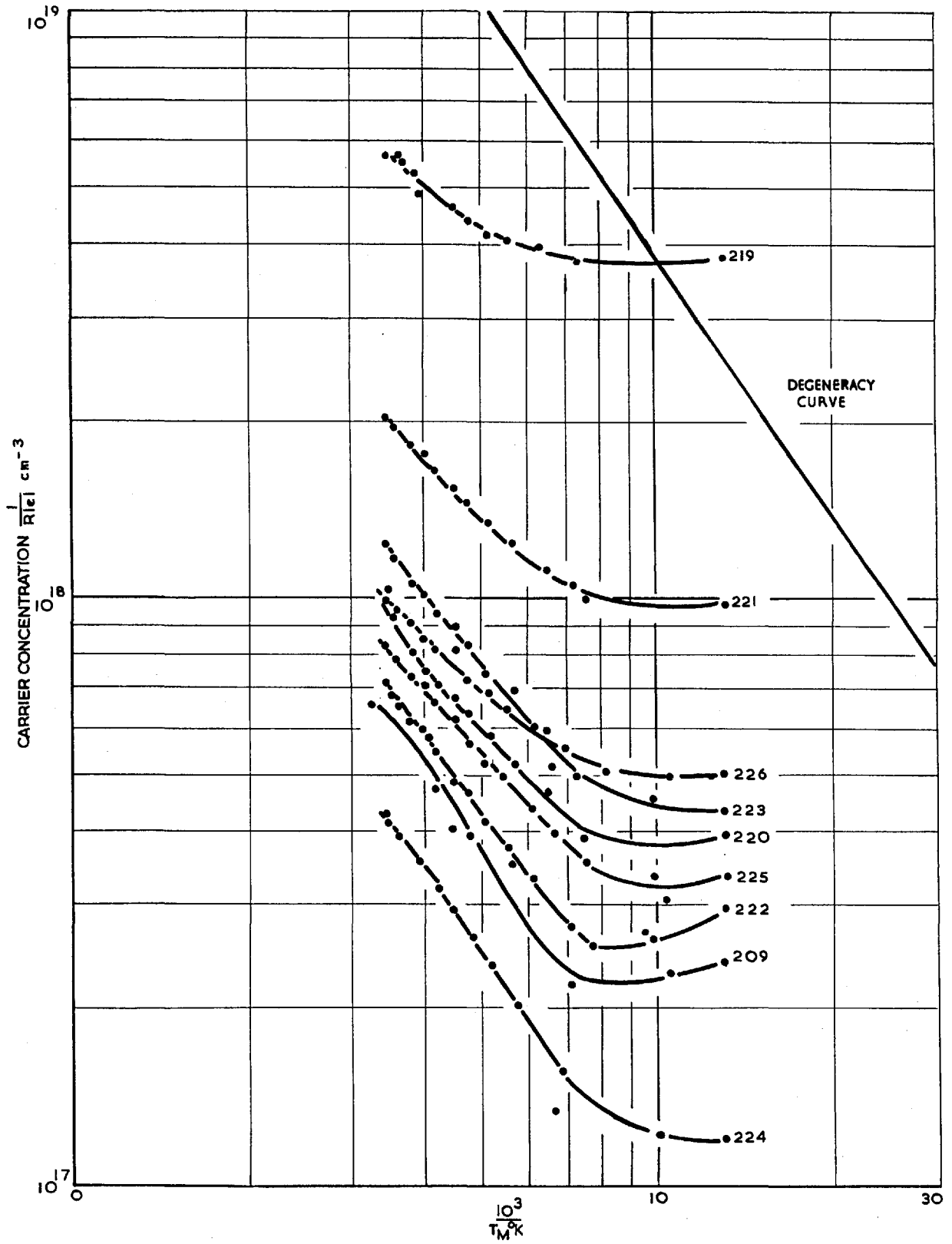
FIG ▪ 7.6

THE VARIATION OF HALL MOBILITY μ_H WITH DEPOSITION TEMPERATURE T_D FOR Ge FILMS GROWN ON <1TO2> Al$_2$O$_3$
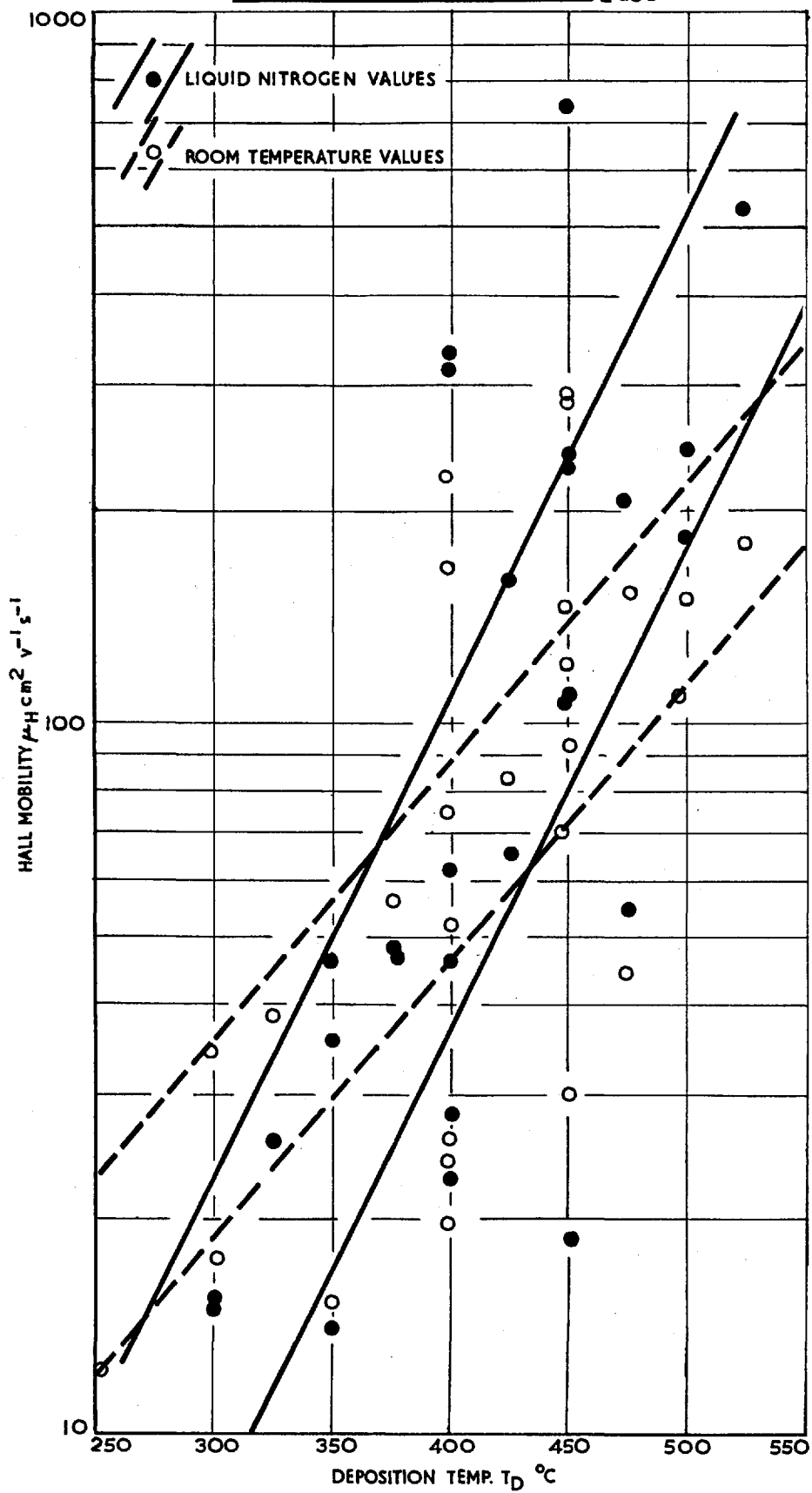
FIG 7.7
THE VARIATION OF HALL COEFFICIENT, R_H WITH DEPOSITION TEMPERATURE, T_D, FOR Ge FILMS GROWN ON <1TO2> Al_2O_3.

FIG ■ 7.8
THE VARIATION OF RESISTIVITY, ρ WITH DEPOSITION TEMPERATURE T_D
FOR Ge FILMS GROWN ON<1 TO 2> Al_2O_3
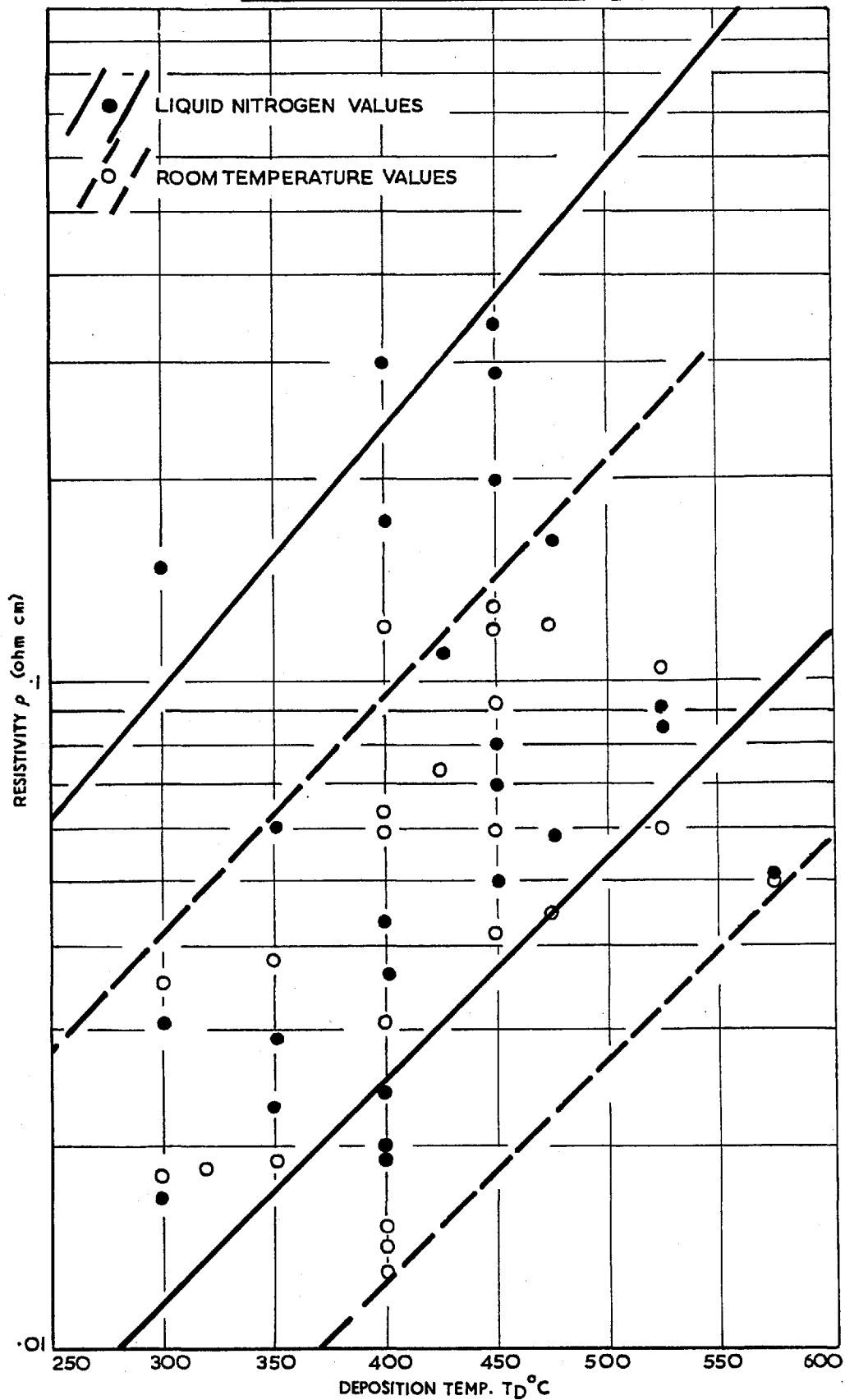
FIG 79
THE VARIATION OF MAJORITY CARRIER CONCENTRATION, $1/R_{lel}$, WITH DEPOSITION TEMPERATURE T_D.
FOR Ge FILMS GROWN ON <ITO2> Al$_2$O$_3$.
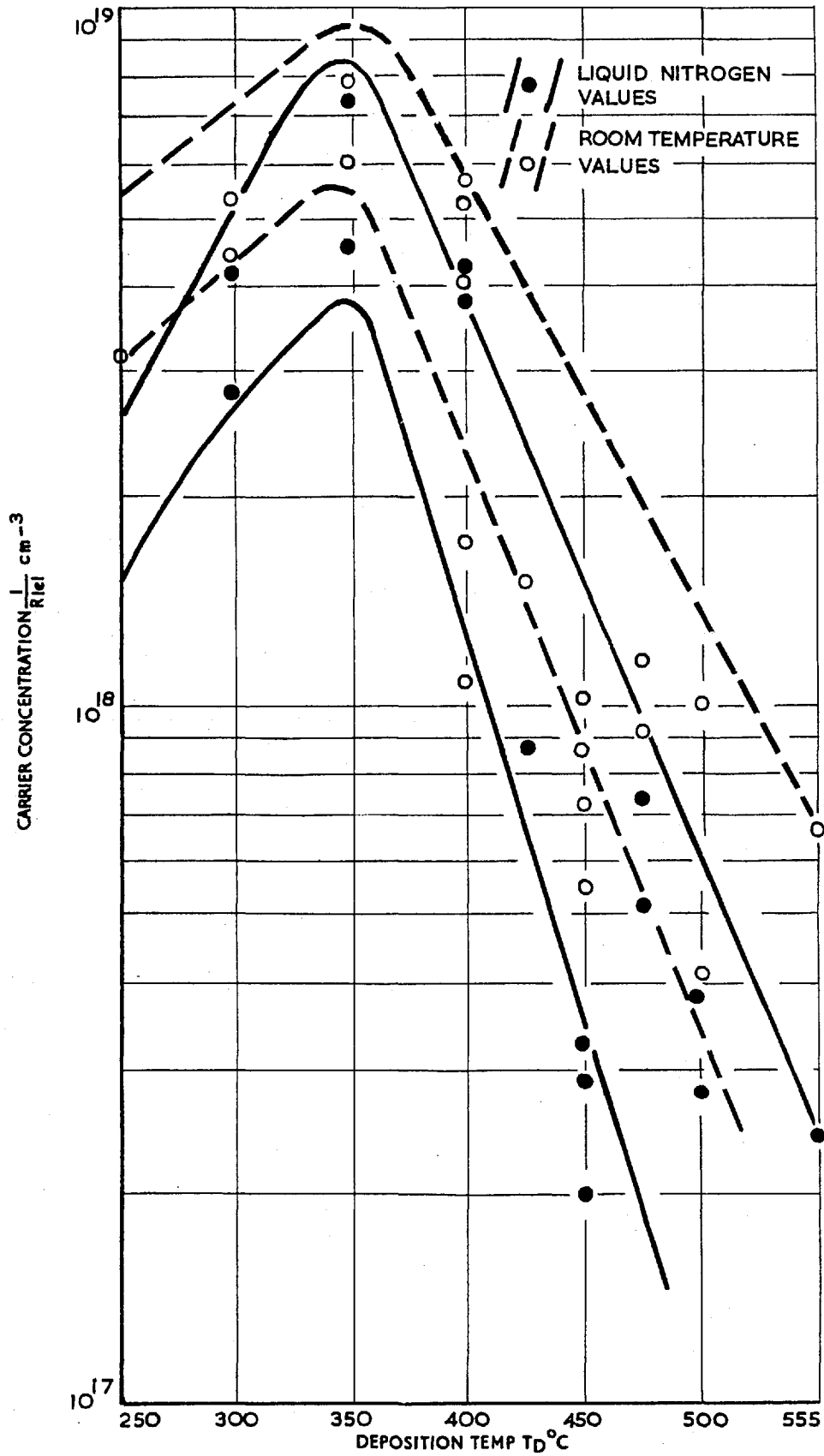
Galvanomagnetic properties of the films were measured as for Ge on Al_2O_3. The results for two of the films are shown in Fig. 7.10 (a) and 7.10 (b). In calculating R_H and σ, the film thickness had to be estimated from Ge/Al_2O_3 data as it was not possible to measure film thickness on the actual substrate. The results show that the films are largely degenerate having an unexpectedly large carrier concentration. Thus, although the Hall mobilities are similar to those obtained from films grown on Al_2O_3, direct comparison in terms of structure is not justifiable. The reasons for the higher carrier concentration in this case is not clear and more definitive experiments are required.

7.3.3. Cd₃As₂/Various Substrates

The target material of bulk n-type Cd_3As_2 was obtained from R.R.E. Malvern. Films were deposited under the conditions indicated in Chapter 5 onto various substrates indicated in Table 1, properties were measured as for Ge/Al_2O_3 from room temperature down to $77^{\circ}K$ and are shown in Figures 7.11 - 7.14. The results are tabulated overleaf.

From these results it can be seen that the electron concentration is very high, as one might expect from a low band gap material ($Eg = 0.13$ eV for bulk Cd_3As_2 at room temperature). The results of annealing show the mobility to have decreased with annealing with an associated decrease in the electron concentration. The effect of deposition rate on carrier concentration (as indicated by 1/Rlel) is found to be insignificant over the range studied. The films are extrinsic and degenerate. The bulk properties of the Cd_3As_2 target material are unknown but, from the work of Lovett (1967), it should have a bulk mobility of around 20000 $cm^2/V.sec$.

7.3.4 InSb, Bi₂Te₃, GaAs, PbTe/Various Substrates

The galvanomagnetic properties of InSb were found to be very poor indeed. The measured mobility of a film grown on mica or alumina at $325^{\circ}C$ and a rate of 1.6 Å/s was found to be only 50 $cm^2 \, V^{-1} \, s^{-1}$. A room temperature deposition

FIG ▬ 7.10(a)

THE VARIATION OF HALL MOBILITY, μ_H, AND HALL COEFFICIENT, R_H, WITH MEASURING TEMPERATURE, T_M, FOR Ge FILMS GROWN ON Cr DOPED Ga As
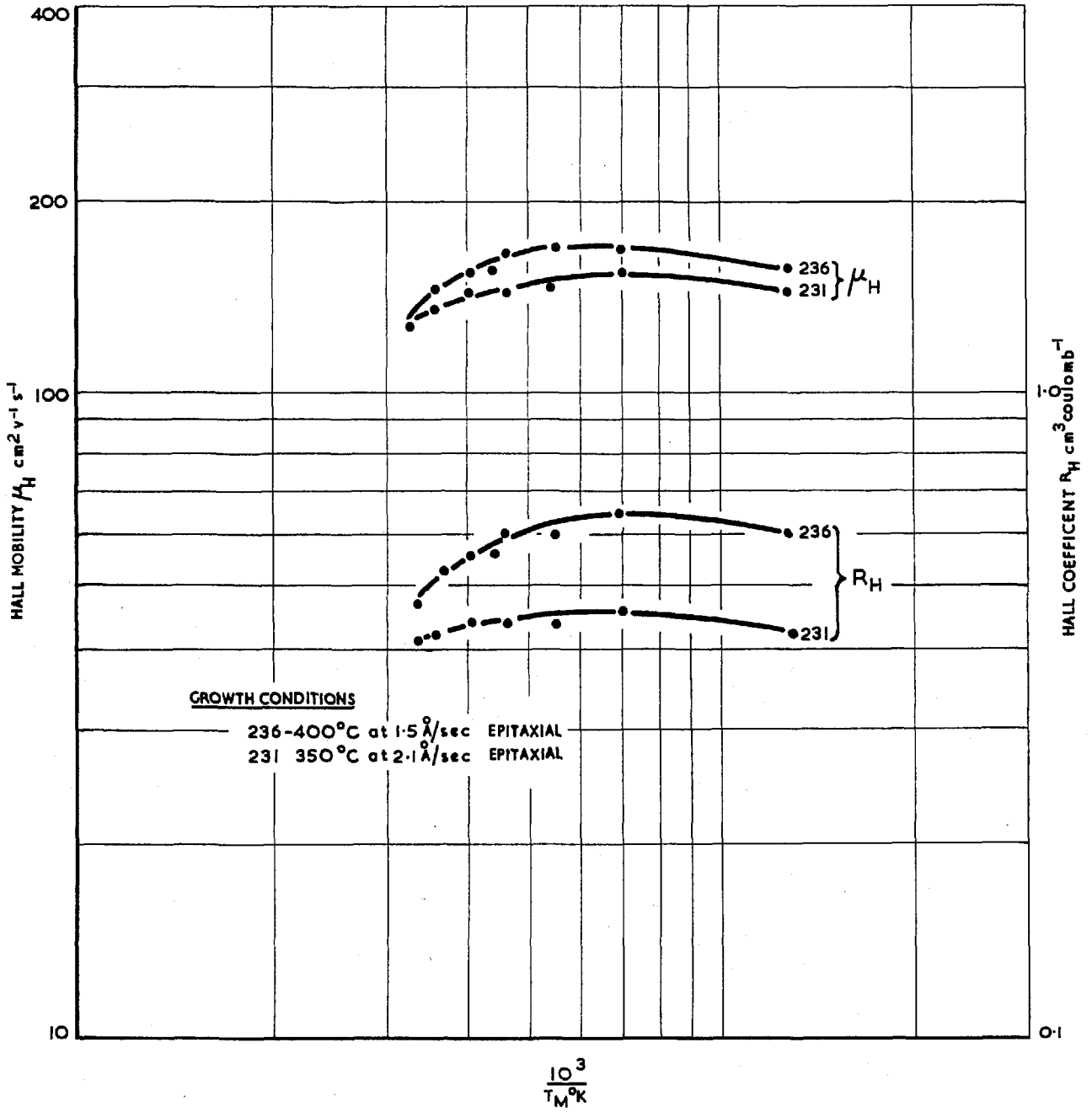
FIG 7.10(b)

THE VARIATION OF CONDUCTIVITYσ AND MAJORITY CARRIER CONCENTRATION $1/R|e|$ WITH MEASURING TEMPERATURE T_M
FOR Ge FILMS GROWN ON Cr DOPED Ga As
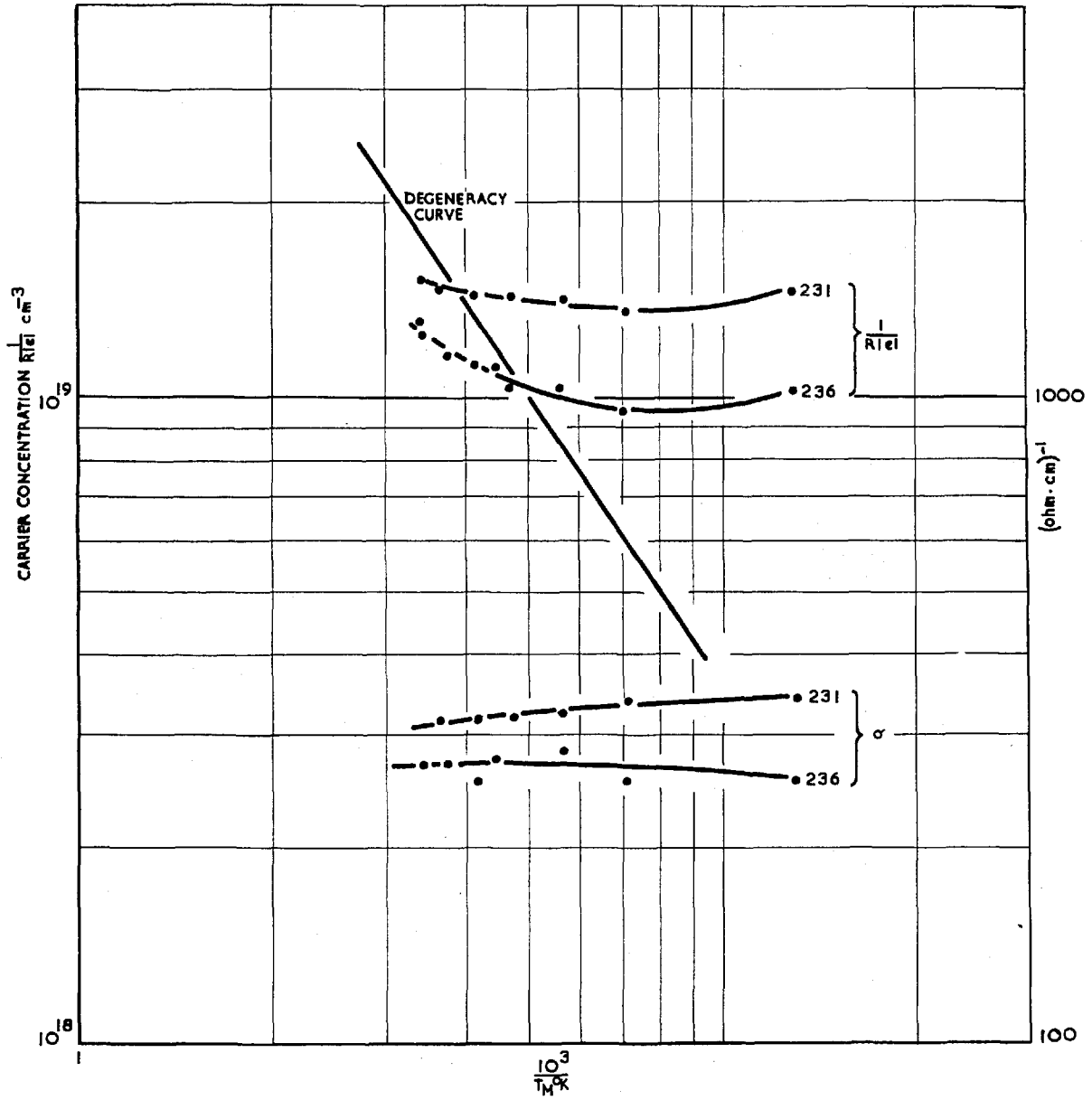
TABLE 1

Galvanomagnetic properties of Cd_3As_2 films deposited onto various substrates – measured at $300°C$

Specimen No.	Substrate Material	Temp. °C	Rate Å/s.	Thickness Å	μ_H cm²V⁻¹s⁻¹	R_H cm³/ coul.	σ Ω cm⁻¹	$1/R|e|$ cm⁻³
							Tm = $300°K$	
LX1	mica	25	?	1875	78.8	1.28	61	4.9
LX1/ann'd	"	"	"	"	564	1.8	310	3.5
LX4	"	"	"	1690	861	1.1	630	5.5
LX5	glass	"	"	840	583	0.72	800	8.6
LX6	"	63	0.7	1250	661	0.43	1500	14.3
LX6/ann'd	"	"	"	"	153	4.2	365	1.5
LX7	"	68	0.7	1330	669	1.4	500	4.5
LX7/ann'd	"	"	"	"	215	5.2	500	1.2
LX8	"	80	0.6	920	611	0.9	680	6.9
LX9	"	25	0.4	670	506	0.85	595	7.4
LX10	"	30	1.25	750	448	0.91	500	6.9
LX11	NaCl	65	1.0	60	260	0.69	375	9.1
LX12	Mica	"	"	"	272	0.92	295	6.8

Note: Specimens LX11 and LX12 are not corrected for specimen electrode geometry (as detailed in Section 7.2). They are included for comparison with each other since they have similar geometries.

FIG 7.11
THE VARIATION OF HALL MOBILITY, μ_H WITH MEASURING TEMPERATURE T_M FOR Cd_3As_2 FILMS
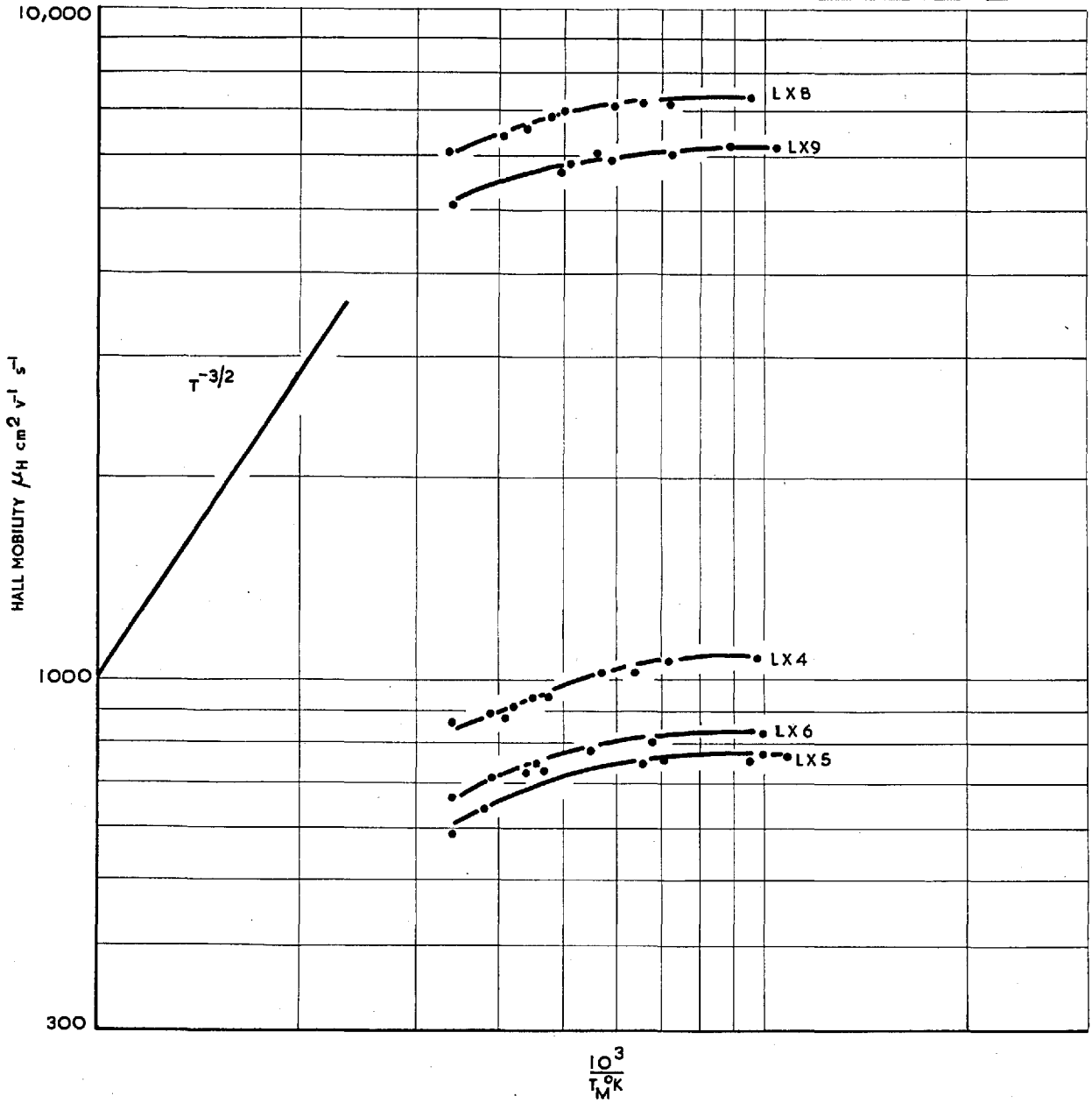
FIG. 7.12

THE VARIATION OF HALL COEFFICIENT, R_H, WITH MEASURING TEMPERATURE, T_M,
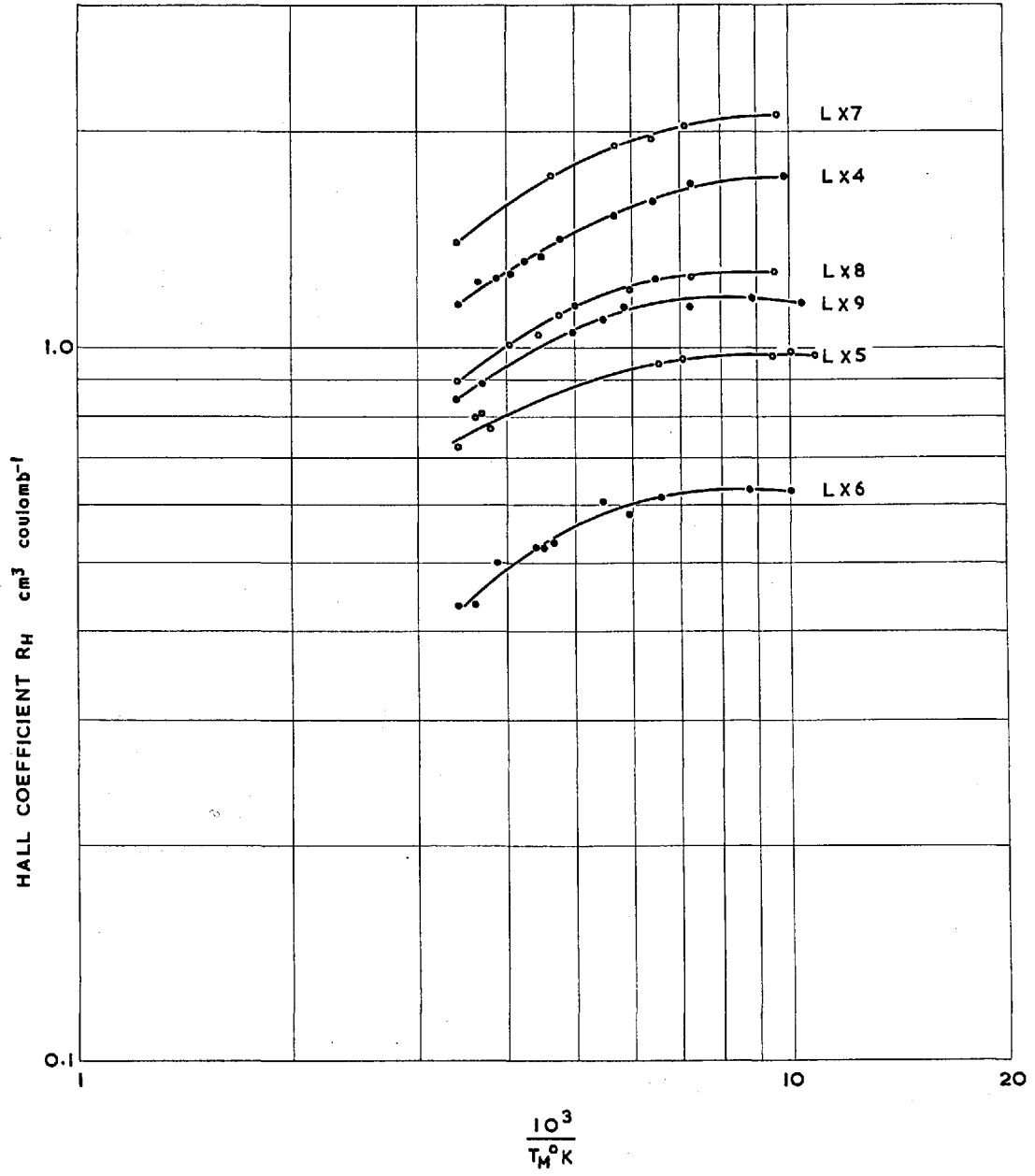
FOR $Cd_3 As_2$ FILMS

FIG. ■ 7.13

THE VARIATION OF CONDUCTIVITY, σ, WITH MEASURING TEMPERATURE, T_M, FOR Cd_3As_2 FILMS
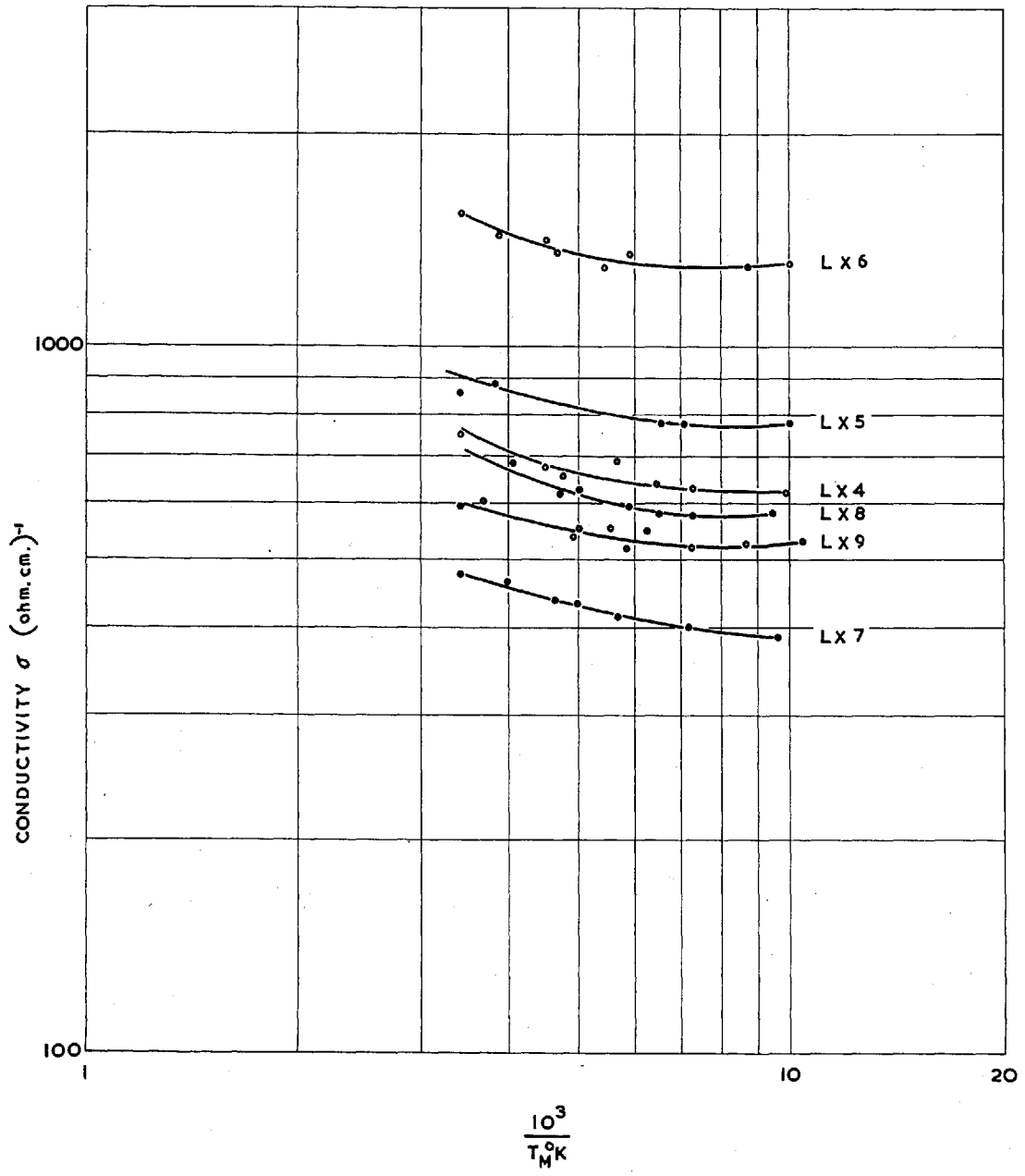
FIG. 7.14

THE VARIATION OF MAJORITY CARRIER CONCENTRATION, $1/R|e|$, WITH MEASURING TEMPERATURE, T_M, FOR Cd_3As_2 FILMS
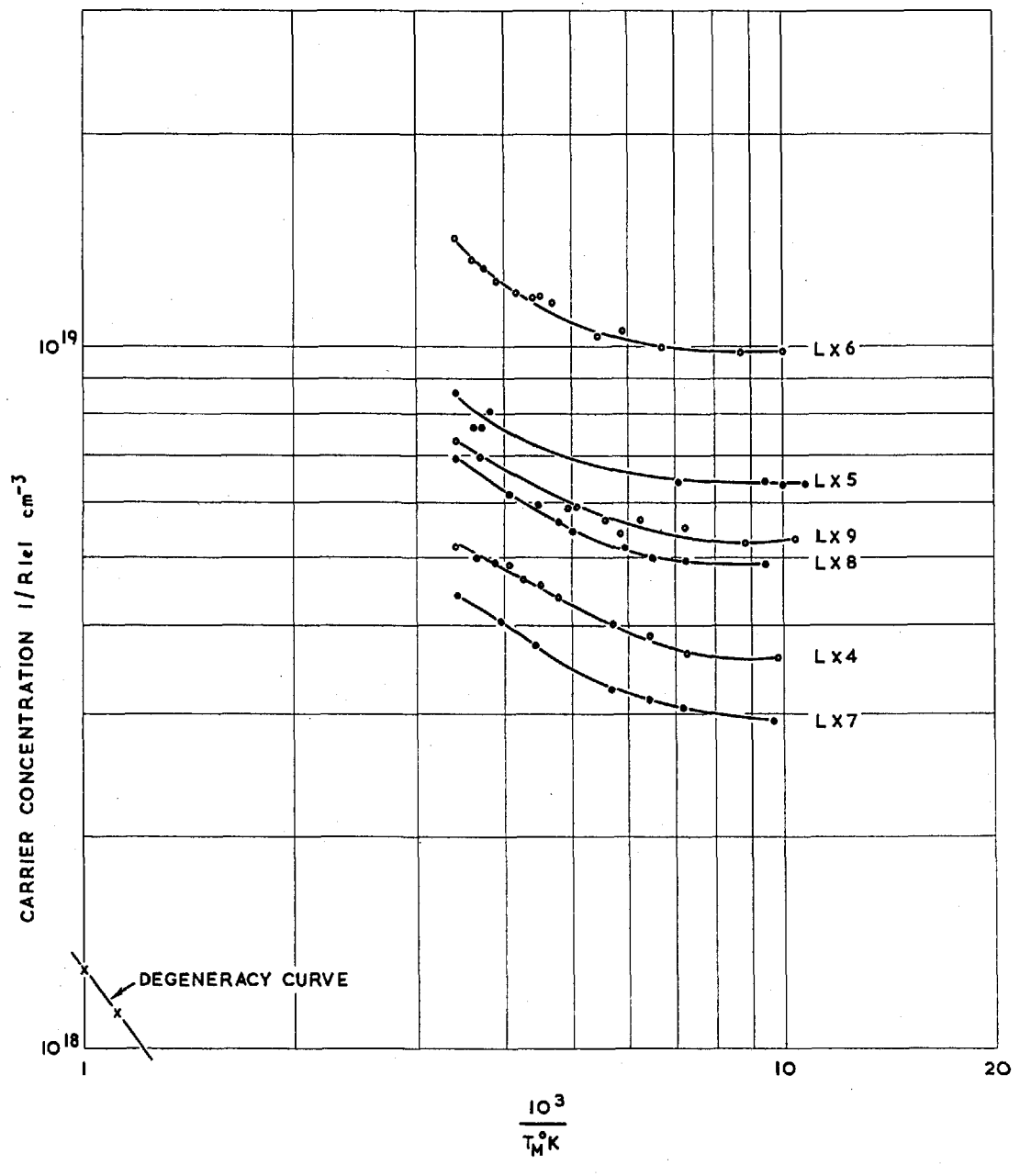
onto mica at the same rate produced a mobility of only 10 $cm^2 V^{-1} s^{-1}$ and onto glass a value of 35 $cm^2 V^{-1} s^{-1}$ (deposited at 1/10 the rate). Annealing the films increased the mobility to 130 $cm^2 V^{-1} s^{-1}$. None of the films were measurable at $77^\circ K$ as the resistance had increased too much. The results of the measurements are tabulated below.

TABLE 2

Galvanomagnetic properties of InSb films deposited onto various substrates – measured at $300^\circ K$

No.	Sub-strate	Temp. $^\circ C$	Rate $\overset{\circ}{A}$/sec.	Thick-ness $\overset{\circ}{A}$	μ_H $cm^2 V^{-1} s^{-1}$	R_H cm^3/coul.	σ Ωcm^{-1}	$1/R|e|$ cm^{-3}
LY4	Al_2O_3	325	1.6	4200	43	12.6	3.4	5×10^{17}
LY6	mica	25	2.0	3500	10	4.4	2.3	1.3×10^{18}
LY6/ann'd	"	"	"	"	140	50.6	3.6	1.3×10^{17}
LY7	"	300	–	–	48	thickness unknown		
LY8	glass	25	13	850	34	1.03	34	6.1×10^{18}

The conclusions to be drawn from this table are that higher substrate temperature and deposition rate produce films nearer to intrinsic and that annealing is also a definite advantage.

The other films which were sputtered, apart from Cd_3As_2, also showed disappointing galvanomagnetic properties. Bi_2Te_3 films produced no measurable Hall effect. It was found, however, that from the p-type target used, films of both conductivity type could be produced depending upon the substrate temperature. Films produced at $100^\circ C$ were n-type, while those produced at $200^\circ C$ were p-type. The film thickness and deposition rate were approximately constant.

Electrical measurements on GaAs films were not successful. This was thought to be due to the oxide content in, and on the surface of the films. PbTe films also showed only limited success. A 2600Å film grown at 4Å/s onto a 200°C alumina substrate produced a room temperature mobility of only 70 $cm^2 V^{-1} s^{-1}$.

7.4. DISCUSSION OF RESULTS

7.4.1. Germanium

The results of the measurement of galvanomagnetic properties in the germanium films proved interesting and valuable. From the curves shown in Fig. 7.5. it is clear that the films are very extrinsic in nature. The impurity level is not so high as to render the films degenerate over the temperature range considered, as is indicated by the degeneracy condition curve of Fig. 7.5. This curve is derived from the expression given by Pearson and Bardeen (1949).

$$T_o = \left(\frac{h^2}{8km_h}\right) \left(\frac{3}{\pi}\right)^{2/3} p^{2/3} \qquad (7.1)$$

where h = Plancks constant   k = Boltzmann constant

m_h = mass of hole   p = hole concentration

To = temperature for which the energy of a hole corresponding to the energy

at the surface of the Fermi distribution is equal to kTo . Putting

m_h = m = free electron mass.

$$T_o = 4.2 \times 10^{-11} p^{2/3} \qquad (7.2)$$

The films can be shown to be extrinsic by consideration of the equation:

$$p_i^2 = n_i^2 = N_c N_v T^3 \exp\left(\frac{-E_g}{kT}\right) \qquad (7.3)$$

(A full discussion of this equation is given by R.A. Smith (1964) p.76)

The value of T for which p_i is of the same order as the impurity concentration can be found by graphically solving the above equation in which p_i = p, N_c, N_v and E_g are known. This is done in Fig. 7.15 for various values

FIG. 7.15

PLOT OF EQUATION 7.3 FOR THE SOLUTION FOR INTRINSIC CONDUCTIVITY IN Ge FILMS

STRAIGHT LINES — $\log T - \log p_i / N_c N_v$ CURVED LINES — $\dfrac{\pm E_g}{kT}$

$\dfrac{0.663}{kT}$

$\dfrac{0.33}{kT}$

$\dfrac{0.11}{kT}$

$p_i = 2.2 \; 10^{13}$

$p_i = 10^{15}$

10^{17}

$p_i = 10^{18}$

10^{19}

$f(T)$

T °K
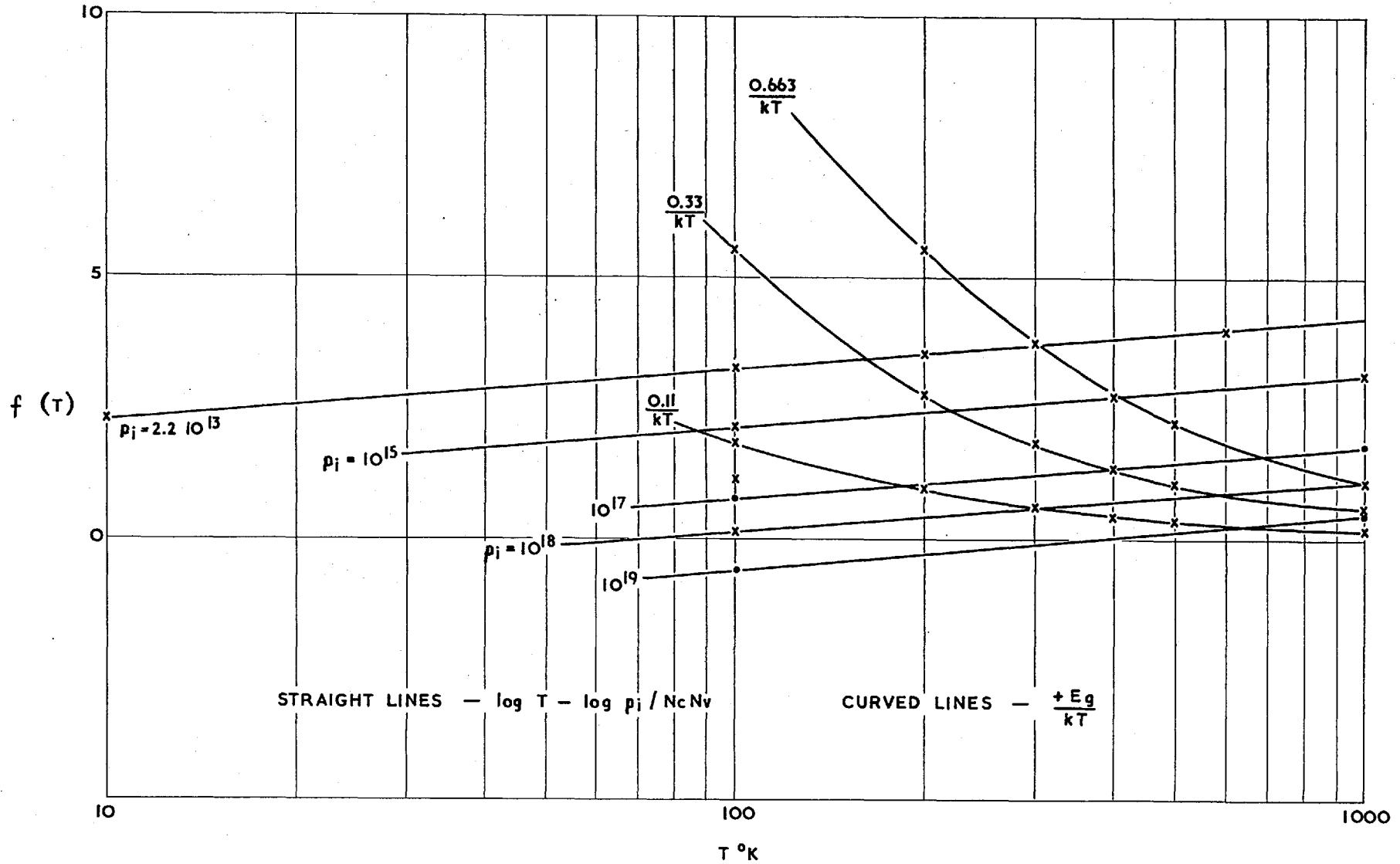
of n_i and E_g. The values of N_c and N_v are assumed equal (i.e. $m_e = m_h = m$) and E_g has been assumed constant with temperature. The solution of the equations are not precisely accurate therefore, but since m_e, m_h and E_g are unknown for our particular specimens to do otherwise would be unjustified. The curves show that the intrinsic temperature is considerably higher than the upper temperature limit of our experiments ($300^{\circ}K$) unless the band gap of the material is very low. This is unlikely. Thus we are safe in assuming the conduction processes to be extrinsic and need consider only a single charge carrier - namely, holes.

The degree of electrical conduction in a material depends upon the amount of scattering present. In a semiconductor there are two main types of scattering processes, assuming negligible surface effects, thermal vibration scattering and ionised impurity centre scattering. As might be expected, the former predominates at high temperatures. Associated with each of these processes is a relaxation time τ (or mean collision time). These are generally not the same, but when both types of scattering are operating, the two may be combined to give an average τ given by (Shockley 1950).

$$\frac{1}{\tau} = \frac{1}{\tau_1} + \frac{1}{\tau_i} \tag{7.4}$$

where τ_1 = lattice scattering relaxation time.

τ_i = impurity " " "

(N.B. this assumes τ to be independent of velocity)

From consideration of the current density and the average drift velocity, it can be shown that the conductivity mobility for holes is given by

$$\mu_c = \frac{e\tau}{m_h} \tag{7.5}$$

(e = electronic charge)

so that

$$\frac{1}{\mu_c} = \frac{1}{\mu_1} + \frac{1}{\mu_i} \tag{7.6}$$

It may be further shown that:

For thermal vibration (lattice) scattering $\tau_l \propto T^{-3/2}$

For impurity scattering $\tau_i \propto T^{3/2}$

We can therefore write

$$\frac{1}{\mu} = a\, T^{-3/2} + b\, T^{3/2} \tag{7.7}$$

where the first term represents impurity scattering and the second term thermal vibration (lattice) scattering. Manipulation of this equation gives

$$\frac{T^{3/2}}{\mu} = a + b\, T^{3} \tag{7.8}$$

so that a plot of $\dfrac{T^{3/2}}{\mu}$ against T^{3} should yield a straight line of slope b and intercept a.

Fig. 7.16 is such a plot for a series of different specimens. It will be seen that the slopes and intercepts are not the same for each film. From these curves and resultant values for the constants a and b, it is possible to calculate the expected variation of mobility with temperature based on just the two scattering processes. Fig. 7.17 is a repeat of Fig. 7.2 with the addition of the calculated curve for each specimen. The agreement is very good in the upper temperature region but in the low temperature region the measured mobility remains fairly constant as the temperature decreases while the calculation predicts a steady decrease. However the calculation neglects the variation of 'a' with temperature which will have the effect of increasing μ_h at low temperatures. The relaxation time for scattering on neutral impurities is independent of temperature and carrier energy, so that the mobility due to this mechanism is also independent of temperature. Grain boundary effects may also predominate at low temperatures where the grain size is small.

The full expression for μ_i and μ_l can be obtained for a non-degenerate semiconductor by consideration of the appropriate wave equations for μ_l and from the theory of Rutherford scattering for μ_i Shockley (1950) and Smith (1964), for example, derive these expressions and give

FIG. ■7.16

DETERMINATION OF COEFFICIENTS a AND b OF EQUATION7.7 FOR Ge FILMS
BY PLOTTING EQUATION7.8
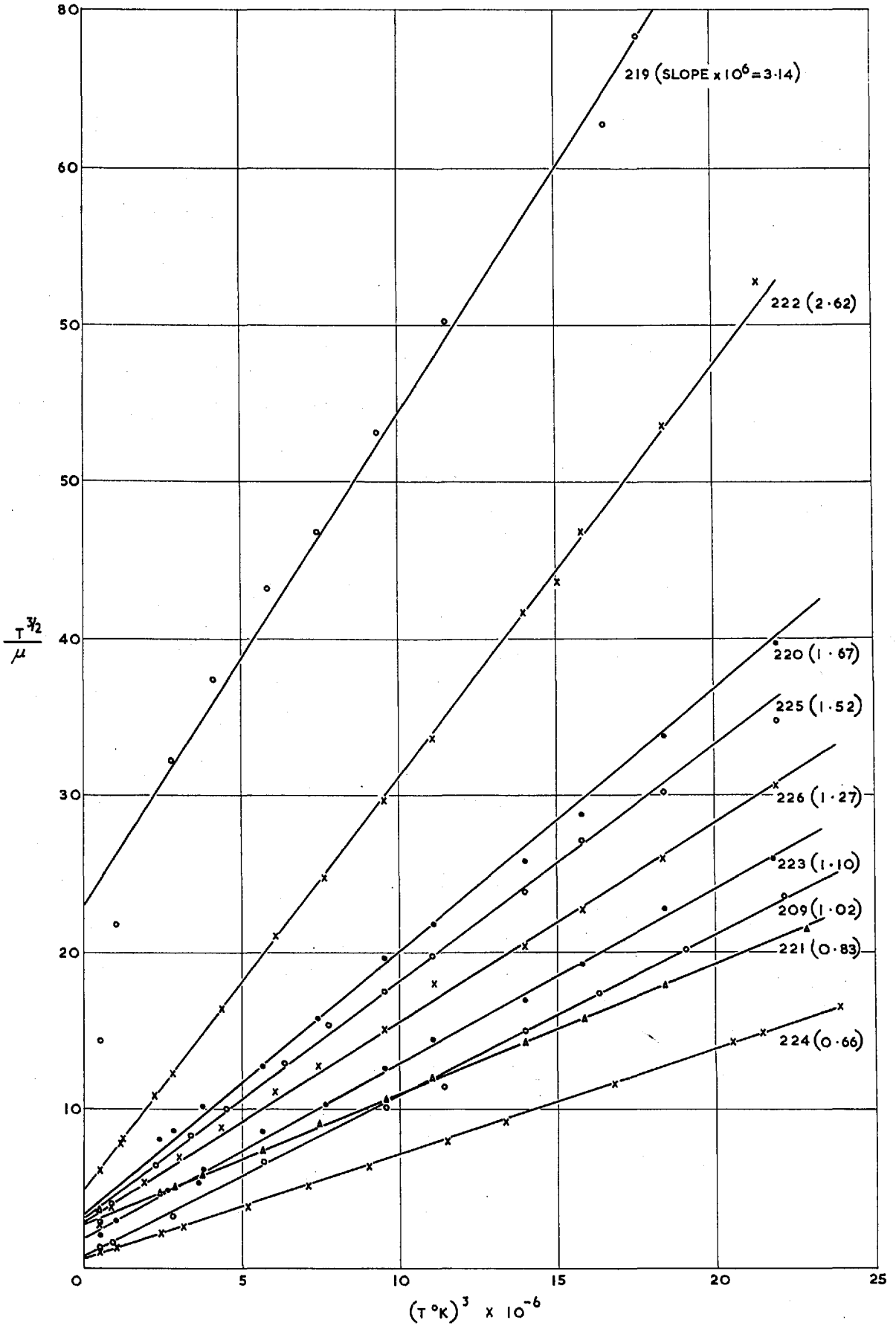
FIG. ▉7.17

VARIATION OF HALL MOBILITY, μ, WITH MEASURING TEMPERATURE, T_M, FOR Ge FILMS GROWN ON <$1\bar{1}02$> Al_2O_3. CALCULATED VALUES ARE FROM THE EQUATION $1/\mu = aT^{-3/2} + bT^{3/2}$ WHERE a & b ARE EMPIRICALLY DEDUCED CONSTANTS (SEE FIG.▉7.16)

—•—•— MEASURED VALUES

—x—x— CALCULATED VALUES FROM $\mu = aT^{-3/2} + bT^{3/2}$
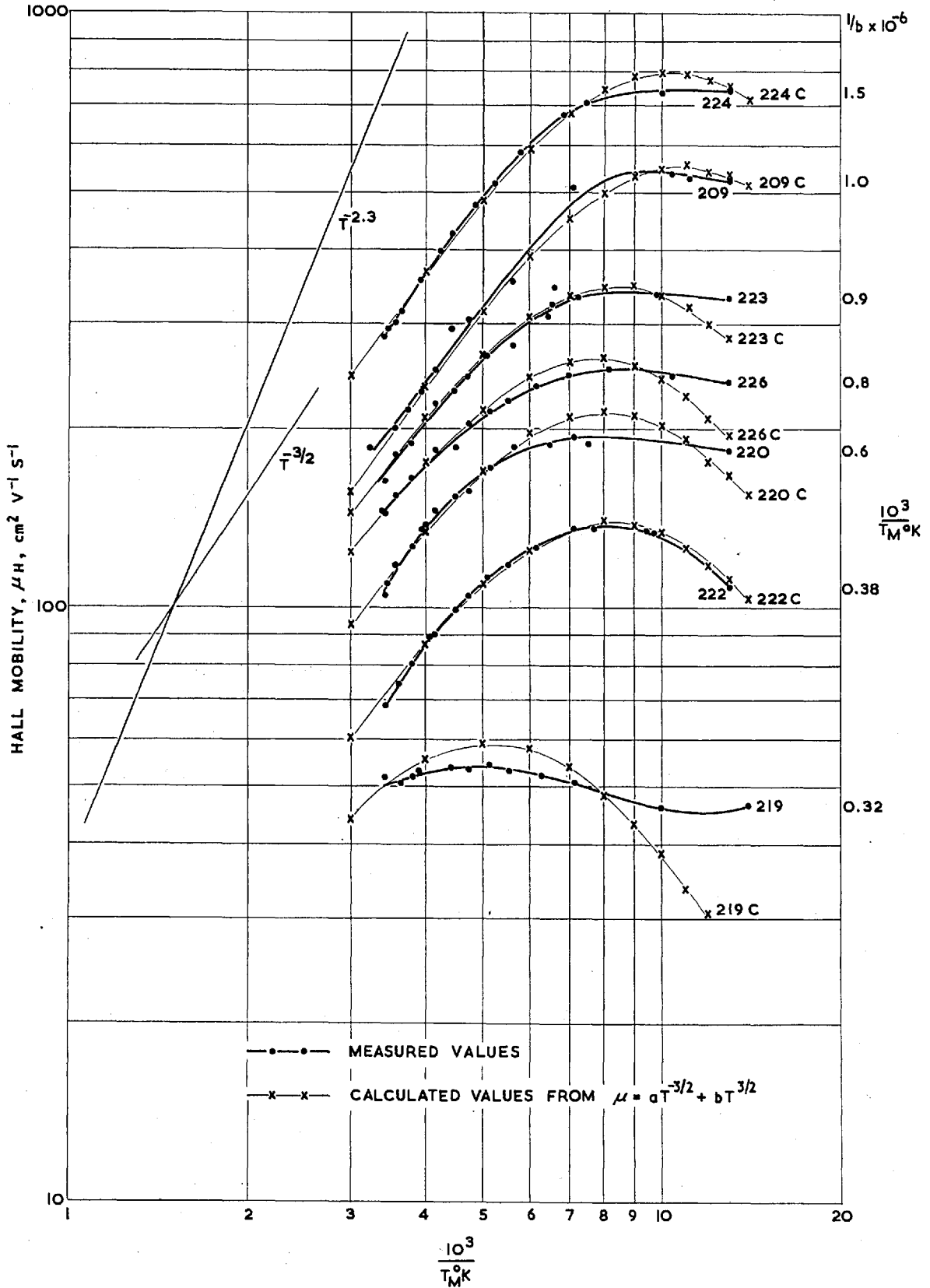
$$\mu_i = \frac{8}{\pi} \left[\frac{2}{\pi} \frac{K^2 (kT)^{3/2}}{N_I e^3 m^{\frac{1}{2}}} \quad \ln \left(1 + \frac{(3K \, kT)^2}{(e^2 \, N_I^{1/3})} \right) \right] \tag{7.9}$$

$$= 8.4 \times 10^{17} \ T^{3/2} / N_I \quad \ln (1 + x^2) \quad \text{for germanium}$$

where $x = 2.4 \times 10^4 \ T/N_I^{\frac{1}{2}}$ and N_I = impurity concentration

k = dielectric constant

And $\mu_1 = \frac{2\sqrt{2\pi}}{3} \frac{e \, \hbar^4 \ C_{11}}{E_{1n}^2 \, m^{5/2} k^{3/2}} \ T^{-3/2}$ (7.10)

where C_{11} = elastic content

E_{1n} = change in band edge per unit dilatation of crystal

(constants for a given material at NTP)

The constants a and b are therefore given by

$\frac{1}{a} = \frac{8.4 \times 10^{17}}{N_I \ln (1 + x^2)}$ (7.11a) and $\frac{1}{b} = \frac{2\sqrt{2\pi}}{3} \frac{e \, \hbar^4 \ C_{11}}{E_{1n}^2 \, m^{5/2} \, k^{3/2}}$ (7.11b)

The graphical values of 1/a agree fairly well with the value calculated from the above quotation as demonstrated below in Table 3.

TABLE 3

Spec. No.	209	219	220	221	222	223	224	225	226
N_I	2.2×10^{17}	3.8×10^{18}	3.7×10^{17}	9.8×10^{17}	2.9×10^{17}	4.3×10^{17}	1.2×10^{17}	3.3×10^{17}	5.1×10^{17}
$\frac{1}{a}$ graph	1.25	0.04	0.30	0.37	0.20	0.53	1.16	9.33	0.34
$\frac{1}{a}$ calc.	3.80	0.22	2.27	0.85	2.90	1.95	7.00	2.55	1.65

The constant 1/b is related to the mean free path of the carriers in the thermal scattering region. The above equations have assumed a semi-conductor with spherical constant energy surfaces and for such a system the mean free path, l, is given by Shockley (1950), p.269.

$$l = \frac{\hbar^4 \ C_{11}}{E_{1n}^2 \, k \, T \, m^2} \tag{7.12a}$$

$$= \frac{1}{b} \times \frac{3T}{2e} \sqrt{\frac{m \, k \, \pi}{2}} \tag{7.12b}$$

Hence the "mean free path" as a function of temperature may be determined for each film. The value at $300^{\circ}K$, calculated from equation 7.12b are given in Table 4 below for the specimens indicated. Also shown is the measured Hall mobility for each specimen at $300^{\circ}K$. The mobility is observed to increase as the value of l increases

TABLE 4

Spec. No.	209	219	220	221	222	223	224	225	226
$b \times 10^6$	1.03	3.14	1.67	0.83	2.62	1.1	0.66	1.52	1.27
$l \, \overset{\circ}{A}$	1350	440	830	1670	530	1260	2270	990	1180
$\frac{\mu}{cm^2} \, v^1 \, s^{-1}$	180	50	105	215	65	160	270	120	140

By comparing the above table with Fig. 7.2. it is immediately apparent that the highest room temperature mobility is observed for these films with the largest "mean free path". From bulk behaviour this is as expected. The most interesting feature is that the values of l in the films is very much lower than that found for bulk at the same temperature. There would thus seem to be a direct correlation between structure and electrical properties.

One of the features of thin film growth is that the layer grows initially as an island structure. The islands increase in size as the deposition continues eventually joining up to form a continuous layer. The film consists then of a mosaic structure of crystallites which may or may not be oriented with respect to each other, dependent upon the temperature. A typical value for island size is $500 - 2000\overset{\circ}{A}$ dependent upon substrate temperature. In a perfect single crystal there will be no grain boundaries to act as traps for the carriers but in a thin film, epitaxial or not, such boundaries will exist. It might be expected therefore that the effective mean free path of a carrier might be reduced by the presence of such boundaries. The mean island size increases with deposition temperature and film thickness.

Comparison of the "mean free path" values given in Table 4 with the growth conditions shown in Fig. 5.26 shows that the trend is for the higher mobility films to occur under growth conditions conducive to large grain size.

A further point, particularly relevant to sputtering, is that the arriving atoms have considerable energy at all stages of the growth period. A fair degree of damage may therefore be induced in the growing film. At high substrate temperatures such damage has a higher probability of being annealed out. One would therefore expect a film with low defect density and/or large crystallite size to have a larger mean free path and hence a higher mobility. This is shown to be the case by Marucchi (1965) who examined Ge layers of varying thicknesses deposited by evaporation.

It is interesting here to note the results of Sloope and Tiller (1963) on evaporated germanium films on CaF_2. They found that substrate temperature had a profound effect upon the measured mobility, it increasing with temperature, and also that increased film thickness showed an increase in mobility. They found that decreasing rate produced a lower defect density. Bearing in mind the fact that the films grown by sputtering are subject to a flux of high energy particles, the conclusions of Sloope and Tiller are very similar to ours above. They conclude that defects such as dislocations, stacking faults and microtwins appear to dominate the conduction processes. The defects have been suggested (Tramposch, 1966) as acting as acceptor states in the material. The mobility of Sloope and Tiller's films is very similar to the present ones grown under like conditions. They, however, find a $T^{-2.3}$ variation in mobility as the magnitude of the mobility increases. Fig. 7.2. shows our curves to follow a $T^{-1.5}$ law - typical of pure phonon scattering.

The suggestion of defects acting as acceptor states is strengthened by the fact that the plot of Hall co-efficient as a function of $1/T$ yields an ionisation energy value of ~ 0.03 eV. This value is obtained by plotting $\log (RT^{\frac{3}{4}})$ against $1/T$ derived from the expression (see Blakemore (19) p. 135).

$$p = \left(\frac{NvNa}{2}\right)^{\frac{1}{2}} \quad \exp \left(\frac{-Ed}{kT}\right) \qquad (7.13a)$$

for impurity conduction
when $N_A \gg N_D$

$$Nv = 2\left[\frac{2\pi mk T}{h^2}\right]^{3/2} = \text{Const.} \times T^{3/2}$$

$$\therefore \quad p = \text{const.} \times T^{\frac{3}{4}} \exp. \left(\frac{-Ed}{kT}\right) \qquad (7.13b)$$

Since $\quad R = \dfrac{1}{pe} = \text{const.} \times T^{-\frac{3}{4}} \exp. \left(\dfrac{Ed}{kT}\right)$

then $\quad RT^{\frac{3}{4}} = \text{const.} \times \exp. \left(\dfrac{Ed}{kT}\right) \qquad (7.14)$

This equation is plotted in Fig.7.18 for typical specimens. The measured value
of 0.03 eV is high for impurity levels in Ge which are typically ~0.01 ev. Only
impurities which can trap more than one electron (e.g. Au, Mn, Zn) have levels
as high as this. Such impurities are extremely unlikely in our system and it
is therefore a reasonable conclusion that the acceptor states are indeed due to
structural defects.

Wolsky (1966) has deposited Ge onto fused quartz substrates by sputtering
and his results are very similar to those reported here. He observes the mobility
to decrease with decreasing measuring temperature, this tendency being less for
increasing deposition temperature. This is precisely as the present findings
and is undoubtedly due to a decrease in scattering centres (lattice defects) as
the deposition temperature increases in association with an increase of grain
size. His plot of [1]/Rlel as a function of 1/T gives a crude estimation for
acceptor ionisation energy of 0.1 eV leading him to similar conclusions to those
given above. It should be mentioned that Wolsky's deposition was carried out at
a residual gas pressure of ~10^{-9} which, by comparison with these results, would
suggest that oxygen does not play a significant role in determining the

FIG. 7.18

DETERMINATION OF ACCEPTOR IONISATION ENERGY FOR Ge FILMS
BY SOLUTION OF EQUATION 7.14
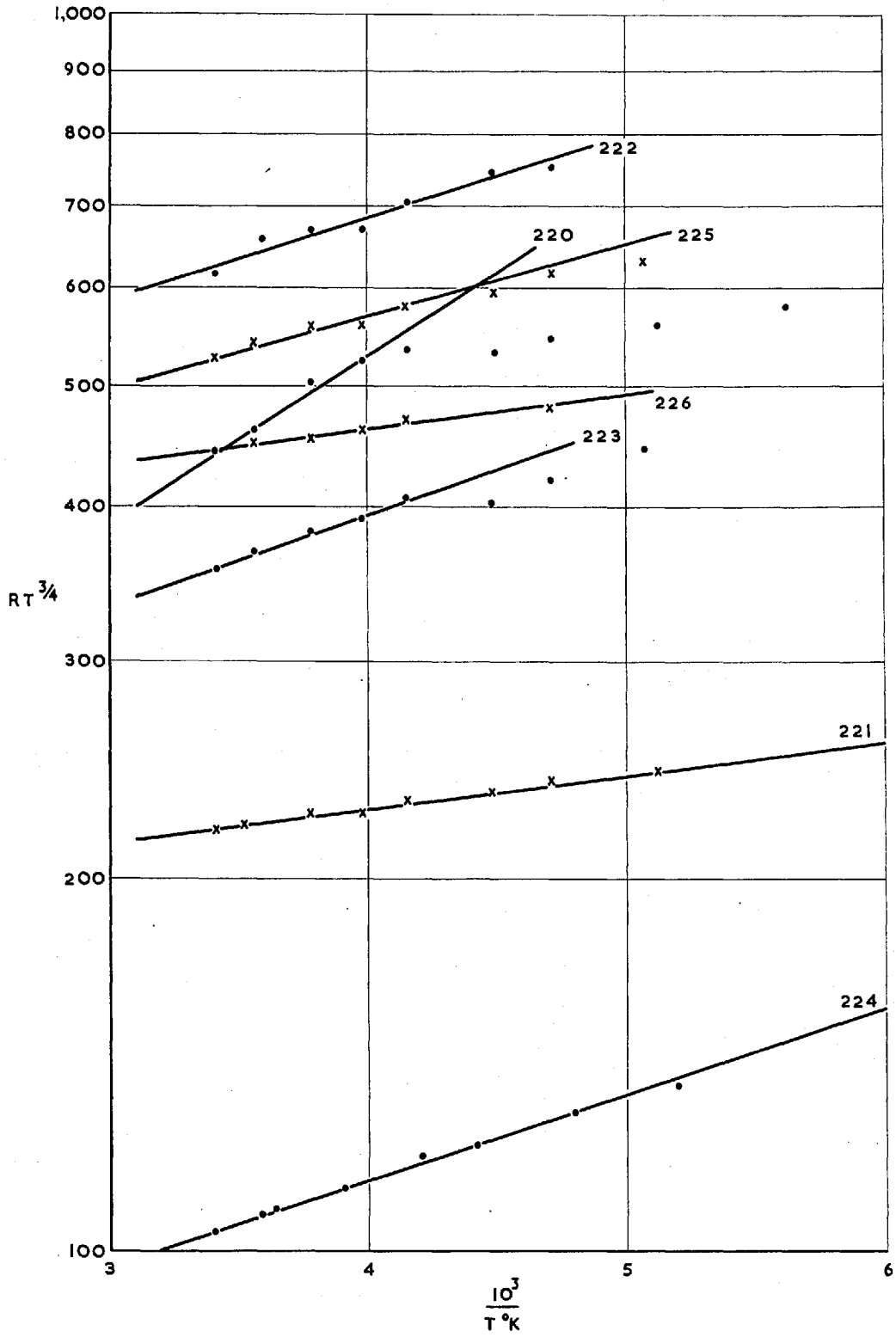
electrical properties. Wolsky also found that the mobility increased and the hole concentration decreased as the film thickness increased, reaching constant values at ~2.5μ from the interface.

7.4.2. Cadmium Arsenide

A thorough investigation of the electrical properties of Cd_3As_2 was not intended as part of the project. The main purpose was to determine whether such a material could be grown in thin film form by sputtering and, if so, what were the general electrical characteristics. Films were grown as described in Chapters 4 and 5. The overall electrical behaviour was rather similar to the germanium films as regards the form of the curves, e.g. mobility increasing as temperature decreased, carrier concentration decreasing as temperature decreased. Application of the same type of analysis as for the germanium films did not yield successful results however. This was due to the fact that the films were degenerate, as is shown by consideration of the degeneracy equation given earlier. Lovett (1967) has examined bulk Cd_3As_2 and finds an effective mass ratio $\left(\frac{m_e}{m}\right)$ of approximately 0.05, which is the figure used in calculating the degeneracy condition. Because of the low band gap of this material (~0.13 eV) the conductivity is almost certainly both intrinsic and extrinsic over the temperature range employed, which again makes analysis difficult. It is not possible to determine an energy value from th slope of the Hall co-efficient against 1/T curve since the films are never wholly extrinsic nor wholly intrinsic. However the following general conclusions can be drawn from the experimental results.

1) Films can be grown on amorphous substrates (glass) at low temperatures (<100°C) with mobilities between 500 and 1000 $cm^2 V^{-1} s^{-1}$.

2) Over the range of rate of deposition used, μ_H is independent of rate.

3) Mobility increases with increasing substrate temperature. The increase is approximately proportional to $T^{-1/3}$ which is lower than would be expected from impurity scattering. Grain size effects may again be predominating.

4) Carrier concentration decreases with increasing substrate temperature.

5) Films have high conductivity ($400 - 800$ $(Ohm.cm)^{-1}$) indicative of a low band gap material.

6) Annealing the films decreases the film carrier concentration but decreases the electron mobility.

This latter conclusion is somewhat anomalous since it was expected that annealing would increase the grain size and reduce structural defects. Annealing was carried out with a deposited overlayer of SiO to prevent loss of one or both of the constituents. It may be possible, therefore, that SiO reacted with the Cd_3As_2 in some way. Further examination of the effects of annealing in a way similar to that carried out on InSb by Juhasz and Anderson (1965) is required before conclusions can be drawn from this observation.

The reasons why Cd_3As_2 should produce films of usable mobility values on amorphous substrates at low temperatures, while other compound semiconductors grown at elevated temperatures on crystalline substrates have very low mobilities, is not clear. One obvious difference between Cd_3As_2 and the other compounds studied is that of crystal structure. InSb etc. have a cubic structure whereas Cd_3As_2 is tetragonal. If the stacking fault energy were higher, or if the dislocation density were lower for a tetragonal material than for a cubic material grown under similar conditions, then the overall defect density would be lower. This would yield a higher value of mobility since there would be fewer scattering centres. Although there is no experimental evidence to support this suggestion, Seeger (1955) has shown that the stacking fault energies in hexagonal materials are higher than in, for instance, cubic noble metals. The stacking fault energy does not depend only on crystal structure, however, so the above must be considered only as a possible explanation for the observed result.

CHAPTER VIII.

SUMMARY AND CONCLUSIONS

The investigation of epitaxial growth by sputtering has attracted a good deal of attention in recent years and the work described in this Thesis has provided further information on the manner by which thin films may be grown by the sputtering technique. The results of the study may be summarised as follows:

(1) Epitaxial films of both metals and semiconductors (elemental and compound) may be grown by sputtering in an inert atmosphere at temperatures considerably lower than the temperature required for epitaxial growth by evaporation.

(2) There is evidence to suggest that, over the range of deposition conditions studied in this work, the films are not epitaxial from the onset of nucleation, i.e. the film orientation increases with thickness.

(3) The relationship between deposition rate and epitaxial temperature follows the expected trend of an energy-controlled phenomenon, i.e. increased orientation with increased substrate temperature and/or decreased deposition rate.

(4) The application of a bias to the substrate so as to attract energetic ions to its surface, increases the degree of orientation, particularly for metal on rocksalt. The orientation improves with bias potential up to a certain value, then deteriorates.

(5) Computer calculation has shown that the energy of arrival of sputtered atoms at the substrate may be considerable even in a glow discharge. Under triode sputtering conditions there is virtually no attenuation of the ejected atom energy distribution.

(6) By triode sputtering, the epitaxial temperature is even lower than that by diode sputtering. The apparent activation energy for epitaxy, derived in terms of substrate temperature and deposition rate, is lower than for evaporation.

(7) Tentative observations of island density in the early (saturation) stages of growth indicate no difference between nucleation by evaporation or by sputtering.

(8) The island density of Ge grown onto (111)Ge shows similarities to vapour phase growth, but the density is approximately an order of magnitude higher.

(9) In all films, there is less twinning at higher substrate temperatures (as observed by electron diffraction). This is as expected since annealing out of defects is an energy dependent process.

(10) The galvanomagnetic properties of the semiconductor films show that in electrical terms the films are far from perfect. The maximum Hall mobility observed for hole conduction in p-type germanium films was approximately 20% of bulk value.

(11) Analysis of the variation of galvanomagnetic properties with temperature showed that impurity scattering was a predominant process. The high impurity concentration in the films supports this.

(12) All galvanomagnetic properties were improved at increased substrate (deposition) temperature. The variation of property with measuring temperature was also found to be dependent upon deposition temperature.

(13) Compound semiconductor films could be readily deposited apparently without loss of stoichiometry, though their galvanomagnetic properties were generally very poor.

One of the overall conclusions to be drawn from this work is that the mechanics of the growth of thin films by sputtering is not widely different

from that by evaporation. Both processes are activation energy dependent, the major difference between the two being the source of the energy required to overcome the various energy barriers. The energy analysis of the sputtered beam shows that the arrival energy of particles at the substrate is significant even by diode sputtering, and the discussion presented in Chapter 6 attempts to demonstrate how this energy may be dissipated on arrival at the substrate. One of the criticisms of the accepted nucleation theories is that they do not allow for arrival energy in their predictions. Complete thermal accommodation is assumed, whereas Cabrera has shown this to be true only for energies below ~ 5 eV.

That the energy of arrival appears to be of greater importance than charge is supported by the evidence of thickness dependence of orientation. Since it has been proposed by various authors that charge, particularly on alkali halide substrates, influences the nucleation stage, differences in nucleation densities as well as initial orientation might have been expected. It should not be concluded, however, that charge plays no part. In the case of diode sputtering, in which the electron flux at the substrate is considerable, the possibility of preferred nucleation sites or charge trapping within the initial islands must be considered. The latter phenomenon, particularly, would provide energy additional to the target atom arrival energy, by way of recombination with thermal ions.

The conclusion to be drawn from the results of the electrical measurements is that defects such as grain boundaries and stacking faults (and dislocations, though the evidence was not so apparent for these) contribute strongly to the scattering mechanisms so as to decrease the mean free path and hence the mobility of the carrier compared to bulk. It is thought that such defects may act as acceptor states, but a detailed description of the nature and effect of such acceptor states is not available

in the literature for p-type germanium, bulk or films. Thus good epitaxial

semiconductor films may be produced by sputtering at relatively low

substrate temperatures, but the structural analysis shows the films to

be full of defects unless the substrate temperature is raised or the

deposition rate lowered. The electrical results are consistent with the

structural findings insofar as the properties approach bulk properties as

the substrate temperature increases, i.e. defect density decreases. The

properties are probably also related to grain size, so that annealing,

high temperature depositions or any other method of increasing the grain

size, should improve the characteristics.

APPENDIX

Computer Calculation of Velocity Attenuation of Sputtered Particles as a Function of Pressure

(Assistance of R.W. Allen is acknowledged)

LAYOUT OF PROBLEM
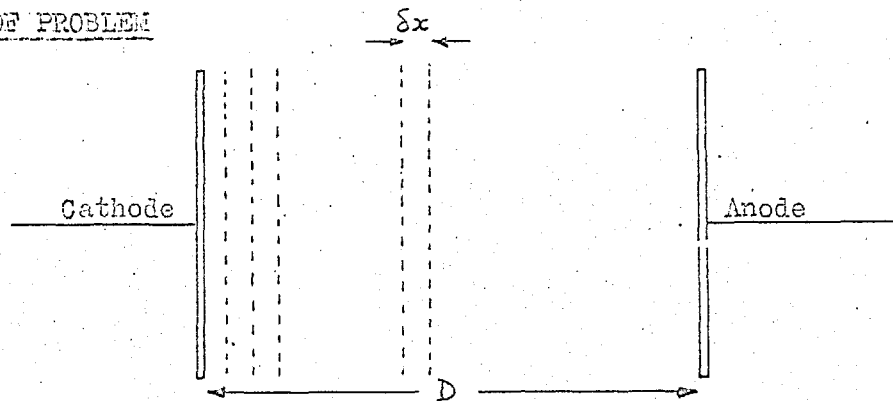
Inter-electrode spacing - D cm. divided into N slabs each of width δx.

Cross-sectional area - 1 cm^2.

Gas density N_A atoms/cm^3.

Collision cross-section $a = C'/V^x$ where x is some power.

$C' = a_o V_o^x$ where a_o = measured collision cross-section at relative velocity V_o.

P = area occupied by the gas atoms in a single slab.

= no. of atoms x collision cross-section at velocity V.

$$= \frac{N_A D}{N} \cdot x \cdot \frac{a_o V_o^x}{V^x}$$

For computation purposes

Put $x = B$ $\qquad N_A D \cdot a_o V_o^x = N_A D C' = C$

$\qquad P = Z$

$\qquad = \frac{C}{N} V^{-B}$

If $V(J) = \log_{10} (\text{velocity} (J))$

then
$$Z(J) = \frac{C}{N} \, e^{-B \times \log_e 10 \times V(J)}$$

Velocity before collision $= V_{BC}$

Velocity after collision $= V_{AC}$

From the Cravath equation for average energy loss, the value for Ag/A is 0.5. Thus, in terms of velocity

$$V_{AC} = \frac{1}{\sqrt{2}} \, V_{BC}$$

$$\log_{10} V_{AC} = \log_{10} V_{BC} - \log_{10} \sqrt{2}$$

If $\log_{10} V_{BC} = V(K)$, then $\log_{10} V_{AC} = V(K - L)$

where $L = \dfrac{\log_{10} \sqrt{2}}{\text{chosen increment for } \log_{10} V}$

In first slab:

$U(J)$ = no. of atoms with velocity $V(J)$ entering

$U(J) \times Z(J)$ collide in slab and leave with velocity $V(J - L)$

$U(J) \times [1-Z(J)]$ do not collide and continue with velocity $V(J)$

In the second slab:

$[U(J) \times Z(J)] \times Z(J-L)$ collide for second time and leave with $V(J-2L)$

$[U(J) \times (1-Z(J))] \times Z(J)$ collide for first time and leave with $V(J-L)$

$[U(J) \times Z(J)] \times [1-Z(J-L)]$ do not collide for second time and leave

$$\text{with } V(J-L)$$

$[U(J) \times (1-Z(J))] \times [1-Z(J)]$ do not collide and continue with $V(J)$

and so on, throughout the slabs.

If $(J-L) \leqslant 0$, these particles are no longer of interest and are ignored in further slabs.

The computer programme sums at the receiver electrode over the velocity range for all the atoms in each group.

COMPUTER PROGRAMME

DECK01   —   EFN   SOURCE STATEMENT — IFN(S) —

```
C SECOND COMPILATION MODIFIED FORM OF FIRST 4 MARCH 66
      REALU(100),V(100),F(100),Z(100),W(100)
      INTEGER S
    1 READ(5,20)N,C,B,L,M,NDATA
   20 FORMAT(I4,F8.4,F3.2,I2,I3,I2)
      IF(N.LE.0)GOTO10
      C=C/FLOAT(N)
      IF(NDATA.LE.0)GOTO6
      READ(5,21)(U(I),V(I),I=1,M)
   21 FORMAT(F6.3,F5.3)
    6 DO11J=1,M
      Z(J)=C*EXP(-B*ALOG(10.)*V(J))
   11 F(J)=0.
      READ(5,23)H,A,R,E,Y,D,O,G
   23 FORMAT(8A6)
      WRITE(6,24)H,A,R,E,Y,D,O,G
   24 FORMAT(1H1,8A6)
      WRITE(6,30)N,C,B,L
   30 FORMAT(1H0,2HN=,I4,2X,2HC=,F7.4,2X,2HB=,F3.2,2X,2HL=,I2)
      FC=0.
      DO12J=1,M
      WC=0.
      DO13K=1,J
   13 W(K)=0.
      W(J)=U(J)
      I=1
    2 K=J
    3 P=Z(K)*W(K)
      S=K-L
      IF(S.LE.0)GOTO4
      W(S)=W(S)+P
      GOTO5
    4 WC=WC+P
    5 W(K)=W(K)-P
      K=S
      IF(K.GE.1)GOTO3
      I=I+1
      IF(N.GE.I)GOTO2
      DO14K=1,J
   14 F(K)=F(K)+W(K)
      FC=FC+WC
   12 CONTINUE
      WRITE(6,25)
   25 FORMAT(1H0,1X,6HLOG10V,6X,7HN(INIT),6X,8HN(FINAL))
      WRITE(6,26)FC
   26 FORMAT(1H0,9HTOO SMALL,5X,4HZERO,7X,F9.5)
      WRITE(6,27)(V(I),U(I),F(I),I=1,M)
   27 FORMAT(1H ,F7.3,F13.5,F14.5)
      GOTO1
   10 STOP
      END
```

PRESSURE=10MTORR D=10CM. AG/A B=0.4   CU/HG DISTN

N= 500   C= 2.2920   B=.40   L= 3

LOG10V	N(INIT)	N(FINAL)
TCC SMALL	ZERO	932.35130
5.000	8.64900	8.55719
5.050	12.15000	8.08322
5.100	16.16600	7.60858
5.150	21.52000	6.78342
5.200	29.03600	6.22028
5.250	33.46400	5.66757
5.300	49.42300	4.80494
5.350	60.64700	4.23693
5.400	75.37100	3.69699
5.450	87.52100	2.91762
5.500	99.15600	2.44016
5.550	102.86200	2.00826
5.600	98.43500	1.42303
5.650	87.00600	1.10432
5.700	73.00200	0.83789
5.750	56.83700	0.49751
5.800	40.15700	0.34362
5.850	25.94700	0.23138
5.900	12.97400	0.09746
5.950	6.48700	0.05337
6.000	2.88300	0.02947
6.050	0.30900	0.00389

PRESSURE= 1MTORR D=10CM. AG/A B=0.4   CU/HG DIST.

N= 500   C= 0.2292   B=.40   L= 3

LOG10V	N(INIT)	N(FINAL)
TCC SMALL	ZERO	64.65103
5.000	8.64900	22.52107
5.050	12.15000	27.68461
5.100	16.16600	32.10729
5.150	21.52000	40.27924
5.200	29.03600	47.44273
5.250	33.46400	53.65598
5.300	49.42300	62.95230
5.350	60.64700	69.84658
5.400	75.37100	75.99430
5.450	87.52100	78.76164
5.500	99.15600	79.73104
5.550	102.86200	76.82495
5.600	98.43500	69.54584
5.650	87.00600	59.03946
5.700	73.00200	47.93845
5.750	56.83700	35.80449
5.800	40.15700	25.05100
5.850	25.94700	16.16857
5.900	12.97400	7.94950
5.950	6.48700	4.02223
6.000	2.88300	1.82648
6.050	0.30900	0.39903

```
PRESSURE=.1MTCRR D=1CCM. AC/A B=C.4  CU/HC DIST.

N= 5CC   C= 0.C229   B=.4C   L= 3

UNDRFLCW AT 04344 IN MQ

UNDRFLCW AT 04367 IN MQ
```

LCG1CV	N(INIT)	N(FINAL)
TCO SMALL	ZERC	4.23237
5.000	8.64900	9.84520
5.C50	12.15CCC	13.61589
5.1CC	16.16600	17.58056
5.150	21.52000	23.65999
5.200	29.02600	31.28056
5.250	33.46400	36.30402
5.3CC	49.42300	51.64724
5.350	60.64700	62.63491
5.4CC	75.37100	76.36306
5.45C	87.521CC	87.28697
5.5CC	99.156CC	97.42497
5.55C	102.86200	1C0.15248
5.6CC	98.4350C	95.23923
5.65C	87.0C6CC	83.77967
5.7CC	73.0C2C0	70.02845
5.750	56.83700	54.27958
5.8CC	40.15700	38.30785
5.85C	25.047CC	24.74793
5.9CC	12.974CC	12.35373
5.950	6.487CC	6.18435
6.CCC	2.88300	2.75441
6.050	0.3C9C0	0.29582

REFERENCES

Almen,O. and Bruce,G.   Nucl.Inst.& Methods 11 279 1961

Almen,O. and Bruce,G.   Nucl.Inst.& Methods 11 257 1961

Anderson,G.S. and Wehner,G.K.   J.Appl.Phys. 31 2305 1960

Bassett,G.A.   Proc.Eur.Conf.Electron Microscopy,Delft. 1 270 1960

Becker,R. and Doering,W.   Ann.Phys. 24 719 1935

Bickley,W.P. and Campbell,D.S.   Vide 99 214 1962

Blakemore,   Semiconductor Statistics

Campbell,D.S. and Stirland,D.J.   Phil.Mag. 9 703 1964

Chapman,B.N.   Ph.D.Thesis Univ.of London 1969

Cozens,J.   Research Project, Imperial College, London 1968

Cravath,A.M.   Phys.Rev. 36 248 1930

Davidse,P.D. and Maissel,L.I.   12th.Nat.Vac.Symp.,American Vacuum Soc.,

1965. Pergamon 1966

Fetz,H.   Z.Phys. 119 590 1942

Francombe,M.H. and Norika,A.J.   J.Appl.Phys. 32 978 1961

Francombe,M.H.,Flood,J.J. and Turner,G.L'E.   Proc.5th.Int.Conf.Electron

Microscopy,1962,Paper DD8   Academic N.Y.1962

Frenkel,J.   Z.Phys. 26 117 1923

Frerichs,R.   J.Appl.Phys. 33 1898 1962

Fruth,H.F.   Physica 2 280 1932

Gawehn,H.   Z.Angew.Phys. 14 458 1963

Gibson,J.B.,Goland,A.N.,Milgram,M. and Vineyard,G.H.   Phys.Rev. 120 1229 1960

Grove,W.   Phil.Trans. 142 87 1852

Guntherschulze,A. and Meyer,K.   Z.Phys. 62 607 1930

von Hippel,A.   Ann.Phys. 80 672 1926

von Hippel,A.   Ann.Phys. 81 1043 1926

Hall,J. and Thompson,M.W.   Brit.J.Appl.Phys. 12 495 1961

Halpern,V.   Brit.J.Appl.Phys. 18 163 1967

Hersch

Hirth,J.P. and Pound,G.V.   Condensation and Evaporation.   Pergamon 1963

Honig,R.E.   J.Appl.Phys. 29 549 1958

Jacobs,M.H.; Pashley,D.W. and Stowell,M.J.   Phil.Mag. 13 121 1966

Janeff,W.   Z.Phys. 142 619 1955

Juhasz,C. and Anderson,J.C.   3rd.Int.Vac.Cong.,1965,Vol.2,Part 1,p333
                    Pergamon11963

Kaminsky,M.   Atomic and Ionic Impact Phenomena on Metal Surfaces.
                    Springer Verlag 1965

Keywell,F.   Phys.Rev. 97 1611 1965

Kistemaker,J. and Snoek,C.   Coll.Int.C.N.R.S. No.113   Paris 1962, p.51

Klick

 Koedam,M.   Physica 25 742 1959

Koedam,M.   Ph.D. Thesis.   State Univ. Utrecht 1961

Kopitzki,K. and Stier,H.E.   Z.Naturforsch. 169 1257 1961

Krikorian,E. and Sneed,R.J.   J.Appl.Phys. 37 3665 1965

Langmuir,I. and Tonks,L.   Phys.Rev. 34 896 1929

Layton,C.K. and Campbell,D.S.   J.Mat.Sci. 1 367 1966

Lewis,B.   Thin Solid Films 1 85 1967

Lewis,B. and Campbell,D.S.   J.Vac.Sci.Tech. 4 209 1967

Lewis,W.   Thin Films and Surfaces.   English Univ. Press 1938

 Longden,A.C.   Phys.Rev. 11 40 1900

Lovett,D.R.   Ph.D. Thesis. Univ. of London,1967

Macdonald,R.J. and Haneman,D.   J.Appl.Phys. 37 1609 1966

Maissel,L.I. and Schaible,P.M.   J.Appl.Phys. 35 237 1965

Martynenko,Y.V.   Phys.Stat.Sol. 15 767 1966

Marruchi,J.   C.R.Acad.Sci.,Paris 260 6580 1965

Matthews,J.W.   Phil.Mag. 6 1347 1961

Matthews,J.W.   Phil.Mag. 12 1143 1965

Matthews,J.W.   Physics of Thin Films(eds.Hass & Thun) 4 137 1967

Matthews,J.W. and Allinson,D. Phil.Mag. 8 1283 1963

van der Merwe, Proc.Int.Symp."Basic Problems in Thin Film Physics"

Clausthal,1965. Vandenhoek and Ruprecht 1966

Miller,R.C. and Kusch,P. Phys.Rev. 99 1314 1955

Morgulis,N. and Tishenko,V. Bull.Acad.Sci.USSR Phys.Ser. 20 1082 1956

Moulton,C. Nature 195 793 1962

Nelson,R.S. Phil.Mag. 11 291 1965

Nelson,R.S. and Thompson,M.W. Proc.Roy.Soc. 259A 458 1961

Ogawa,S., Watanabe,D. and Ino,S. Acta Cryst. 16 A133 1963

Oliphant,

Palmberg, P, Rhodin,T.N. and Todd,C.J. Appl.Phys.Letters 10 122 1967

Palmberg,P , and Rhodin,T.N. Published in J.Phys.Chem.Sol. 1968

Pashley,D.W. and Stowell,M.J. Proc.5th. Int.Conf.Electron Microscopy

Philadelphia,1962. Academic N.Y. 1963

Pashley,D.W. Adv.in Physics 14 327 1965

Pearson,G.L. and Bardeen,J. Phys.Rev. 75 865 1949

Penney,W. and Moubis, Proc.Amst.Acad. 43 41 1940

Putley,E.H. The Hall Effect and Related Phenomena. Butterworth 1960

Reizman,F. and Basseches,H. Metallurgy of Semiconductor Materials.

Wiley 1962, p.169

Rhodin,T.N., Palmberg,P , and Todd,C.J. Published in Mol.Processes on

Solid Surfaces 1968

Rol,P.K., Fluit,J.M. and Kistemaker,J. Physica 26 1009 1960

Rothe,E.W. and Bernstein,R.B. J.Chem.Phys. 31 1619 1959

Seeger,A. in Defects in Crystalline Solids. London Phys.Soc. 1955

Seeliger,R. and Sommermeyer,K. Z.Phys. 93 1935

Shockley,W. Electrons and Holes in Semiconductors. Van Nostrand N.Y.1950

Silsboo,R.H. J.Appl.Phys. 28 1246 1957

Sloope,W. and Tiller,C.O.   J.Appl.Phys. 37 887 1966

Sloope,W. and Tiller,C.O.   Jap.J.Appl.Phys. 2 308 1963

Smith,R.A.   Semiconductors.   C.U.P. 1964

Stirland,D.J.   in "Uses of Thin Films in Physical Investigations."
                        (J.C.Anderson,ed)   Chapman and Hall   1966

Stirland,D.J.   Appl.Phys.Letters 8 326 1966

Stuart,R.V. and Wehner,G.K.   Phys.Rev.Letters 4 409 1960

Stuart,R.V. and Wehner,G.K.   9th.Nat.Vac.Symp., American Vacuum Soc.,1962
                        p.160.   Macmillan, N.Y. 1963

Stuart,R.V. and Wehner,G.K.   J.Appl.Phys. 33 2345 1962

Theurer,H.C. and Hauser,J.J.   J.Appl.Phys. 35 554 1965

Thompson,M.W.   Physics Letters 6 24 1963

Thompson,M.W.   Sussex Univ. Report, 1967

Tramposch,R.F.   Bull.Am.Phys.Soc. 11 460 1966

Volmer,M. and Weber,A.   Z.Phys.Chem. 26B 277 1925

Walton,D., Rhodin,T.N., and Rollins,R.   J.Chem.Phys. 38 2695 1963

Wehner,G.K.   Adv. in Electronics and Electron Physics 17 1955

Wehner,G.K.   J.Appl.Phys. 31 1392 1960

Wehner,G.K.   U.S.Patent No.3021271   1962

Wehner,G.K. and Medicus,G.   J.Appl.Phys. 25 698 1954

Wehner,G.K. and Rosenberg,D.   J.Appl.Phys. 31 177 1960

Weimer,P.K.   I.R.E. Trans. on Electron Devices 8 421 1961

Widmer,H.   3rd.Int.Vac.Cong.,1965,Vol.2 Part 1, p.309.   Pergamon 1967

Wolsky,S.P., Piwkowski,T.R. and Wallis,G.   Research Report 1965
                        P.R.Mallory Labs., Burlington, Mass., U.S.A.

Wolsky,S.P. and Wallis,G.   13th. American Vacuum Soc. Meeting 1966(Abstract)

Wright,A.W.   Amer.J.Sci.& Arts 13 49 1877